POLITECHNIKA GDAŃSKA

Imię i nazwisko autora rozprawy: Michał Maciejewski

Dyscyplina naukowa: Inżynieria Materiałowa

ROZPRAWA DOKTORSKA

Tytuł rozprawy w języku polskim: Struktura i właściwości fizyczne szkieł i szkło-ceramik fosforanowych domieszkowanych jonami ziem rzadkich

Tytuł rozprawy w języku angielskim: Structure and properties of phosphate glasses and glass-ceramics doped with rare earth ions

Promotor
prof. dr hab. inż. Barbara Kościelska

Gdańsk, rok 2025

GDAŃSK UNIVERSITY OF TECHNOLOGY

The author of the doctoral dissertation: Michał Maciejewski

Scientific discipline: Materials Engineering

DOCTORAL DISSERTATION

Title of doctoral dissertation: Structure and properties of phosphate glasses and glass-ceramics doped with rare earth ions

Title of doctoral dissertation (in Polish): Struktura i właściwości fizyczne szkieł i szkło-ceramik fosforanowych domieszkowanych jonami ziem rzadkich

Supervisor
prof. dr hab. inż. Barbara Kościelska

Gdańsk, year 2025

POLITECHNIKA GDAŃSKA

OŚWIADCZENIE

Autor rozprawy doktorskiej: Michał Maciejewski

Ja, niżej podpisany(a), oświadczam, iż jestem świadomy(a), że zgodnie z przepisem art. 27 ust. 1i 2 ustawy z dnia 4 lutego 1994 r. o prawie autorskim i prawach pokrewnych (tj. Dz.U. z 2021 poz. 1062), uczelnia może korzystać z mojej rozprawy doktorskiej zatytułowanej: „Struktura i właściwości fizyczne szkieł i szkło-ceramik fosforanowych domieszkowanych jonami ziem rzadkich" do prowadzenia badań naukowych lub w celach dydaktycznych.[1]

Świadomy(a) odpowiedzialności karnej z tytułu naruszenia przepisów ustawy z dnia 4 lutego 1994 r.o prawie autorskim i prawach pokrewnych i konsekwencji dyscyplinarnych określonych w ustawie Prawo o szkolnictwie wyższym i nauce (Dz.U.2021.478 tj.), a także odpowiedzialności cywilno- prawnej oświadczam, że przedkładana rozprawa doktorska została napisana przeze mnie samodzielnie.

Oświadczam, że treść rozprawy opracowana została na podstawie wyników badań prowadzonych pod kierunkiem i w ścisłej współpracy z promotorem prof. dr hab. inż. Barbarą Kościelską.

Niniejsza rozprawa doktorska nie była wcześniej podstawą żadnej innej urzędowej procedury związanej z nadaniem stopnia doktora.

Wszystkie informacje umieszczone w ww. rozprawie uzyskane ze źródeł pisanych i elektronicznych, zostały udokumentowane w wykazie literatury odpowiednimi odnośnikami, zgodnie z przepisem art. 34 ustawy o prawie autorskim i prawach pokrewnych.

Potwierdzam zgodność niniejszej wersji pracy doktorskiej z załączoną wersją elektroniczną.

Gdańsk, dnia ....

Ja, niżej podpisany(a), wyrażam zgodę na umieszczenie ww. rozprawy doktorskiej w wersji elektronicznej w otwartym, cyfrowym repozytorium instytucjonalnym Politechniki Gdańskiej.

Gdańsk, dnia ....

[1] Art. 27. 1. Instytucje oświatowe oraz podmioty, o których mowa w art. 7 ust. 1 pkt 1, 2 i 4–8 ustawy z dnia 20 lipca 2018 r. – Prawo o szkolnictwie wyższym i nauce, mogą na potrzeby zilustrowania treści przekazywanych w celach dydaktycznych lub w celu prowadzenia działalności naukowej korzystać z rozpowszechnionych utworów w oryginale i w tłumaczeniu oraz zwielokrotniać w tym celu rozpowszechnione drobne utwory lub fragmenty większych utworów.
2. W przypadku publicznego udostępniania utworów w taki sposób, aby każdy mógł mieć do nich dostęp w miejscu i czasie przez siebie wybranym korzystanie, o którym mowa w ust. 1, jest dozwolone wyłącznie dla ograniczonego kręgu osób uczących się, nauczających lub prowadzących badania naukowe, zidentyfikowanych przez podmioty wymienione w ust. 1.

GDAŃSK UNIVERSITY OF TECHNOLOGY

STATEMENT

The author of the doctoral dissertation: Michał Maciejewski

I, the undersigned, declare that I am aware that in accordance with the provisions of Art. 27 (1) and
(2) of the Act of 4th February 1994 on Copyright and Related Rights (Journal of Laws of 2021, item1062), the university may use my doctoral dissertation entitled: "Structure and properties of phosphate glasses and glass-ceramics doped with rare earth ions" for scientific or didactic purposes.[1]

Gdańsk,..... .....

Aware of criminal liability for violations of the Act of 4th February 1994 on Copyright and Related Rights and disciplinary actions set out in the Law on Higher Education and Science (Journal of Laws 2021, item 478), as well as civil liability, I declare, that the submitted doctoral dissertation is my own work.

I declare, that the submitted doctoral dissertation is my own work performed under and in cooperation with the supervision of prof. dr hab. inż. Barbarą Kościelską.

This submitted doctoral dissertation has never before been the basis of an official procedure associated with the awarding of a PhD degree.

All the information contained in the above thesis which is derived from written and electronic sourcesis documented in a list of relevant literature in accordance with Art. 34 of the Copyright and Related Rights Act.

I confirm that this doctoral dissertation is identical to the attached electronic version.

Gdańsk,..... .....

I, the undersigned, agree to include an electronic version of the above doctoral dissertation in the open, institutional, digital repository of Gdańsk University of Technology.

Gdańsk,..... .....

[1] Art 27. 1. Educational institutions and entities referred to in art. 7 sec. 1 points 1, 2 and 4–8 of the Act of 20 July 2018 –Law on Higher Education and Science, may use the disseminated works in the original and in translation for the purposesof illustrating the content provided for didactic purposes or in order to conduct research activities, and to reproduce for thispurpose disseminated minor works or fragments of larger works.

2. If the works are made available to the public in such a way that everyone can have access to them at the place and timeselected by them, as referred to in para. 1, is allowed only for a limited group of people learning, teaching or conducting research, identified by the entities listed in paragraph

GDAŃSK UNIVERSITY OF TECHNOLOGY

DESCRIPTION OF DOCTORAL DISSERTATION

The Author of the doctoral dissertation: Michał Maciejewski

Title of doctoral dissertation:

Structure and properties of phosphate glasses and glass-ceramics doped with rare earth ions

Title of doctoral dissertation in Polish:

Struktura i właściwości fizyczne szkieł i szkło-ceramik fosforanowych domieszkowanych jonami ziem rzadkich

Language of doctoral dissertation: English

Supervisor: prof. dr hab. inż. Barbara Kościelska

Date of doctoral defense:

Keywords of doctoral dissertation in Polish: szkło fosforanowe, luminescencja jonów Eu^{3+}, struktura szkła, szkło-ceramiki, kontrolowana krystalizacja, SrF_2, KF, AlF_3, Ag

Keywords of doctoral dissertation in English: phosphate glass, Eu^{3+} ions luminescence, glass structure, glass-ceramics, controlled crystallization, SrF_2, KF, AlF_3, Ag

Summary of doctoral dissertation in Polish:

Wytworzono oraz zbadano serie szkieł oraz szkło-ceramik opartych na opracowanej nowej matrycy fosforanowej P_2O_5 – K_2O – Bi_2O_3 – Nb_2O_5 (PKBN). Przeprowadzone modyfikacje dzieliły się na trzy grupy obejmujące: I) wprowadzenie dodatku SrF_2 w celu uzyskania w procesie wygrzewania nanokryształów w matrycy szkła oraz określenie ich wpływu na luminescencję domieszki Eu; II) wprowadzenie dodatku KF oraz AlF_3 w celu określenia ich wpływu na strukturę, właściwości oraz luminescencję domieszki Eu; III) zmniejszenie udziału Bi_2O_3 w składzie szkła macierzystego, domieszkowanie go Ag oraz Eu oraz określenie wpływu wygrzewania i obecności Ag na luminescencję jonów Eu^{3+}. Struktura materiałów została zbadana metodami XRD oraz FTIR, określono ich charakterystyki termiczne za pomocą technik DTA/DSC oraz zmierzono ich właściwości optyczne przy zastosowaniu technik spektroskopowych. Przeprowadzone badania potwierdziły uniwersalność syntezowanych materiałów oraz ich wysoki potencjał aplikacyjny w roli luminoforu w diodach LED.

Summary of doctoral dissertation in English:

A series of glasses and glass-ceramics based on the developed novel phosphate matrix P_2O_5 – K_2O – Bi_2O_3 – Nb_2O_5 (PKBN) were synthesized and studied. The modifications performed were divided into three groups, including: I) introduction of SrF_2 addition in order to obtain nanocrystals in the glass matrix during the annealing process and determination of their effect on the luminescence of the Eu dopant; II) introduction of KF and AlF_3 addition in order to determine their effect on the structure, properties and luminescence of the Eu dopant; III) reduction of the Bi_2O_3 share in the composition of the parent glass, doping it with Ag and Eu and determination of the effect of annealing and the presence of Ag on the luminescence of the Eu^{3+} ions. The materials were structurally characterized using XRD and FTIR measurements, their thermal characteristics were determined using DTA/DSC techniques and their optical properties were measured using spectroscopic techniques. The conducted research confirmed the universality of the synthesized materials and their high application potential as a luminophore in LEDs.

Pragnę złożyć serdeczne podziękowania mojej Pani Promotor, prof. dr hab. inż. Barbarze Kościelskiej za daną mi szansę, nieocenione wsparcie i cierpliwość. Jestem ogromnie wdzięczny za poświęcony mi czas i pomoc w procesie tworzenia tej pracy.

Praca w zespole Fizyki Nanomateriałów była dla mnie przyjemnością, zawsze mogłem liczyć na cenne uwagi, rozmowy pełne przemyśleń i inspirującą współpracę, za co bardzo dziękuję.

Dziękuję również Koleżankom i Kolegom z Instytutu Nanotechnologii i Inżynierii Materiałowej za wszelką pomoc, przekazaną wiedzę oraz dni pełne uśmiechu.

Z całego serca dziękuję moim Kochanym Rodzicom i Rodzeństwu, bez Waszego poświęcenia i ciągłego wsparcia droga, którą obrałem nie byłaby możliwa. Stało się to wszystko, choć tak niedawno „trochę" się bałem.

Za to, że byłaś przy mnie ten cały czas, nieustannie wspierałaś, dawałaś nadzieję i siłę. Bez Ciebie nie poradziłbym sobie.
Dziękuję Justynko

Table of content

Abbreviations

τ – radiative decay lifetime

C_b – position of the band center

DSC – Differential Scanning Calorimetry

DTA – Differential Thermal Analysis

FT-IR – Fourier Transform Infrared Spectroscopy

GC – glass-ceramic

H-BiP – high-temperature monoclinic $BiPO_4$ phase

M-BiP – monoclinic monazite-type $BiPO_4$ phase

Q_n – number of bridging oxygens in PO_4 tetrahedron

R/O – red to orange ratio

R_a – relative area of the band

RE – rare earth elements

RO – modifying oxide

S – Saad-Poulain parameter

SSL – Solid-State Lighting

T_c – crystallization temperature

T_g – glass transition temperature

T_m – melting temperature

T_x – onset of the exothermic maximum

UnP – unknown crystalline phase

UV-Vis – Ultraviolet-Visible Absorption Spectroscopy

XRD – X-Ray Powder Diffraction

1. Introduction

To understand the principles governing amorphous solids, one must demonstrate patience and imagination. Although this statement may be considered accurate for most materials, in the case of glasses it contains a deeper meaning - among others, peculiarly related to the conditions of transition to the glass phase described later. The first of the listed features indirectly expresses the amount of time necessary to obtain and characterize the newly created material. There is no widely known method that, analogous to X-ray diffraction in crystals, would allow for an unambiguous and exhaustive description of the internal structure of multicomponent glasses. Apart from empirically created principles defining the "ease" of vitrification of a given group of components, there is also no universal principle indicating whether and under what conditions it will be possible to vitrify an experimental mixture of compounds. At this point, it is appropriate to outline the second of the cited features, which allows for a basic understanding of what the postulated internal structure is, and thus provides for finding answers to problematic aspects of synthesis. The typical division of solids into crystals characterized by a periodic atomic structure and amorphous solids devoid of this property could suggest that in glasses at the microscopic level, atoms, not finding an energy minimum, are immersed in complete chaos. Imagination, which in this case is a broad term that includes not only invention but also the ability to reason, allows us to observe the relationships between atoms, creating probable visions of coordinated systems of structural units, which as a result form a "glass network". Based on the differences in the properties of chemical compounds constituting the components of glass, it is, therefore, possible to guess their role in the internal structure of the amorphous solid, but the way in which they fill the space often remains a riddle, in which a sharp mind puts together an answer using data on the nearest neighbors.

Having described the most important characteristics of a glass researcher, it is necessary to turn our attention to the subject of study itself. In this work, among the many questions and issues that arise, I would like to begin with the question "What is glass?" and lead the narrative so fluently that the answer to the last question "Why glass?" becomes obvious.

1.1. General characteristics of glasses

Each of the questions asked deserves an answer, in the case of the previously posed "What is glass?" it should first be given a bit of elegance and transformed into the form "What is the definition of glass?". When looking for this definition, we can start by observing everyday life, as a result of which we can state with a clear dose of obviousness that we are surrounded by amorphous solids. Starting with kitchen containers and ending with all kinds of screens, we can surmise that these objects are made of glass. The question therefore arises: on what basis is

it possible to make this distinction, i.e. which material features do we consider necessary to assign glasses? Of course, transparency, fragility, and universality can certainly be mentioned. Awareness of them allows us to construct the first, "everyday" definition of glass as a material that is characterized by the above-mentioned properties. As can be seen, rooting the definition in the unique features of the material is a good direction, but it requires much greater precision and selectivity, in particular emphasizing the previously mentioned division that places crystalline solids against glasses. In contrast to crystals, amorphous solids lack long-range order, and thus periodicity, which would guarantee a relatively simple mathematical description of the structure. However, this does not mean a complete lack of order – short-range order is observed in the internal structure. This feature, referring only to the way atoms are arranged, and not to their types and bonds formed, constitutes a universal criterion that can characterize materials as amorphous. There is no doubt that the presented condition is sufficient in its simplicity and could constitute a second, this time already 'professional' definition of the described group of solids. However, it concerns a purely microscopic observation, which is a consequence of the glass transition observed macroscopically. Its occurrence is therefore a complementary criterion for the classification of amorphous solids. This transition can be considered based on the dependence of enthalpy as a function of temperature, an example of which is presented in Figure 1.

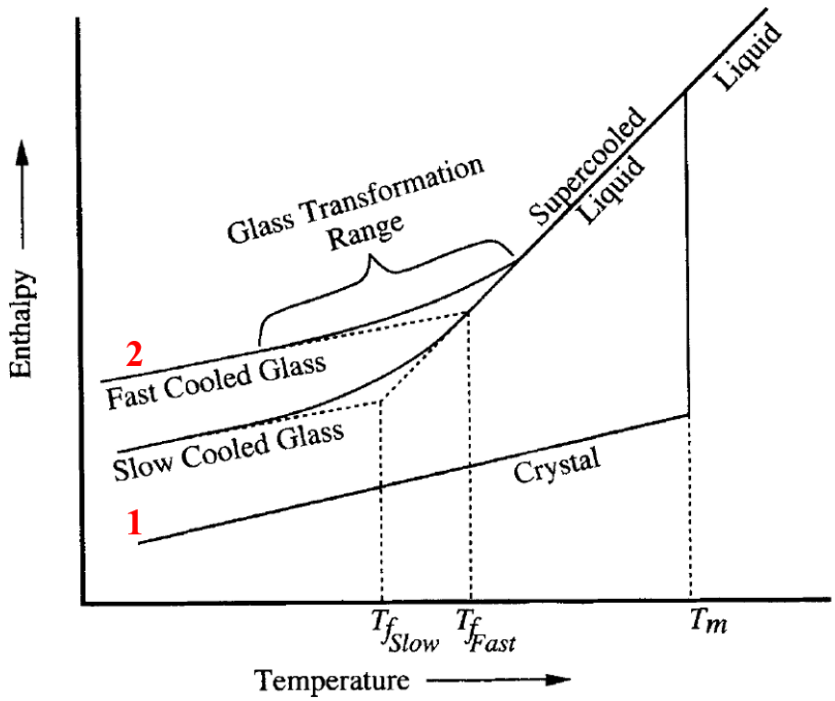

Fig. 1 Schematic diagram of the dependence of enthalpy on temperature obtained for the glass-forming liquid during cooling. The variants of the processes taking place are marked with 1 and 2: 1 – crystallization, 2 – transition to the glass phase [1]

Analyzing the process described in Figure 1, one can observe how a gradually cooled liquid at the melting temperature T_m undergoes a phase transition, rapidly reducing (the graph shows a discontinuity in the function) its enthalpy to the level characteristic of a solid – crystallization occurs. As can be seen, following the path of the process marked with No. 2, as a result of cooling, one can obtain a solid with an enthalpy slightly higher than that observed for a crystalline solid in a given temperature range. The aforementioned patience, identified with providing the right amount of time, in the case of cooling a liquid in most cases leads to obtaining a material with a crystalline structure. Peculiarly, cooling a liquid sufficiently quickly at the crystallization temperature does not cause any noticeable process, and the curve continuously reaches a slope corresponding to a solid. For a supercooled liquid, a glass transition occurs in the region close to the glass transition temperature T_g, the atoms not having enough time to occupy their preferred equilibrium positions due to the drastic increase in viscosity in the transition region (with decreasing temperature) solidify to form an amorphous solid. Due to the fact that the transition to the glass phase is continuous and occurs in a temperature range (no well-defined beginning and end), for practical reasons the temperature T_g that characterizes it can be defined based on various concepts as a single value, but a precise description would require including a temperature range. Moreover, the curve corresponding to the enthalpy function characteristic for glasses in Figure 1 branches near the end of the glass transition. This is a manifestation of the kinetic feature of the glass transition - the value of T_g depends on the rate of cooling applied. Unifying the presented postulates, it is possible to put forward a final definition: a glass is any isotropic material that exhibits a glass transition in the temperature range described by the parameter T_g and whose structure is completely devoid of long-range order described by translational symmetry [1].

Based on the adopted description, it can be concluded that the transition to the glass phase is not a special feature exhibited only by some group of materials, but in the physics of the condensed phase, although less stable, in many aspects equivalent to the crystal state of matter, available for most compounds under certain conditions. David Turnbull in his work [2], considering the latter, cites the cooling rate ($\bar{T}$), reduced surface tension at the crystal-liquid boundary (α), and reduced glass transition temperature (T_{gr}) as parameters whose higher values have a positive effect on the tendency to form glasses. On the other hand, its improvement can also be achieved by reducing the grain density (ρ), the fraction of acceptors on the crystal surface (f), and the volume of the liquid (V_c). Some of the above-mentioned quantities are material constants, so the actual control of the process is limited to changing the volume of the liquid and the cooling rate. A smaller volume of liquid, and thus the amount of cooled substance, has a greater chance of solidifying in an amorphous form due to the fact that despite the

homogeneous nature of the glass transition, heat flow from the sample occurs mainly through its surface (in the case of conventional methods of preparation), and thus, with fixed values of the other parameters, limits its maximum dimensions. Considering that obtaining glass is directly related to maintaining the state of a supercooled liquid, in which nucleation and growth do not occur, the problem of the possibility of obtaining a glassy form of the material can be transformed into the problem of avoiding crystallization during cooling. To do this and obtain a glass of a given composition, the critical value of the cooling rate must be provided to the sample by conducting the experiment. The previously used term "sufficiently fast cooling" was defined by Richard Zallen [3] as cooling sufficiently fast and strongly, where fast refers to ensuring the fastest possible exceedance of the temperature range corresponding to the supercooled liquid without crystallization occurring, and strongly expresses cooling below the glass transition temperature T_g defined for the beginning of the transition. For this reason, the tendency to form glass can be directly identified with the cooling rate required by a given material to obtain it in an amorphous form. It may therefore seem that regardless of the selected substance, in the form of a mixture of compounds or single elements, increasing the cooling rate will allow vitrification of each of them, which is partially proven by metallic glasses obtained using $\overline{T}$ = 10^5 – 10^8 K/s [3]. However, with the increasing value of $\overline{T}$, the decreasing volume of obtained samples is partially correlated. As a result, materials are sought that constitute a compromise of properties and tendency to form glasses so that they could have practical applications.

Deviating slightly from the formulation of the definition of glasses, it is worth considering the essence of their structure. It was mentioned earlier that in the absence of long-range order, short-range order occurs in them, but what is it in reality? Its presence certainly means that the positions of the atoms forming the glass network are macroscopically arbitrary, but at the same time not completely random. Randomness would mean in this case that, just like in an ideal gas, the atoms do not interact with each other and can occupy any positions at a given moment limited only by the atomic radius. As it turns out, however, when analyzing the mutual positions of atoms in the structure of glasses, one can observe clear correlations in their immediate surroundings, which are a consequence of the occurrence of chemical bonds. The presence of bonds defines the interatomic distances between the closest neighbors and is the reason for the existence of a certain trend in the angles in the units forming the structure. Randomness therefore refers to any way of arranging well-defined structural units relative to each other and determines a certain statistical distribution describing the lengths of bonds and their angles in the structure of glasses.

The first attempts to create a theory describing the process of glass formation focused on the classification of compounds that can be easily obtained in glassy form and the features

accompanying them. Collectively, they were called the structural theory of glass formation. The breakthrough work in this trend was the theory of the continuous random network of glasses proposed by Zachariasen in 1932 [4].

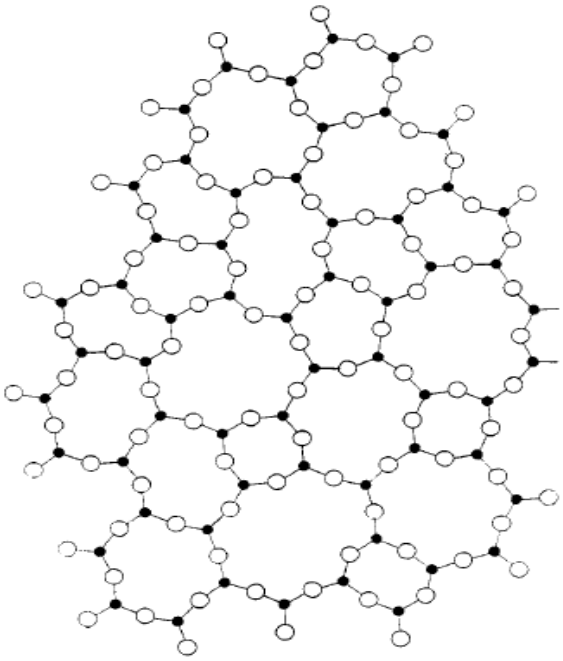

Fig. 2 Schematic diagram of the structure of oxide glass with the general formula A_2O_3 proposed by Zachariasen [4]. Oxygen atoms are marked with empty circles

Having noticed the similarity of mechanical properties of glasses and crystals, he concluded that this was a sign of the same interatomic forces in both the crystal and the glass, and therefore of ultimately similar internal energies. This idea was presented in the well-known diagram (Figure 2) showing a two-dimensional proposal of the glass network. Zachariasen's outstanding achievement was to combine the above observations and propose, based on the principles of crystal chemistry, oxygen polyhedra as the basic units forming the glass network. This gave rise to four empirical principles relating to structural properties, which at that time explained why some oxides were easier to obtain in amorphous form. The principles were formulated as follows: 1) an oxygen atom is linked to not more than two glass-forming atoms; 2) the number of oxygen atoms surrounding glass-forming atoms must be small; 3) the oxygen polyhedra share corners with each other, not edges or faces; 4) at least three corners in each oxygen polyhedron must be shared – forming a three-dimensional network. The proposed model, although groundbreaking in the concept of the structure of an amorphous covalent solid, is only applicable to oxide glasses

In the above work, a division of cations into glass-forming defined as those capable of forming glassy oxides (capable of isomorphic substitution), and thus the skeleton of glasses, and network modifiers in the form of large cations with a small charge, which occupy naturally occurring random holes for a continuous network, was proposed. Currently, based on the above division, glass components are grouped according to the role they play in the structure. Glass-forming compounds such as SiO_2 or B_2O_3 form the basic structure of the glass, compounds classified as intermediates such as Nb_2O_5, depending on their content, may act as glass-forming or be a modifier. The latter form a large group of compounds by means of which the properties of the obtained amorphous material are controlled.

Further development of theories describing the formation of glasses led to a change of approach from empirically selecting favorable compositions and glass-forming features to determining the conditions necessary to obtain glass of a given composition. Those that focused on determining the critical cooling rate at which the reorganization of the structure to the crystalline state is impossible were collectively called kinetic theories of glass formation. In these considerations, the mutual interactions between the models of the nucleation rate (I) and growth rate (U) as a function of temperature and time are discussed. On their basis, it is possible to determine the volume fraction of the crystalline phase in the sample, the value of which in isothermal conditions is given by the relationship:

$$\frac{V_x}{V} = 1 - exp\left(-\frac{\pi}{3} I_v {U_l}^3 t^4\right), \quad (1)$$

where V_x is the volume of the crystalline phase, V is the sample volume, I_v is the nucleation rate per unit volume, U_l is the linear rate of crystal growth, and t is the time during which the sample was at a fixed temperature. Knowing the forms of the I_v and U_l functions from the temperature, it is possible to plot the dependence in the coordinates of time and temperature. Based on the adopted specific value of V/V_x, a function called the time-temperature-transformation (TTT) curve is obtained. An example of the shape of the TTT dependence is presented in Figure 3.

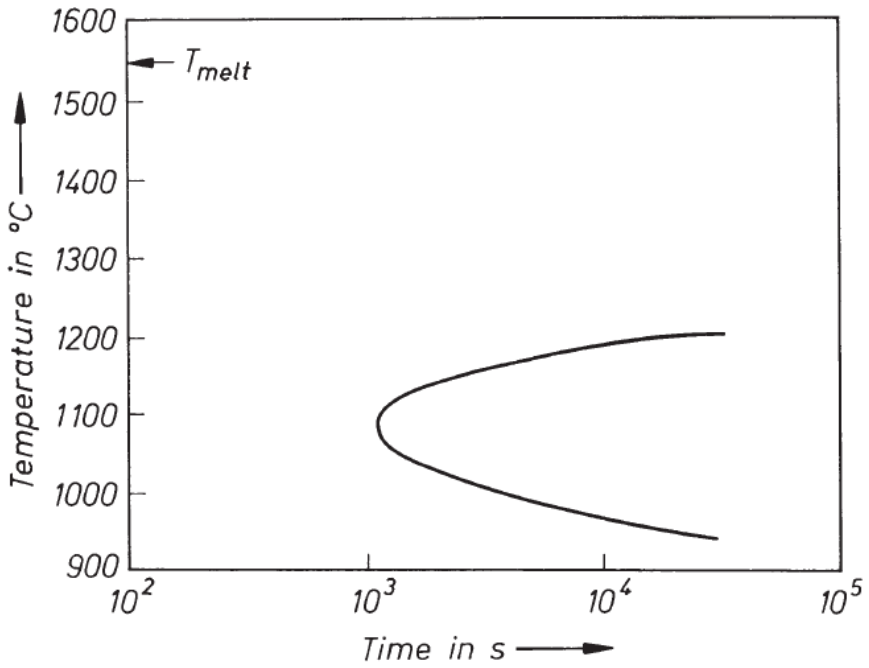

Fig. 3 Example of TTT curve obtained for $V_x/V = 10^{-6}$ [5]

The assumed value of the $V_x/V = 10^{-6}$ parameter is considered [6] as the limiting value of the degree of crystallinity that can be detected in the sample, so in this case, it is a well-defined condition, the fulfillment of which guarantees to obtain a crystalline structure instead of an amorphous one. The characteristic shape of the curve is dictated by the competing processes of atomic mobility, which increases with increasing temperature, and the driving force for crystallization, which decreases with increasing temperature. The appearing "nose" of the function corresponds in this case to the shortest time necessary for a given part of the volume to crystallize. The usefulness of the presented concept comes from the possibility of determining the critical cooling rate necessary to obtain the glassy state. This is done by drawing a tangent, when the initial conditions are assumed to be the melting temperature (T_m) at time t = 0, the approximate expression then has the form:

$$\left(\frac{dT}{dt}\right)_c \approx \frac{(T_m - T_n)}{t_n}, \tag{2}$$

where $(dT/dt)_c$ is the critical cooling rate, and T_n and t_n are the values (temperature and time, respectively) of the coordinates of the TTT inflection point. Studies on the kinetics of the glass formation process conducted by Uhlmann [7] allowed him to conclude the material features promoting the occurrence of this process. The first observation made was a high viscosity at the point (T_n/t_n) on the TTT diagram, which could be a sign of high viscosity at the temperature T_m and an increased probability of a strongly increasing viscosity dependence with a decrease in

temperature below T_m. He also mentioned a high energy barrier for nucleation and the absence of potential heterogeneous nuclei. In addition, it is advantageous to use complex, multicomponent alloy compositions.

The narrative so far has focused on the description of glasses and the process of their creation as a result of skillful "avoidance" of crystallization. It could have remained in this form if in 1953 a small mistake had not been made by the then-employee of Corning Glass Works S.D. Stookey, who accidentally heated a sample of glass (lithium disilicate) containing silver precipitates to 900 °C instead of 600 °C. To his surprise, instead of a melted glass mass, he found in the furnace a cloudy material with a shape not different from the initial one [8]. Unwittingly, he thus obtained a material called glass-ceramic, in which the glass is a matrix for the crystalline precipitates formed in a controlled process. Referring again to the topic of definitions, in this case, it is worth mentioning the work of Deubener et al. [9], which proposes an updated definition of glass–ceramics: "*Glass-ceramics are inorganic, non-metallic materials prepared by controlled crystallization of glasses via different processing methods. They contain at least one type of functional crystalline phase and a residual glass. The volume fraction crystallized may vary from ppm to almost 100%*". The standard procedure for the production of glass-ceramics consists of at least two stages, the first of which consists of the synthesis and shaping of the glass, typical for a given composition (additionally containing a nucleating agent), which is then heated in the carefully controlled manner at a temperature above T_g. Among the classical methods of preparation, a single-stage and two-stage process are distinguished [10]. In the case of the first of the mentioned, one annealing temperature is used, at which nucleation and crystal growth occur simultaneously. Due to the simple form, there is limited control over the form of the precipitated phase, and it is also necessary for the processed material to show a strong overlap of the nucleation and growth rate curves as a function of temperature. The two-step process separates the nucleation and growth factors, thus providing greater control over the density and size of the crystals. It begins with annealing at a temperature corresponding to the highest nucleation rate (slightly higher than T_g), followed by a second annealing at a higher temperature determined for the maximum growth rate of the crystalline phase. A critical factor determining the controlled crystallization is the internal, homogeneous nucleation of the introduced agent, which then constitutes the heterogeneous center for the other crystalline phase, thus ensuring its simultaneous growth in the entire volume of the material [11]. The properties of glass-ceramics can be considered as directly dependent on the constituent factors, which are the glass matrix and the crystalline phase, but also on the composition and microstructure, the type of which can significantly affect the properties of individual phases [12].

With technological progress, a branch of materials emerged naturally, named for the size of precipitated crystallites <100 nm nano-glass-ceramics. Apart from the unique thermo-mechanical properties and durability one of the most often emphasized features of these materials, especially in the field of optical applications, is their transparency. It is obtained by controlling the growth of nanocrystals so that their size does not surpass 30 nm, which, in accordance with Hopper's turbidity model [13], ensures good transparency of glass-ceramics while taking phase differences of up to 0.3 refractive index into account [14].

1.2. Phosphate glasses

Of the five major glass families, one of the (seemingly) non-obvious compounds for the manufacture of optical glasses is the P_2O_5. In this field, phosphate glasses offer unique properties, such as low phonon energy, high transparency to UV light, and high solubility of rare earth ions [15] but their choice is not obvious due to poor chemical durability. Due to their above-average characteristics, phosphate glasses could be a direct technological competitor to silicate glasses, if not for the water corrosion occurring in them. Understanding and counteracting the processes taking place is therefore crucial for the realization of practical applications of this material. Considering the loss of weight over time for metaphosphate composition, dissolution which proceeds uniformly can be described in two stages, the initial stage where water diffuses through the glass surface causing hydration of polyphosphate chains, and the subsequent constant loss of mass characterized by the linear relationship as reported by Bunker et. al [16]. Therefore, the reaction mechanism attributed to the above process, such as the congruent dissolution of the glass network or disparate leaching of alkali ions from the glass as a result of ion exchange reactions with hydrogen-containing species (H^+, OH^-) [17] must be limited to allow the widespread use of phosphate glass.

Improvement of chemical durability can be achieved by nitridation [18] where substitution of oxygen by di- and tri-coordinated nitrogen causes the increase of crosslinking between mixed $P(O, N)_4$ tetrahedra [19]. A different approach is to modify the composition to incorporate cations exhibiting strong covalent bonding character or characterized by high valence into the glass structure. This convention was followed by the work of Reis et al. [20], which demonstrated a significant improvement in chemical resistance of $(40 – x)ZnO - xFe_2O_3 – 60P_2O_5$ glasses with increasing Fe_2O_3 content – Fe^{3+} cations replace phosphorus in P-O-P bonds, creating more stable Fe-O-P bonds. Another example is $ZnO – P_2O_5$ double glasses containing 50 – 70 mol% ZnO proposed by Takebe et al. [21]. Based on solubility measurements, an increased resistance of glass samples containing more than 65 mol% ZnO was noted. The effect of enhancing chemical resistance in phosphate glasses may also be obtained due to the addition of Nb_2O_5. The inhibition of the P-O-P bond hydrolysis is caused by the presence of oxygen octahedra associated with the Nb^{5+} cation, which attach to the phosphate skeleton, creating stronger Nb-O-P bonds, as suggested by Teixeira et al. [22]. As a result, they observed a significant increase in the resistance of glasses to water corrosion with the increasing share of niobium oxide in the studied glasses. The presented solutions provide amorphous materials based on P_2O_5 with sufficient strength, and what is worth emphasizing, they do not constitute difficult compromises and in many cases also have a positive effect on other properties.

The description of the internal structure of phosphate glasses can begin with the case of the glassy P_2O_5. The basic unit of the amorphous oxide structure is PO_4 tetrahedra spatially coordinated with each other through P-O-P bonds. Due to the pentavalent nature of the phosphorus ion, the presence of a double bond with one of the oxygen atoms (terminal oxygen O_T) is required to ensure the neutrality of the individual. The figure below (Figure 4) shows a diagram of the probable connection of four PO_4 units in the glass structure.

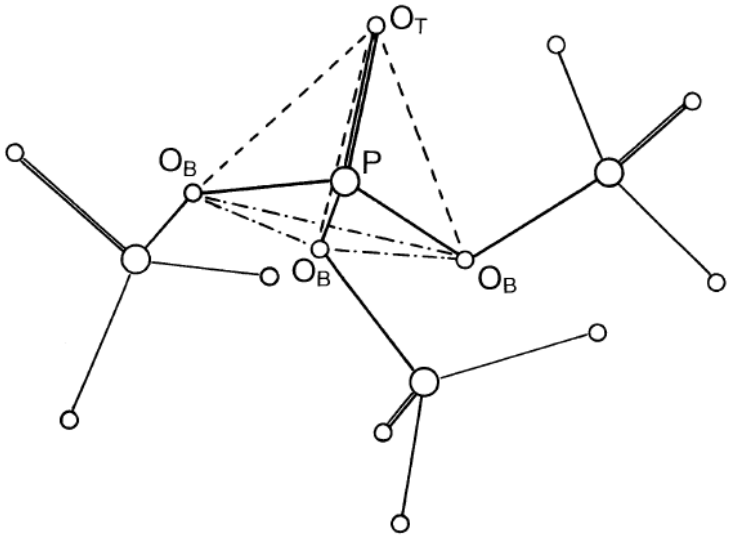

Fig. 4 Schematic representation of a fragment of glassy P_2O_5, where O_T denotes the double-bonded terminal oxygen atom, while O_B denotes the bridging oxygen atom [23]

The bond lengths in the PO_4 tetrahedron forming the amorphous solid were determined based on neutron diffraction [23] and X-ray [24]. As a result, it was found that the P–O_B bond has a length (bridging atom) of ~1.58 Å, P-O_T ~1.43 Å and the average distance between P atoms in the tetrahedra connected by vertices is ~2.94 Å. The P-O_T double bond is much shorter due to its π-bonding character, which was proved by Uchino and Ogata [25] based on ab initio calculations. Due to the presence of terminal oxygen in glassy P_2O_5, the structural units only connect to 3 vertices, which leads to lower rigidity than for example silicate glass structure (4 vertices connected) as a result of which these materials are characterized by a very low glass transition temperature. It is presumed that P_2O_5 layers of oxygen polyhedra between which the Van der Waals interaction is present [17].

When interpreting the structure of phosphate glasses, the Q_n nomenclature, originally developed for the description of silicate glasses by Lippmaa et al. [26], is often used. It takes into account the number of bridging oxygen n in the PO_4 tetrahedron, which is schematically shown in Figure 5.

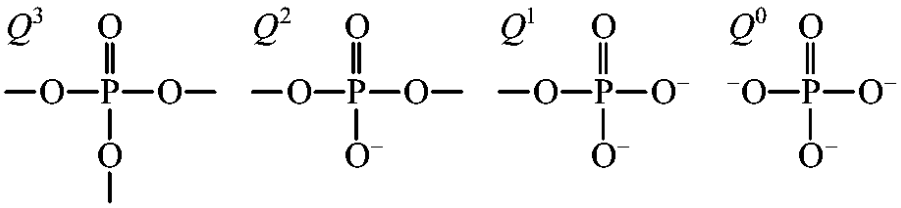

Fig. 5 Schematic representation of the basic structural units of phosphate glasses in the Q_n notation [15]

In simple binary phosphate glasses, the evolution of the groups presented above takes place as follows - modifying oxide is introduced into the P_2O_5 glass network, which results in breaking the P-O-P bonds, resulting in the formation of non-bridging oxygen connected with the modifier cation. Increasing the modifier content leads to a gradual depolymerization of the structure of the glass network. Achieving the metaphosphate composition is equated with the moment when only Q_2 units in the form of chains and rings remain in the glass. Then, with a still-growing share of the modifier, the units depolymerize to Q_1 until the appearance of orthophosphate groups Q_0. The latter ones show a high tendency to crystallize, thus defining the limit of glass formation in the presented system. Following the work of Van Wazer [27, 28], it can be stated that depending on the composition and thus the O/P ratio, the internal structure of simple phosphate glasses can be defined by a whole range of structures: starting from a three-dimensional network of Q_3 tetrahedra in glassy P_2O_5 (O/ P = 2.5) and a mixture of tetrahedra and linear structures formed by depolymerization in the ultraphosphate glasses (2.5 < O/P < 3), through the aforementioned long quasi-polymer structures in metaphosphate glasses (O/P = 3). Subsequently, in the compositions, in which ratio 3 < O/P < 3.5 the structure of short Q_2 chains was observed, which are terminated with Q_1 units, for O/P = 3.5 mainly dimers of two connected Q_1 units are present, which constitute pyrophosphate glass, finally the occurrence of orthophosphate Q_0 units is described for glasses with an O/P ratio of > 3.5.

The above criteria, despite the obvious presence of the modifier, do not specify what mutual structural role its cations have in the glass network, because apart from causing network depolymerization, these ions also become its integral part. It was therefore extremely important to develop a theory unifying previous studies and observations. In 1995, Hoppe proposed a structural model of phosphate glasses that was extremely important for understanding the essence of amorphous solids based on P_2O_5 [29]. Considering the scope of ultraphosphate glasses, he proposed that all non-bonding oxygens (along with double-bonded oxygen) tend to coordinate modifier cations (M). The proposed coordination leads to the stabilization of the glass network through re-polymerization occurring independently of the mechanism of P-O-P bond breaking. This phenomenon takes place through the formation of M-O-P bonds that guarantee

that PO_4 units are connected with phosphorus or modifier atoms. The evolution of the glass structure was described in the model as dependent on the available amount of O_T per number of modifier cations, which will be characterized by a certain coordination number N_M. Depending on the majority ratio between terminal oxygen per modifier ion (M_T) and the coordination number, Hoppe distinguished two regions: $M_T > N_M$ – there is a sufficient amount of O_T per each modifier cation, they form isolated coordination polyhedra; $M_T < N_M$ – due to the insufficient number of O_T, the cations must share available oxygen atoms, the resulting coordination polyhedra have common edges and bridge neighboring Q_2 units. Based on the above model, it was possible to explain the behavior of the packing density and coordination numbers describing M-O. In the case of metaphosphate and polyphosphate glasses, a detailed description of the structure and properties is presented in the work by Brow [30].

1.3. Luminescent glasses and glass–ceramics doped with rare earth ions

It is difficult to imagine the current world without electricity, but one of the most severe consequences would certainly be the lack of artificial lighting, with which we are surrounded by various lamps and screens - this vision, although bordering on sci-fi, allows us to realize the constantly growing demand for solid-state lighting (SSL). The observed increase in the average maximum efficacy of commercial LEDs (currently approx. 120 lm/W, target forecast approx. 255 lm/W) and their decreasing cost of an LED to the displacement of conventional light sources from the market, which may lead up to a 4% decrease in lighting electricity consumption by 2030 [31,32]. Taking into account the emerging economic and ecological issues, the improvement of the existing and the creation of new SSLs is a promising direction of research, which gives a real possibility of introducing solutions to an actively developing market.

SSLs in the form of white LEDs are most often implemented by integrating monochromatic diodes containing primary colors or by using a phosphor which, when illuminated with an appropriate wavelength in the UV range, converts the absorbed radiation and emits white light [33]. Despite the constant development, and thus the increasing efficiency and lifetime of the systems obtained, the above technological solutions face some limitations. Namely, the former is characterized by a troublesome structure that requires different driving currents for individual component diodes, which, as a result of the degradation and instability of driving currents, may lead to an unstable color temperature [34-36]. The latter are marked by lower efficiency which is an inevitable consequence of energy losses in the down-conversion process [34]. Moreover, in these devices, material limitations are leading to the necessity to choose between the efficiency and the high color rendering [37], and multifaceted degradation is observed [38-40]. In particular, phosphor failures consequent on high-temperature stress exposure and related thermal quenching effects are extremely important to overcome to further improve LED reliability, whereby thermal stability enhancement of phosphors has gained a lot of attention in recent years [41-44].

Using the unique properties of glasses, such as chemical resistance unattainable for other materials combined with special optical and thermal characteristics, it was possible to create an alternative to standard LEDs by synthesizing a bulk phosphor through doping the glass matrix with rare earth ions (RE). These elements, due to the screening of the incompletely filled 4f shell from the environment by the externally filled $5s^2$ and $5p^6$ orbitals, are characterized by a small influence of the host material on optical transitions occurring inside the $4f^n$ configuration. At the same time, the observed sharp spectral lines of rare earth ions associated with electric dipole transitions in the 4f shell contradict the Laporte's selection rule, according to which they

are forbidden for an isolated atom. The explanation of the intensity of the mentioned electronic transitions was independently proposed by G. Ofelt [45] and B. Judd [46] in 1962. For an atom in a non-centrosymmetric ligand perturbation field, it is possible to mix wave functions of opposite parity from higher shells into 4f wave functions – in this way the selection rule is relaxed and the probability of the transition is increased. Apart from the RE ion constituting the active center, the ion environment is therefore extremely important, and one should consider what can be expected from such a system if the environment is an amorphous solid. Understanding the relationships between the characteristics of luminescent glasses doped with RE ions and their structure is certainly necessary for the optimal synthesis of luminophores in this technology. Attempts to describe the above issue were undertaken by Wang et al. [47] who proposed the application of crystal chemistry principles to formulate a model of the local structure of rare earth ions in glasses. The starting point of the work was the adoption of the modified random network (MRN) model developed by Greaves [48], which is a modernized version of continuous random network CRN. The CRN model from the 1930s was confronted with the results of research on spectroscopic techniques (especially EXAFS) and diffraction techniques that were not available at that time. In the face of inaccuracies, it was "replaced" with the MRN model, in which the following observations were postulated: a) the immediate surroundings of the modifier cations are better defined, and their coordination number and bond lengths remain little variable with concentration; b) the glass network consists of interlacing sub-networks that create regions rich in matrix or modifier atoms (percolation channels appear), the occurrence of which is not homogeneous. This short digression allowed us to present the initial system used to determine the local surroundings of RE ions, where Wang et al., due to the fact that modifier cations in oxide glasses are most often ionically bonded, applied the rules of crystal chemistry for ionic structures. As a result, the following model guidelines were proposed: a) the coordination number of the rare earth cation depends on the mutual ratio of the ionic radii of the RE cation and ligands (most often the oxygen anion), where for the coefficient value of 0.732 a transition from six-coordinated to states described by higher coordination numbers is observed; b) the scatter of the distances of ligands to the central ion decreases with the progressive depolymerization of the glass network and the decreasing radius of the RE ion; c) the presence of additional modifier ions improves the dispersion of RE cations, preventing the formation of active ion clusters, in which the chance for luminescence quenching would be increased. The presented model allows for the explanation and prediction of the spectral properties of rare earth ions in oxide and fluoride glasses, starting from the local structure through the fluorescence decay characteristics to concentration quenching.

Recently, Herrmann et al. [49] investigated the relationship between molecular structure and optical properties of aluminosilicate glasses containing variable addition of MgO/BaO modifiers, doped with Er^{3+}, combining spectroscopic results with analysis in the Judd–Ofelt theory and molecular dynamics simulations. It was observed that with the increasing content of BaO, which guarantees lower field strength, the overall coordination number of the RE cation associated with oxygen decreases, but the probability of higher coordination of these ions by non-bridging oxygens increases, which results in the observed splitting of absorption peaks. In the above work, it was suggested that modifier ions with high field strength compete with RE ions for positions in the structure that guarantee high coordination of non-bridging oxygens. Additionally, the authors observed that lattice modifiers with a large ionic radius and low field strength reduce the symmetry of the position occupied by Er^{3+} ions, which may affect the intensity of hypersensitive transitions. The conducted studies emphasize the complexity of the problem of the influence of the glass network on the optical properties of doped RE ions, in particular, the number of factors influencing the immediate surroundings of the active center may be a challenge and at the same time, it shows how many changes in the luminescence characteristics can be introduced by appropriate selection of the glass composition.

Moving from the subject of theory and observed optical relationships to their practical implementations, it is worth mentioning at the outset the concept of obtaining white light in the case of glasses doped with rare earth ions. The first glass capable of "generating" white light was presented by Zhang et al. [50]. In the conducted experiment, they used a borate matrix containing mainly additives of alkali metal and alkaline earth metal oxide modifiers, to which Ce^{3+}, Tb^{3+}, and Mn^{2+} ions were implemented. The mentioned glasses were produced by mixing the appropriate amounts of substrates and melting at a controlled cooling rate, which is a simple and therefore cheap synthesis method that guarantees to obtain a complete luminescent material with all the advantages of the glassy matrix used - this is the first of the main advantages of using this technology. To obtain white light, the selection of active centers was carried out in such a way that, apart from compatibility with the matrix, their emission wavelengths covered the region of blue light – Ce^{3+}, green light – Tb^{3+}, and red – Mn^{2+}, respectively, thus constituting a complete set of primary colors. In the case of this system, Ce^{3+} cations, apart from emitting blue light, act as a sensitizer for the remaining two active centers. Moreover, due to the dependence of its emission band position on the content of modifiers, it is possible to adjust the optimal overlap with the excitation bands of Tb^{3+} and Mn^{2+}. As a result, the authors of the work, by simultaneously exciting three active centers embedded in the borate matrix with UV light with a wavelength of λ_{ex} = 365 nm, obtained white light emission. Another feature of the presented

solution is included in Figure 6, which presents the dependence of the obtained emission color on the composition of the glasses on the CIE chromaticity diagram.

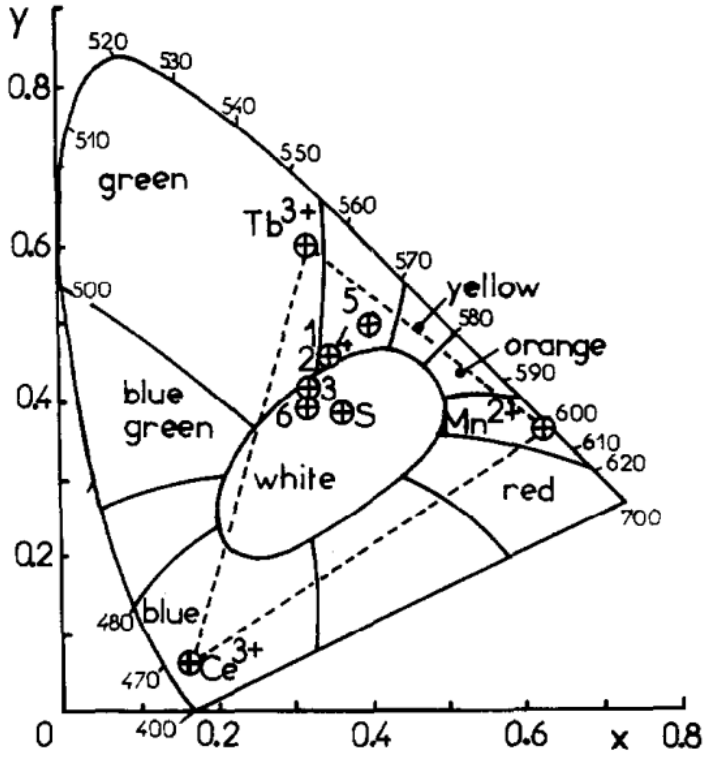

Fig. 6 The simultaneous emission shown in the CIE chromacity diagram for the excitation wavelength λ_{ex} = 254 nm [50]. The diagram shows the dependence of chromacity on the composition of the glasses using points. The composition closest to the center of the white range marked (6) was as follows: $60B_2O_3 – 21.5Li_2O – 10BaO – 2Al_2O_3 – 0.5\ As_2O_3 – 3La_2O_3 – 1Ce_2O_3 – 1Tb_2O_3 – 1MnO$

This example highlights another advantage of luminescent glasses, which is the direct control of luminescent properties by modifying their composition. Another unique feature is a certain freedom in the selection of specific ions due to the existence of many combinations of active centers (mainly double and triple dopant systems), which, as a result of simultaneous emission, produce white light [51]. It is worth mentioning that the activator contents used are usually small, in the order of several percent (in the above example 1% of each compound), which allows for reducing the cost and environmental impact of this solution.

The issue of emission tunability was raised in the work of Liu et al. [52], where a multicomponent luminescent glass based on a borosilicate matrix doped with a system of three rare earth ions: Eu^{3+} (red), Eu^{2+} (blue) and Tb^{3+} (green) was studied. The control of the final emission of the material was carried out at the synthesis stage by changing the composition of the atmosphere used during the melting process. Due to the need to obtain Eu^{2+} cations, a reducing H_2/N_2 mixture with a variable ratio of component gases was used. The authors suggested that under strongly reducing conditions, the larger amount of Eu^{2+} formed (at the

expense of Eu^{3+}) provides a larger share of blue light and at the same time allows for a more efficient energy transfer to Tb^{3+} ions, thus enabling the control of the simultaneous emission of the luminescent glass. Another approach to the mentioned issue was described by Gou et al. [53], who used a strontium-borate matrix to implement active centers in the form of Tb^{3+} and Eu^{3+} ions (the content of Eu^{3+} ions was a variable of 0–10%). With the increase of the Eu_2O_3 content in the glass, an intensification of the energy transfer from Tb^{3+} ions to Eu^{3+} was observed, the noticeable effect of which was a gradual change of emission from yellowish green to yellowish white at excitation λ_{ex} = 365 nm. It is worth noting that the type of environment provided by the matrix for the active centers is also extremely important. In the cited examples, despite the presence of one different dopant, similar white light emissions were obtained, the slight difference being its obtained color temperature. The use of a different pair of rare earths, namely Pr^{3+} and Dy^{3+} in the conducted experiment was decided in [54]. For the studied series of borate-tellurium glasses at a constant Dy_2O_3 content (0.5 mol%), the Pr_6O_{11} content was changed in the range of 0 – 1 mol%. Depending on the excitation wavelength used, two cases were found: a) when λ_{ex} = 388 nm, energy transfer from Dy^{3+} ions to Pr^{3+} occurs, the efficiency of which increases with the increasing Pr_6O_{11} content, as a result of which white light emission is observed; b) when λ_{ex} = 437 nm, energy transfer from Pr^{3+} to Dy^{3+} is taking place, as a result of which for the same samples it is possible to obtain orange light emission, which changes into white with the increasing Pr^{3+} ion content.

In the case of optical phosphate glasses, their usefulness as luminescent matrices can be indirectly evidenced by the words of Doris Ehrt contained in the article [55] summarizing her over 30 years of work with these materials: "*Phosphate and fluoride phosphate glasses have been doped with nearly all rare earth ions, and the static and time-resolved photoluminescence have been investigated as a function of glass composition and doping concentration*." This quote expresses in a non-literal way that phosphate glasses easily combine with rare earth ions, and the materials obtained in this way exhibit observable luminescence. The above statement is confirmed by numerous works published in recent years. Linganna et al. [56] proposed a lead phosphate glass singly doped with Dy^{3+} ions. They used a characteristic feature of the rare earth cation, which exhibits two intense emission lines - blue (486 nm) and yellow (576 nm), of which the latter transition is hypersensitive, and therefore strongly depends on the host glass environment. By selecting the matrix composition, it is possible to control the blue-to-yellow intensity ratio (Y/B), which for pure phosphate is about 2 [55]. With the increase in the Dy_2O_3 content (added at the expense of PbO), the Y/B gradually increased to a maximum of 4.5 for 1 mol% of the dopant, and then drastically decreased to 3.3 for the sample containing 2 mol%, as a result of which the achieved color change was negligible. At the same time, for concentrations

greater than 0.5 mol%, luminescence lifetime quenching caused by dipole-dipole interaction between Dy^{3+} ions or cross-relaxation was observed. A similar concept using only the Dy^{3+} ion dopant was implemented by Vidhi et al. [57] in the form of a multicomponent aluminophosphate glass containing a variable share of ZnO/Dy_2O_3. Based on the photoluminescence results (λ_{ex} = 350 nm), it was suggested that due to the significantly higher intensity of the $^4F_{9/2} \rightarrow {}^6H_{13/2}$ transition corresponding to the yellow emission (electric-dipole) compared to the intensity of the $^4F_{9/2} \rightarrow {}^6H_{15/2}$ transition characterized by blue emission (magnetic-dipole), the dopant ions occupy sites of lower symmetry having an inversion center. The determined Y/B coefficient decreased with the increasing Dy_2O_3 share to the level of 1.94 at 1.5 mol%, which in the case of this glass guaranteed coordinates on the chromaticity diagram corresponding to cold white light. The extension of the system containing the Dy^{3+} dopant with Tm^{3+} ions was considered in the work of Chen et al. [58], where a phosphate glass containing SrO, ZnO, and TiO_2 additives was selected as the matrix. The authors observed that both the excitation wavelength (352 – 360 nm) and the change of the dopant content, in particular Dy_2O_3 at a fixed Tm_2O_3 content (0.6 mol%), provide significant tuning of the optical properties in the white light range. The observed changes were attributed to the energy transfer via resonant transfer modes between Tm^{3+} and Dy^{3+} ions, the efficiency of which, calculated based on lifetimes, increases with the increasing Dy_2O_3 content. At the same time, for samples in which the Tm_2O_3 content was variable (Dy_2O_3 constant – 0.8 mol%), it was concluded that energy transfer occurred between Dy^{3+} and Tm^{3+}. Due to the mutual energy transfer occurring in both cases, the increase in the intensity of transitions characteristic for the acceptor will increase at the expense of the intensity of donor transitions, enabling multi-plane control of luminescence.

An equally widely used rare earth element in phosphate luminescent glasses is Eu, which, depending on the oxidation state, can be characterized by different luminescent properties. In the case of Eu^{2+}, this ion shows 5d → 4f emission that can change in the UV to yellow range depending on the covalency and crystal field strength of the matrix, while Eu^{3+} is characterized by a well-defined emission in the red range and a $^5D_0 \rightarrow {}^7F_2$ transition, which is a hypersensitive forced electric-dipole transition that can serve as a probe of the ion's immediate surroundings [59]. In the work of Jha et al. [60] the emission properties of zinc-phosphate glasses doped with Eu^{3+} ions were investigated, changing the type of modifying oxide RO (where R = Mg, Ca, Sr, and Ba) in the composition. As a result of the conducted measurements, it was found that the highest quantum efficiency was achieved for compositions containing BaO, for which the Eu_2O_3 content (3 – 9 mol%) was subsequently optimized. With the increasing dopant content, an increase in the emission intensity was observed, especially for samples containing 7 and 9 mol% Eu_2O_3. For the two glasses mentioned, the ratio of the intensity of the $^5D_0 \rightarrow {}^7F_2$ do $^5D_0 \rightarrow {}^7F_1$

transitions also changed drastically, the low value of which was identified with the incorporation of ions into an environment with higher symmetry. The clear change was caused by partial precipitation of the crystalline phase at the synthesis stage, as a result of which the emission color shifted from red to orange for samples containing 7 and 9 mol% Eu_2O_3. The described glasses turned out to be an optimal environment for active centers and can therefore be a starting point for further modification in terms of white light emission. One of the available possibilities is the one presented by Francisco-Rodrigez et al. [61] concept, in which lithium-aluminum-zinc phosphate glasses were activated with Tb^{3+} and Eu^{3+}. Due to the simultaneous doping with both rare earth ions (1 mol% each), light emission was obtained, which can be tuned from reddish-orange through warm white to neutral white, using different excitation wavelengths, respectively 318, 359, and 340 nm. It is important that due to the arrangement of energy levels in the Eu^{3+} ion, direct excitation using λ_{ex} = 340 nm is not possible. Based on the measurements made, it was observed that energy transfer occurs between Tb^{3+} and Eu^{3+} ions, the most probable mechanism of which is electric dipole-dipole interaction. A comparison of two binary dopant systems similar to those described above was made by Górny et al. [62] who synthesized lead-phosphate glasses containing Tb^{3+}/Eu^{3+} and Tb^{3+}/Sm^{3+} ions. While maintaining a constant Tb_2O_3 content of 0.5 mol%, the share of other dopants was changed in the range of 0.5 – 1.5 mol%. In the case of luminescence (λ_{ex} = 377 nm) of glasses containing Eu_2O_3, the increased dopant content led to an increase in the energy transfer efficiency ($Tb^{3+} \rightarrow Eu^{3+}$) from 52% to 71%. At the same time, in the case of the applied matrix, the exceptionally efficient energy transfer caused the CIE chromatic coordinates to be strongly red-shifted already at the lowest acceptor content. The same effect was observed for doubly doped samples containing samarium. Additionally, based on luminescence measurements, the authors observed that the increased dopant content caused a decrease in the intensity of all observed transitions at the excitation wavelength λ_{ex} = 378 nm.

The idea of luminescent glasses doped with RE ions seems to be without flaws at first glance. Due to its simplicity and the number of modification possibilities, this concept can seemingly be compared to an imaginary kitchen, in which, regardless of the ingredients used, you always get a perfect dish that oddly does not taste good but shines. Unfortunately, in reality, these materials, despite their promising properties, are characterized by insufficient efficiency to replace other SSL synthesis technologies. The method that allows one to maintain all the advantages of luminescent glasses and at the same time exceed their emission limits is the controlled production of a crystalline phase in the glass volume. As a result, one get luminescent glass-ceramics (GC), which exhibit improved active optical and mechanical properties and, with appropriate control of crystallite growth - high transparency. The reason for the occurrence of

the first of the mentioned features can be described in two ways, where the first contribution is the occurrence of self-segregation of dopant atoms in the formed crystallites [63,64], and the second one, directly dependent on the first one, is the environment of RE ions with higher symmetry and lower phonon energy provided by crystalline precipitates [65]. The above-described phenomenon of selective incorporation of dopants into crystallites is particularly pronounced in the case of fluoride crystals and is explained by the strong affinity of fluoride anions to lanthanides [66]. This conclusion designates the set of fluorine compounds as one of the most frequently used crystallization agents in RE-doped glasses. One of the first successful realizations of an emitting material for infrared up-conversion based on the concept of glass crystallization was presented by Auzel et al. in 1975 [64]. In this work, many compositions melted based on the scheme: glass-forming oxide + PbF_2 + RE oxides were investigated. Two compositions of GeO_2 – PbF_2 – Yb_2O_3 – Er_2O_3/ Tm_2O_3 were distinguished, which were optimized for up-conversion efficiency. Due to the presence of microcrystalline precipitates rich in rare earth ions, these materials were characterized by an efficiency almost twice as high as the commercial crystalline luminophore LaF_3:Yb:Er. However, due to the uncontrolled crystallization process, the above-described glass–ceramics were not transparent. A certain breakthrough in the field of materials with similar purposes was the transparent oxyfluoride glass–ceramics presented by Wang and Ohwaki, obtained in a simple annealing process at 470 °C. The size of the obtained $Pb_xCd_{1-x}F_2$: (Er^{3+}, Yb^{3+}) precipitates was determined based on X-ray diffraction measurements and was ~20 nm. As a result, for the studied glass–ceramics, the observed emission intensity increased almost 100 times compared to the unannealed sample.

The harmfulness of lead compounds and the rationalization of solutions by reducing costs have directed the attention of the scientific community towards low-toxic alkaline earth fluorides. The work of Wang et al. [67] is in line with this trend and describes the characterization of silicate glass-ceramics (heat treatment 2h, 660 °C) with the initial composition of $50SiO_2$ – $10Al_2O_3$ – $20ZnF_2$ – $20SrF_2$: Eu^{3+}. Based on the measurements carried out, homogeneous precipitation of SrF_2 crystallites with an average size of 20 nm was found in the matrix volume. The results of energy dispersive spectroscopy confirmed the predominant incorporation of Eu^{3+} ions into nanocrystals, the effect of which was observed in the form of almost 9-fold luminescence enhancement compared to as-prepared glass. BaF_2 was used in the synthesis of fluorosilicate glass-ceramics doped with 3 mol% ErF_3 by Qiao et al. [68]. Based on the results of differential thermal analysis, characteristic temperatures of the glasses were determined, which provided a reference point for the selection of the annealing temperature T_{HT} = 650 °C. This process was carried out four times in the range of 1 – 64 h in order to determine the effect of annealing time on the intensity of the up-conversion luminescence of Er^{3+} ions for the excitation

wavelength λ_{ex} = 980 nm. It was suggested that with increasing annealing time, the amount of BaF_2 nanocrystallites increases, which in turn causes an increase in the measured luminescence intensity. It is worth emphasizing that due to the high energy of the matrix phonons and the high sensitivity of the up-conversion luminescence of Er^{3+} ion in unannealed glass, practically no emission was observed.

An interesting example of the production of glass–ceramics based on $49SiO_2 – 20Al_2O_3 – 30CaF_2 – 1EuF_2$ glass was described by Secu et al. [69]. In order to obtain the crystalline phase, unusual annealing parameters were used, T_{HT} = 760 °C and exceptionally short times: 2, 8, 15 and 25 minutes. As a result, a milky color sample was obtained for the 15-minute process (cloudy in the case of 25 minutes), in which a cubic nanocrystalline phase of CaF_2 was identified based on X-ray diffraction and transmission electron microscope images. Additional two reflections at 2θ = 31.82° and 26.6° were identified as the effect of substitution of Ca^{2+} ions in the crystal lattice by Eu^{3+} ions formed during synthesis in an oxidizing atmosphere and Eu^{2+} ions, respectively. The emission spectra measured at the excitation wavelength λ_{ex} = 315 nm showed a broad emission of Eu^{2+} ions centered at 425 nm and a weak emission in the red region characteristic of the Eu^{3+} dopant. With the formation of the crystalline phase in the glass, an increase in the intensity of blue light emission and an increasing Stark splitting of the $^5D_0 \rightarrow {}^7F_2$ transition of the Eu^{3+} ion were observed, interpreted by the authors as the effect of changing its environment to non-centrosymmetric CaF_2 nanocrystals. In the matter of using RE-doped phosphate glasses as a base for glass-ceramics, one of the concepts studied involves obtaining phosphate precipitates from controlled crystallization of the matrix itself, such as $NaZnPO_4$ [70], $LiPO_3$/ TiP_2O_7 [71] and $BiPO_4$ [72] nanocrystals. At the same time, there are few works that would address the topic of luminescent phosphate glass-ceramics containing fluoride precipitates, in particular from the aforementioned group of alkaline earth fluorides. Considering the unique characteristics of phosphate glasses, the lack of sufficient information on the properties of such materials provides an undoubted motivation for research in this area.

1.4. Glass modifications leading to enhanced luminescence

1.4.1. SrF_2

The strontium fluoride mentioned in the previous chapter, in reference to the role played in luminescent glasses, can be classified as a crystallizing fluoride. The distinction introduced divides this group of compounds into the aforementioned crystallizing ones, which are introduced into the glassy matrix in order to obtain their nanometric precipitations in the process of controlled annealing, and non-crystallizing fluorides, which are only to modify the structure and properties of glasses. SrF_2 crystallizes in a cubic system (a = 5.784 Å) with the Fm-3m symmetry group [73]. Its crystals doped with RE ions are characterized by a low refractive index, good mechanical strength, and low hygroscopicity [74]. In addition, they show high-temperature emission stability in the range of up to 200 °C [75]. The above-mentioned advantages, together with the benefits provided by glassy matrices, already at the outset explain the motivation for research on the implementation of this crystalline phase in luminescent materials. The comparison of the influence of SrF_2 and BaF_2 (20 mol%) crystallites on the properties of silicate glass-ceramic doped with Gd^{3+} was made by Antuzevics et al. [76]. Measurements made using a transmission electron microscope showed that in the case of glass-ceramics containing SrF_2 crystallites, they are evenly dispersed in the sample volume and are characterized by a small size scatter compared to the BaF_2 phase. Additionally, based on electron paramagnetic resonance spectroscopy measurements using Gd^{3+} ions as a probe, it was found that they occupy centers of regular symmetry in SrF_2 crystallites when annealing takes place at 600 °C and additionally trigonal and tetragonal centers at higher process temperatures – accessible due to differences in charge compensation mechanisms. These findings may be crucial in systems of two dopants, in which gadolinium would act as a donor.

A different binary system of Ce^{3+}/Tb^{3+} dopants in a similar silicate matrix was proposed by Luo et al. [77]. The addition of 20 mol% SrF_2 was used as a crystallization agent, from which, as a result of a series of two-hour annealings at temperatures in the range of 570 – 590 °C, nanocrystalline precipitates were obtained with an average size increasing with temperature from 11 to 16 nm. The confirmed incorporation of RE^{3+} ions into nanocrystallites resulted in a clearly higher intensity of Tb^{3+} emission (λ_{ex} = 310 nm) than in the unannealed glass. An increase in the efficiency of energy transfer between Ce^{3+} and Tb^{3+} was proposed as an explanation for this observation, which could occur due to the shortening of the distance between ions in the very low phonon energy (~290 cm^{-1}) environment of the SrF_2 crystal lattice. Consistent conclusions were reached by Qiao et al. [78] by studying the spectroscopic properties of glasses of the composition $50SiO_2 – 10Al_2O_3 – 20ZnF_2 – 20SrF_2$ doped with Er^{3+}/Yb^{3+}. The selected rare

earth element system in the parent glass showed up-conversion luminescence at the excitation wavelength λ_{ex} = 980 nm, characterized by two main bands described as transitions $^4S_{3/2} \rightarrow {}^4I_{15/2}$ (541 nm) and $^4F_{9/2} \rightarrow {}^4I_{15/2}$ (654 nm). Despite the different excitation mechanisms, a significant increase in the emission intensity was observed for the glass–ceramic, the cause of which was found in the improved efficiency of energy transfer between dopant ions incorporated into SrF_2 nanocrystals - analogously to the previously described case. Moreover, the authors demonstrated the existence of a correlation between the annealing temperature (570 – 660 °C), average crystallite size and the emission intensity, which (taking into account the ends of the ranges) increased almost 20 times with temperature. The proposed explanation is based on the thesis that a larger crystallite size allows for the "accommodation" of a larger number of ions and thus ensures optimal emission conditions.

The justification for using SrF_2 additive (10 and 20 mol%) in Eu^{3+}-doped bismuth borate glasses was verified by Milewska et al. [79]. The annealing carried out in a wide temperature range from 450 °C to 590 °C (1 or 24 h) was correlated with X-ray diffraction measurements and on their basis, T_{HT} = 560 °C was distinguished as the optimal temperature - due to the compromise between the growth of the SrF_2 phase and the crystallization of the matrix causing the loss of transparency. The analysis of luminescence decay times and Judd–Ofelt parameters allowed the authors to conclude that some of the Eu^{3+} ions were incorporated into SrF_2 nanocrystals, which resulted in the enhancement of the observed luminescence for the sample containing 20 mol% fluoride additive. As can be seen, the versatility of SrF_2, especially in the form of nanocrystals, is expressed by its effectiveness in enhancing luminescence, which was confirmed in several different systems – differing both in the doping method and the type of matrix.

1.4.2. AlF_3 and KF

Due to the fact that the title compounds belong to the previously defined group of non-crystallizing fluorides, they will be described together in this paragraph. However, this does not mean that the effect they cause in glasses is also completely convergent, and the final result can often be strongly dependent on the content and interaction with the matrix and other components of the glasses. For this reason, the described pair of fluorides can be called "silent" modifiers, which are usually used to tune the properties of glasses. This fact causes that there are not many works, especially in the field of phosphate glasses, which would systematically describe their action. In general, the addition of AlF_3 can increase the luminescence intensity of RE ions and improve the cohesion of the glass network by creating Al-O-NFC bonds (network-forming cation) and less probable Al-F-Al cross-links, thus increasing the stability of the glasses.

On the other hand, KF can have a beneficial effect on the luminescence of rare earth dopants, providing both lower phonon energy and increased glass compactness. An unambiguous statement of the effects obtained with the addition of the above fluorides requires direct measurements in specific amorphous systems

The description of the effect of AlF_3 addition on the luminescence properties of $Eu^{3+}/Tb^{3+}/Tm^{3+}$ doped tellurium glasses was developed by Walas et al. [80]. The compositions without AlF_3 and containing 18 mol% fluoride were compared in two configurations of dopant molar ratios. The differential scanning calorimetry measurements showed that the glass containing the AlF_3 additive is characterized by a glass transition temperature 60 °C higher than the parent glass and the lack of an exothermic crystallization maximum. Based on the results of infrared spectroscopy, it was suggested that this is the effect of the formation of stronger Te-O-Al bonds, the presence of which, by reducing the mobility of atoms, leads to greater stability of the glasses containing the AlF_3 additive. The common emission of dopants was obtained using two excitation wavelengths λ_{ex} = 395 nm and 410 nm, and in both cases, a clear enhancement of luminescence was observed for the samples with AlF_3. The same dopant system was used in a series of bismuth borate glasses studied by Milewska et al. [81], in which the content of AlF_3 was varied (0–20 mol%). Despite the high content of fluoride, contrary to the previous example, no significant changes in the thermal characteristics and structure of the glasses related to its introduction were observed. However, its presence was confirmed by X-ray photoelectron spectroscopy and indirectly by photoluminescence measurements. Luminescence measurements of glasses doped singly with Eu^{3+} (as a probe due to the hypersensitive $^5D_0 \rightarrow {}^7F_2$ transition) containing 0, 10, and 20 mol% AlF_3 showed a significant increase in the band intensity for the sample containing 10 mol% of the modifier. Interestingly, the sample containing the largest share of fluoride was characterized by lower emissions than the parent glass. The proposed explanation referred to the increase in symmetry in the immediate vicinity of RE ions in the presence of a sufficiently high content of AlF_3. Finally, a tunable luminophore capable of emitting white light at excitation λ_{ex} = 355 nm was achieved, in which energy transfer between Tb^{3+} and Eu^{3+} was found (it cannot be ruled out that its efficiency increased due to the addition of fluoride). When introducing fluorides into the composition of glasses, one should be aware of the partial evaporation of fluorine, which results, among others, from the conditions of synthesis. Partially related to the issue of the role of fluorine anions in glasses, Liang et al. [82] studied the effect of the F/O ratio on the properties of silicate glasses by controlling the share of Al_2O_3 and AlF_3 in the composition. Interestingly, the luminescence measurements performed showed that the highest emission intensity was characteristic of the sample for which the F/O ratio value was in the middle of the tested range. Samples containing a higher content of AlF_3, in

a manner similar to the sample containing 20 mol% AlF_3 in the work of Milewska et al. [81], were characterized by deterioration of properties. This indirectly confirms the important role of fluorine anions in luminescent glasses and the necessity of maintaining the balance between oxygen and fluorine.

In the case of KF, one of the few works describing its effect on luminescence in glasses was published by Sarumaha et al. [83]. They compared two Eu_2O_3-doped fluorophosphate glasses, one of which contained an addition of 10 mol% KF introduced at the expense of P_2O_5. Based on the measurements carried out in glasses with KF, an enhancement of the luminescence of Eu^{3+} ions was found, which, according to the authors, was caused by providing active ions with greater asymmetry in their coordinating environment. This thesis was also confirmed by measurements of the luminescence decay time, which was longer in the case of the mentioned sample - the calculated quantum efficiency increased by almost 6%. From a different perspective, the effect of KF was presented by Takahashi et al. [84] who studied the up-conversion luminescence of Er^{3+} ions and the luminescence of Eu^{3+} in fluoride glasses based on ZrF_4. The measurements showed that among the alkali metal fluorides used (Li, Na, K, Rb, Cs), the composition containing KF was characterized by the most intense emission of Er^{3+} ions (λ_{ex} = 800 nm). The explanation proposed by the authors takes into account the measurements of the multiphonon decay rate, the value of which was the lowest for glasses with the addition of KF. The examples presented clearly show that the concept of a simple additive to glasses that does not require additional thermal treatment may be a promising (also more ecological) concept of enhancing the luminescence of glasses doped with RE ions.

1.4.3. Ag

The first mention of the use of, as stated in the title, “small silver particles” in Eu^{3+}-doped glasses comes from the work of Malta et al. from 1985 [85]. As a result of $AgNO_3$ reduction occurring during melting, metallic Ag particles were obtained and dispersed in the B_2O_3 – CaF_2 glass matrix, which showed strong absorption with a maximum located at ~314 nm. Luminescence (λ_{ex} = 314 nm) measured for these materials was characterized by an enhancement of 560% compared to glasses without silver addition. The increase in intensity was associated with the occurrence of surface plasmon resonance (SPR), which by inducing a localized electromagnetic field near the metallic particles affects the electron transition properties in RE ions. Currently, this phenomenon is extensively studied in various luminescent glass systems in terms of optimizing the conditions leading to luminescence enhancement – mainly by controlling the process of obtaining particles of the desired size.

Amjad et al. [86] studied the effect of silver nanoparticles on the luminescence of Eu^{3+} ions embedded in the zinc tellurium glass matrix. Due to the probability of luminescence quenching caused by energy transfer from RE ions to Ag nanoparticles in the case of concentration of metallic particles exceeding the concentration of the active dopant, it was decided to use constant contents of AgCl – 0.3 mol% and Er_2O_3 – 0.5 mol%. Using three different times (4, 12, and 24 h) of annealing the samples at 350 °C, metallic silver nanoparticles were obtained with average sizes increasing with increasing process time. The results of photoluminescence at excitation with a wavelength of 395 nm showed a gradual increase in emission intensity for glasses annealed for 4 and 12 h. The sample subjected to 24h of annealing was characterized by lower intensity than the glass without AgCl additive, the proposed reason was related to the quenching of luminescence caused by the transfer of energy from Eu^{3+} ions to nanoparticles, the excessive growth and agglomeration of which led to a decrease in their mutual distances. The demonstrated luminescence enhancement, according to the authors, apart from the increased local field caused by SPR, has its genesis in the reduction of phonon sidebands caused by the presence of Ag nanoparticles.

The analysis of the influence of metallic silver precipitates also in tellurite glasses containing in this case the PbO additive was undertaken by Dousti et al. [87]. The presence of Ag nanoparticles formed as a result of annealing the glasses for 9h at 340 °C (25 °C above T_g) was confirmed based on transmission electron microscope measurements – the average size was ~10 nm. The measurements of the emission of Eu^{3+} ions performed for this sample allowed to observe the enhancement of luminescence by a factor of close to 2, resulting from the presence of metallic particles dispersed in the glass. As can be seen from the two examples above, the type of additives used has little effect on the formation and properties of Ag nanoparticles, which are clearly more dependent on the type of glassy matrix. Remaining with the same RE dopant, it is worth taking a closer look at a different matrix proposed in the work of Saad et al. [88]. They used sodium phosphate glass doped with 1 mol% Eu_2O_3 and 0.5 mol% $AgNO_3$, respectively, which was subjected to annealing at 305 °C, varying its duration from 10 to 30 h. Similarly to the previously described cases, the maximum of luminescent properties was observed for the sample annealed for 20 h. This sample was characterized by the average size of Ag nanoparticles equal to 10 - 30 nm, the presence of which allowed the enhancement of the luminescence of Eu^{3+} ions by a factor of 2.3 (compared to the unannealed glass). As the reason for this observation, the authors proposed that, apart from the local field effect stimulated by SPR, the occurrence of energy transfer between Ag nanoparticles and Eu^{3+} ions. This modification presents an elegant form of minimally invasive increase of the capabilities of luminescent glasses, which can be used together with other modifications to some extent. At the same time,

due to the characteristics of this solution, it is not as universal as the concepts described in the remaining points, because not in all glasses it is possible to obtain well-defined metallic nanoparticles without unwanted crystallization or loss of transparency of the material.

Pursuing delicate balance in multicomponent amorphous materials containing Ag can also draw attention to the relationships between individual components. It is worth emphasizing, among other things, the occurrence of eutectic in the Bi_2O_3 – Ag phase system, the diagram of which is presented in Figure 7 [89].

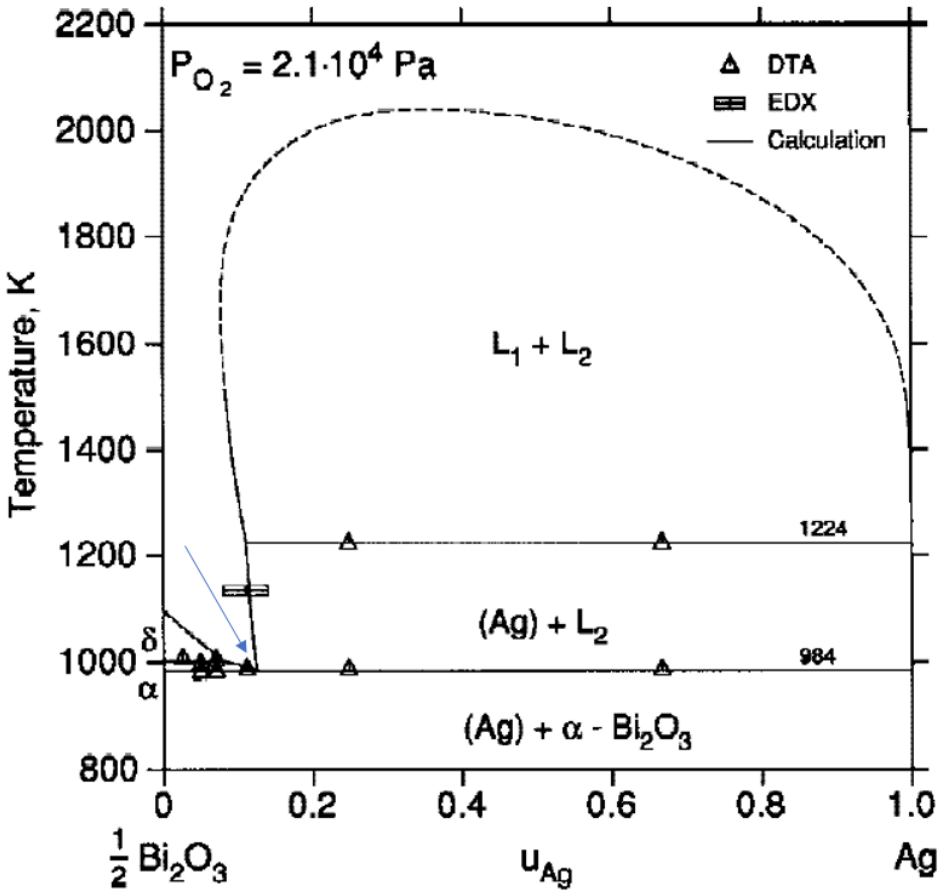

Fig. 7 Phase diagram of Ag – Bi_2O_3 [89]. The eutectic point is marked with arrow – (~12.5 mol% Ag/87.5 mol% Bi_2O_3, 710.9 °C)

The presence of this unique property of the Bi_2O_3 - Ag system can be directly used to facilitate synthesis of Ag nanoparticles in a bulk material, which was presented in the work published by Sadecka et al. [90]. Based on the composition corresponding to the eutectic point, a composite material containing nanometric Ag precipitates embedded in a crystalline Bi_2O_3 matrix was obtained. The annealing of the synthesized material at 600 °C carried out in the next stage, resulted in obtaining Ag nanoparticles, enabling observation of LSPR band. Strictly controlled process conditions in the above-described experiment led to obtaining a well-defined

nanometric Ag phase. However, transferring this issue to the example of optical glasses, also the presence of the Bi_2O_3 crystalline phase becomes crucial, as well as, as reported by Sadecka et al. [90], the possibility of the appearance of metallic Bi nanoparticles. The moment at which the phase transition would occur in the case of amorphous materials is the melting process, where during rapid cooling of the melt there is a chance for crystallization of the aforementioned phases. Therefore, due to the dynamic characteristics of the glass synthesis, it is not possible to strictly control its conditions. High process temperature and unique features of amorphous solids can lead to the occurrence of local conditions in which microscopically the Ag - Bi_2O_3 ratios will correspond to eutectic. High temperature (>1000 °C) can also result in the occurrence of Bi_2O_3 thermoreduction [91]. The metallic bismuth formed in this way creates a phase system with silver presented in Figure 8 [92], in which eutectic is also present, giving the possibility (assuming dynamic melting conditions) of obtaining the Ag crystalline phase at a much lower temperature.

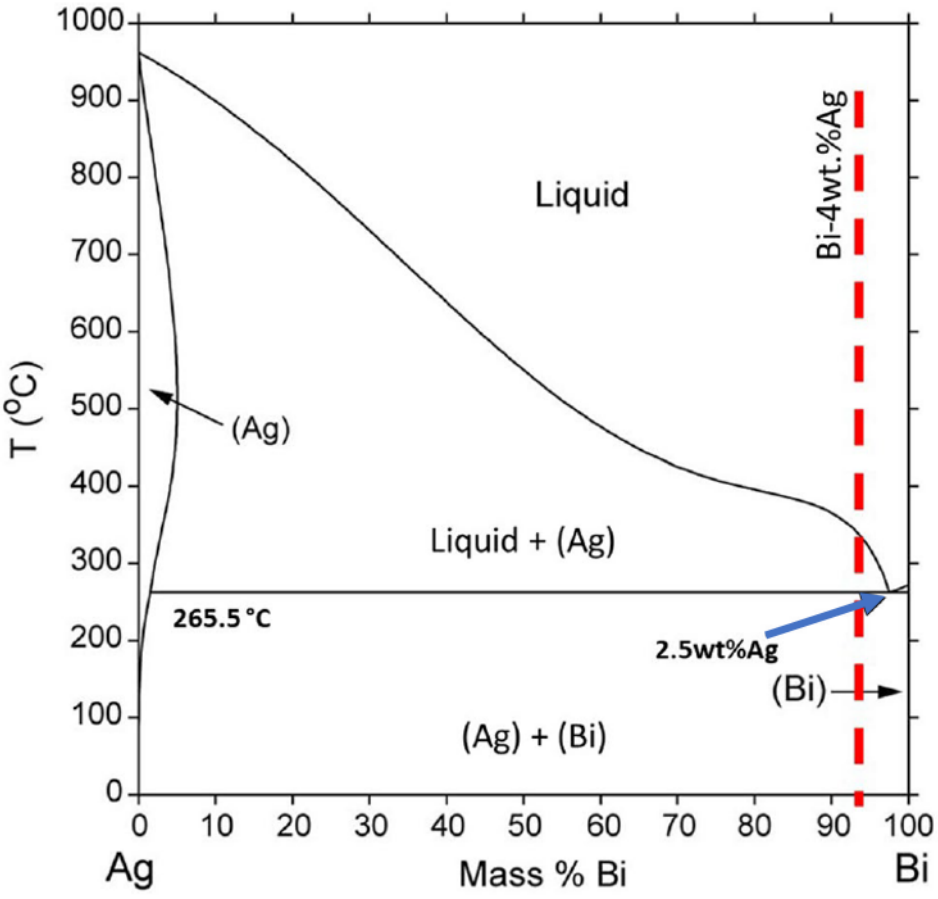

Fig. 8 Phase diagram of Ag – Bi [92]. The eutectic point is marked with arrow – (4.73 mol% Ag/95.27 mol% Bi, 265.5 °C)

In the case of glasses containing an Ag dopant, the presence of Bi_2O_3 in the composition has a dual nature. On the one hand, due to the eutectics present, it increases the probability of

obtaining Ag nanoparticles. Additionally, the specificity of the glass-forming melt allows for the occurrence of local conditions that facilitate the fulfillment of these dependencies to a greater extent. On the other hand, this system is burdened with randomness and it is much more difficult to control the effects obtained in a melt that, apart from Ag and Bi_2O_3, has additional components. The greatest challenge still remains, even in the case of successful obtaining of Ag precipitations, the simultaneous crystallization of Bi compounds, the extensiveness of which may prevent the use of optical glass, and thus negate the assumptions and sense of producing optically active Ag particles.

1.5. Motivation and objectives

The motivation for conducting research on phosphate luminescent glasses has been initially outlined in the presented literature review, and its essence is formulated as follows: *In response to the growing needs and requirements for solid-state lighting, it is necessary to provide a technological solution characterized by advantages in the fields of efficiency, resistance, versatility, and price. The concept that can meet the above requirements is the synthesis of luminescent glasses and glass-ceramics containing rare earth ion dopants. A suitable implementation of this idea due to the set of features consistent with the assumptions is a glass with the symbolic composition* $P_2O_5 – K_2O – Bi_2O_3 – Nb_2O_5$*, which, due to the used components, not only allows for the full use of the advantages of glassy* P_2O_5 *but also provides an ideal environment for rare earth ions. In addition, as a starting matrix, it offers a wide range of modification possibilities allowing for the adjustment of properties and an uncomplicated change of the material's character through the annealing process.* The implementation of the presented concept is a promising candidate for a luminophore that can be used in modern LEDs and directly determines the direction of ongoing research.

The aim of this work was therefore to develop and characterize a new stable phosphate glass matrix, modify its composition and properties, and optimize it for luminescent applications, in particular visible light emission using rare earth elements doping. The aforementioned modification of the obtained amorphous materials focused on two aspects: changes in the relative shares of individual matrix components, including the introduction of additives in the form of fluorine and silver compounds, and conducting an extensive series of annealing in order to obtain a glass-ceramic with improved optical properties. Due to the undertaking of producing a material not previously described in the literature, the above main goal was realized within the ongoing research process through emerging component goals:

- development of the synthesis parameters and compositions of homogeneous, durable optical glasses based on phosphorus oxide,

- conducting the doping process with Eu_2O_3 at the synthesis stage in order to introduce active centers capable of emitting visible light when excited with UV light into the amorphous matrix,

- development of a method and optimal parameters of the heat treatment process of glass containing a crystallizing agent in the form of SrF_2, enabling the production of glass-ceramics

with improved properties, ensuring the enhancement of the luminescence of rare earth ions embedded in the material

- introduction of KF and AlF_3 modifying compounds and determination of their influence on the properties and structure of the obtained amorphous materials, especially enhancement of light emission

- conducting composition modification by minimizing the Bi_2O_3 content and performing controlled annealing of derivative glasses containing $AgNO_3$ to obtain metallic particles in the glass volume and determine their effect on the luminescence of Eu^{3+} ions.

The scope and means of implementation of the above issues are included in Chapter 2, which describes the research methods, and Chapter 3, which covers the results.

1.6. Research hypotheses

In present doctoral dissertation the following research theses were defined:

1) For phosphate glasses of $P_2O_5 – K_2O – Bi_2O_3 – Nb_2O_5 – SrF_2$: Eu_2O_3 composition it is possible to obtain a nanocrystalline phase of SrF_2 dispersed in the glass matrix, thanks to which the luminescence of Eu^{3+} ions is enhanced; the glass-ceramics obtained in this way remain transparent.

2) The introduction of various KF and AlF_3 contents into the composition of $P_2O_5 – K_2O – Bi_2O_3 – Nb_2O_5$: Eu_2O_3 glasses allows for the modification of its properties and structure and, with the appropriate content, leads to the enhancement of the luminescence of Eu^{3+} ions.

3) It is possible to reduce the Bi_2O_3 content in $P_2O_5 – K_2O – Bi_2O_3 – Nb_2O_5$: Eu_2O_3 glasses without losing transparency and chemical durability; introducing an $AgNO_3$ dopant into compositions with a reduced Bi_2O_3 content allows obtaining Ag nanoparticles during the heat treatment process, the presence of which has a positive effect on the emission of Eu^{3+} ions.

2. Materials and methods

2.1. Synthesis

The synthesis of phosphate glasses with the nominal composition P_2O_5 – K_2O – Bi_2O_3 – Nb_2O_5 (PKBN) was carried out using the melt-quenching technique. Due to the modifications to which the PKBN parent glass was subjected, four series were distinguished containing the following additives: SrF_2 (PKF), AlF_3 (PKA), KF (PFF and PF), and $AgNO_3$ (PB). In the series containing KF, two additional sub-series were distinguished, of which PFF, similarly to the methodology used for the other fluorides (SrF_2 and AlF_3), was characterized by a proportional addition of the modifier in the range of 5 – 15 mol% while maintaining constant ratios between the basic components of the glass. This allowed for the separation of effects related to the incorporation of variable fluoride contents into the matrix structure. The addition of the modifier in the PF series was determined to be disproportionate due to the different method of using KF, in which it was introduced in a 1:1 ratio at the expense of K_2O, while the contents of the remaining glass components were close to those of the PKBN matrix. The PB series glasses are the implementation of the concept of reducing the Bi_2O_3 content from the initial 20 mol% to 0 mol%, which was carried out to increase the probability of reducing the $AgNO_3$ introduced into the glass to the form of metallic Ag. However, due to the insufficient chemical resistance demonstrated by the compositions containing less than 10 mol% Bi_2O_3, they were not subjected to doping and further studies. The listed series of materials, regardless of the content of the modifiers used, were doped with 0.5 mol% Eu_2O_3. The compositions of the studied glasses divided into series are included in Tables 1 a-d (Table 1a additionally contains the composition of the PKBN matrix).

Sample	P_2O_5	Bi_2O_3	Nb_2O_5	K_2O	SrF_2	Eu_2O_3
PKBN	50	20	10	20	-	-
PKBN 05Eu	49.75	19.9	9.95	19.9	-	0.5
PKF5	47.5	19	9.5	19	5	-
PKF10	45	18	9	18	10	-
PKF15	42.5	17	8.5	17	15	-
PKF5 05Eu	47.25	18.9	9.45	18.9	5	0.5
PKF10 05Eu	44.75	17.9	8.95	17.9	10	0.5
PKF15 05Eu	42.25	16.9	8.45	16.9	15	0.5

Table 1a. Compositions of PKBN glasses and those containing SrF_2 additives (mol%), along with their designations, which will be used in this work

Sample	P_2O_5	Bi_2O_3	Nb_2O_5	K_2O	AlF_3	Eu_2O_3
PKA5	47.5	19	9.5	19	5	-
PKA10	45	18	9	18	10	-
PKA15	42.5	17	8.5	17	15	-
PKA5 05Eu	47.25	18.9	9.45	18.9	5	0.5
PKA10 05Eu	44.75	17.9	8.95	17.9	10	0.5
PKA15 05Eu	42.25	16.9	8.45	16.9	15	0.5

Table 1b. Compositions of glasses containing AlF_3 additive (mol%) along with their designations that will be used in this work

Sample	P_2O_5	Bi_2O_3	Nb_2O_5	K_2O	KF	Eu_2O_3
PF5	50	20	10	15	5	-
PF10	50	20	10	10	10	-
PF15	50	20	10	5	15	-
PFF5	47.5	19	9.5	19	5	-
PFF10	45	18	9	18	10	-
PFF15	42.5	17	8.5	17	15	-
PF5 05Eu	49.75	19.9	9.95	14.925	4.975	0.5
PF10 05Eu	49.75	19.9	9.95	9.95	9.95	0.5
PF15 05Eu	49.75	19.9	9.95	4.975	14.925	0.5
PFF5 05Eu	47.25	18.9	9.45	18.9	5	0.5
PFF10 05Eu	44.75	17.9	8.95	17.9	10	0.5
PFF15 05Eu	42.25	16.9	8.45	16.9	15	0.5

Table 1c. Compositions of glasses containing KF additives (mol%), along with their designations, which will be used in this work. PF denotes the series with disproportionately introduced KF, and PFF denotes proportional addition

Sample	P_2O_5	Bi_2O_3	Nb_2O_5	K_2O	Ag	Eu_2O_3
PB0	62.5	0	12.5	25	-	-
PB1	61.875	1	12.375	24.75	-	-
PB5	59.375	5	11.875	23.75	-	-
PB10	56.25	10	11.25	22.5	-	-
PB15	53.125	15	10.625	21.25	-	-
PB10 05Eu	55.97	9.95	11.19	22.39	-	0.5
PB15 05Eu	52.86	14.93	10.57	21.14	-	0.5
PKA10 05Eu 05Ag	55.69	9.9	11.14	22.28	0.5	0.5
PKA10 05Eu 1Ag	55.41	9.85	11.08	22.16	1	0.5
PKA15 05Eu 1Ag	52.33	14.78	10.47	20.93	1	0.5

Table 1d. Glass compositions for which an attempt was made to reduce the Bi_2O_3 content and containing an Ag dopant (mol%), along with their designations, which will be used in this work. Compositions marked in gray were characterized by too low resistance to water corrosion

The raw reagents ($(NH_4)_2HPO_4$, $Bi_5O(OH)_9(NO_3)_4$, KNO_3, Nb_2O_5, SrF_2, KF, AlF_3, $AgNO_3$ and $EuCl_3 \cdot 6H_2O$) were weighted taking into account the contents listed in tables 1 a-d, ground finely in a mortar to obtain a homogeneous powder and placed in a porcelain crucible. In the case of glasses containing fluoride modifiers, to remove gaseous by-products that could lead to inhomogeneities in the glass, decomposition was carried out at 450 °C for 2 hours. The PB series, due to the differences in compositions, required extending the decomposition process to three stages, in which the sample was successively heated at 200, 300, and 400 °C for 1.5 h each. Then, the decomposed, preheated batches were directly transferred to a chamber furnace, where they were subjected to target melting and homogenization in air at temperatures ranging from 1000 to 1150 °C. The melting process time was optimized to ensure a sufficient degree of alloy uniformity while minimizing spontaneous evaporation of components and, as a result, was in the range of 10 - 40 min depending on the composition. Then, the contents of the crucible were poured onto a steel plate preheated to ~200 °C and immediately pressed with a second steel plate to ensure an appropriate cooling rate. As a result, transparent glass samples of approximately 1 mm thick were obtained, which were left to cool down.

Glass-ceramics were produced in a controlled crystallization process by heating in an air atmosphere the glasses whose compositions are given in Table 1a (the target PKF series containing SrF_2 as a crystallization agent and the reference PKBN matrices). Glass samples were subjected to two distinct annealing processes. In the first process, for Eu - undoped glasses, a series of 10-hour annealings every 10°C was carried out, starting from 485 °C and ending at 605 °C, which gave a total of 13 annealing. The aim of the above experiment was to determine the

effect of heat treatment on the structure of glasses and the characteristics of crystallization, including the analysis of precipitating crystalline phases. The second annealing process consisted of three stages and involved Eu-doped glasses. In the first stage, the PKBN 05Eu - PKF15 05Eu samples were heated at 525 °C, 545 °C and 585°C for 10h. Part of the materials obtained in annealing at 525 °C was reheated at 545 °C or 585 °C for 10h, which was the second stage of annealing. In the last stage, part of the glass-ceramics obtained in the second stage was used and heated again at the same temperatures for 12 hours. As a result, for each composition (0 - 15 mol% SrF_2), 3 as-prepared samples were heated single, two samples were heated doubly for 10 hours (higher temperature annealing time) at 525/545 °C and 525/585 °C, and two samples were heated triply, for a total of 22 hours at 525/545 °C and 525/585 °C. Such a complex process of thermal treatment was aimed at examining the influence of the glass crystallization process on the luminescent properties of the Eu^{3+} ions embedded in them.

For selected Eu_2O_3-doped glasses from the PFF and PKA series, separate annealing tests were carried out to check the susceptibility of atypical compositions to controlled thermal treatment. The annealing process included two series carried out at 585 °C for 8h or 10h.

Glasses with reduced Bi_2O_3 content - PB10 and PB15 containing an Ag dopant were subjected to a series of annealings, the aim of which was to determine the possibility of obtaining metallic Ag nanoparticles dispersed in the glass matrix. To determine the effect of silver content on the properties, PB10 05Eu 1Ag and PB10 05Eu 05Ag glasses (1 and 0.5 mol% Ag, respectively - Table 1d) were selected, which were annealed at 500 °C for 3, 6, and 22 h, respectively. Meanwhile, in the case of PB15 05Eu 1Ag glass, a different approach was chosen, in which the samples were annealed at two temperatures at 500 and 550 °C for 3, 6, 12, 24, and 48 h.

In the case of heat treatment carried out for glass series, a tube furnace was used. To ensure proper temperature control, glass samples were introduced into the furnace and heated to the set temperature in a simple cell made of Al_2O_3, which ensured repeatable process conditions. In particular, it was possible to precisely position the samples in the center of the heated furnace in the appropriate heating zone and additionally measure the temperature close to the sample. The scheme of the system used is shown in Figure 9.

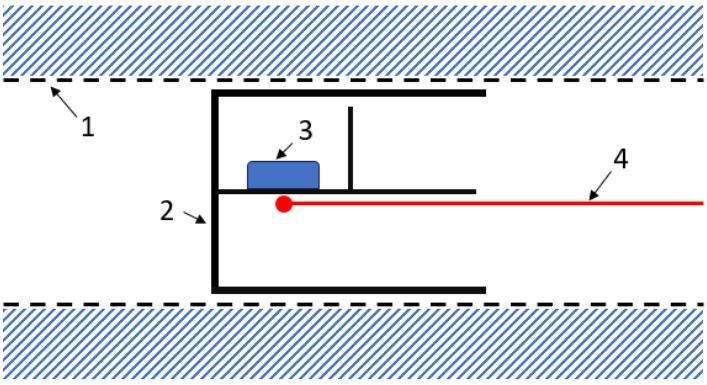

Fig. 9 Schematic diagram of the system used for glass annealing (cross-section). 1 – tube constituting the furnace chamber, 2 – sample cell, 3 – sample, 4 – external thermocouple

2.2. X-ray Powder Diffraction (XRD)

X-ray diffraction is a non-destructive method of characterizing the structure of materials, which uses the interaction of electromagnetic radiation with matter. In structural analysis, radiation with energy in the range of 5 – 60 keV [93] is most often used, which is equivalent to the wavelength range of 2.5 – 0.2 Å. These values are comparable to the interatomic distances in the crystal lattice, so they satisfy the relationship $\lambda \leq 2d$ (λ – incident wavelength; d – distance between atomic planes) and allow Bragg reflection to take place. As a result, X-ray diffraction occurs, the constructive interference of which is described by Bragg's law: $2d\sin\theta = n\lambda$, where n is a natural number called the order of reflection, and θ is the angle between the lattice plane and the incident ray.

Therefore, this technique is a basic tool for identifying unknown crystalline phases and characterizing their structure. It also allows for determining the presence of nanocrystallites in the material and determining their size based on the broadening of diffraction reflections. The relationship describing the average crystallite size D is known as the Scherrer equation:

$$D = \frac{K\lambda}{\beta_c \cos\theta} \tag{3}$$

where K is the Scherrer constant and β_c is the corrected half-width taking into account, among other things, apparatus factors.

In the case of amorphous solids, the lack of periodicity means that it is not possible to distinguish directions in the structure for which constructive or destructive interference would occur unambiguously. As a result of the measurement, a curve in the form of a broad maximum is observed, which only indicates the occurrence of a statistical preference for a specific interatomic distance and means that the atoms forming this material are quite tightly packed

[94]. At the same time, due to its characteristic form, this result can be a confirmation of the amorphous nature of the synthesized material. However, this study is crucial in the case of glass-ceramics, as it allows for the confirmation of the presence of the desired crystalline phases and the determination of the average crystallite size.

The obtained glasses and glass-ceramics were thoroughly ground and characterized by powder X-ray diffraction (XRD) on a Philips X'PERT PLUS diffractometer equipped with a Malvern PANalytical PIXcel1D detector, using Cu-Kα radiation. Measurements were performed at room temperature in the 2θ range of 10° - 90° with a 0.0131° step.

2.3. Fourier Transform Infrared Spectroscopy (FT-IR)

Fourier transform infrared spectroscopy is related to the oscillations of atoms that form molecules or sets of atoms that form functional groups in the studied material. The absorption of a quantum of infrared radiation is possible only when the electric dipole moment of the molecule changes during the oscillation - this defines the general selection rule for infrared spectroscopy. On the basis of this technique, it is possible to determine the lengths of bonds, their force constants, and the general evolution of the material structure.

The use of the Michelson interferometer in infrared spectroscopy allows for the measurement to be carried out using a wide-band of infrared radiation and thus recording the modulation of the beam intensity in time-space, and not in the frequency characteristic of the continuous wave method. The interferogram obtained in this way can be transformed using the Fourier transform into a target spectrum presenting the intensity dependence as a function of frequency. This solution is characterized by a high signal-to-noise ratio, the possibility of using a single detector without a slit, and precise calibration of the wavelength [15].

In the case of glasses, the manifestation of structure are separate molecular clusters, which are building units that maintain the short-range order. At this scale, this structure can be roughly regarded as close to a randomly distorted crystal lattice and as it turns out this distortion (compared to an ideal crystal) manifests itself in small changes in the vibrational force constant, which only leads to a moderate widening of the absorption bands in the vibrational spectrum, despite the complexity of the system [95]. Thus, infrared spectroscopy is a very useful technique in the analysis of the internal structure of glasses, including the determination of the presence and evolution of structural units characteristic of glass-forming compounds. Stoch and Środa [96] studying the structure of various oxide glasses emphasized the importance of the Mid-infrared (MIR – from ~500 to 4000 cm^{-1}) range, in which bands originate from network former atoms bound to oxygen. It was established that based on MIR spectra it is possible to track changes in structure caused by the introduction of a new component or changes in proportions in the

composition. In the case of alkaline and alkaline earth modifiers, it was also concluded that the observed band shifts indicate changes in the structure caused by depolymerization; moreover, it is possible to track changes in the nature of the bonds and the coordination number of cations.

FT-IR measurements were obtained on a Perkin-Elmer MIR/FIR spectrometer with a TGS detector using KBr/glass pellets mixed in a weight ratio of 50:1. The spectra were collected at room temperature in the range of 4000 – 400 cm^{-1} with a resolution of 2 cm^{-1} as the average of 32 scans. The infrared spectra of the glasses containing SrF_2, KF and AlF_3 addition were modeled by adjusting the minimum number of Gausians (corresponding to single absorption bands) allowing for an acceptable representation of the shape of the envelope. Considering the spectrum's complexity, the yielded sets of functions represent one of the probable combinations that meet the requirement of physically possible vibrations in the materials under investigation. The relative area of the band $R_a = A_b/A_s$ was calculated to assess changes in the share of individual bands in the spectrum (for the purposes of this work also called intensity), where A_b stands for band area, and A_s for the total area enclosed by the modeled spectrum envelope.

2.4. Thermal analysis

Thermal analysis is defined as the analysis of a change in a property of a sample, which is related to an imposed temperature alteration [97]. Although very concise, this definition captures the idea of observing thermal events occurring in a material along with the implementation of a given temperature program. In the case of glasses, the most important effect is the transition to the glass phase, which is most often observed using Differential Scanning Calorimetry (DSC) and Differential Thermal Analysis (DTA). The characteristic temperatures determined from the measurements allow to estimate the stability of the tested amorphous solids, an example may be the Saad-Poulain parameter [98], which, based on the glass transition, crystallization, and onset of the exothermic peak temperature values from the measurements, gives approximate information about the stability against crystallization of a given composition. Additionally, using the mentioned values of characteristic temperatures, it is possible to estimate the optimal temperatures of the thermal treatment in which the phase, for example nanocrystalline, of the nucleating agent introduced into the glass is obtained, and at the same time, it is possible to avoid the bulk crystallization of the glass matrix. This optimization assumes obtaining a nucleation rate much higher than the growth rate of the crystalline phase, so temperatures in the range from T_g to T_g +50°C are usually used [99]. However, due to the risk of strong matrix crystallization effects in the case of a narrower range between T_g and T_c, it is more advantageous (in terms of process control) to use temperatures slightly higher than the glass transition temperature.

2.4.1. Differential Scanning Calorimetry (DSC)

Differential Scanning Calorimetry measurement involves recording the change in the difference in the heat flow rate to a test sample and a reference sample when they are subjected to a controlled temperature program [100]. This concept is implemented in two ways in the form of heat-flux and power compensation DSC calorimeters. The heat-flux DSC calorimeter uses a precisely defined heat conduction path with a well-known thermal resistance to measure heat exchange with the environment. The directly measured value is the temperature difference, which determines the heat exchange intensity - the heat flow rate is proportional to it. The principle of operation of power compensation DSC is based on maintaining both the sample and the reference sample at the same temperature during the temperature program. The signal in this system is the difference in power supplied to the sample to achieve the above goal.

This technique provides information on the thermal characteristics of the material, most often these will be the temperature values of exothermic or endothermic events, to which the reactions or transitions taking place can be attributed. Therefore, it is a key tool in the characterization of amorphous solids, allowing not only to track changes occurring in the internal structure of glasses along with the introduced modifications but also providing information necessary for the precise execution of controlled annealing processes.

2.4.2. Differential Thermal Analysis (DTA)

This measurement technique is closely related to DSC but allows only the determination of characteristic temperatures, while the DSC measurement also gives information on thermal parameters such as heat of crystallization or heat of fusion. In this case, the temperature difference between the sample and the reference is measured as they are subjected to a temperature program. This idea is implemented in a similar way as in the previously described measuring system, two samples are placed in the furnace chamber, one of which is the tested material and the other is the reference - Al_2O_3 is often used due to its well-known stability in a wide temperature range. For each sample, the temperature is measured with thermocouples spaced at a minimum distance from the samples (crucibles with a convex bottom are often used, which are placed directly on the thermocouple, so the distance is equal to the thickness of the crucible material), then the difference of these two values is plotted against the temperature/time during temperature program with a certain heating rate. Due to the significant similarity of techniques, the thermal events present for DSC occur as well in DTA measurements. In DTA, unlike DSC, it is not possible to measure heat capacities due to the constant heat flow during the measurement. Moreover, the practically identical analysis process in both

measurement techniques causes DTA as a less universal technique to be gradually replaced by DSC. At the same time, DTA is a much cheaper option for measurements at high temperatures due to the materials used in it and allows the use of larger sample weights. Therefore, it is still a choice for the thermal characterization of glasses.

The thermal properties of the glasses were investigated using differential thermal analysis techniques performed on a Netzsch Simultaneous Thermal Analyzer STA 449 F1 Jupiter® in a covered alumina crucible (sample mass ~ 50 mg) and differential scanning calorimetry performed on a Netzsch Thermal Analyzer DSC 204 F1 Phoenix® in a covered aluminum crucible (sample mass ~ 5 mg). Measurements were performed using a heating rate of 10 K/min in a synthetic air atmosphere. The use of two measurement techniques was due to the impossibility of unequivocally determining the glass transition based only on the DTA curve. As a result, it was decided to carry out an additional measurement using the DSC technique in the range from 45 to 550 °C. The glass transition temperature (T_g) and crystallization temperature (T_c) of the materials under study were clearly determined thanks to the combined results of the aforementioned techniques.

2.5. Photoluminescence Spectroscopy

Photoluminescence spectroscopy is a measurement technique that utilizes the interaction of photons with matter, as a result of which the absorbed quantum of electromagnetic radiation (most often in the UV range) leads to electronic excitation in the examined material - energy is exchanged and electron occupies higher energy state. Due to the high energy of the excited electronic state, at room temperature, a non-radiative mechanism is less likely, so after some time at the excited state (lifetime) the system can return to the ground state spontaneously under emission of a photon [101]. The light emitted in the above process is characterized by a frequency lower (less often equal) than the frequency of the excitation wave, this is the so-called Stokes's rule - observed as a shift of the frequency of the emitted wave towards lower frequencies (in relation to the excitation wave) caused by the loss of excess vibration energy of the active unit to the surroundings.

The basic equipment used in the measurements consists of a light source, a detector coupled to an analyzing unit, a sample chamber, and two monochromators. The light source is usually a xenon lamp which emits polychromatic radiation with a wavelength in the range 200 - 1400 nm. The sample excited with the appropriate wavelength emits light which is analyzed by the emission monochromator directing only light of a fixed wavelength to the photomultiplier. As a result, the fluorescence intensity is measured as a function of the wavelength. The measurement can take place as described above when for a constant excitation wavelength, the

emission intensity is monitored in a certain wavelength range - an emission spectrum is obtained. The excitation spectrum is obtained by observing the intensity of radiation with a selected emission wavelength as a function of the excitation wavelength. By analyzing the measured spectra, information is obtained about the luminescent properties of the studied material, the types of active centers, and their surroundings. In particular, this technique enables one to study the influence of the glass matrix in which they are located on rare earth ions and, conversely, the influence of the RE dopant content and its type on the luminescent properties of the material. As a result, knowing the excitation and emission spectra of active centers in a given material, it is possible to select them in such a way that a favorable (from the experimental point of view) energy transfer occurs between them, numerous examples of which are presented in the first chapter of this work. Finally, in the case of luminescent glasses, this technique enables direct observation of the emission effect, which is the target application of these materials.

Photoluminescence emission and excitation spectra were collected using the SCINCO FluoroMate FS-2 fluorescence spectrometer using the following measurement parameters: integration time – 40 ms, response time – 0.02 s, and 0.25 nm measurement interval. The samples were prepared in uniform pellets by mixing glass with KBr in a weight ratio of 1:1.

2.6. Time-resolved Emission Spectroscopy

Valuable information about the microscopic nature of the active center, its environment and the recombination process can be inferred from the luminescence decay curves and the resulting lifetime of the excited state obtained with time-resolved emission spectroscopy [101]. The idea of the technique is to measure the rate of population change in the excited state. This concept, in simple terms, is implemented by illuminating the sample with a short excitation pulse of a specific frequency and the following measurement of the intensity of the emission obtained as a function of time t. Due to the proportionality of the luminescence intensity I(t) to the population in excited state, there is a dependence on the exponential decay:

$$I(t) = A\, exp\left(\frac{-t}{\tau}\right), \tag{4}$$

where τ is the radiative decay time (its reciprocal is the transition probability) and A is an amplitude. In addition, the analysis of lifetimes distinguishes between the average lifetime considering amplitudes $\langle\tau\rangle_{Amp}$ and the average lifetime considering intensities $\langle\tau\rangle_{Int}$, these parameters are defined as follows:

$$< \tau >_{Amp} = \frac{\sum A_i \tau_i}{\sum A_i}, \quad (5)$$

$$< \tau >_{Int} = \frac{\sum A_i \tau_i^2}{\sum A_i \tau_i}. \quad (6)$$

The obtained decay curves do not always have to correspond to the above equation and be single-exponential functions, this deviation may be a valuable source of information, inter alia, about the change in the active ion's environment and the resulting energy transfer, which is an additional method of decay for the excited ion, thus shortening the lifetime. In glass-ceramics doped with rare earth ions, the presence of two-exponential luminescence decay can be interpreted as information about two different environments in which the ion is located: the long lifetime is determined by the environment with high symmetry, and the short life time by the low symmetry environment of the dopant ion [102].

Time-resolved emission spectra were collected using pulsed spectrofluorometer system [103] based on laser system PL2251-20 with Nd:YAG laser and PG 401/SH parametric optical generator from EKSPLA with signal analyzed by Bruker Optics 2501S spectrograph and the Hamamatsu streak camera C433-01 model. All apparatus and measurements are controlled by the original Hamamatsu HPDTA software, allowing for real-time data analysis. Decay times were obtained by slicing the streak camera image at a certain time interval.

2.7. UV–Visible Absorption Spectroscopy (UV-Vis)

Absorption spectroscopy in the ultraviolet and visible radiation range, as the name suggests, examines the interaction of matter with radiation in the wavelength range of ~10 – 800 nm. The condition for absorption of a photon, followed by the transfer of an electron from a lower to a higher energy level, is the matching of the photon energy to the difference between energy levels. The relationship connecting the above-described discrete atomic or molecular electronic states with the frequency of electromagnetic radiation is the Bohr–Einstein relation in the form:

$$\Delta E = E_2 - E_1 = h\nu, \quad (7)$$

where E_i is the energies of the levels between which the electron transition occurs, h is Planck's constant, and ν corresponds to the frequency of radiation. The above expression is the first selection rule of electron absorption spectroscopy. The second selection rule refers to the transition probability *W* between the initial state Ψ_i and the final state Ψ_f, which must be

nonzero, expressed by the relation $W = B_{if}\ \rho \neq 0$, in which the letter ρ denotes the radiation density and B_{if} denotes the Einstein coefficient proportional to the transition dipole moment. The third of the approximate selection rules is the condition of maintaining the same multiplicity of states between which the transition occurs. The relatively high energy of photons in the UV–Vis range causes the observed spectra to be electronic-oscillatory-rotational, but according to the Franck–Condon rule, during electron transitions energy cannot be allocated to vibrational or rotational transitions, which causes electronic transitions to be much faster and, as a result, are characterized by a high-resolution spectrum [104].

In a UV-Vis spectrophotometer, the irradiated beam is split by an optical chopper into a reference beam providing the intensity I_0 and a beam incident on the sample, which is characterized by the intensity I as a consequence of the absorption taking place. As a result, it is possible to calculate the transmittance ($T = I/I_0$) of the sample as a function of the incident wavelength. This approach allows one to get rid of the influence of instrument factors and obtain only the sample response. In the case of luminescent glasses, UV-Vis spectroscopy allows one to determine the width of the optical window, in particular high transparency for UV radiation (absorption edge), which is necessary due to the need to excite RE ions located inside the amorphous matrix. The presence of these ions can be confirmed on the basis of narrow absorption bands corresponding to characteristic electronic transitions. In addition, for glasses containing an $AgNO_3$ additive, it is possible to determine the formation of metallic precipitates in the material by observing the surface plasmon resonance band.

Absorption spectra of the glasses were obtained using a UV-Vis Perkin-Elmer Lambda 35 spectrophotometer. The studies were carried out in the transmission mode range from 190 to 1100 nm with a resolution of 2 nm.

3. Results and discussion

3.1. Materials containing addition of SrF_2

DTA and DSC

The obtained PKF glass series, together with the parent glass PKBN, were thermally characterized using DSC and DTA techniques. The results of these measurements are presented in Figure 10, where the measurement curves from the mentioned methods were scaled and compared to each other in order to provide a comprehensive picture of the thermal properties in the range from 40 to 800 °C. Based on the DSC results (left), it was possible to observe glass transitions, which were characterized by glass transition temperatures T_g (in this work the concept of determining T_g for the transition center was adopted). The influence of the SrF_2 addition on the transition position is particularly pronounced, after its introduction the glass transition temperature increases significantly reaching a maximum of T_g = 522 °C for PKF10, which is equivalent to an increase of 34 °C compared to the PKBN parent glass. Interestingly, further addition leads to a decrease in T_g in the case of the PKF15 sample.

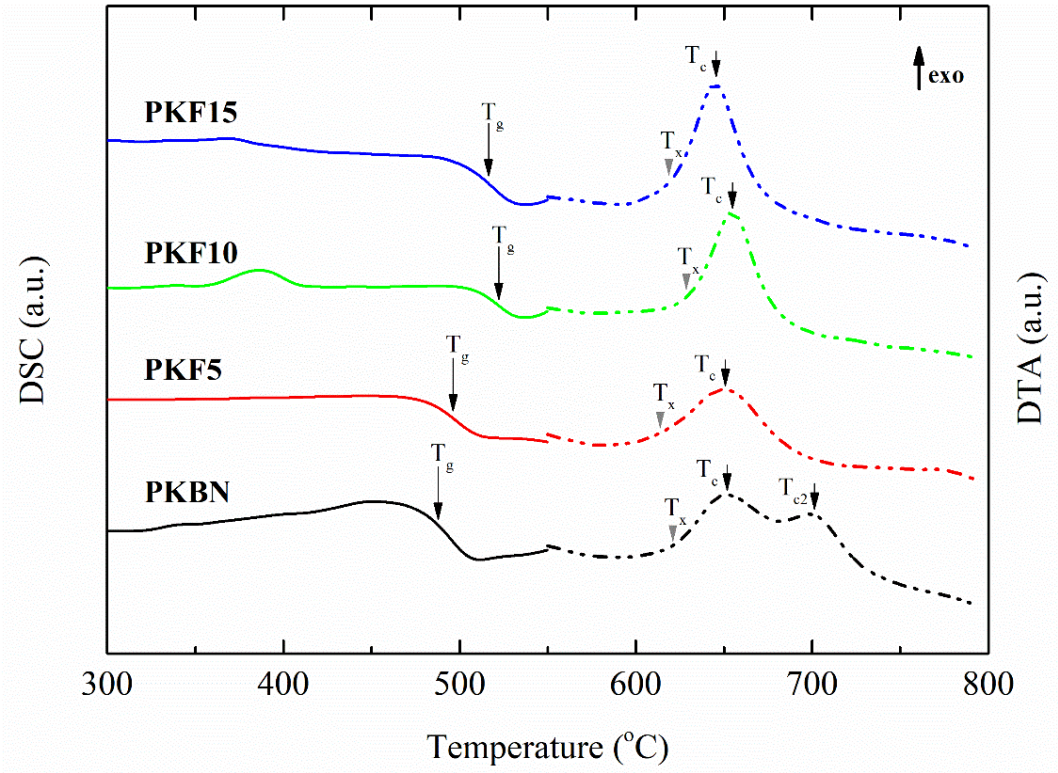

Fig. 10 Results of DSC (continuous line) and DTA (dashed line) measurements of PKF and PKBN parent glass series. The curves corresponding to the two techniques were rescaled and compared to each other to present the overall characteristics of the measured glasses. Characteristic temperatures are marked with arrows: T_g – glass transition temperature, T_x – onset temperature related to T_c, which is the crystallization temperature (exothermic maximum)

Other parameters such as the temperature of the onset of exothermic maximum (T_x) and the value of its center known as the crystallization temperature (T_c) were read from the results of the DTA analysis. In this case, the addition of SrF_2 caused smaller differences in the values, for PKBN and PKF5 the T_c value was similar and equal to ~650 °C. Moreover, the PKBN glass was the only one characterized by the second exothermic maximum T_{c2} = 698 °C, the occurrence of which can be identified with the crystallization of the second, high-temperature crystalline phase. The growth of this phase is probably inhibited by the addition of SrF_2, which would explain the lack of its signs in the PKF series. Glasses with a higher fluoride content showed different trends - compared to the PKBN matrix, the crystallization temperature increased by 5 °C for PKF10 and decreased by 5 °C for PKF15. A summary of the characteristic temperatures of the measured glasses is included in Table 2.

	DSC	DTA		*S*
	T_g	T_x	T_c	
PKBN	488	621	651 (698)*	*10.02*
PKF5	496	614	649	*10.80*
PKF10	522	631	655	*6.11*
PKF15	516	619	645	*6.5*

Table 2. Characteristic temperatures (°C) determined on the basis of DTA/DSC measurements. The symbols used are analogous to those introduced in Fig. 8. The table also includes the calculated values of the Saad–Poulain (S) parameter. The value marked by an asterisk indicates the position of the second exothermic maximum

The values of the obtained temperatures were used to calculate the parameter proposed by Saad – Poulain [98] in the form:

$$S = \frac{(T_c - T_x)(T_c - T_g)}{T_g}. \quad (8)$$

It allows for a relative assessment of the stability against crystallization of selected compositions and for tracking changes in this property along with their modifications; the values calculated for the PKBN glass and the PKF series are included in Table 2. It should be noted that the use of the S parameter in this work involved the use of two measurement techniques, in which, although the same heating rate of 10 K/min was set, the tested samples were not characterized by identical geometry, therefore, the S values are only used for comparative analysis within this work. Moving on to this analysis, it can be seen that the obtained values divided the tested

glasses into two groups - PKBN and PKF5 with the value of S ≈ 10, while for PKF10 and PKF15, S ≈ 6. This is an indication of the influence of SrF_2 on the stability of the glasses, which is reduced for the share close to 10 mol% and higher (based on the parameter values). In this approach, PKF5 glass can be considered as a transitional material between the PKBN matrix and other compositions, in which the influence of SrF_2 on its properties is clearly stronger. This is supported by the dual nature of this material, which is characterized by the value of the S parameter almost identical to PKBN glass and, at the same time, does not show the presence of a second exothermic maximum, which is similar to glasses with higher fluoride content.

A particularly interesting comparison of DTA results is presented in Figure 11. It contains fragments of identically conducted measurements of the PKF15 sample (same as in Figure 10) and its version doped with only 0.5 mol% Eu – PKF15 05Eu. With the introduction of the dopant, the recorded temperatures characterizing the exothermic maximum increased collectively by ~13 °C, which resulted in a shift of the thermal effect towards higher temperatures without changing its form – compared to PKF15. The above observations may mean that Eu^{3+} ions in the case of the described glasses are more likely to behave as lattice modifiers, building themselves into the glass lattice, thus increasing the resistance to crystallization. Similar conclusions were reported in [105], where the increasing share of the Eu_2O_3 dopant positively influenced the stability of bismuth-alumino-borate glasses and decreased the degree of crystallinity of the samples subjected to annealing.

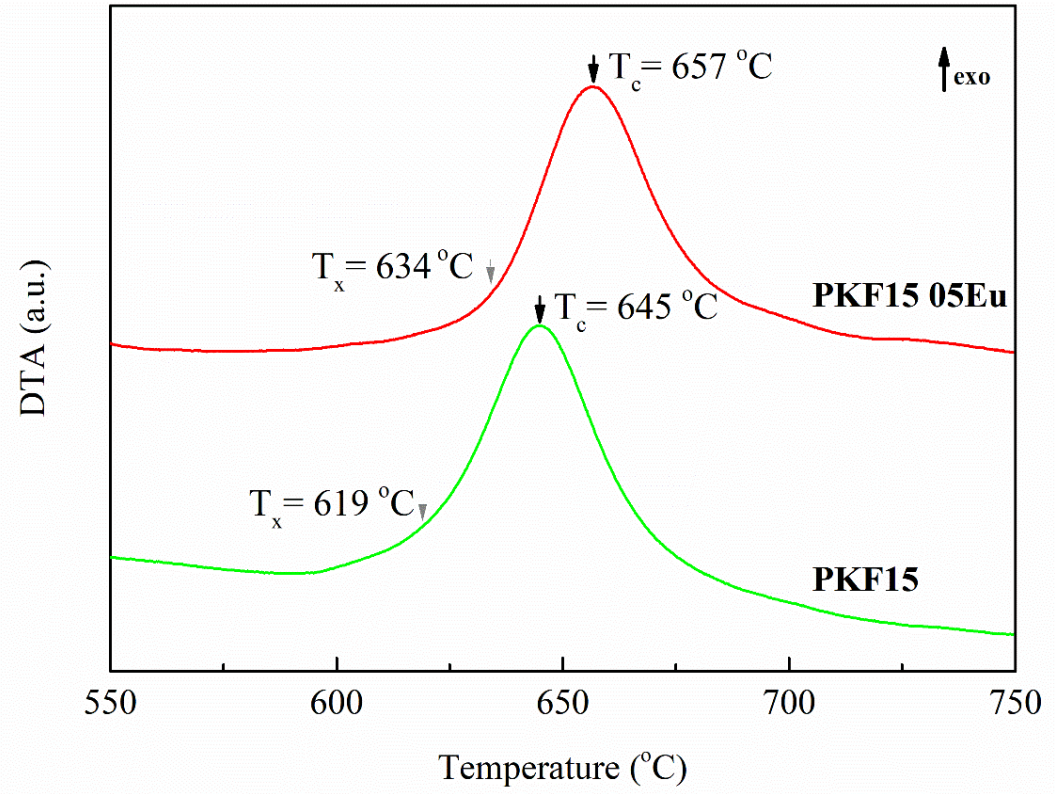

Fig. 11 Comparison of fragments of the DTA measurement curve obtained for the PKF15 matrix and its Eu_2O_3-doped version PKF15 05Eu. The presented exothermic maximum illustrates the influence of a relatively small dopant (0.5 mol%) on the characteristic temperatures of the derived materials

The thermal analysis performed was crucial in determining the range of annealing parameters that would allow for controlled growth of the SrF_2 crystalline phase in the glass matrix. However, the observed differences in values of characteristic temperatures (Table 2) between the studied glasses made it difficult to select one general annealing temperature directly. The uniqueness of this temperature is emphasized by the fact that it should provide optimal annealing effects for each of the compositions, which in this approach is equivalent to maintaining control over the growth of the desired crystalline phase (SrF_2) and hindering the bulk crystallization of the matrix so that it is possible to conclude about the influence of the modifier content on the properties of the obtained materials. As a result, it was decided to "scan" the range of available temperatures from 485 to 605 °C (determined based on DSC/DTA) and experimentally select the optimal temperature through a series of 10 h of annealing with an interval of 10 °C.

XRD

The results of X-ray diffraction measurements allowed us to confirm the amorphous nature of the PKBN matrix and the PKF glass series - the corresponding diffraction patterns are included at the bottom of Figures 13 - 16. Analogous conclusions about the shapes of the glasses additionally doped with 0.5 mol% Eu could be reached based on the shape of their diffraction patterns presented in Figure 16 a). Photos of samples of as-prepared glasses are presented in Figure 12 (first row). As can be seen, the obtained materials were homogeneous and characterized by high transparency with a slightly yellow tint.

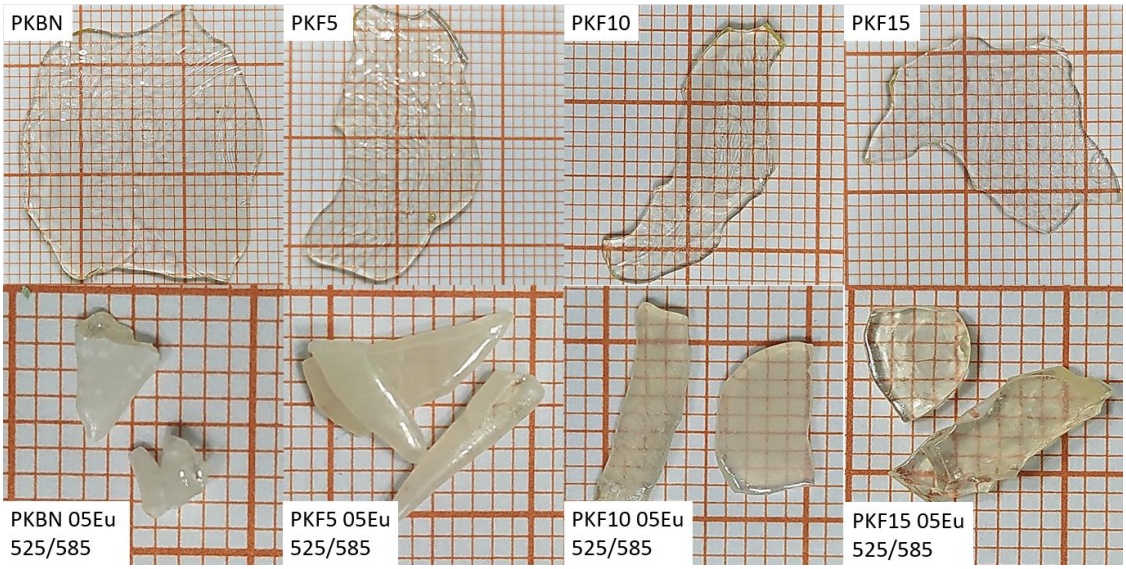

Fig. 12 Comparison of photos of as-prepared glasses (top row) and their doped counterparts after double annealing initially at 525 °C and then at 585 °C (bottom row). The second row clearly shows the loss of transparency of the PKBN glass and the gradual improvement with increasing SrF_2 content

Undoped glasses, which were subjected to a series of 10 h of annealing in the range of 485 –605 °C (the summary of the parameters of individual processes is included in Table 3), were subjected to XRD characterization in order to optimize the annealing temperature and to obtain a systematic description of the crystallization process, the measurement results are summarized in Figures 13 – 16. Due to the demonstration of the purely amorphous nature of the samples annealed in the range of 485 to 555 °C, these results were not included in the work. This procedure provided greater transparency of the compared data.

Series	Glasses	Annealing parameters
1	undoped	every 10°C from 485°C -605°C range for 10h
2	with 0,5 mol% Eu	525°C, 545°C, 585°C for 10h
3	with 0,5 mol% Eu; annealed at 525°C for 10h	545°C, 585°C for 10h

Table 3. Summary of the parameters of the annealing process performed for the PKF series

Regardless of the series of glasses subjected to the annealing process, the last temperature, which, according to the observations made, guaranteed a completely amorphous material devoid of crystalline phase reflections that stood out beyond the wide maximum was 565 °C. On this basis, it was possible to conclude that the limiting parameters of the annealing process, after which the first signs of the appearance of crystalline precipitates in the glass matrices of PKBN - PKF are noticeable are 575 °C and 10 h. Materials obtained using these conditions are characterized by reflections of very low intensity, which may be equivalent to information about a small share of the newly formed crystalline phase. As a result, the above-mentioned annealing parameters can be considered as limiting, which ensures the presence of detectable crystallite content, taking into account a specific detection threshold resulting from the applied XRD measurement technique. The hardware limitations and the conclusions about the temperature characteristics based on the thermal analysis led to the conclusion that in the case of lower temperatures, the presence of nanocrystalline precipitates formed as a result of annealing, which remains outside the detection threshold, cannot be completely excluded. Unfortunately, in most cases, the reflections originating from crystallites dispersed in the matrix overlap with the strong halo of the amorphous matrix. As a result, it is difficult to recognize or characterize poorly defined reflections associated with nanometric precipitates.

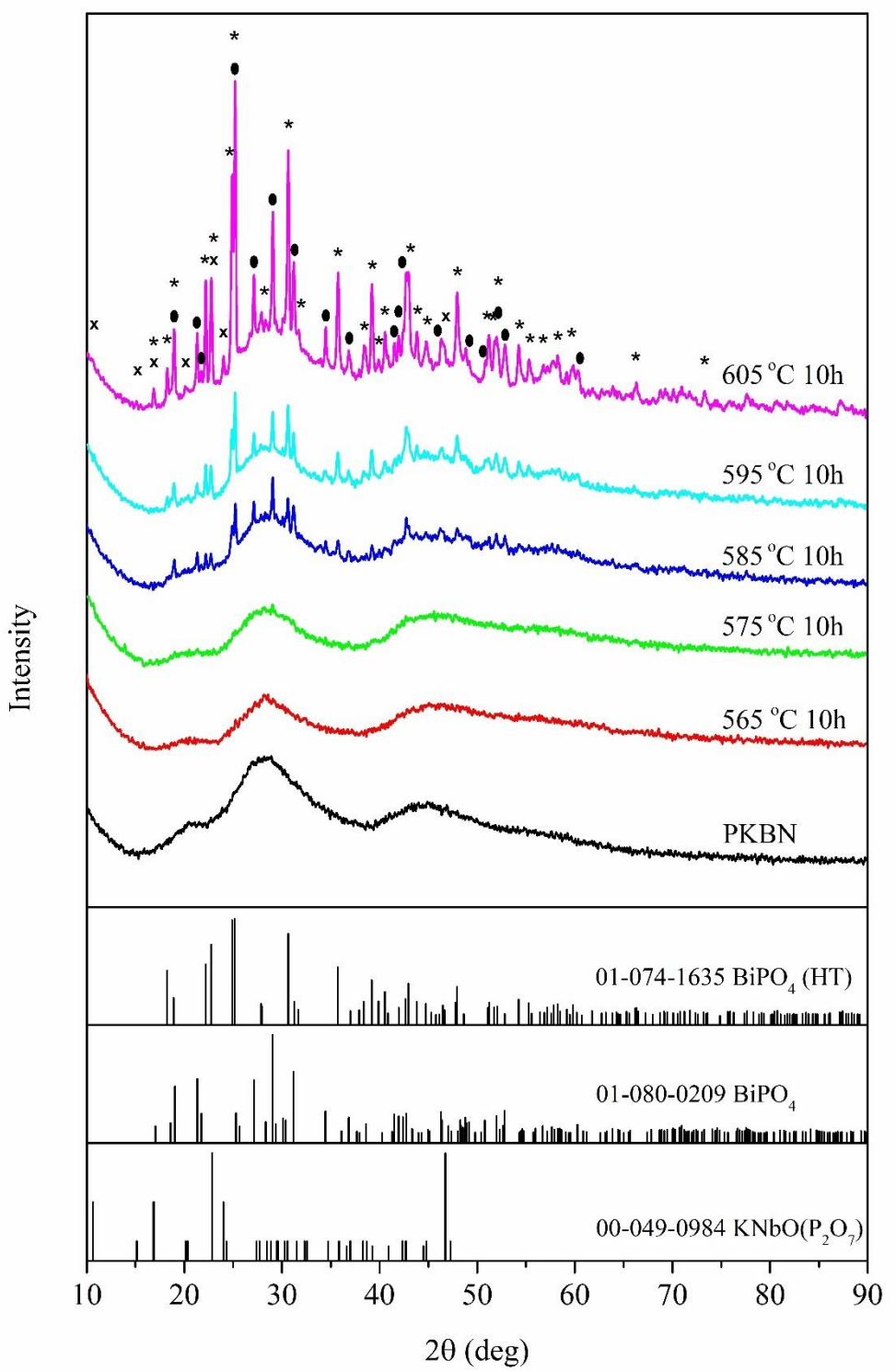

*Fig. 13 Comparison of diffractograms obtained as a result of measurements of PKBN glass samples subjected to annealing in the range of 565 - 605 °C for 10 h. Additionally, the diffractogram of the unannealed sample is included at the bottom. The identified crystalline phases formed as a result of annealing the amorphous material are marked with symbols, these are respectively: * - high temperature monoclinic $BiPO_4$; ● - monoclinic $BiPO_4$; **X** - $KNbO(P_2O_7)$, standard XRD patterns of these phases were shown in the lower part of the figure*

Well-defined reflections in the diffractograms of PKBN samples appear in the case of annealing at 585 °C, which is presented in the comparison in Figure 13. In the next step, a higher process temperature (595 °C) led only to a slight increase in the peak intensity. Only in the case of the last annealing at 605 °C a sudden increase in intensity was observed, which could be correlated with the increase in the sample crystallinity. It was certainly influenced by the growth of three crystalline phases, which were identified based on the recorded reflections (Figure 13) as monoclinic monazite-type $BiPO_4$ (M-BiP) phase (ICDD no. 080–0209), its high-temperature equivalent (H-BiP) (ICDD no. 074–1635) and $KNbO(P_2O_7)$ (ICDD no. 049–0984), occurring only in glasses annealed at 605 °C.

In the case of the described PKBN series, the evolution of the crystalline phases indicates that the second exothermic maximum observed for this glass (Figure 10; T_{c2} = 698 °C) can probably be attributed to the crystallization of the H-BiP phase. Similar observations were made by Mooney-Slater in her work [106], where she studied polymorphic forms of bismuth phosphates. The transformation M-BiP → H-BiP was defined by her as occurring rather in a gradual manner, where one phase is replaced by the other by reconfiguration, than destructively with the participation of numerous bond breaks. However, it is worth emphasizing that both the work of Mooney-Slater and the studies presented by Romero et al. [107] mentioned that the above transformation occurs above 600 °C, but in order to produce the high-temperature $BiPO_4$ variant, they use annealing in the range of 750 - 800 °C - the process is also described as slow (lasting several days). The fact that the presence of the H-BiP phase was demonstrated in the tested glasses already in samples annealed at 585 °C can be explained in two ways, but in each of them it is important to take into account the influence of the glass structure on the crystallization process. The first of the probable mechanisms assumes, analogously to the examples described above, the growth of the M-BiP phase as the first, which at a certain stage of the process would gradually transform into the high-temperature version of $BiPO_4$. The second option is the simultaneous growth of the M-BiP and H-BiP phases, supported by the environmental conditions of the glass matrix. The argument in favor of the second thesis is the occurrence of both phases in samples obtained in the process characterized by a relatively low temperature and short duration - H-BiP reflections were recognized already for 585 °C. Moreover, the crystal structure of both phases in the short-range order does not differ significantly from the units constituting the parent glass network, which would allow for easier reorganization of the atoms. On the other hand, following the conclusion presented by Romero et al. [107], which defines the structural changes occurring during the M-BiP → H-BiP transformation as very small, related mainly to the slight rotation of the PO_4 tetrahedra, the mechanism presented first can be considered probable. The outlined situation suggests that a

common compromise with a clear threshold near 600 °C is more probable than the isolated action of individual mechanisms when describing the observed changes. In this proposed explanation, below 600 °C, mainly spontaneous crystallization of both phases occurs, M-BiP dominates, and a small part of it is simultaneously transformed into the high-temperature phase. Exceeding the mentioned annealing temperature threshold makes the transformation into H-BiP more probable and dynamically occurs at the expense of the second phase. This concept would explain the trend in the intensity of diffraction reflections present in Figure 13.

The addition of SrF_2 was introduced to the PKF glass series in order to obtain a nanocrystalline SrF_2 cubic phase by controlled annealing. The glass-ceramics obtained in this way turned out to contain more than one crystalline phase, which was confirmed by the XRD results presented in Figures 14 - 16.

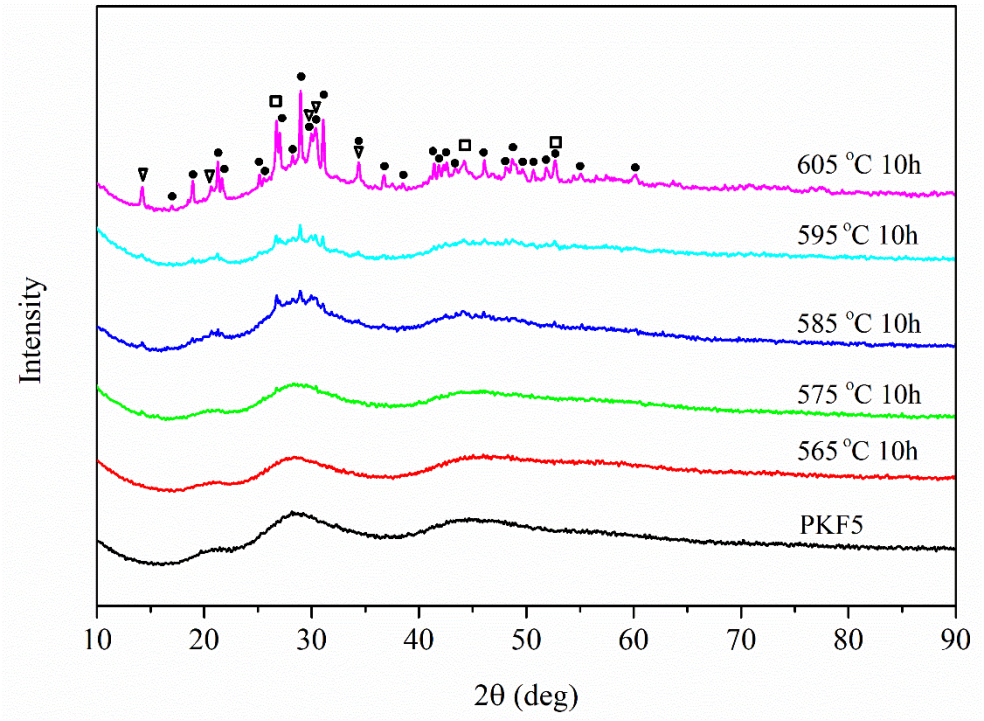

Fig. 14 Comparison of diffraction patterns obtained from measurements of PKF5 glass samples heated in the range of 565 - 605 °C for 10 h. Additionally, the diffraction pattern of the unheated sample is included at the bottom. The identified crystalline phases formed as a result of heating the amorphous material are marked with symbols, these are respectively: ● - monoclinic $BiPO_4$; □ - SrF_2; ▽- unknown phase

As can be seen, the complexity of the initial amorphous system resulted in its susceptibility to modifications, which is particularly evident in the XRD analysis of the annealed samples. It showed that the introduction of as little as 5 mol% SrF_2 significantly affects the structure of the glasses and, indirectly, the resulting crystallization properties. It was observed that even the smallest SrF_2 content used completely inhibits the possibility of growth of the H-BiP phase (which

is confirmed by the corresponding DTA curves lacking the second exothermic maximum). As a result, in the PKF 5-15 glass-ceramics, the following was identified: the M-BiP phase, with high probability some of the reflections were assigned to the cubic phase of SrF_2 (ICDD no. 086–2418) and the presence of an unknown phase (UnP) was detected, which could not be identified. Analysis of this issue, apart from the complications resulting from the amorphous nature of the material, is even more convoluted due to its multicomponent nature, which results in broad and complex XRD peaks. The width of the reflection, most often described by full width at half maximum (FWHM), can be changed by two factors, the overlap of closely located peaks originating from different crystalline phases and the sizes of individual crystallites. Precipitates whose diameters do not exceed the order of tens of nanometers will be characterized by reflections with FWHM so large that in the case of a multicomponent sample, it is impossible to unambiguously characterize and identify the crystalline phases.

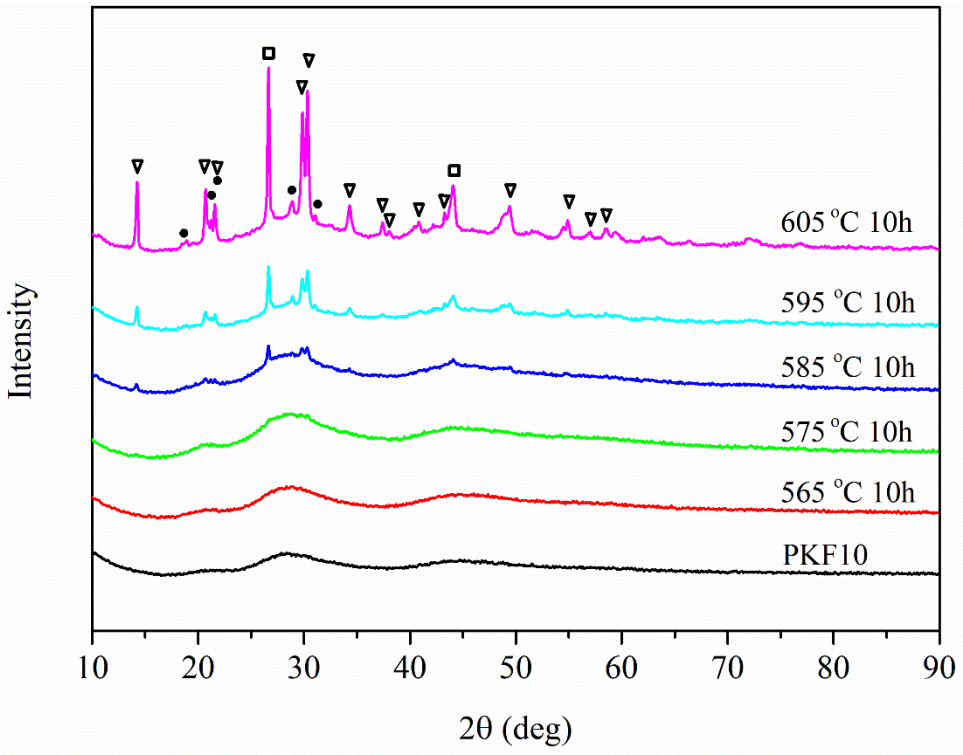

Fig. 15 Comparison of diffraction patterns obtained from measurements of PKF10 glass samples heated in the range of 565 - 605 °C for 10 h. Additionally, the diffraction pattern of the unheated sample is included at the bottom. The identified crystalline phases formed as a result of heating the amorphous material are marked with symbols, these are respectively: ● - monoclinic $BiPO_4$; □ - SrF_2; ▽ - unknown phase

The analogous dependence of the differences in the intensity of reflections on the annealing temperature described earlier for the PKBN glass-ceramic was also observed for other compositions. However, with the increasing share of SrF_2, the nature of this trend changed, in

which the relative differences in intensity (especially visible between samples annealed at 595 and 605 °C) significantly decreased. These changes may be related to the crystallization of the UnP phase, the appearance of which probably significantly limits the growth of the M-BiP phase - this relationship is particularly visible in the case of PKF10 and PKF15 glass-ceramics obtained at 605 °C. However, this division is not unambiguous for the PKF5 glass-ceramics, their transitional nature is again revealed, and both the main M-BiP phase dominant in the PKBN glass-ceramics is present in them and SrF_2 crystallites and the UnP phases appear (Figure 14). Moreover, the distinct properties of this composition are expressed by very low intensity, poorly defined reflections isolated for samples annealed at both 585 and 595 °C. The reason for the above observation is not clear, as neither the results of thermal analysis nor the type of crystalline phases formed differ significantly from the other PKF compositions.

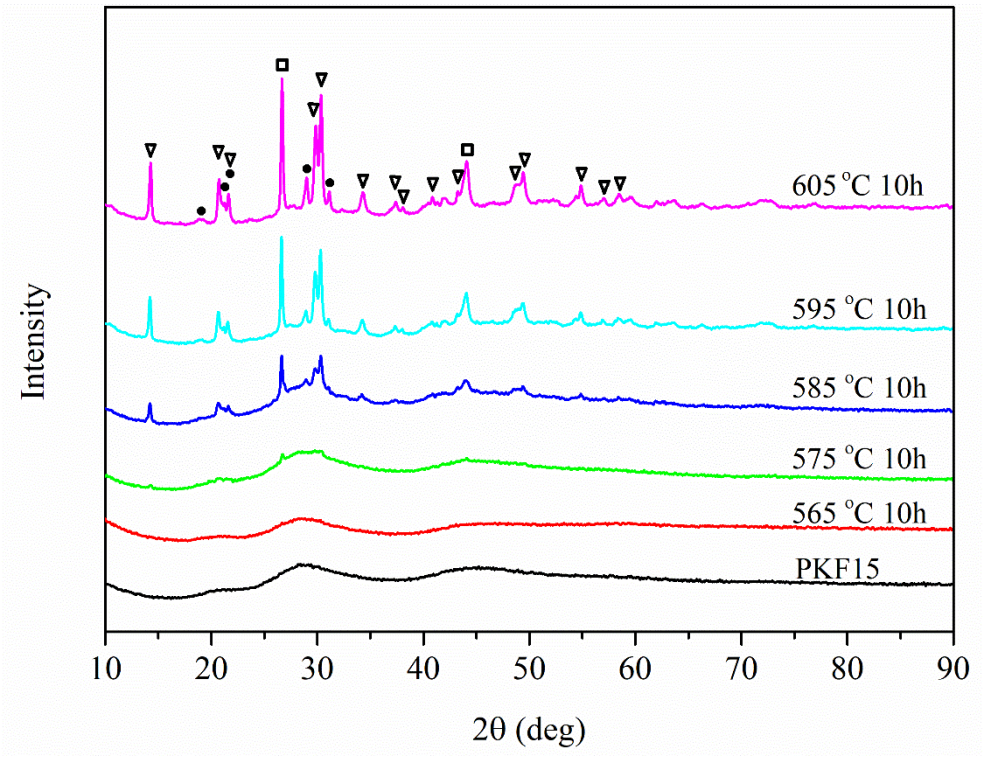

Fig. 16 Comparison of diffraction patterns obtained from measurements of PKF15 glass samples heated in the range of 565 - 605 °C for 10 h. Additionally, the diffraction pattern of the unheated sample is included at the bottom. The identified crystalline phases formed as a result of heating the amorphous material are marked with symbols, these are respectively: ● - monoclinic $BiPO_4$; □ - SrF_2; ▽ - unknown phase

The PKF5 glass-ceramic case has already initially suggested that samples with a higher modifier content exhibit mutual similarity in crystallization characteristics. In particular, they are distinguished by well-defined peaks of the SrF_2 and UnP phases, with negligible intensity of reflections corresponding to M-BiP. This disappearance is probably closely related to the

appearance of UnP crystallites, which are formed at the expense of M-BiP. The occurrence of this correlation may indicate that the UnP phase is a phosphate, which includes, among others, strontium atoms, unfortunately, the complexity of the studied system did not allow its unambiguous identification.

The intensity of reflections in the presented diffraction patterns, which increased with the temperature of the annealing process, also provides information about changes in the morphology of the obtained samples. With the increasing annealing temperature, the surface of the resulting materials became somewhat cloudy, and a thorough analysis allowed us to notice minor streaks in glasses annealed already at 565 °C. To summarize, the degree of transparency of the obtained glass-ceramics increased with the increasing share of SrF_2 and was inversely proportional to the temperature used for their production. Taking into account the above-mentioned relationships and the measurement results that were their basis, it was decided to select T_H = 585 °C as the main annealing temperature, which for all compositions could meet the compromise of sufficient transparency while ensuring an increase in detectable amounts of the crystalline phase. In order to extend the systematics of the study, two additional parameter values were distinguished: low annealing temperature T_L = 525 °C and medium annealing temperature T_M = 545 °C. The first of the above was defined as a temperature slightly higher than the experimentally determined highest glass transition temperature – T_g = 522 °C for PKF10. The T_M temperature is expressed as an average of the T_H temperature values and the averaged T_g values of PKBN – PKF15 glasses.

Summarizing the effects of annealing of undoped glasses presented so far, it can be stated that based on the XRD results, the crystallization characteristics of these materials were initially outlined. They consisted of identifying the occurring crystalline phases, their evolution related to the introduction of different SrF_2 contents, and optimizing the annealing parameters for practical applications. The collected information allowed for the analysis of the properties of glass-ceramics doped with 0.5 mol% Eu_2O_3, the results of which diffraction measurements are presented in Figure 17. At first glance, it is clear that the recorded reflections were characterized by very low intensity and direct identification would be impossible - this confirms the justification for creating a "guide" in the first stage of the experiment describing the behavior of the tested glasses subjected to a series of systematic annealings.

As expected, the diffraction patterns presented in Figure 17, which were obtained for glasses heated at b) 525 °C, c) 545 °C and e) 525/545 °C, were devoid of any signs of crystalline precipitates (irrespective of composition). The remaining annealings, d) 585 °C and f) 525/585 °C, resulted in obtaining crystallites dispersed in the glass matrix, which was confirmed by diffuse peaks in the diffractograms of PKF5 05Eu and PKF10 05Eu, to which phases analogous to those

identified for undoped counterparts were assigned. Among the listed glass-ceramics, there was no PKF15 05Eu sample, for which, contrary to expectations (established on the basis of data from Figure 16), both in the case of single and double annealing, only an amorphous halo was obtained as an XRD result.

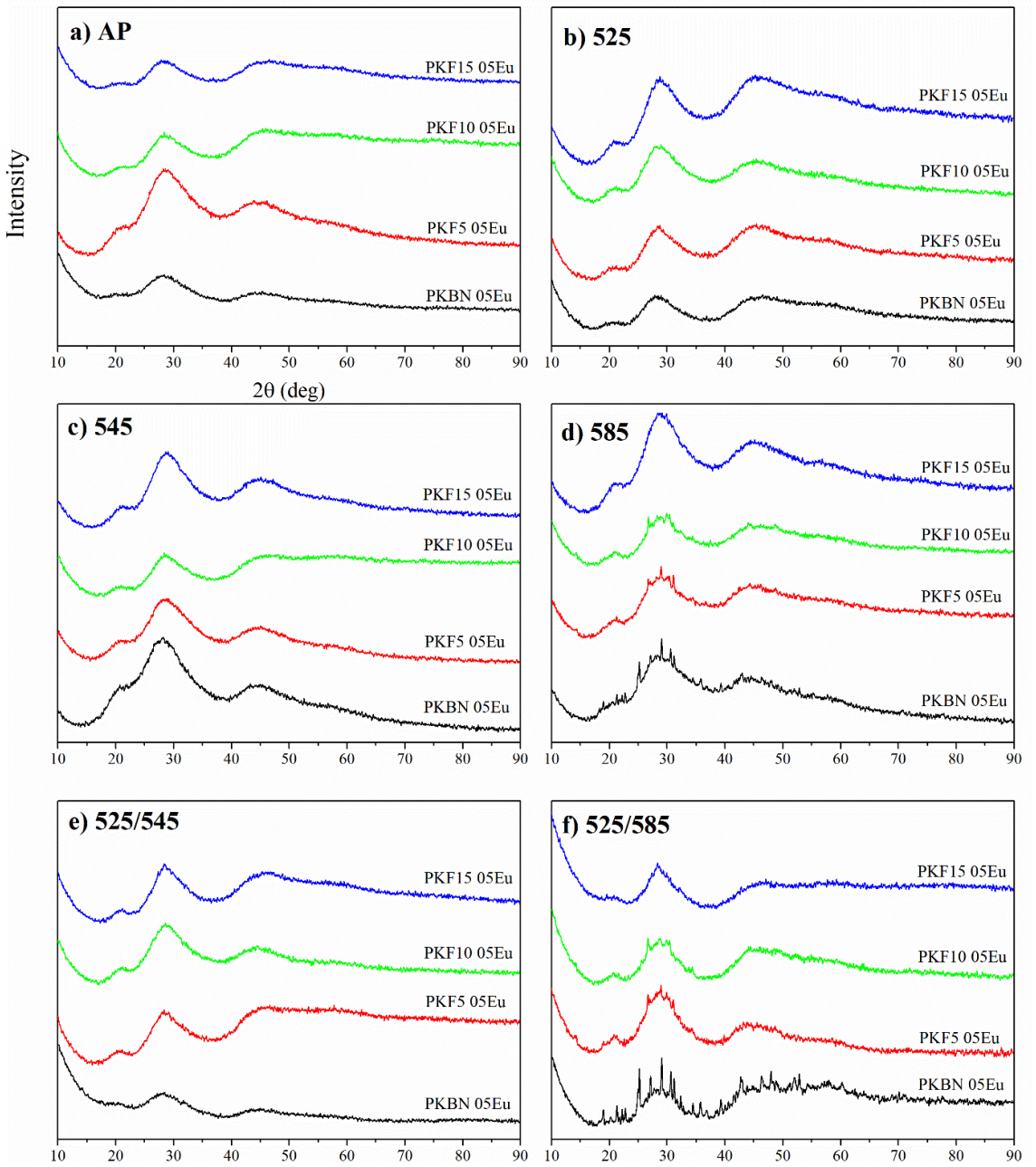

Fig. 17 Comparison of diffractograms of a series of glasses doped with 0.5 mol% Eu, which were subjected to annealing. For all compositions 0 - 15 mol% SrF_2, the graphs show the annealing results defined by the parameters: a) as-prepared glasses; b) 525 °C/10 h; c) 545 °C /10 h; d) 585 °C /10 h; e) 525 °C /10 h + 545 °C /10 h; f) 525 °C /10 h + 585 °C /10 h. For the sake of clarity, the shared axes are described only for graph a)

Due to identical process conditions, the only factor that could cause the observed difference was the modification of the composition by introducing the Eu dopant. The effect caused by such a small Eu_2O_3 dopant (0.5 mol%) could seem insignificant in principle, but as revealed in the comparison of DTA measurements presented in Figure 11, the dopant used in the case of this composition significantly affects the structure of the glasses. As a result, by making the glass more resistant to crystallization, it limits the growth of the expected crystalline phases in the annealing process characterized by the given parameters (585 °C and 10 h). The results also show that this effect is not separated from other parameters and becomes more significant with the increasing SrF_2 content. The indirect effect of this correlation is visible in Figure 12 (bottom row), where the surface appearance of the samples subjected to double annealing at 525/585 °C is presented. With the increasing content of the modifier, the surface turbidity acquired during thermal treatment decreases. Attention should be paid to the degree of turbidity of the PKBN and PKF5 samples, which is much greater than it could be deceptively shown solely based on the diffraction measurements performed for them.

The process of identifying crystalline phases carried out for the PKBN 05Eu glass-ceramic heated singly and doubly in T_H showed the presence of M-BiP and H-BiP phases in both samples. In the case of extended heating, additional reflections were also observed ($2\theta \approx 32.3°$ and 32.8°), which could not be assigned, and may be a sign of the formation of an additional phase appearing only in specific conditions guaranteed by the performance of double heating. The diffractograms of the remaining glass-ceramic compositions, although in the case of the above heating parameters were characterized by visible reflections, due to their low intensity and blurred form did not allow for direct identification of the formed phases. To some extent, taking into account the Eu effect, it can be assumed that these are crystallites of phases revealed during the series of heat treatments of samples without a dopant.

The observed effect of the Eu_2O_3 dopant brings another conclusion about the probable mutual influence of Eu^{3+} ions and the glass network. Due to the scale of the effect caused by a very small amount of dopant on the glass-ceramic structure, it is possible that the structural units forming this material together with the crystallites can equally strongly modify the environment of Eu^{3+} ions, and thus affect their properties, in particular luminescence.

FT-IR spectroscopy

The structural analysis of PKBN – PKF glasses, apart from the extensive XRD characterization, was based on infrared spectroscopy measurements, in which spectra in the range of 4000 – 400 cm^{-1} were obtained. The summary of the obtained results is presented in Figure 18.

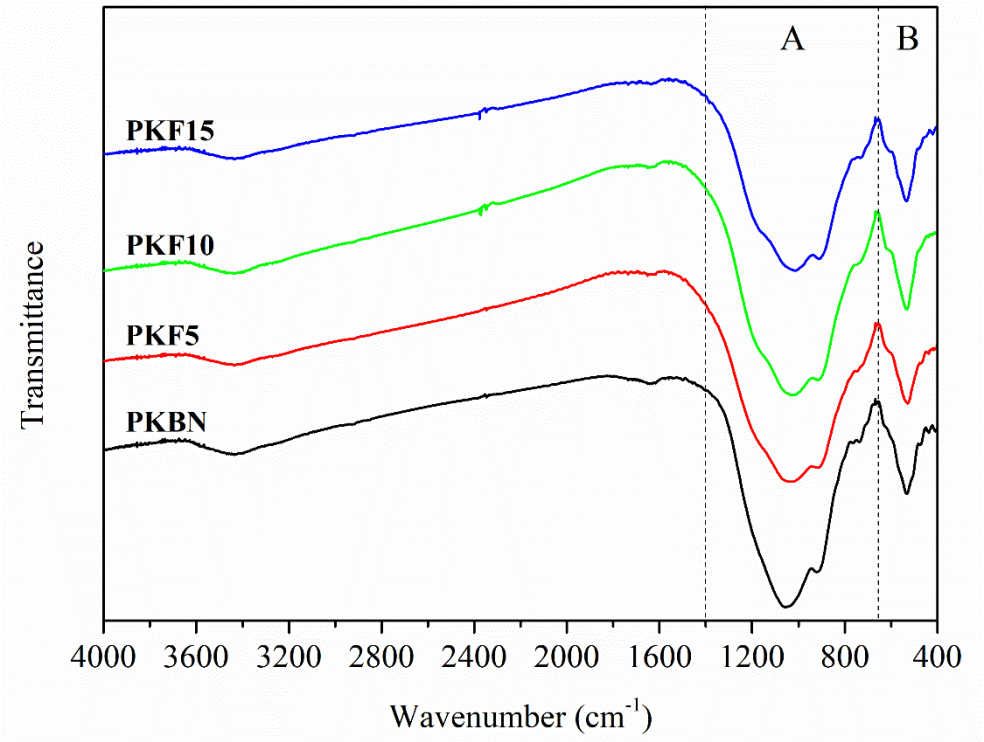

Fig. 18 Summary of FT-IR spectra obtained for as-prepared glasses in the range of 4000 – 400 cm^{-1}. The vertical dashed lines indicate the areas A and B, which were subjected to detailed analysis due to the bands characteristic of the tested glasses

Due to the position of the main bands containing information on the internal structure of the materials, the detailed analysis was limited to the range of 1400–400 cm^{-1}. For the convenience of description, this range can be divided into two dominant, complex minima, the first of which is located around 1400 – 670 cm^{-1} (marked with the letter A in Figure 18), and the second is located at 650 – 410 cm^{-1} and in this case marked with the letter B. The detailed measurement data are presented in Figure 19 using a short-dashed line. Based only on the general comparison of the spectral shapes, it can be stated that the change in the SrF_2 content in the range of 0 – 15 mol% does not lead to significant differences, especially in the form of new bands or large shifts. However, with the introduction of fluoride, a broadening of the left part of the A minimum can be observed, which is accompanied by the appearance of a new inflection of the curve located around 1180 cm^{-1}. Moreover, with increasing the SrF_2 content, it was observed that the most intensive minimum (in the case of PKBN ~1050 cm^{-1}) shifts towards lower wave numbers, up to the value of 1015 cm^{-1} read for PKF15. A common feature of the detected absorption bands is their large width. Moustafa and El-Egili [108] in their work on IR spectroscopy measurements of sodium-phosphate glasses suggested that the broadening of the bands is the effect of the

diversity of ways in which the structural groups can be connected to each other and ultimately the increased number of vibration modes resulting from their presence. This observation is also indirect information about the structural disorder of the phosphate groups in the material.

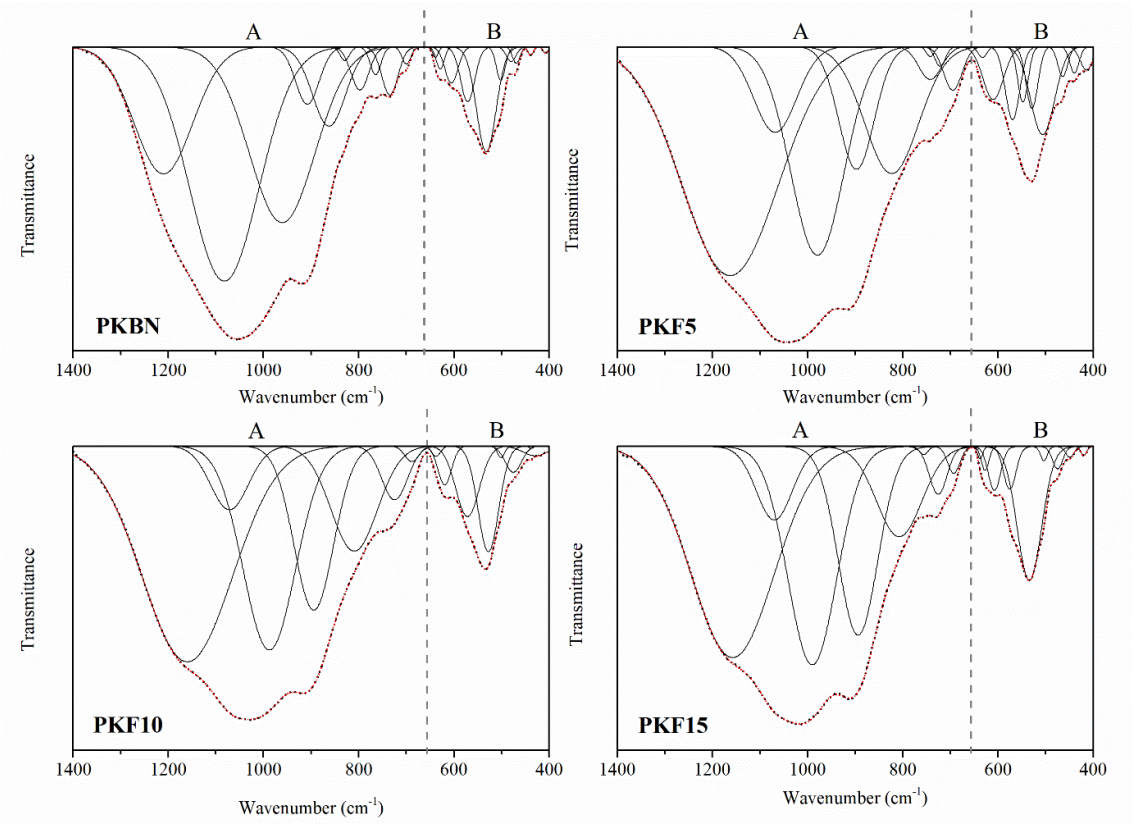

Fig. 19 Results of deconvolution (modeling) performed for fragments (1400 – 400 cm^{-1}) of IR spectra of as-prepared glasses containing from 0 to 15 mol% SrF_2. The experimental curves are marked with a short-dashed line, the matched components of the bands (Gaussian) are marked with a solid line, and the envelope of the simulated spectrum is marked with a red dotted line. The vertical dashed line separating the studied fragment into two main maxima is located at ~670 cm^{-1}

Tracing the structural evolution caused by the addition of SrF_2 required identification and analysis of individual bands. Due to the complex form of the spectra, which made it impossible to make the above assignment directly, it was decided to model them (deconvolution) in the A and B ranges - in total in the range of 1400 - 400 cm^{-1}. The results of this operation in the form of fitted curves are included in Figure 19, the parameters characterizing them are collected in Tables 4a and 4b (the assumptions of this process were described earlier in subsection 2.3).

PKBN	C_b	1210	-	1082	961	908	862	829	798	765	735	700
	R_a	16.3	-	35.7	25.5	3.0	5.8	0.3	1.7	0.7	1.7	0.3
PKF5	C_b	-	1163	1068	979	897	-	-	823	743*	722	695
	R_a	-	39.3	6.6	19.8	7.7	-	-	12.2	1.4	0.4	1.4
PKF10	C_b	-	1160	1072	988	894	-	-	809	-	725	688
	R_a	-	38.6	4.8	21.1	12.8	-	-	9.6	-	2.7	0.4
PKF15	C_b	-	1158	1070	990	894	-	-	808	756	726	693
	R_a	-	36.1	5.4	22.0	15.3	-	-	8.4	0.1	1.7	0.7

Table 4a. Parameters of the curves obtained in the process of modeling the IR spectra of PKBN - PKF glasses. The C_b values correspond to the band center positions and are expressed in cm^{-1}, while R_a - relative area of the band, was defined as the percentage ratio of the band area to the area of the obtained model envelope

PKBN	C_b	639	629	605	571	-	532	502	480	469	439	-
	R_a	0.1	0.4	1.0	1.7	-	4.5	0.7	0.3	0.3	0.1	-
PKF5	C_b	633	-	610	570	548	529	506	464	-	440	414
	R_a	0.2	-	1.9	1.9	1.0	1.3	3.8	0.5	-	0.4	0.5
PKF10	C_b	638	-	619	571	-	528	501	475	-	438	429
	R_a	0.2	-	1.0	3.3	-	4.3	0.2	0.8	-	0.0	0.5
PKF15	C_b	638	627	608	576	-	534	504	475	-	449	420
	R_a	0.1	0.4	1.1	1.1	-	6.7	0.2	0.5	-	0.2	0.1

Table 4b. Parameters of the curves obtained in the process of modeling the IR spectra of PKBN – PKF glasses (continued)

The first of the distinguished bands in the proposed model (starting from higher wave numbers) occurs only for the PKBN sample with the center located at about 1210 cm^{-1}. It was assigned to the stretching vibrations of the P=O bond [108-110]. This band does not occur for samples containing the SrF_2 additive. It is also possible that its intensity decreases to such an extent that it is no longer distinguishable in the spectrum. Regardless of the method, the disappearance of the band may be related to the strong reconfiguration of the glass structure under the influence of fluoride. It can be understood as the effect of the "cracking" of the P=O bond, which, due to the freedom provided by the depolymerization of the network, starts to coordinate intermediate M cations to form P-O-M bonds, where the cation, acting as a network

former, increases the cross-linking of the glass structure [110]. This is probably one of the factors causing the measured glass transition temperatures for the PKF glass series (Figure 10) to be higher compared to the PKBN matrix. With the introduction of 5 mol% SrF_2 into the compositions in the range corresponding to the above-mentioned absorption, a strong band appears located at ~1163 cm^{-1}, to which asymmetric stretching vibrations of P-O- (NBO) bonds in PO_2^- groups [105] were assigned. Assigning this band to asymmetric vibrations, based on the findings presented in Robinson's work [111], may mean that the band of corresponding symmetric vibrations may be located at about 1030 cm^{-1}, but in the case of the glasses studied it was not directly observed. Increased SrF_2 content in PKF10 and PKF15 samples leads to a gradual decrease in relative intensity and a slight shift of the band towards lower wave numbers. One of the probable reasons for these changes is the probable appearance of phosphate groups PO_3^{2-} [110], which is a sign of the presence of pyrophosphate units $P_2O_7^{4-}$.

The influence of SrF_2 on the glass structure is particularly visible in the case of the band evolution, which for the PKBN matrix was distinguished at ~ 1080 cm^{-1} and was attributed to the asymmetric stretching of the $P\text{-}O^-$ bond in Q_1 units (chain terminator) [112, 113]. The initially large relative field (R_a for PKBN ≈ 36 %) decreases several times after the introduction of fluoride and the band center shifts towards lower wave numbers. The observed changes may be related to the transformation of the glass network, as a result of which the weakened and shifted band probably corresponds in this case to the symmetric stretching in PO_2 units [114]. The key to explaining the changes occurring with the introduction of the modifier is to take into account the simultaneous disappearance of the band interpreted as the effect of P=O bond vibrations and the decreasing intensity of the aforementioned absorption as the effect of the equilibrium described as $2Q_1 = Q_2 + Q_0$ [115, 116] established under the influence of SrF_2 addition, which determines the observed changes in the description and characteristics of the band. The neighboring band is characterized by the highest R_a value in the case of PKBN glass, for PKF5 the minimum value of this parameter was noted, followed by its gradual increase with the increasing share of SrF_2. The changes in the relative field of the band were accompanied by a significant shift of its center, from the position of 960 cm^{-1} determined for PKBN to 990 cm^{-1} determined for PKF15. It probably corresponds to the asymmetric stretching of the P-O-P bond associated with large metaphosphoric rings [105, 112]. The mentioned changes induced by fluoride addition may be related to the increasing share of Q_0 units, for which the characteristic deformation vibration band is located at ~990 cm^{-1} [114]. One of the results of the proposed evolution describes a band located at about 900 cm^{-1}, which can be attributed to the stretching vibrations of P-O-P bonds associated with metaphosphate chains [105]. Considering the fact that with increasing SrF_2 content in the samples the relative field systematically increases and the center shifts towards

lower wave numbers, it is possible that this is an image of a gradual disintegration of the ring units, which take the form of chains.

The bands located around 862 cm^{-1} and 829 cm^{-1} were distinguished only in the case of modeling the spectrum of PKBN glass and were assigned to the vibrations of BiO_6 octahedra and BiO_3 pyramidal units [117]. It is also probable that the vibrations of the Nb-O bond contribute partially to these bands.

Symmetric stretching vibrations of the P-O-P bond were described as the cause of the absorption band located at ~800 cm^{-1} [108]. Initially, the weak band determined for PKBN was significantly enhanced, reaching the highest intensity after the introduction of 5 mol% SrF_2. At the same time, the aforementioned enhancement was accompanied by a significant shift towards higher wave numbers (823 cm^{-1}). In the case of PKF10 and PKF15 glasses, the corresponding band was located near 810 cm^{-1} and was characterized by a decreasing R_a value, which may be due to partial replacement of symmetric P-O-P bonds by P-O-M induced by structural changes related to the appearance of the modifier. The adjacent weak band, depending on the composition, was located in the range of 765 – 740 cm^{-1} (absent for PKF10) and could not be identified. The absorption band characterized by the center located at ~735 cm^{-1} has been described as a possible effect of symmetric stretching of P-O-P bonds forming ring units [105, 112]. The changes induced by the addition of 5 mol% SrF_2 are revealed by a strong reduction in intensity and a shift towards lower wave numbers (720 cm^{-1}), which can be understood as a consequence of the breaking of bonds forming rings. However, a further increase of fluoride content probably leads to an increase in the cross-linking of the structure, and a renewed increase of the relative field is observed as well as a small shift of the band towards higher wave numbers.

The band located at about 700 cm^{-1} probably corresponds to the deformation vibrations of the corner-shared NbO_6 octahedra [118], and the absorption located at ~640 cm^{-1} can be attributed to the vibrations of the Bi-O bond [112]. Based on the analysis of the compositions of the glasses, it can be concluded that in these materials there are generally structural units based on Bi and Nb atoms, most probably in different coordinations 3 and 6-coordinated. The changes occurring with the introduction of different SrF_2 contents, in the case of Bi and Nb, are concentrated around the incorporation of these cations into the glass structure, and thus are the effects of the transition from the role of a modifier to a conditional network former. The next band occurs only for PKBN and PKF15 glasses and is located at ~627 cm^{-1} and is related to the presence of oxygen polyhedra NbO_6 [108, 118], similarly to the ~700 cm^{-1} band it describes deformation vibrations.

The band located at ~605 cm^{-1} together with the neighboring band at ~570 cm^{-1} were jointly described as the effect of the Bi-O bond vibrations in strongly deformed octahedra [117]. The first of the mentioned absorptions reaches the maximum of the relative field for the PKF5 sample with a simultaneous significant shift towards higher wave numbers, while the second one is characterized by the highest R_a value for PKA10 and a slightly shifted band center for PKF15. Two bands in the range of 548 – 528 cm^{-1} were identified as related to the deformation vibrations of Q_0 units [105, 112, 113]. The first of the bands is characterized by low intensity and was observed only for PKF5. The changes in the parameters of the second band, analogously to the tendency already observed in these materials, are the strongest when 5 mol% of the modifier is introduced. It is worth mentioning that in the work of Glasstwin et al. [114] the band around ~530 cm^{-1} was determined to originate from the coupled deformation vibrations of Q_0 units with the vibrations of the Nb-O bond, which could explain the increase in R_a with the increasing fluoride content in the glasses. The band around 500 cm^{-1} is characterized by a significant relative field only in the case of the PKF5 sample and was assigned to the vibrations of the Nb-O bond related to the occurrence of edge-shared NbO_6 octahedra [118]. In this case, the transient nature of Nb is visible, which with the increasing fluoride content is more likely to be randomly incorporated into the lattice than to form highly coordinated units. The spectral components around 475 cm^{-1} and 470 cm^{-1} (occurring only in PKBN) were assigned to the deformation vibrations of the O-P-O bond [105] or bonds in the BiO_3 unit [112, 119]. The band located at ~440 cm^{-1} may be the effect of the Bi-O bond vibration in strongly distorted BiO_6 octahedra [117]. The last of the bands located at ~420 cm^{-1} was observed only for the PKF series and was identified as the Nb-O bond vibration [114].

UV-Vis analysis

Figures 20 and 21 present the comparisons of absorption spectra obtained in the wavelength range of 190 – 1100 nm for the base glasses PKBN - PKF and their counterparts doped with 0.5 mol% Eu, respectively. The data in Figure 20 indicate that in the case of as-prepared glasses, there are no excess absorption bands originating from the matrix components themselves, which could modify or adversely affect the emission properties of the material. The recorded level of transmittance of the glasses in the visible light region is in a fairly wide range from ~75% for PKBN to ~50% for PKF10, but these results do not show an unambiguous dependence of this parameter on the SrF_2 content. The same conclusion can be reached by analyzing the spectra of samples containing the Eu dopant (Figure 21). The origin of the differences is probably mostly related not so much to the material properties themselves (transparency, comparison with Figure 12), but to the specificity of the measurement, which was

performed on mechanically unprocessed samples. This choice was motivated by the difficulty of polishing the samples, which resulted from the small thickness of the melted glasses, and the type of information requested because the focus was mainly on the occurrence of absorption bands and qualitative delineation of the transparency range of the samples. Apart from the exclusion of the occurrence of excess absorptions for glasses containing a share of Eu, two characteristic bands were observed, resulting from electronic transitions in Eu^{3+} ions, regardless of the composition of the glasses, these were the transitions $^7F_0 \rightarrow {}^5L_6$ (395 nm) and $^7F_0 \rightarrow {}^5D_2$ (465 nm). In this way, both the usefulness of the synthesized glasses in optical applications and, indirectly, the fact of the incorporation of Eu^{3+} ions into the glass matrix were confirmed.

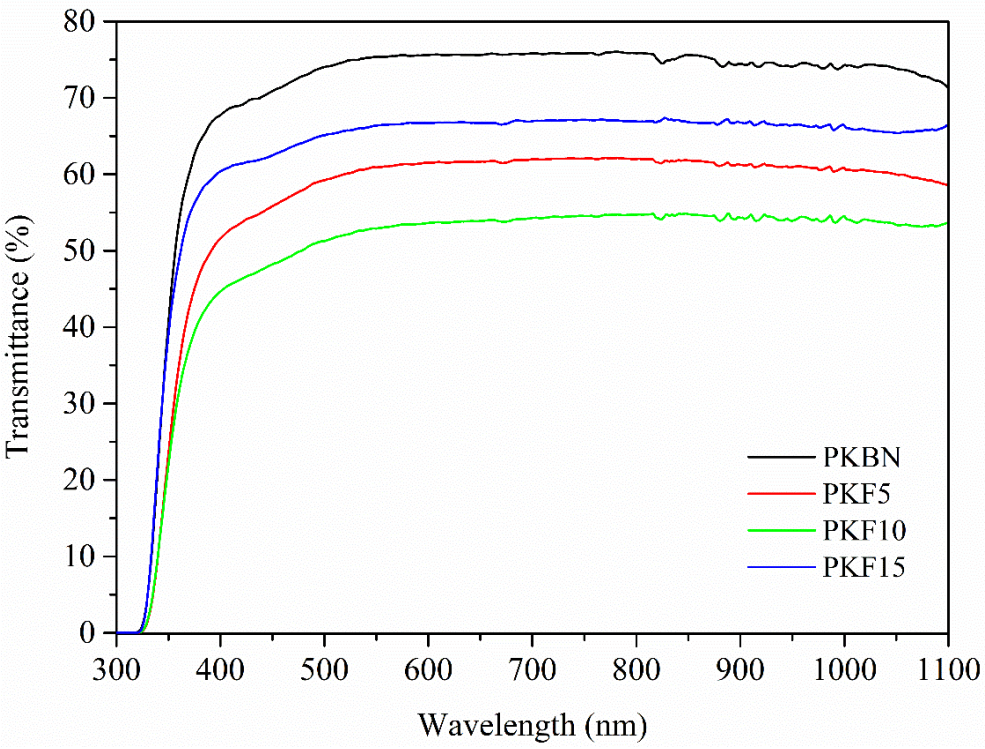

Fig. 20 UV–Vis spectra obtained for undoped PKBN - PKF glasses

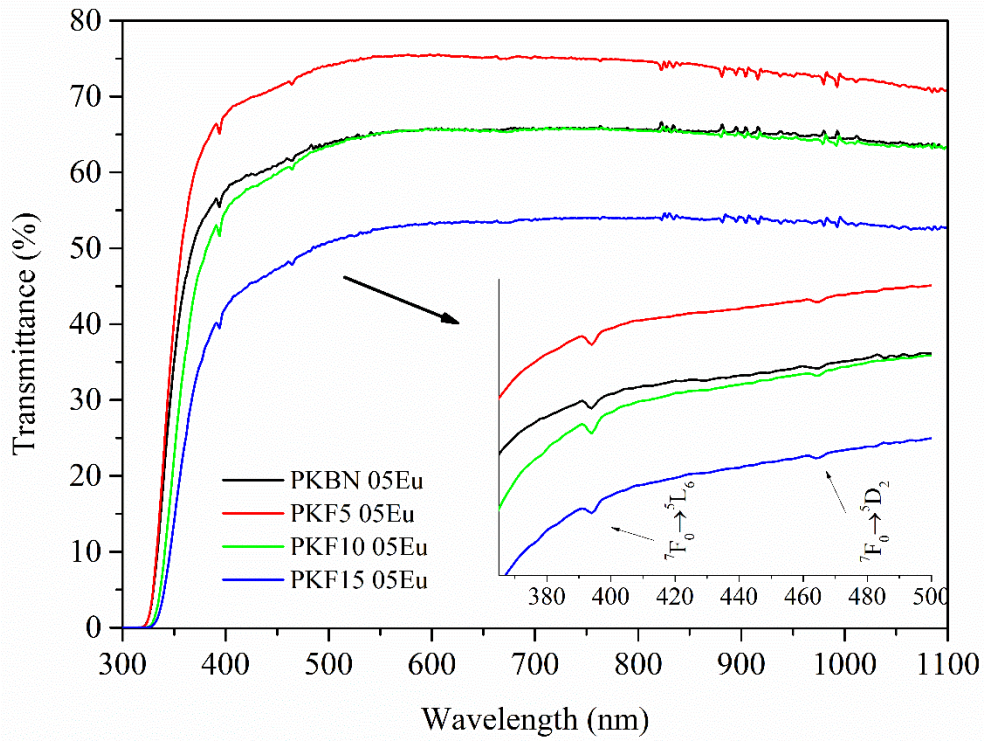

Fig. 21 Comparison of UV-Vis spectra obtained for Eu doped PKBN - PKF glasses. Enlarged spectral range include a description of Eu^{3+} absorption bands

Luminescence analysis

Luminescence measurements carried out for both as-prepared glasses doped with Eu and the series subjected to annealing allowed for the analysis of the effect of SrF_2 content and thermal treatment process on the emission properties of Eu^{3+} ions. Figure 22 presents a comparison of excitation spectra recorded for unannealed glasses at the observation of the wavelength λ_{em} = 615 nm (a) and emission spectra obtained using the excitation wavelength of λ_{ex} = 465 nm (b). The following method of data presentation allowed for a more convenient highlighting of the effects induced in PKBN – PKF 05Eu glasses by the change in fluoride content.

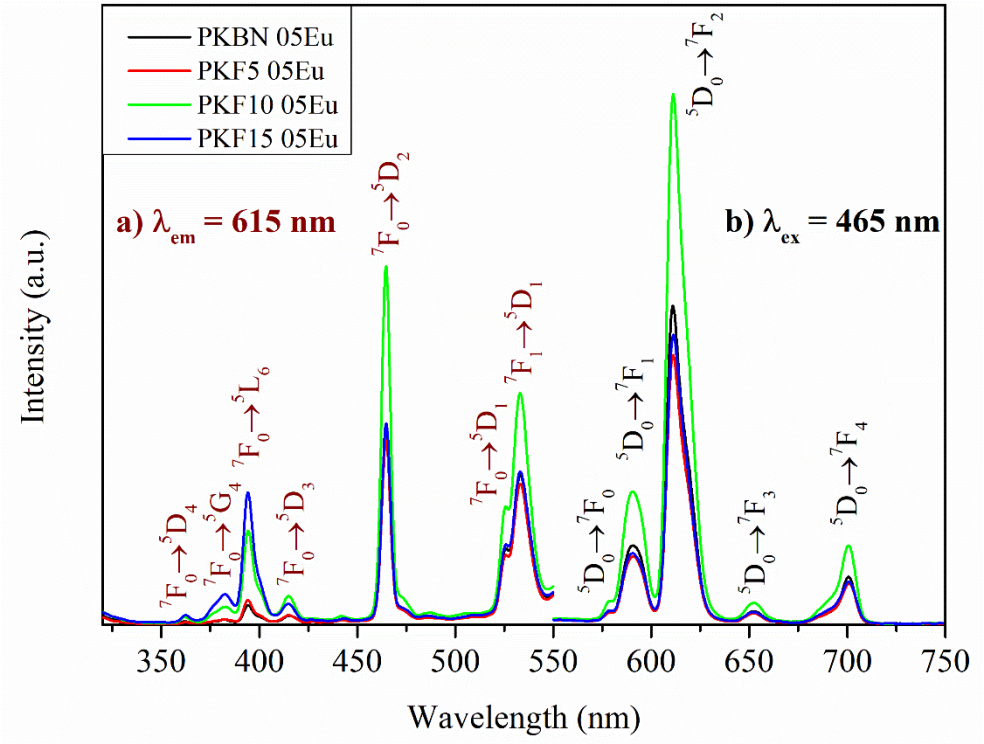

Fig. 22 Summary of a) excitation (λ_{em} = 615 nm) and b) emission (λ_{ex} = 465 nm) spectra recorded for as–prepared glasses doped with 0.5 mol% Eu

The form of excitation spectra contains distinguishable information in the form of 7 maxima representing electronic transitions of Eu^{3+} ions. These transitions are: $^7F_0 \rightarrow {}^5D_4$ (362 nm), $^7F_0 \rightarrow {}^5G_4$ (383 nm), $^7F_0 \rightarrow {}^5L_6$ (395 nm), $^7F_0 \rightarrow {}^5D_3$ (415 nm), $^7F_0 \rightarrow {}^5D_2$ (465 nm), $^7F_0 \rightarrow {}^5D_1$ (525 nm) and $^7F_1 \rightarrow {}^5D_1$ (533 nm). The highest intensity of the mentioned electronic transitions was observed at wavelengths of 395 nm, 465 nm, and 533 nm. Among the listed maxima, it can be seen that in the case of the measurement performed for the PKF10 05Eu glass, they are distinguished by a significantly higher intensity when compared to the other compositions. However, this statement does not include the maxima observed for wavelengths smaller than 425 nm, where, disproportionately to the rest of the excitation spectrum (comparing the data recorded for PKBN 05Eu and PKF5 05Eu, one could expect similar values in the ultraviolet also for PKF15 05Eu), a higher intensity was recorded for the PKF15 05Eu glass. Taking into account the dependencies observed in the excitation measurements, in the case of emission properties studies, it was decided to use the excitation wavelength λ_{ex} = 465 nm in all experiments concerning these materials. The emission spectra recorded for the corresponding parent glasses were also summarized in Figure 22 in part b), thus providing a complete picture of the luminescence properties of these materials. Despite the differences between the glasses tested, no new bands or their significant shift were observed. For each composition, it was possible to distinguish

maxima associated with the radiative transitions of Eu^{3+} ions from the excited $^5D_0$ level to the ^7F_J states (J = 0, 1, 2, 3, 4). They were located at wavelengths of 579, 590, 611, 652, and 701 nm, respectively. Similarly to the results of excitation measurements, based on a simple comparison, it can be stated that in the case of PKF10 05Eu glass, almost twice as high emission intensity was observed compared to the intensities observed for the other glasses.

The influence of the process itself and the annealing parameters on the emission properties was determined, among others, on the basis of the emission spectra presented in Figure 23. Sections a - d were separated accordingly to the compositions of the compared glasses and glass-ceramics.

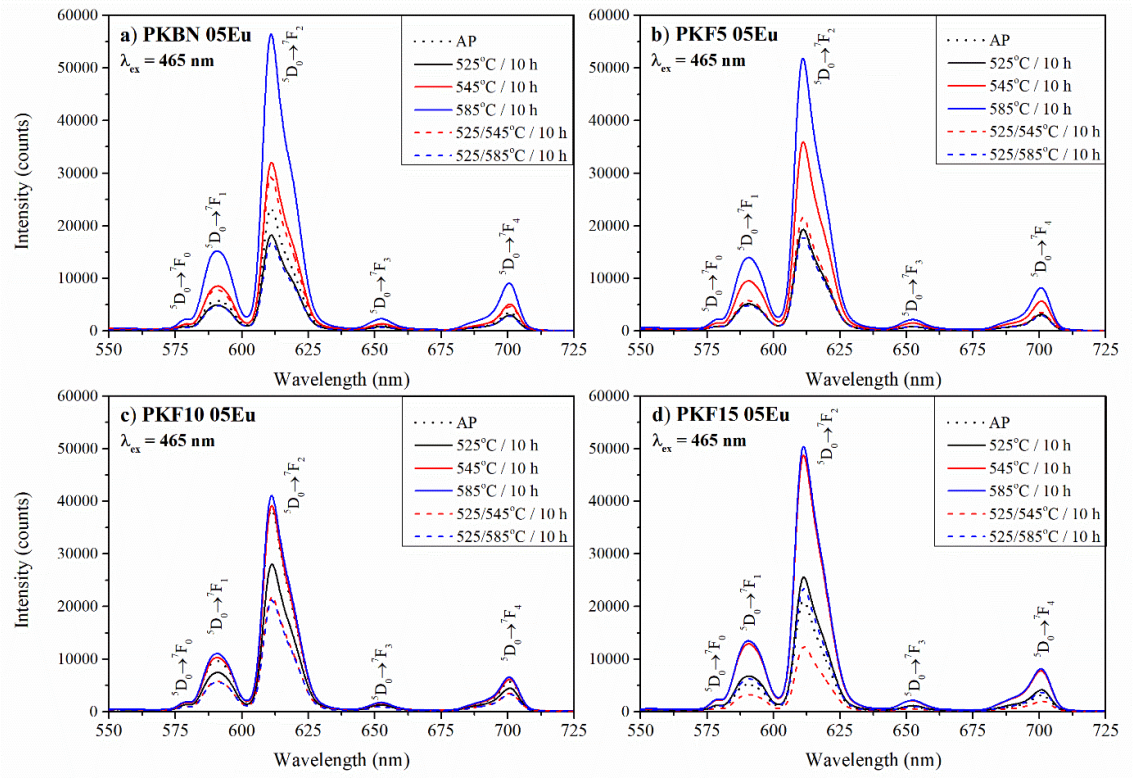

Fig. 23 Summary of emission spectra (λ_{ex} = 465 nm) of glasses and glass-ceramics illustrating the effect of the performed annealing on the luminescent properties. The results were grouped according to the compositions, respectively: a) PKBN 05Eu, b) PKF5 05Eu, c) PKF10 05Eu and d) PKF15 05Eu

Each section contains a summary of emission spectra at excitation λ_{ex} = 465 nm of as-prepared glasses (identical to the curves in Figure 22 b), glasses annealed individually at 525, 545, and 585 °C for 10 h, and glasses subjected to two-stage annealing, in which the first stage took place at 525 °C for 10 h and the second at 545 or 585 °C for 10 h. The main of the generally observed changes (for all compositions) caused by the annealings performed is the change in the intensity of the bands, in particular, it is important to emphasize the effect of the enhancement of the luminescence of Eu^{3+} ions. Apart from that, no new bands were observed, excepting those identified for the matrices in Figure 22.

Focusing on the evolution of the obtained spectra within specific compositions, first of all, the comparison presented in Figure 23 a) containing the results of materials obtained in the process of thermal treatment, for which the initial matrix was PKBN 05Eu glass, should be analyzed. As can be seen, for samples heated individually at 545 °C and 585 °C and twice at 545 °C the intensity recorded was higher than for the glasses not subjected to annealing, at the same time the glass-ceramics obtained at the highest of the above-mentioned temperatures was characterized by the most intense emission – almost 3 times higher compared to the as-prepared glass sample. It is surprising to note the weakening of luminescence in the case of the sample heated at 525 °C, for which, taking into account thermal and XRD measurements, no significant changes influencing the luminescent properties would be expected. In Figure 23 b) the collected spectra show dependencies similar to those observed for the PKBN 05Eu series, in particular, for the two materials showing the highest emission intensity (545 and 585 °C 10h). The addition of 5 mol% SrF_2 caused that both the samples subjected to double annealing and those singly annealed at 525 °C were characterized by an intensity similar to the as-prepared sample. As shown earlier, for the unannealed PKF10 05Eu glass, a distinctively high luminescence intensity was recorded, the slight increase of which was noted only for the materials annealed at 585 °C (section c of Figure 23). Apart from the sample subjected to thermal treatment at 545 °C, the other process variants led to obtaining materials with significantly lower emission intensity. The introduction of 15 mol% SrF_2, despite the relatively low intensity shown by the as-prepared glass, turned out to have a beneficial effect on the properties of the annealed materials. A luminescence enhancement was observed, similar in nature to that shown by PKF10 05Eu, but taking into account the reference of as-prepared glass, the increase is more than twofold. The general conclusion from the data presented in Figure 23 is the highest intensity of Eu^{3+} ion emission in materials subjected to annealing at 585 °C for 10 h, regardless of composition. The role of single annealing at 545 °C should also be highlighted, which in the case of PKF10 05Eu and PKF15 05Eu glasses guaranteed an intensity slightly lower than that obtained at 585 °C. Taking into account the above observations and economic and ecological considerations, annealing at 545 °C can be considered a competitive alternative if limited to compositions containing 10 and 15 mol%. In this respect, the PKF15 05Eu sample annealed at 545 °C is the most promising of all, combining high intensity with optimal annealing process parameters. Taking the above point of view, in which the set of parameters is "optimized" in a non-binding way for the application, it is worth mentioning the unannealed PKF10 05Eu sample, which in economic criteria, in the absence of annealing, is able to guarantee a promising level of emission intensity. Although it is inferior in parameters to the annealed equivalent with 15 mol% SrF_2, it is an interesting case to consider.

In order to emphasize the effect of the variable SrF_2 content in the annealed glasses on their emission properties, Figure 24 presents a summary of spectra grouped according to the annealing parameters used. Due to the low intensities and slight differences between the spectra obtained for the samples annealed twice at 585 °C, they are omitted in the following summary

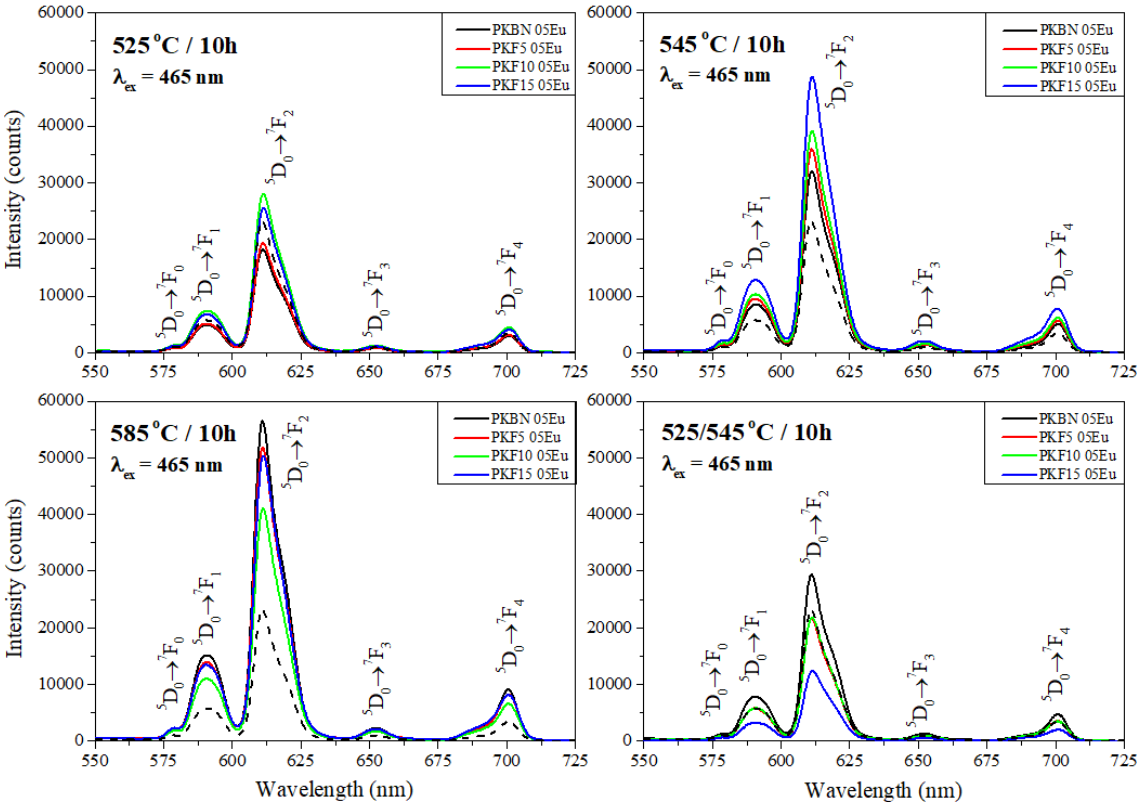

Fig. 24 Emission spectra (λ_{ex} = 465 nm) of PKBN 05Eu – PKF15 05Eu samples subjected to annealing at 525, 545, 585 °C for 10 h, respectively, and double annealing at 525/545 °C. The dashed line additionally shows the spectrum of as-prepared PKBN, which serves as a reference in this case

Starting the analysis from the lowest of the applied temperatures, a clear demarcation is visible, which is determined by the spectrum of the unannealed PKBN 05Eu, which is the reference. In accordance with the previously outlined dual nature: samples PKBN 05Eu and PKF5 05Eu (similar in properties) after heat treatment are jointly characterized by a weakening of the emission, and for materials containing 10 and 15 mol% of fluoride, higher intensities were recorded than those observed in the reference spectrum. Although this effect is subtle, due to the slight disturbance of the glassy system caused by the relatively low annealing temperature, the tendency shown in the developed crystallization characteristics and thermal measurements is visible. At the same time, it should be emphasized that annealing had the most noticeable effect on the PKF10 05Eu sample, whose spectrum before the process, characterized by an intensity much higher than the others, significantly lost its intensity after its occurrence. One of the probable explanations suggests that this could be due to the occurrence of structural reorganization, which ultimately

led to the disappearance of the optimal emission conditions obtained during the melting process itself. Glasses subjected to a 10 h process at 545 °C (upper right part of Figure 24), despite a relatively slightly higher temperature, present a slightly different situation. With the increasing share of fluoride in the compositions, the annealed materials showed a gradual increase in the emission intensity with a slightly distinguishable PKF15 05Eu spectrum.

The image of the SrF_2 effect in the case of annealing with, as it was possible to determine, the most favorable parameters (585 °C 10 h) was presented in the lower left section of Figure 24. As can be seen, this way of presenting the data brought an unexpected result, because it emphasized that the highest emission intensity was recorded for the PKBN 05Eu glass-ceramic. The proposed explanation of this state of affairs can be based on the previously presented DTA/DSC results (Figure 10) and XRD of doped glass-ceramics (Figure 17). The glass transition temperature determined based on the thermal analysis of the PKBN glass is clearly lower than the values determined for the glasses containing a share of SrF_2, which may result in greater susceptibility to crystallization. Moreover, convergent conclusions about the weaker cross-linked structure of this glass were obtained on the basis of the FTIR spectra analysis (Fig. 17). As shown by XRD measurements characterizing the crystallization of undoped glass (Fig. 11), the above observations indicate that annealing the PKBN matrix, in comparison to the other compositions, can lead to the formation of a material containing a larger share of the spontaneous crystalline phase. Therefore, it can be expected that the glass-ceramics formed by thermal treatment of PKBN 05Eu at 585 °C for 10 h will be characterized by a high degree of crystallization with a dominant $BiPO_4$ phase. It cannot be ruled out that the presence of crystallites of the latter compound as well as partial segregation of Eu^{3+} ions ultimately leads to the enhancement of the luminescence of active centers. Reports describing the usefulness of $BiPO_4$ as a host for rare earth ions described in [120-122] confirm the above-proposed explanation. However, this is not the only factor conditioning the luminescence enhancement, which is confirmed by the PKBN 05Eu sample annealed twice at 585 °C, which showed a surprisingly low emission intensity, despite the clear presence of $BiPO_4$ precipitates. The factor behind the observed distinction is probably subtle and concerns change in the immediate vicinity of Eu ions, which could have occurred due to the extended time of the double thermal treatment experiment.

Apart from the case of PKBN 05Eu, it is also worth considering the second of the extreme results obtained for glasses heated at 585 °C for 10 h, namely PKF10 05Eu, for which a significantly lower emission intensity was noted than for other samples from the PKF series subjected to the heating process with the above-mentioned parameters. This result is particularly interesting due to the fact, emphasized in the characterization process, of its great similarity to PKF15 glass; the proposed explanation for this observation is as follows. Considering

compositions containing the SrF_2 additive, the emission intensity observed for PKF5 05Eu can be explained similarly to PKBN 05Eu by the dominant presence of $BiPO_4$ crystallites (phases characteristic of higher fluoride contents are still a minority), in this case the transitional nature of this composition is evident. However, when comparing the diffractograms of the annealed samples PKF10 05Eu and PKF15 05Eu (Fig. 15 d), a clear difference can be seen – in contrast to PKF15 05Eu, in the case of lower SrF_2 content, reflections indicating the presence of a crystalline phase were observed. Of course, the presence of nanocrystals below the detection threshold in the material with 15 mol% cannot be unequivocally ruled out. Taking into account the additionally developed crystallization characteristics, in particular the appearing phases, one can put forward a hypothesis that excessive growth of crystallites of the phase marked as UnP, appearing for these compositions, adversely affects the emission processes of Eu^{3+} ions dispersed in it.

The lower right part of Figure 24 presents a comparison of spectra of materials subjected to double annealing at 525/545 °C. By assessing based on the highest of the maxima, it can be seen that only for the annealed PKBN 05Eu glass the intensity (which is the reference) observed for as-prepared PKBN 05Eu was exceeded. In the remaining recorded cases the emission intensity is lower - in the case of PKF5 05Eu and PKF10 05Eu it was slightly lower, while in the case of the sample containing 15 mol% SrF_2, its level was significantly lower. Analyzing the results of luminescence measurements of samples subjected to double annealing, one can reach a general conclusion that this technique adversely affects the emission properties of the studied glasses, especially if they are compared with the spectra constituting their "components". The curves obtained in XRD measurements will not be of much use in this case, as can be seen in Figure 17 e, no reflections were recorded on them except for the amorphous halo. Individual observations suggest that the low spectral intensities observed for the doubly annealed samples are not so much related to the applied temperatures, but to the re-annealing threshold phenomenon itself, regardless of whether an observable crystalline phase is formed as a result or not. It is possible that this is an effect similar to that described for the as-prepared PKF10 05Eu sample, whose emission intensity decreases significantly when annealed already at 525 °C. Therefore, it is likely that it is the process carried out at 525 °C that affects the glassy system in such a way that it creates an unfavorable initial state for the next annealing carried out at a higher temperature.

The analysis presented above was based on a simple concept of comparisons, but thanks to it, it was possible to determine promising directions of glass modification by analyzing the conditions of the annealing process allowing to obtain their optimal emission properties. As a result, it was possible to determine the mutual influence of annealing conditions and SrF_2

content on luminescence, including the justification for using this process in a single-stage and two-stage version. In the case of the latter, the problem of structural reconfiguration introduced with the first annealing at 525 °C was outlined, which ultimately led to completely different results than in the case of direct application of the target temperature. One of the possibilities is the occurrence of nucleation of a new phase in the material, the premises of which are provided by the diffraction pattern of the PKBN 05Eu glass-ceramic obtained in double annealing at 585 °C, on which single reflections of an unknown phase not appearing in other samples were recorded.

Taking advantage of the fact that in the case of Eu^{3+} ions the $^5D_0 \rightarrow {}^7F_2$ transition is hypersensitive, i.e. strongly dependent on the symmetry of the ion environment, and the $^5D_0 \rightarrow {}^7F_1$ transition is a magnetic dipole transition independent of the ligand field, the ratio of their intensities known as the red/orange ratio (R/O) was calculated. This parameter describes the strength of ionic or covalent interactions between Eu^{3+} ions and the surrounding ligands, and its decrease after annealing can be interpreted as a confirmation of the partial incorporation of active centers into the higher symmetry environment of the precipitated crystallites [77,123,124]. The results of the calculations are presented in Figure 25, where the R/O values are compared with the annealing conditions in which the corresponding materials were formed. As can be seen, regardless of the SrF_2 content, the glasses before annealing were characterized by a significantly higher value of the parameter, which decreased after the thermal treatment, which may indicate the occurrence of Eu^{3+} ion segregation. Analyzing the trends of R/O changes with increasing annealing temperature, two trends can be distinguished: in the case of PKF5 05Eu, the parameter value decreases almost linearly with increasing single annealing temperature, while PKF10 05Eu and PKF15 05Eu samples were characterized by practically constant R/O values for both single and double annealing processes. Clearly different behavior in the case of double annealing at 525/585 °C was demonstrated by glass-ceramics based on PKBN 05Eu and PKF5 05Eu – the R/O parameter values were significantly lower for them.

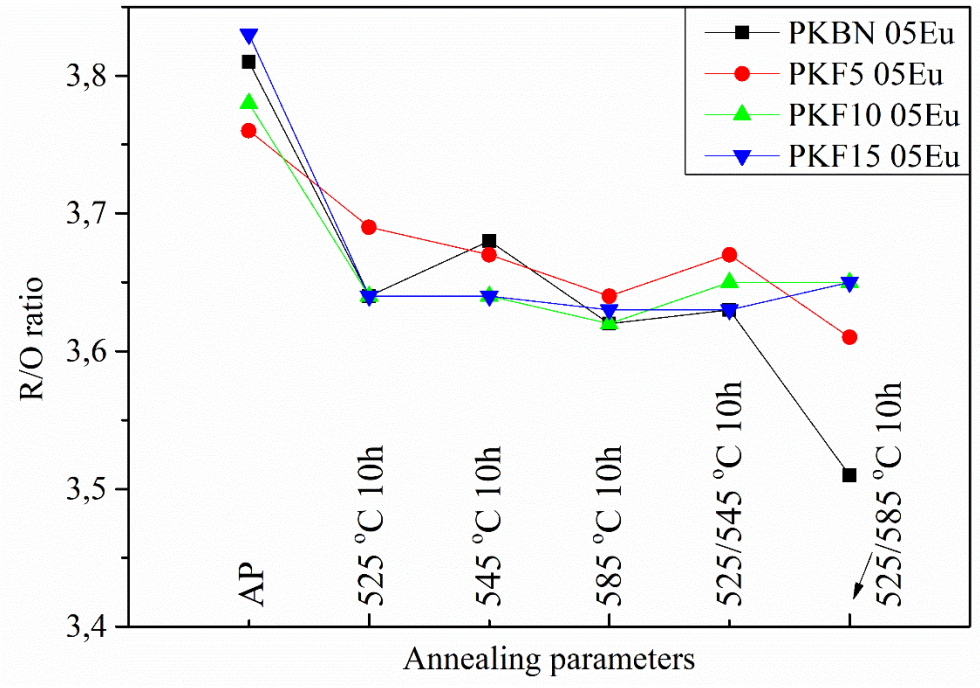

Fig. 25 Graph showing the evolution of the R/O parameter calculated for glasses and glass-ceramics subjected to annealing processes, the parameters of which are included on the X-axis. The lines connecting the points serve only as a guide for the eye to see the occurring trend

The above analysis provides indirect evidence for the segregation of Eu^{3+} ions into precipitates formed during controlled crystallization. This allows for comprehensive conclusions about the effect of annealing on the emission of deposited active centers, which complements the findings collected using XRD. Thus, despite the lack of visible reflections of crystalline phases, the above comparison directly emphasizes that Eu^{3+} ions in each of these cases (different annealing parameters) experienced a change of environment to one characterized by higher symmetry. It should be realized that this is only another aspect of the same phenomenon and only guarantees simple qualitative information about the change of environment after any annealing because no correlation with the emission intensity shown by these materials was quantitatively observed.

Luminescence decay measurements

Additional insight into the relationship between the immediate environment and the emission properties of Eu^{3+} ions contained in the tested glasses and glass-ceramics was provided by measurements of the luminescence decay by observing the $^5D_0 \rightarrow {}^7F_2$ (615 nm) transition at 465 nm excitation ($^7F_0 \rightarrow {}^5D_2$). The results obtained for the PKBN – PKF 05Eu matrices are presented in Figure 26. Already at the first stages of the analysis it was observed that regardless

of the composition, the recorded decay curves are characterized by a double-exponential character [125], which can be written as the relation:

$$I(t) = A_1 e^{\frac{-t}{\tau_1}} + A_2 e^{\frac{-t}{\tau_2}}, \quad (9)$$

where τ_1, τ_2 are the lifetime components, A_1, A_2 are the corresponding amplitudes and the variable t corresponds to the time

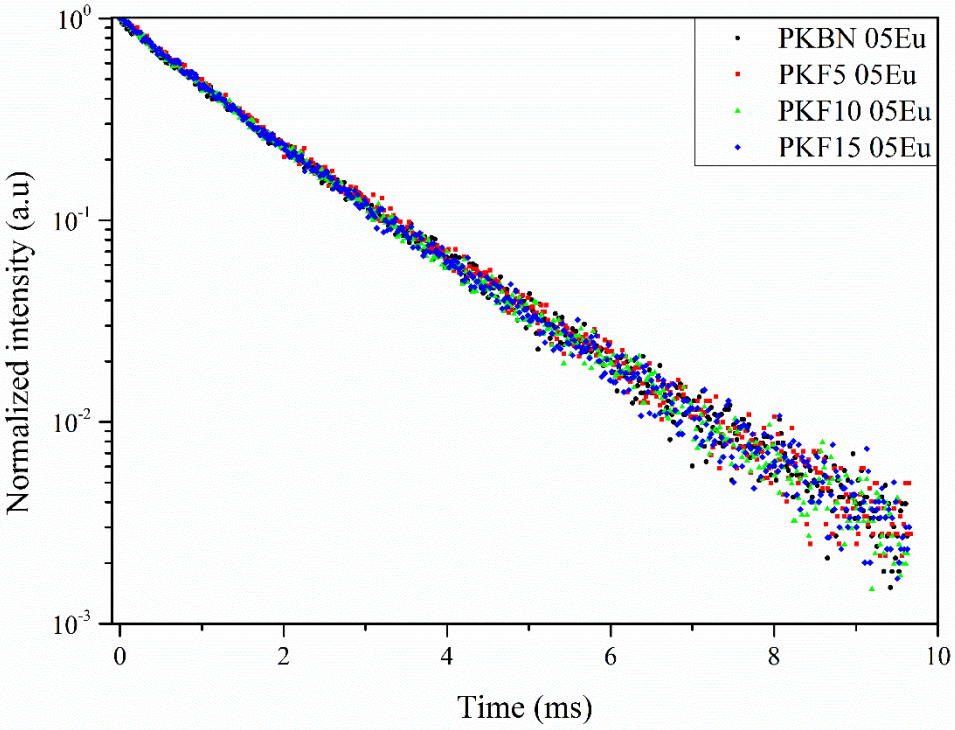

Fig. 26 Comparison of luminescence decay curves obtained for PKBN – PKF15 glasses doped with Eu^{3+} ions

The modeling of the measurement data carried out with the above expression allowed for the extraction of key parameters, which are presented in Table 5, additionally, the calculated average decay times are included there. The unusual observation of the double-exponential decay for both as-prepared matrices and samples subjected to annealing could indicate that Eu^{3+} ions experience two different types of closest environments. In this interpretation, a longer lifetime is associated with an environment with higher crystal field symmetry, while a shorter one with lower [124,126,127]. The general occurrence of the complex form of the curves suggests a dual segregation of dopant ions in theoretically homogeneous materials, which was demonstrated in the case of unannealed glasses. The explanation of the above peculiarity can be based on the

probability of spontaneous micro-separation occurring at the melting stage, as a result of which Eu^{3+} ions found themselves in slightly different configurations of the amorphous glass network, guaranteeing a difference in symmetry. At the same time, it is not possible to clearly determine directly from the data contained in Table 5 whether the material described by a given set of parameters is glass or glass-ceramics, so there is no simple correlation of decay times with heat treatment conditions and emission properties. However, in the case of amplitude average lifetimes, a general increase in the value of this parameter was observed for samples that were annealed.

	PKBN 05Eu	PKF5 05Eu	PKF10 05Eu	PKF15 05Eu	PKBN 05Eu 525°C 10h	PKBN 05Eu 585°C 10h	PKF10 05Eu 525°C 10h	PKF10 05Eu 585°C 10h
τ_1	0.89	2.04	1.51	0.90	0.70	0.44	0.59	0.70
τ_2	1.74	1.09	0.56	1.71	1.68	1.58	1.57	1.68
$<\tau>_{Int}$	1.53	1.57	1.45	1.50	1.56	1.52	1.50	1.56
$<\tau>_{Amp}$	1.37	1.44	1.36	1.40	1.79	1.89	1.78	1.79
A_1	0.39	0.36	0.84	0.41	0.30	0.21	0.22	0.30
A_2	0.59	0.65	0.16	0.60	0.94	1.14	1.05	0.94

Table 5. Parameters obtained by fitting decay curves measured for doped PKBN–PKF15 matrices and selected glasses annealed for 10 h at 525 and 585 °C. Based on the above data, intensity and amplitude average lifetimes were calculated. The lifetime values were given in ms

3.2. Materials containing addition of AlF_3 and KF

XRD

The XRD measurements confirmed the amorphous nature of the synthesized glasses and provided insight into the crystallization process occurring during the annealing series. The curves presented in parts a) and b) of Figure 27 are devoid of any crystalline phase reflections and in the range from 20 to 50 ° the occurrence of an amorphous halo characteristic of glasses was observed.

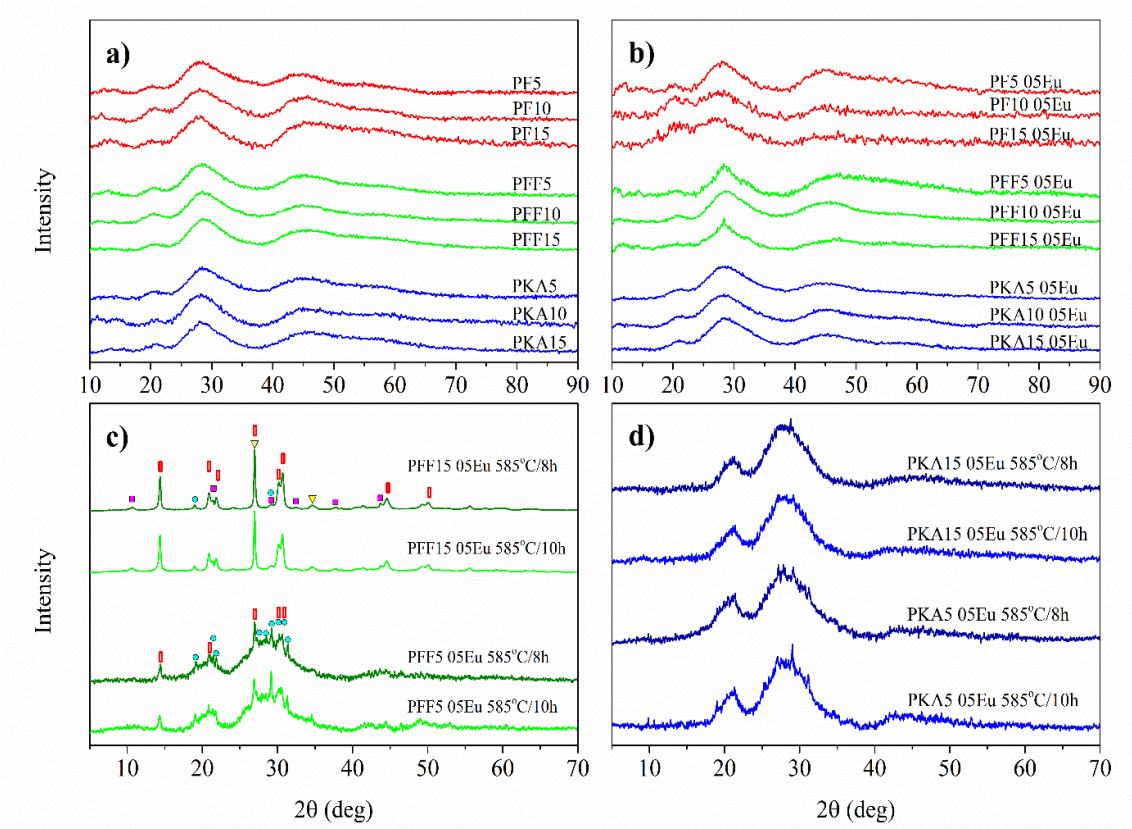

Fig. 27 Comparison of diffraction patterns: three series of as-prepared glasses a) undoped and b) doped with 0.5 mol% Eu_2O_3. Due to their form, these results confirm the amorphous nature of all obtained materials. In addition, the lower part of the figure contains diffraction patterns of glasses and glass-ceramics obtained in the process of annealing selected compositions from the c) PFF and d) PKA series. In the case of the first of the above-mentioned, the following crystalline phases were observed: circle - monoclinic $BiPO_4$; rectangle – unknown phase; square - KNb_3O_5; triangle - Bi_2O_4

The selected compositions were additionally subjected to annealing at 585 °C for 8 or 10 h in order to extend the analysis, in particular, to find the answer whether, despite other purposes, “non-crystallizing” fluorides can affect the luminescence properties of these materials. Analysis of the results presented in Figure 27 c indicated that as a result of heat treatment of PFF5 05Eu and PFF15 05Eu glasses, multiphase crystalline precipitates were obtained in them. Among the reflections observed in the diffractograms of glass-ceramics based

on PFF5 05Eu glass, peaks belonging to the crystalline phase of monoclinic $BiPO_4$ and an unidentified phase were distinguished, which with high probability may be the UnP phase (or its variant) observed in previously described glass-ceramics containing an SrF_2 additive. In the case of PFF15 05Eu, crystallites identified as KNb_3O_5 and Bi_2O_4 were additionally distinguished in the better-defined diffractogram. The first conclusion from the comparison presented in Figure 27 c is the lack of significant differences between the diffractograms of the samples heated for 8 and 10 h, in both cases the maxima correspond to each other in terms of intensity and position. The second, more important conclusion is the difference in the XRD results obtained for glass-ceramics containing different KF contents. Clearly, for higher fluoride content, the heated samples were characterized by better-defined reflections and the lack of dominant amorphous maxima (compared to the PFF5 05Eu glass-ceramics), these features may suggest that the discussed glass-ceramics may have a higher degree of crystallinity. Thus, the proportional addition of KF reduces the stability of glasses to crystallization, and this effect is proportional to the applied share.

The opposite situation to the one described above was observed for the annealed samples from the PKA series, the diffraction patterns of which are shown in Figure 27 d. Regardless of the AlF_3 content and the annealing time, all the curves had a similar form with strongly outlined amorphous halo and few maxima protruding slightly above their envelopes. They probably come from the initially forming crystalline phase. Due to the form of the supposed reflections being at the border of measurement noise, it was impossible to make an identification. As can be seen, in accordance with expectations, the addition of AlF_3 influenced the cross-linking of the glass structure, thus leading to an increase in their stability against crystallization. In the case of the glass-ceramics described above, it is particularly beneficial to correlate the obtained XRD results with the photos of the corresponding samples taken after the thermal treatment process (10 h at 585 °C). These photos are shown in Figure 28.

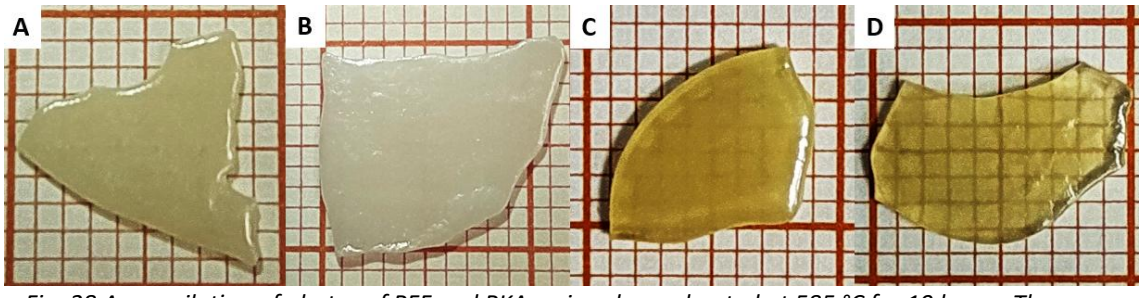

Fig. 28 A compilation of photos of PFF and PKA series glasses heated at 585 °C for 10 hours. These are respectively: A – PFF5 05Eu; B – PFF15 05Eu; C - PKA5 05Eu; D – PKA15 05Eu

Undoubtedly, at first glance it is possible to match the photos to the appropriate diffraction pattern of the PFF or PKA series from Figure 27. In the case of glass-ceramics from the first of the above-mentioned series, as a result of crystallite growth, they lost transparency, became uniformly opaque with partially melted edges. The difference in the form of samples A and B, i.e. PFF5 05Eu and PFF15 05Eu glass-ceramics, respectively, is significant in this case. The greater crystallinity of sample B is manifested by the loss of the characteristic yellowish color in favor of white, thus resembling a ceramic material. At the same time, the sample did not lose its surface features, which would occur in the case of complete melting. This case is exceptionally interesting due to the fact that based on XRD and the photo alone, without knowing the history of the material, it would be impossible to unequivocally assign it an amorphous nature. This conclusion emphasizes the scale of the effect exerted by KF on the internal structure of the glasses and the resulting extreme annealing results. On the other side of this extreme are the samples from photos C and D in Figure 28, which only slightly became cloudy after the annealing process. Despite almost congruent diffractograms, the samples differing in AlF_3 content showed a different reaction to heat treatment, which results in the difference in their transparency observed in the photos.

DSC and DTA

DSC and DTA measurements conducted for glass matrices from three series (PF, PFF, and PKA) allowed one to determine the thermal characteristics of these materials, which, apart from characteristic temperatures, included conclusions on the influence of the type and content of fluorides introduced into the glasses on their thermal properties. The obtained measurement curves were compared and presented in Figure 29 in the convention introduced in Figure 10. The temperatures read from the graphs together with the temperatures determined for the PKBN matrix, which facilitated the comparison of results, were collected in Table 6. Starting the analysis from glass transitions, it should be noted that regardless of the type or method of introducing fluorides (in the case of PF5/PFF5) into the compositions, their mere appearance in the glass led to an increase in the T_g value compared to the initial PKBN glass. This general observation is not obvious, especially in the light of the performed annealing, it could be expected that the addition of KF in the highest content used would lower the glass transition temperature. This reveals another level of complexity of the glasses tested, which will be expressed in the following analysis of mutual changes in the characteristic temperature values.

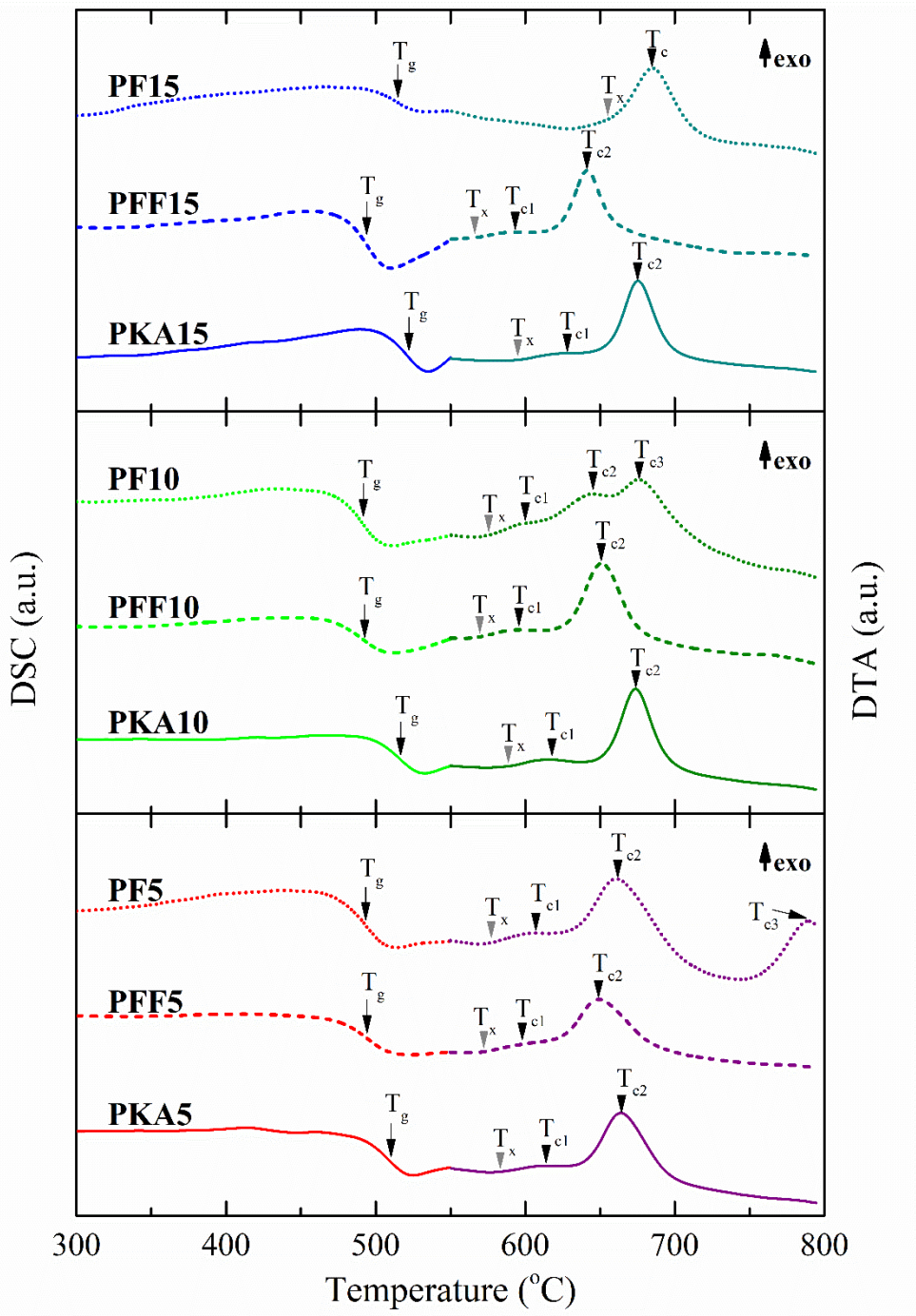

Fig. 29 Results of DSC (left part) and DTA (right part) measurements of glasses from the PF, PFF and PKA series, for modifier contents of 5–15 mol%. The curves corresponding to the two techniques were rescaled and compared to each other to present the overall characteristics of the measured glasses. Characteristic temperatures are marked with arrows: T_g – glass transition temperature, T_x – onset temperature associated with the first T_c, which is the crystallization temperature (exothermic maximum)

In glasses containing AlF_3 additive, already in the composition containing 5 mol% of the modifier, the effect of the increase in the T_g value is clearly visible, which can be identified as the effect of increase in the cross-linking of the structure. The probable mechanism responsible for the occurrence of this process is the formation of Al-O-P bonds instead of P-O-P bonds, characterized

by a more covalent character [128,129]. The confirmation of the above thesis can be the gradual increase in the glass transition temperature value with the increasing fluoride content, up to T_g = 522 °C noted for PKA15. This temperature is also the highest among those determined for all compositions from the 3 series of glasses. Considering the glasses from the PF series, practically the same glass transition temperature was recorded for both PF5 and PF10 ($T_g \approx 493$ °C), only a further increase in the KF content leads to a rapid change of almost 22 °C, reaching T_g = 515 °C. In the case of the seemingly twin PFF series, the glass transition temperature is practically independent of the fluoride content used and similar to that recorded for PF5 and PF10. The presented data suggest that in the case of the T_g parameter, a different method of introducing KF into the compositions of the PF and PFF series has an observable effect for a threshold value greater than 10 mol%. Due to the fact that in the PF series, the addition of KF takes place proportionally at the expense of the share of K_2O in the composition, the glass is depleted in K^+ cations modifying its lattice. As a result, the reduced alkali content has a smaller effect on the internal structure of the material, fewer NBOs are formed that weaken the glass network, which is macroscopically manifested by a higher T_g temperature [30,128]. The above interpretation may explain the observation of a higher T_g value for PF15, but at the same time, it emphasizes the different behavior of the PF10 sample, for which an intermediate value would be expected.

Sample	T_g	T_x	T_{c1}	T_{c2}	T_{c3}
PKBN	488	621	651	698	-
PF5	493	577	607	661	789
PF10	492	576	600	646	676
PF15	515	655	685	-	-
PFF5	495	572	598	649	-
PFF10	493	569	595	651	-
PFF15	494	566	593	642	-
PKA5	510	583	614	664	-
PKA10	517	589	617	674	-
PKA15	522	595	628	675	-

Table 6. Characteristic temperatures (°C) determined from DTA/DSC measurements. The notations used are analogous to those introduced in Fig. 29

Moving on to the issue of exothermic maxima observed on the measurement curves (Figure 29), it is necessary to emphasize the twofold tendency separating the series studied. The first group includes the PFF and PKA series. Two exothermic events were recorded for them, the

first of which is not very intense, and the second maximum, which follows it at higher temperatures, is characterized by much higher intensity. The second group includes the PF series and was distinguished due to completely different features, namely, three exothermic maxima were observed for glasses containing 5 and 10 mol% KF, while only a single maximum appears for the PF15 measurement curve. In the case of the DTA curve obtained for PF5, attention should be paid to the maximum described as T_{c3}, because its incomplete form and extreme location with relatively small interference in the composition (compared to other compositions containing 5 mol% fluorides) mean that it cannot be ruled out that it is a measurement artifact. The reason for the observed differences and distinctiveness of the PF series is probably the disproportionate way in which fluoride was introduced into them, thus disturbing the stoichiometry of the components.

The evolution of exothermic effects occurring under the influence of proportional addition of KF (PFF series) was not dictated by drastic changes, similar to the changes in the glass transition position. With a gradual increase in fluoride content, the first maximum T_{c1} (analyzed from left to right of the graph) shifts slightly towards lower temperatures. This change occurs while maintaining a constant width of the maximum, which can be defined, among others, by the expression $T_{c1} - T_x \approx 26$ °C. Thus, while maintaining a constant peak width, with increasing KF content, the shift leads to a gradual decrease in the thermal stability of the glasses, defined as $\Delta T = T_x - T_g$. Using the fact that the heating rate (10 K/min) was maintained during the measurements, it is possible to interpret the correlation between the width of the crystallization maximum and the time necessary for crystallization to occur, as described in [98]. In this approach, it became possible to draw more complete conclusions about the effect exerted by the proportional addition of KF on the properties of the glasses. Hence, it should be emphasized that despite the moderate effect on the thermal characteristics of PFF series glasses, the proportional addition of KF causes that, without a significant change in the crystallization kinetics, the resistance of materials to crystallization decreases with its increasing share. An excellent experimental example of the above relationships was presented in the performed annealings, the results of which are included in part c of Figure 27. It should be emphasized that the considerations so far were based on the analysis of the exothermic maximum T_{c1}, in which the beginnings of the crystalline phase are probably formed, and the actual crystallization process of glasses is represented by the generalized effects of T_{c1} and T_{c2}. It is the change in the position of T_{c2} in the case of PFF15 glass (shift towards lower temperatures) that may be the reason for the increase in the crystallinity of the obtained glass-ceramics, including the appearance of additional crystalline phases.

The strong influence exerted by the addition of AlF_3 on the position of the glass transition of the PKA series samples is also distinguished in the case of exothermic effects observed in DTA measurements. With the increase of the modifier content from 5 to 10 mol%, only a slight increase in the value of the T_{c1} parameter was noted, only in the case of PKA15 the position of the maximum shifts by almost 10 °C towards higher temperatures. A better illustration of the changes taking place is possible by loosely comparing the values shown with those observed for the PFF series. As can be seen in the comparison included in Table 6, regardless of the fluoride content, the T_{c1} and T_{c2} values for PKA glasses are much higher than for their PFF counterparts. In both of the above-mentioned series, the width of the second of the maxima decreases with the increasing share of modifiers. Moreover, the distance between the T_{c1} and T_{c2} peaks is comparable in both series and is the largest for samples with 10 mol% fluoride (~56 °C) and the smallest for 15 mol% (~48 °C).

Moving from the analysis taking into account the mutual dependencies within specific glass series to the approach taking up the subject of changes in thermal characteristics occurring due to the content of modifiers used, it is necessary to start from the lower part of Figure 29 containing a summary of measurements of glasses with the addition of 5 mol% fluorides. Since this is the lowest content used, it can be described as the initial stage of the action of the introduced additives, in which the observed changes in the glasses are still insignificant, but the initial directions of the effects caused are already clear. The disproportion in the compositions, and therefore also in the content of K^+ ions between PF5 and PFF5 is still small enough that minor shifts in characteristic temperatures are observed (excluding the uncertain maximum of T_{c3} for PF5). Of these 3 compositions, the PKA5 sample stands out due to its clearly higher T_g. It should be emphasized that both the introduction of 5 mol% KF and AlF_3 lead to the occurrence of a thermal effect in the form of a maximum marked as T_{c1} (~600 °C), which was not observed in the case of the PKBN matrix. The presence of this peak may indicate a potential narrowing of the thermal stability range, but it should be taken into account that it is not shifted towards lower temperatures. By making an analogous comparison of the measurement curves of glasses containing 10 mol% modifiers (middle part of Figure 29), it can be seen that the trends outlined for the lower content are maintained, thus increasing the mutual differences. Additionally, for the PF10 glass, the appearance of a new exothermic maximum of ~650 °C was noted (assuming that the previously shown maxima did not change their positions significantly). The last of the comparisons (upper part of Figure 29) shows the differences caused by 15 mol% modifiers. Apart from slight shifts of characteristic temperatures in the curves obtained for PKA15 and PFF15, the case of PF15 glass is particularly interesting, for which only a single exothermic maximum strongly shifted towards higher temperatures (T_{c1} = 685 °C) was observed.

The analysis of DSC/DTA measurements made it possible to outline the influence of the applied fluorides on the thermal characteristics of the glasses. At the same time, taking into account that the starting material for the modifications carried out was the PKBN matrix, it was possible to state that the thermal effect, which is manifested in this glass by the first exothermic maximum (T_{c1} = 651 °C) is in a sense "inherited" by all the resulting compositions containing fluoride additions. In the case of the PFF and PKA series, the equivalent of the above-mentioned phenomenon is the second of the observed maxima designated as T_{c2}. For the PF glass series, due to the evolution of exothermic effects forced by changes in composition, this effect maintains its form, but shifts towards higher temperatures with the increase of the KF share in the composition and can be attributed to the T_{c2} maxima for PF5, T_{c3} for PF10 and T_{c1} for PF15, respectively. The occurrence of what could be called in this context secondary exothermic effects is a manifestation of subtle changes in the structure of glasses, which potentially enable the formation of different crystalline phases or, on the contrary, rebuild the configuration of the glass network, preventing crystallization from occurring.

FT-IR analysis

A detailed description of the dependencies occurring in the structure of the studied glasses would allow for a comprehensive understanding of their properties and the effects exerted by the introduced modifiers. This task is extremely difficult due to the very nature of amorphous solids, which is why it was decided to conduct a thorough analysis of the FT-IR spectra of the glasses (Figure 30), based on which it was possible to partially explain the role of non-crystallizing fluorides in the materials. In addition, the importance of taking into account the influence of the Eu dopant on the internal structure of the glass was also considered. The spectra of the studied glasses (matrices and Eu doped) obtained in the range of 4000 - 400 cm^{-1} are presented in Figure 30. As can be seen, no significant changes in their shapes were noted in any of the spectra. Due to the lack of possibility of direct analysis of the effects related to the introduction of additives, it was decided to focus on the region of 1550 – 400 cm^{-1}, where the presence of characteristic absorption bands was demonstrated, the spectra of glasses limited to this region are presented in Figures 31 - 34. These bands are arranged in two main minima in the range of 1550 – 700 cm^{-1} and 700 – 400 cm^{-1} and in order to obtain information on the subtle evolution of the glass structure under the influence of different types and variable contents of modifiers, it was decided to carry out the process of their modeling. The results of this operation are presented in the above-mentioned figures and in Tables 7 a-c (placed at the end of the chapter). The following part proposes descriptions of the specified components of the spectra,

due to the desire to maintain clarity, the description of the band from a given series of glasses was each time preceded by its designation placed in brackets. Furthermore, a concept was used in which the default reference was the modeled PKBN or PKBN 05Eu spectrum (Figure 31), and specific bands were discussed with respect to the increasing fluoride content.

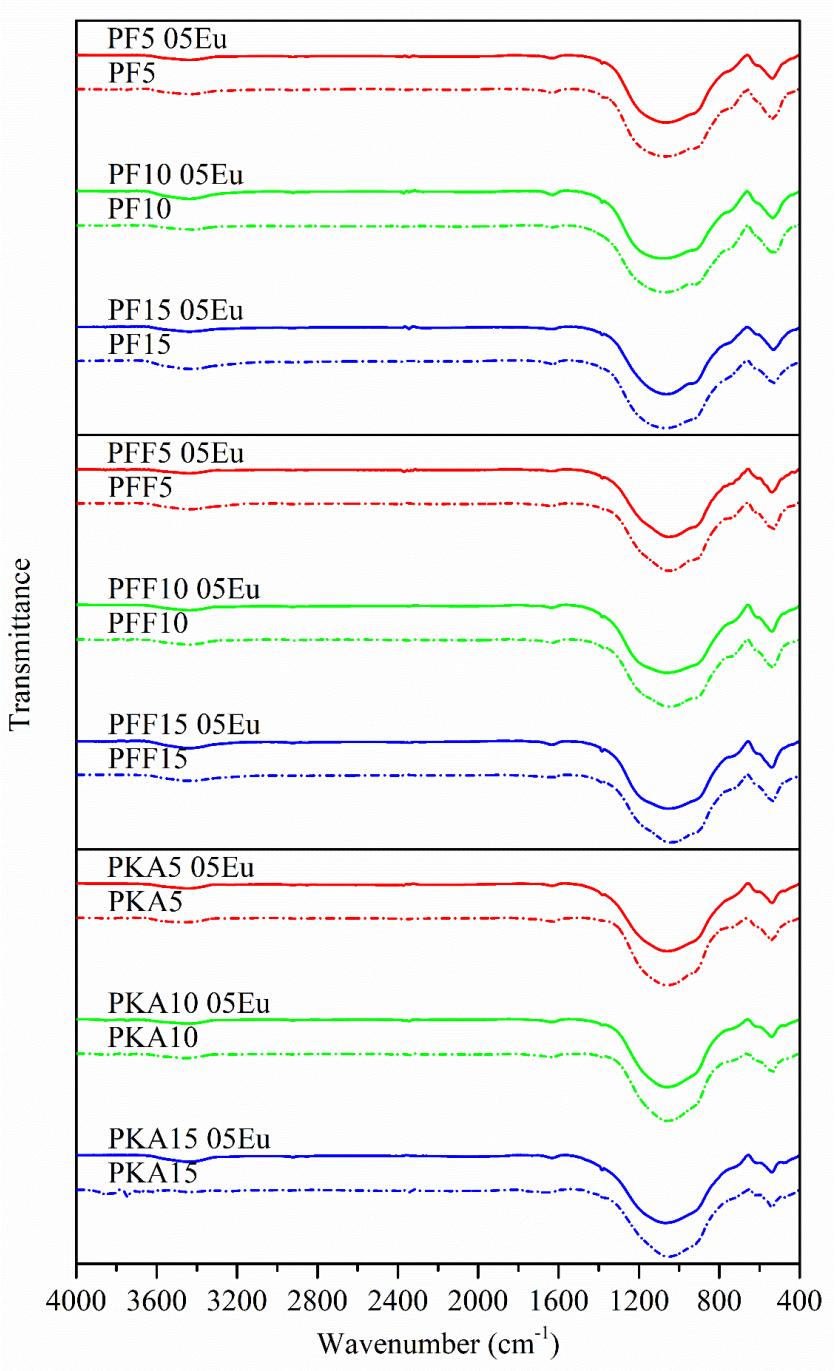

Fig. 30 Summary of FTIR spectra obtained for as-prepared glasses in the range of 4000 – 400 cm^{-1}. The dashed line indicates the spectra obtained for glasses doped with 0.5 mol% Eu

Description of structural changes caused by fluoride addition

(**PF**) Starting the analysis from higher wavenumbers (from the left side of the spectra), a band was distinguished for the PF series glasses, the center of which is located at ~1370 cm^{-1}. Due to its location, the description of this band is ambiguous. Among the probable matches of it are asymmetric stretching vibrations of P-O bonds in PO_4 units [130], additionally overlapping with harmonics of stretching vibrations of P=O bonds [108]. The increasing addition of KF affects the gradual increase of the band intensity, for PF15 the intensity was more than twice as high as in the case of the starting matrix. The reason for this observation may be related to the gradually decreasing amount of K^+ cations resulting from the method of introducing KF at the expense of K_2O (disproportionately in relation to the other components), and thus to the proportionally decreasing probability of "breaking" P=O bonds. (**PFF**) The opposite situation occurs in the case of glasses from the PFF series, where the decreasing band intensity with increasing KF content can be identified with the increased number of broken P=O bonds (the total number of modifier cations increases with the KF content). (**PKA**) For the PKA series, this band, depending on the composition, is in the range of 1380 - 1386 cm^{-1} of the spectrum and is characterized by very low intensity for glasses containing 5 and 10 mol% AlF_3. A further increase in the addition to 15 mol% results in a several-fold increase in the observed absorption band intensity. The noted changes can be explained by the way in which AlF_3 probably interacts with the glass structure, namely it modifies P=O bonds and P-O-Al bonds are formed. As a result, one of the band components disappears, the effect of which is visible as a decrease in the absorption intensity for PKA5 and PKA10 (compared to PKBN). The case of the increase in the band intensity for PKA15 can be considered as the effect of the second proposed band component (stretching asymmetric vibrations of the P-O bond), which becomes dominant under the influence of the modifier. Moreover, it cannot be ruled out that a significant addition of fluoride modifies the vibrations by incorporating fluorine anions into the structural units of the glasses, which would be partially confirmed by the observed shift of the band center towards higher wave numbers.

(**PF**) The next band in the proposed model is located at ~1240 cm^{-1} and can also be attributed to the vibrations of P=O bonds [110,131]. After introducing KF into the glasses, the intensity of this band gradually decreases, reaching a minimum for PF10 and is shifted towards higher wave numbers. This is additional information about the moderate effect of this modifier on P=O bonds and much more complicated dependencies of the internal structure, in which depolymerization cooperates with the coordination of modifier ions. (**PFF**) The band distinguished for the PFF series (1177 – 1208 cm^{-1}) is characterized by a significantly higher intensity, which gradually increases with the KF share. Additionally, these changes are accompanied by a shift of the absorption band centroids towards lower wave numbers. It is

possible that this band represents several types of stretching vibrations of modified PO_2 units [113,132] and a certain variant of the equilibrium described earlier for the PF series is established here, assuming a still significant influence of P=O bond vibrations (**PKA**). In the case of the PKA series, the proposed model did not take this band into account; it is possible that this is the effect of strong cross-linking of the structure occurring in accordance with the mechanism described for the band located at ~1380 cm^{-1}.

(**PF**) The neighboring band (1135–1161 cm^{-1}) was not specified in the PKBN spectrum, while in the case of the PF series it is particularly intense. The increasing addition of KF causes the band center to gradually shift towards higher wave numbers, until reaching the upper limit of the above range in the case of the PF15 sample. The description of this band is related to the joint effect of asymmetric stretching vibrations of the PO_2 bond [108] and vibrations originating from the stretching of the P-O-(NBO) bond (non-bridging oxygen) [109]. The ratio of the individual components mentioned may change with the K^+ content. In addition, the possibility of oxygen exchange by fluorine and the formation of fluorophosphate units should be taken into account, in which the vibrations of mixed O-P-F bonds overlap with the PO_2 vibrations, causing a band shift [133]. (**PFF**) Analogously to the case of the PKBN matrix, this band does not occur in the PFF series. It is particularly interesting that due to the proportional introduction of KF, the increasing amount of K^+ cations, as it might seem, significantly deepens the differences between these compositions. The explanation takes into account the numerous O-P-F bonds formed by the addition of KF in mixed fluorophosphate units (described for the PF series), the presence of which causes the band to be strongly shifted towards higher wave numbers and merges with the neighboring band. This would partially explain the strong increase in its (localized band ~1200 cm^{-1}) intensity and the shift towards lower wave numbers progressing with the increasing KF content. (**PKA**) In the modeled spectra of PKA glasses, the localized bands ~1180 cm^{-1} are characterized by high intensity, which is practically independent of the AlF_3 content. Additionally, comparing the band positions with those noted for the PF series, it can be observed that they are significantly shifted towards higher wave numbers. This suggests that, in addition to the previously described shift associated with the incorporation of fluoride ions, an additional shift occurs due to the incorporation of Al ions, which stiffen the glass structure [134].

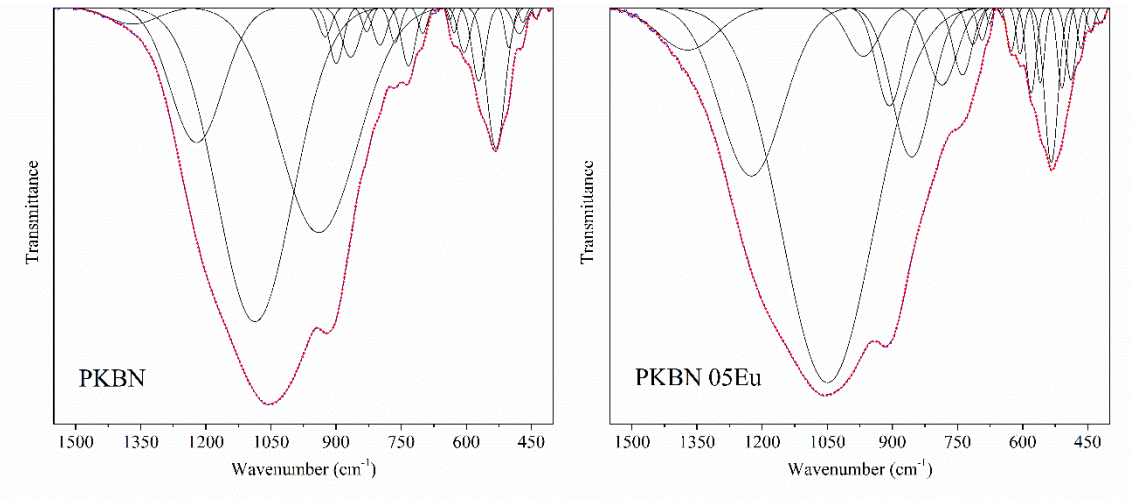

Fig. 31 Deconvolution results performed for fragments (1550 – 400 cm^{-1}) of the IR spectra of the PKBN matrix and its Eu-doped version. The experimental curves are marked with a solid blue line, the matched components of the bands (Gaussian) are marked with a black solid line, and the envelope of the simulated spectrum is marked with a red dotted line

(**PF**) The next band in the case of PKBN glass is located at ~1087 cm^{-1} and does not occur for PF samples. Its probable description is the effect of symmetric PO_2 stretching [114,132] or asymmetric P-O bond stretching (chain terminator) [112,113]. The characteristics of the PF series show that the decreasing K_2O content may be associated with a reduction in the number of Q_1 units, which could be one of the reasons for the absence of this band in the spectrum. (**PFF**) The strong band at about 1050 cm^{-1} in the PFF series glasses can be interpreted analogously to the band at ~1080 cm^{-1} in the spectrum of PKBN glass. The observed evolution under the influence of the increasing KF content in the composition has its genesis in the progressive process of depolymerization of the glass network. These changes are already significant in the case of the sample containing 5 mol%, in which the equilibrium between increasingly shorter phosphate chains and the Q_1 units formed as a result of their cracking leads to an initial increase in band intensity. The mentioned disproportionation reaction [30] of type $2Q_2$ --- $Q_1 + Q_3$ occurring in polyphosphate glasses may, however, be an explanation for the significantly lower intensity of the absorption band observed in the PFF15 spectrum. (**PKA**) The band changes (1042 – 1086 cm^{-1}) occurring with the addition of AlF_3 are twofold; in the case of PKA5 and PKA10, the observed intensity is relatively low, while for the sample containing 15 mol% of the modifier it reaches the level noted for PKBN glass. An analogy of this intensity evolution can be seen to that described for the band located at ~1380 cm^{-1}, but in this case, the absorption specified for PKA15 is strongly shifted towards lower wavenumbers (lower limit of the above range). In order to explain these changes, the reasoning proposed in this paragraph for PKBN can be applied. Considering the slight shifts of the bands for PKA5 and PKA10, the probable reason for their low intensity is the

smaller number of P-O units (chain terminator), resulting from the increasing Al/K ratio, which results in the incorporation of Al^{3+} cations. At the same time, the ongoing cross-linking process of the structure may result in partial replacement of O-P-O bonds by O-Al-O [134], which, apart from the high intensity of the band observed for PF15, would explain its shift towards lower wavenumbers.

(**PF**) The analysis to date clearly indicates that modifications of the PF glass network induced by the addition of KF lead to an increased probability of the occurrence of branched structures in the form of "chains" than in the PKBN glass. Taking into account the above findings, the band located at 940–990 cm^{-1} has been described as the effect of asymmetric stretching vibrations of the P-O-P bond [108,112,132]. Assuming that some of the introduced fluorine ions are incorporated into the glass structure, forming fluorophosphate units, the described band may also be the total effect of vibrations of the F-P-F bonds. In such a system, the increasing share of P-F bonds, due to the higher binding energy, could contribute to the gradual shift of the band towards higher wave numbers. It cannot be ruled out that the described band is partly derived from vibrations related to the presence of strongly deformed NbO_6 octahedra [135]. (**PFF**) In the case of the PFF series, the increasing addition of KF does not significantly affect the position of the band defined as ~970 cm^{-1}, but its intensity changes. The absorption observed for PFF5 and PFF10 is characterized by almost 3 times lower intensity than their counterpart containing 15 mol% KF. This band can be described analogously to the PF series, but the progressive depolymerization leads to a decrease in the number of P-O-P bonds, which would explain the decrease in intensity. Another effect of this process may be the appearance of Q_0 units [114] in the PFF15 glass, whose additional deformation vibrations could explain the increase in the band intensity. (**PKA**) The counterparts of the described band in the case of the PKA series are located in the range of 974 - 994 cm^{-1}, of which for samples containing 5 and 10 mol% AlF_3 a significant shift of absorption towards higher wavenumbers was noted (compared to PKBN). Moreover, the compositions mentioned are characterized by a large relative band area, in contrast to the PKA15 sample, for which a decrease in intensity by almost an order of magnitude was observed. The glass containing the highest content of AlF_3 used seems to be susceptible to abrupt changes in parameters, the explanation of which in this case is probably the effect of cross-linking of the structure through the formation of P-O-Al bonds.

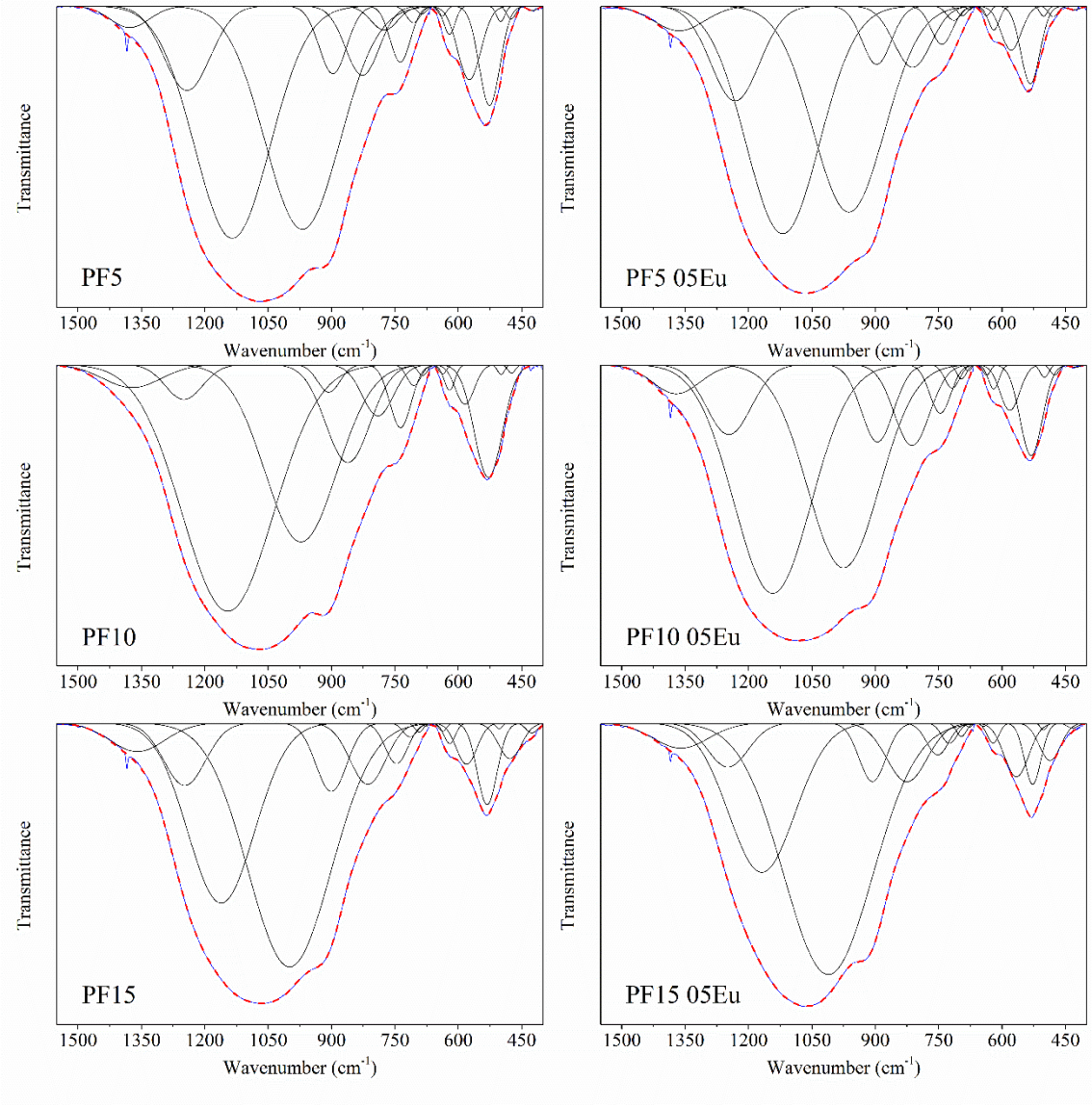

Fig. 32 Deconvolution results performed for fragments (1550 – 400 cm^{-1}) of IR spectra of PF series glasses and their Eu-doped versions. The experimental curves are marked with a solid blue line, the matched components of the bands (Gaussian) are marked with a black solid line, and the envelope of the simulated spectrum is marked with a red dashed line

(**PKBN**) The band centered at ~925 cm^{-1} was distinguished only in the spectrum of PKBN glass. It is characterized by low intensity and can probably be attributed to the stretching vibrations of the P-O-P bonds associated with the ring units [108].

(**PF**) The band located at ~900 cm^{-1} can be classified as the effect of the P-O-P bond stretching vibration associated with Q_2 units [108,136]. Among the PF series samples, it is worth highlighting the glass containing 10 mol% KF, for which the lowest band intensity was recorded with a simultaneous shift towards higher wavenumbers. (**PFF**) Comparison of the bands from the PFF series with that obtained for PKBN reveals that they have an order of magnitude lower

relative field values. Additionally, with increasing fluoride content, they shift towards lower wavenumbers. The use of a different convention of introducing KF into the compositions of PF and PFF glasses means that in the case of the latter, a less compact structure can be expected, in which the presence of Q_2 units is less probable. Referring to the disproportionation principle, this band can be described as a P-O-P bond stretching vibration in Q_3 units [130,133]. (**PKA**) The description of this band in the case of the PKA series will be analogous to that presented for PF glasses. The gradually increasing relative area of the bands with the increasing share of AlF_3 additionally indicates the role of the network strengthening by incorporating Al^{3+} cations into it.

(**PKBN**) The interpretation of the ~860 cm^{-1} band appearing exclusively for the PKBN matrix can be twofold, one of the possibilities are vibrations occurring in NbO_6 octahedra units connected in chains [118,135], which would also be evidence of their presence in the glass. The second description is the stretching vibrations of Bi-O bonds, indicating the presence of BiO_3 units [137]. The conclusion from the above description is the observation that the use of fluoride modifiers in PKBN glasses can partially limit the formation of extended units based on Bi and Nb cations.

(**PF**) The center of the next band is located at ~830 cm^{-1} and after the addition of 5 mol% KF its relative field increases significantly (relative to the low intensity band in the PKBN spectrum) reaching the highest value for PF10 glass. Together with the neighboring band located at ~790 cm^{-1} these bands are probably a representation of symmetric stretching vibrations of P-O-P bonds [108,112,113]. Interestingly, only in the case of the PF15 sample the second band was not isolated, which may be a manifestation of the "closing" of the structure, also visible in the results of thermal analysis. (**PFF**) The increasing addition of KF causes a strong shift towards lower wavenumbers to be observed for PFF10 and PFF15 glasses. For none of the samples from the PFF series, the complementary band observed in the PF series occurred, but apart from the analogous assignment of P-O-P vibrations, it is possible that in the case of 10 and 15 mol% KF, the influence of the vibrations of P-O-P bonds forming ring units is additionally revealed [108]. (**PKA**) Also in the case of the PKA series, the bands (for PKA5 and PKA10 there is a complementary band at ~780 cm^{-1}) were assigned to P-O-P bond vibrations, just like in the case of PF glasses. For the PKA15 sample, an increase in intensity and a shift towards lower wavenumbers were also observed, which together may indicate the effect caused by the additional vibration in AlO_4 units [136].

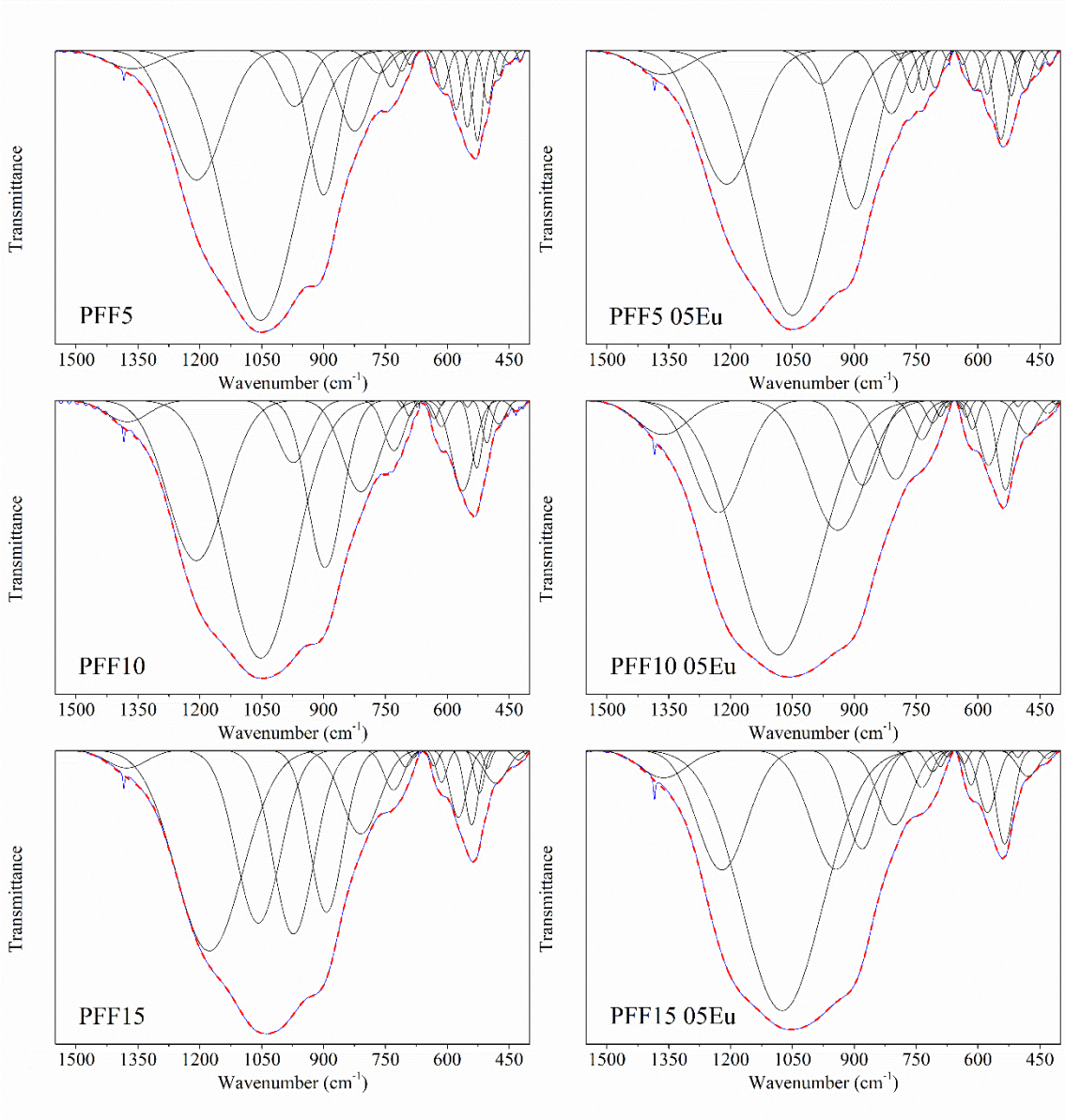

Fig. 33 Deconvolution results performed for fragments (1550 – 400 cm^{-1}) of IR spectra of PFF glasses and their Eu-doped versions. The symbols used are as for figure 32

(**PF**) In the spectrum of glasses from the PF series, the presence of the band located at ~764 cm^{-1} was not noted, which in the case of the PKBN matrix was described as the effect of vibrations related to the presence of structural units containing Bi-NBO [130] or Nb [135]. The occurrence of the described band together with the band located at ~866 cm^{-1} (occurs only for PKBN) seems to be a characteristic feature of glasses with a composition close to PKBN. (**PFF**) For this series, this band occurs only for the PFF5 sample, which does not differ significantly from the composition of the starting matrix and due to the similarity can also be designated as the effect of stretching vibrations of the Bi-NBO bond associated with BiO_6 units [130]. (**PKA**) The situation is more complicated in the case of the series containing the AlF_3 additive, because the discussed band also occurs in the spectrum of the PKA15 sample, which would seemingly

contradict the statement about the condition of similarity to the PKBN composition. However, this may be an effect related to the polyhedron vibrations associated with Al^{3+} ions.

(**PF**) The next band (733 – 746 cm^{-1}) shows a more than twofold increase in relative field after the introduction of 5 mol% fluoride, after which it reaches the maximum value for PF10. At the same time, a gradual shift of absorption towards higher wavenumbers is observed with the addition (the largest in the case of PF15). One of the probable description options are symmetric stretching vibrations of the P-O-P bond forming rings [108], the formation of more complex structures would explain the described evolution of the band parameters. (**PFF**) This band (729–736 cm^{-1}) has been interpreted as representing one of the stretching vibrations of the P-O-P bond [132] and is characterized by the highest intensity for the PFF10 glass. (**PKA**) Apart from the distinctive in terms of position and intensity band distinguished for the PKA10 sample, the addition of AlF_3 did not introduce a clear trend in the changes of the parameters. The shift towards higher wavenumbers and the large relative field may be partly related to the lack of an adjacent band (~750 cm^{-1}) for this composition. This could manifest the transitional nature of the glass containing 10 mol% AlF_3, in which, despite the relatively high content of the modifier, the abrupt changes characteristic of PKA15 are not able to occur, so it changes the glass structure but in a way that is not a direct consequence of the characteristics of the PKA5 sample. Although convoluted, this observation may reflect a delicate balance between the action of fluorine anions on the glass network and the Al cations gradually taking over the role of its formation.

(**PF**) The absorption centered at ~700 cm^{-1} can be attributed to deformation vibrations in the corner-shared NbO_6 octahedra [118,131]. The gradual increase in the band intensity at 5 and 10 mol% KF is reversed at 15 mol% and reaches the level observed for PKBN. Moreover, in the case of PF15, a weak band appears, defined as accompanying (~690 cm^{-1}), the presence of which suggests that in the described octahedra some oxygen atoms were replaced by fluorine. (**PFF**) For the series with proportional addition of KF, the situation is different, because for the PFF10 glass the accompanying band (~692 cm^{-1}) was observed, and the sample containing 15 mol% KF is characterized by band parameters similar to PKBN. A possible matching, apart from the previously described Nb-O vibrations, are symmetric stretching vibrations of Q_1 units [114]. (**PKA**) In this series, the band also corresponds to vibrations associated with NbO_6 octahedra, but its gradually decreasing intensity with the increasing content of AlF_3 may indicate the process of replacing Nb-based units by polyhedra containing the Al^{3+} cation.

(**PF**) In the case of the PF series, a weak band located in the range of 677 – 687 cm^{-1} does not occur in the spectrum obtained for PKBN and has not been identified. Moreover, the increasing share of KF causes this band to lose intensity and shift towards lower wave numbers. (**PFF**) A band located in a similar range is characterized by the lowest relative field for the PFF10

sample. (**PKA**) The description of absorption is even more complicated because it was not distinguished for PKA10, so in each of the studied series a different effect is observed and it is not possible to determine the trend of changes. However, what unites the mentioned cases is the lack of this band in the spectrum of the matrix from which they all originate, so it is reasonable to claim that its presence is related to the presence of fluorine ions in the structure of the glasses.

(**PF**) The band, the position of which (~638 cm^{-1}) is practically independent of the modifier content, can be attributed to the stretching vibrations of the Nb-O bond in slightly deformed NbO_6 octahedra [135] or the Bi-O bond in BiO_6 units [112]. The introduction of the additive causes a small increase in the band intensity, which remains close to constant with the increase of the KF content. (**PFF**) Despite the low-variability of the band position, the proportional addition of KF strongly influenced the intensity of the described effect, leading to its almost 3-fold increase (compared to PKBN). It was described analogously to the case from the PF series. (**PKA**) A strong influence on the glass structure of the introduced AlF_3 appeared in the case of this band, which is characterized by the largest relative field for PKA5, and does not occur at all for PKA15. The increasing content of the modifier leads to the disappearance of the NbO_6 structural units [135], the vibrations of which are presented in the described band.

(**PF**) Another of the isolated absorptions probably corresponds to deformation vibrations of NbO_6 units [118,131] and after introducing a modifier into the composition it shifts from 628 cm^{-1} to 621 cm^{-1}. Further increase of the KF share in the glasses is manifested by a small increase in intensity, which may suggest that the disproportionate addition of KF may have a beneficial effect on the formation of structural units based on Nb. (**PFF**) This band was not observed in the case of spectra of glasses from the PFF series, it may be the result of increased depolymerization of the glass network caused by the proportional addition of KF. (**PKA**) The mechanism described in the previous paragraph may also take place in the case of this band due to their common genesis, which results in the lack of this band for the PKA15 glass and the highest intensity noted for PKA5.

(**PF**) The center of the next band is located at ~605 cm^{-1} and can be described as the effect of vibrations of strongly deformed BiO_6 octahedra [117]. It was not distinguished in the spectra of glasses from the PF series, which may mean that in the case of these glasses, Nb-based units are more strongly promoted than Bi-based units. The opposite conclusion can be reached when analyzing PKBN glasses. (**PFF**) The same conclusions can be reached when analyzing the evolution of the corresponding band (611 – 614 cm^{-1}) in PFF glasses. The slightly increasing intensity for the sample containing 5 mol% KF and comparable with the matrix for higher shares indicate that the structural role of bismuth is particularly important in this series

(compared to Nb). (**PKA**) The observed gradual shift of the band towards higher wavenumbers and its abrupt decrease in relative field after introducing 5 mol% of the modifier indicate that the addition of AlF_3 limits the structural role of Bi. The absorption observed for PKA10 and PKA15 may therefore correspond additionally to the effect of O-P-O bond vibrations coupled to Nb-O [135], which are partially replaced by Al-F bonds, which is confirmed by the shift of the band center.

(**PF**) One of the main bands occurring in the described minimum is located at ~575 cm^{-1}. An increase in intensity was shown for the PF5 glass (almost twice the value noted for PKBN), after which the intensity dropped to a level close to the initial matrix for the subsequent glasses. Due to the unusual evolution and previous observations, the description of the origin of this absorption is complicated. In the case of PKBN glass, it can be attributed to the bending vibrations of the Bi-O bond in BiO_6 units [137], but in the case of samples containing fluoride, the presence of these polyhedra cannot be excluded, but the analysis so far has shown that they are not preferred in their structure. The increase in the relative field of the discussed band in the PF5 spectrum and its form in the case of PF10 and PF15 can therefore be explained by the transitional nature of the glass as a sample containing 5 mol% fluoride and the structural role of fluorine anions. On the one hand, the PF5 sample containing some of the matrix features (as described earlier) may still have an increased predisposition to base structural units on Bi atoms, but at the same time, they are modified with fluorine anions creating mixed Bi(O, F) polyhedra. Samples containing a larger share of KF show the dominance of the F incorporation effect, which results in a strong shift of the band towards higher wavenumbers. (**PFF**) A partially similar description as presented above can be applied to the band in the case of the PFF series, however, it is necessary to take into account the different characteristics of the appearing structural units. The smaller relative area of the bands observed for PKBN and PFF5 (compared to the compositions containing 10 and 15 mol% KF) may indicate a smaller amount of BiO_6 units caused by the presence of BiO_3 units previously demonstrated for these compositions. Analyzing the intensities of the remaining compositions in this convention, it can be stated that in the case of PFF10, only BiO_6 units dominate, while PFF15 containing both types of polyhedra is an intermediate system. (**PKA**) The addition of AlF_3, creating an environment not favorable to the formation of Bi-based polyhedra, caused the observed band (577 – 580 cm^{-1}) in the case of PKA5 to be characterized by an order of magnitude lower intensity compared to the PKBN glass. The slight increase in intensity shown by PKA10 and PKA15 samples probably has its origin in the overlapping stretching vibrations of Al-F bonds in AlF_6 or mixed groups [138].

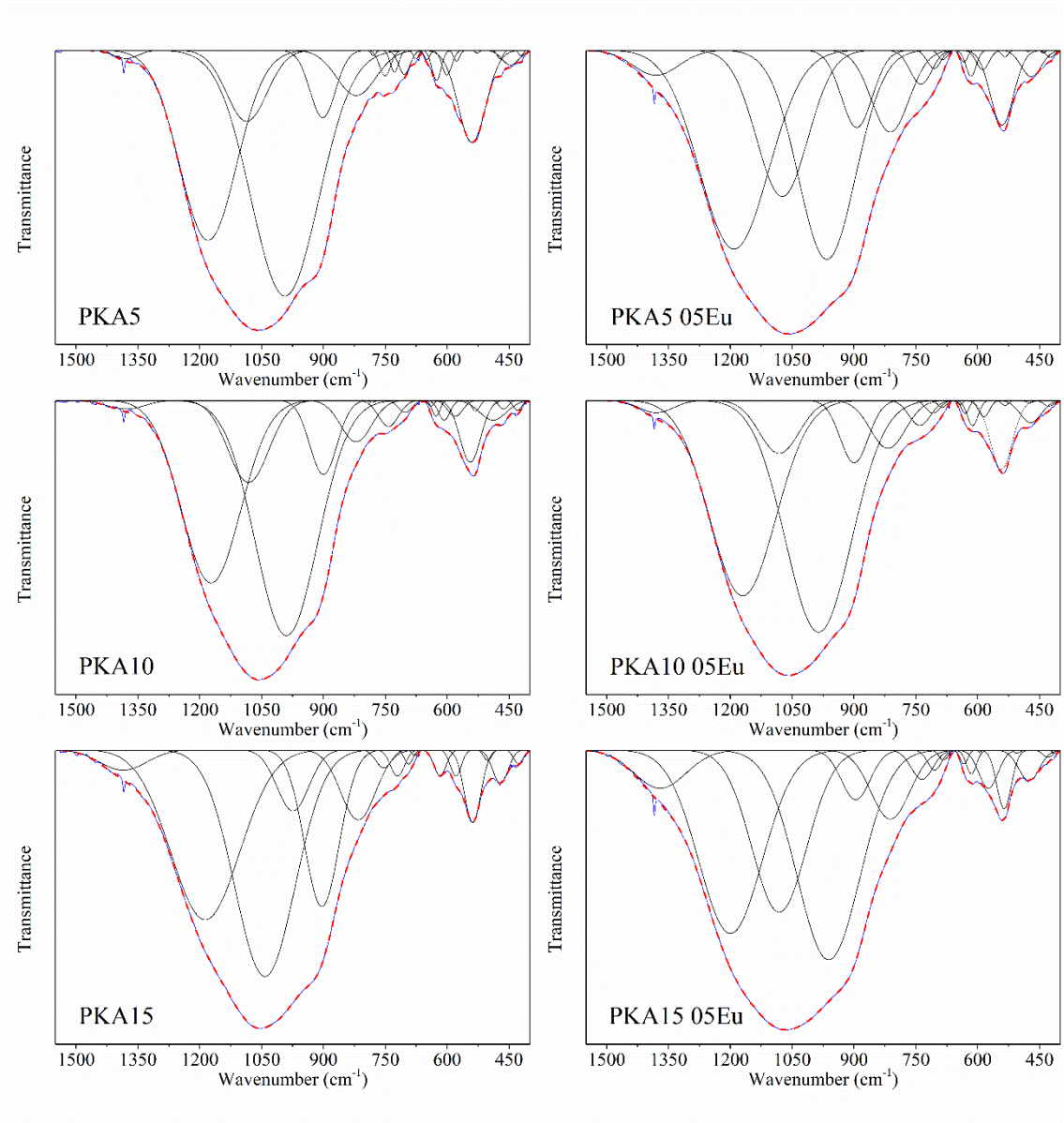

Fig. 34 Deconvolution results performed for fragments (1550 – 400 cm^{-1}) of the IR spectra of PKA series glasses and their Eu-doped versions. The symbols used are as for figure 32

(**PFF**) Absorption centered at ~545 cm^{-1} was not distinguished in the spectra of PKBN glasses and the PF series. The band present for the PFF10 glass, in contrast to the other samples from this series, was characterized by an intensity almost one order lower, which can be explained based on the description presented above for the neighboring band at ~570 cm^{-1}. In this approach, this band would be the effect of bond vibrations in BiO_3 units [117], which would explain the clearly lower relative field noted for the sample with 10 mol% KF. At the same time, the absence of this band in the spectrum of the PKBN glass and the distinctively high intensity of the next absorption suggest that more complex modifications may occur, which could result in band shifts. (**PKA**) In the series containing the AlF_3 additive, the band located at ~540 cm^{-1} is characterized by strong absorption for PKA5 and a clear decrease in its intensity for the other

samples from the series. This band is probably a manifestation of the Bi-O bond bending vibrations [137] and the vibrations of mixed $Al(O, F)_6$ units [139,140]. The occurring change in relative fields may result from the weakening of the influence of the first of the mentioned vibrations under the influence of the increasing share of AlF_3.

(**PF**) In the spectrum of glasses containing disproportionate KF addition, this band (~530 cm^{-1}) is the most intensive component in the low-wavenumber minimum. However, the interpretation of its origin is not unambiguous. As already mentioned in the previous paragraph, the PKBN sample may indicate that this absorption is attributed to the effects related to the bending vibration of the Bi-O bond [130]. Moreover, it should be considered to attribute the observations as the effects of coupled Nb-O bond modes with the bending vibrations of the O-P-O bond in PO_4^{3-} units [113,114]. (**PFF**) The gradual decrease in the relative field value observed for this series with the increasing share of KF in the composition may indicate the increasing role of coordinated K^+ cations in the glass network. (**PKA**) Contrary to glasses from the PKA series, the described band is very weakly intense, and the addition of 15 mol% AlF_3 causes it to disappear at all. Apparently, as a result of the introduction of the modifier, the units associated with the vibrations described above gradually disappear, which emphasizes the important role of Al atoms in the glass network.

(**PF**) The band centered at ~500 cm^{-1} was assigned to vibrations confirming the presence of edge-shared octahedra NbO_6 [118]. Increasing the KF content in the composition led to a gradual weakening of the band, which may be related to the decreasing O/Nb ratio exerted by replacing K_2O with KF. It cannot be ruled out that due to this effect the chance of forming isolated oxygen-niobium units in the glass network decreases. (**PFF**) The discussed component of the spectrum in the case of the PFF series increases rapidly after introducing 5 mol%, and then gradually decreases with increasing KF content in the glass. Due to the proportional way of introducing KF into the compositions, the O/Nb ratio remains constant, while the proportion of K to Nb atoms increases. The intensity changes are therefore probably a consequence of the initial opening of the structure, where, in addition to the previously mentioned ones, there are bending vibrations in the O-Nb-O-P bonds, the intensity of which decreases with the progressing depolymerization (induced by the increasing share of the modifier). (**PKA**) In the case of the PKA series, the band located at ~502 cm^{-1} was distinguished only for the PKA15 sample. The dominance of the structural role of AlF_3 may indicate that this band can be assigned to the deformational vibration of the glass skeleton, which is observable due to the increase in the stiffness of the network of the composition discussed.

(**PKBN**) The absorption localized at ~480 cm^{-1} is probably related to the bending vibration of the Bi-O bond in triangular units [137] and was not observed for the PF and PFF series. (**PKA**)

Interestingly, in the case of the PKA series, the mentioned band occurs only in the sample containing 15 mol% and its origin is ambiguous, although it may be related to the bending vibration of the P-O-P or Bi-O bond.

(**PF**) The evolution of the band located at ~475 cm^{-1} in the case of the PF glass series is as follows. For both the PKBN matrix and the PF5 and PF10 samples, the above band shows relatively low values of the relative field, only after the introduction of 15 mol% KF there is a drastic increase in intensity (by almost an order of magnitude) and a shift towards higher wavenumbers is observed. The probable effect behind this absorption is the bending vibrations of the P-O-P bond [110], and the difference in intensity may be the effect of a lower level of glass depolymerization induced by the addition of the modifier. (**PFF**) The occurrence of the above band in the case of the PFF series is in the range from 475 cm^{-1} to 483 cm^{-1}. As in the case of the PF glasses, these bands represent P-O-P vibrations, but due to the diametrically different nature of these series, the observed gradual increase in their relative field must have a different genesis. The case of PFF10 and PFF15 shows that the observed shift towards higher wavenumbers may be the result of an increased probability of fluorine incorporation into the glass network (among others in the form of F-P-O), the final effect of which is increased absorption. (**PKA**) The bands of the PKA series are slightly shifted towards lower wavenumbers (463 – 472 cm^{-1}) compared to the previous series, and the PKA15 sample is distinguished by a significantly higher intensity compared to the other compositions of the series. Although the main phenomenon behind this band will be, analogously to the above cases, the P-O-P deformation vibration, in the case of glass containing 15 mol% AlF_3, the structural modification of the glass network with Al^{3+} cations and additional vibrations of P-O-Al bonds should also be taken into account.

(**PF**) The band localized at ~439 cm^{-1} was not observed in the spectra of the PF series glasses, while for the PKBN matrix it is the effect of the deformation vibrations of the Bi-O bond in BiO_3 units [117]. (**PFF**) A band similarly described above, in the case of the PFF series, was distinguished only for the sample containing 5 mol% KF is located at ~449 cm^{-1}. (**PKA**) Unusually, also only for the glass containing 5 mol% of the modifier was it possible to distinguish the band at ~446 cm^{-1}. It is possible that it corresponds to the deformation vibrations of the Bi-O bond, due to the proximity of the composition to the initial matrix

(**PF, PFF**) Very weak bands located in the range of 440 – 400 cm^{-1} are probably the effects of deformational vibrations of O=P-O bonds [135] or coupled Nb-O and O-Nb-O-P modes [114]. (**PKA**) Considering the strong influence of AlF_3 on the structure and the increasing intensity of the band located at 421 – 429 cm^{-1} with its content, it can be attributed to deformational vibrations in AlF_6 units [138] (or mixed ones).

Summarizing the general features distinguished on the basis of the above analysis of FTIR spectra, it can be stated that in the case of the PF glass series, the increasing content of disproportionately introduced KF leads, among other things, to the depletion of the glass in K^+ ions, which results in the formation of a more complex phosphate network of the glass. The direct effect is therefore an increased probability of the occurrence of branched structural units in the form of linear chains and rings. In addition, the current modifications of the internal structure may have a beneficial effect on the formation of oxygen polyhedra around Nb cations, in particular octahedra, although the interaction between bismuth and niobium, which perform similar structural functions, is not unambiguous. The studies carried out additionally indicate the possibility of incorporating fluorine ions into the structural units appearing in the glasses (this is a general conclusion for all of the glasses studied, although it manifests itself in different ways in them). A different method of introducing KF in the PFF series contributes to the intensification of the depolymerization process of the glass network. In contrast, short phosphate chains with accompanying Q_1 and Q_0 units will occur more frequently for these glasses. These glasses show an increased preference for the occurrence of systems in which the structural role of Bi is distinguished. Analysis of the PKA series glasses shows that the addition of AlF_3, already from the lowest content used, strongly affects the cross-linking of the glass structure. This effect is particularly manifested by the formation of P-O-Al bonds and the formation of mixed oxygen-fluorine units concentrated around Al^{3+} ions. The case of these glasses also shows the superiority of Al over Bi and Nb in taking over the structural role of the networker. It should be emphasized that the composition of PKA15 is different, which showed abrupt changes in parameters, at the bottom of which there is probably a process of forming a subtle equilibrium between the introduced modifying fluorine ions and the role of the network Al in relation to the content of P and O.

Description of structural changes caused by the presence of Eu dopant

By extending the presented analysis to the spectra of glasses doped with 0.5 mol% Eu_2O_3, an attempt was made to describe the type and scope of structural changes caused by the presence of the dopant. The parameters of doped and undoped glasses obtained in the modeling process were compared, but the complexity of the obtained data did not allow for a direct analysis of the changes taking place. As a compromise, a concept was adopted in which "representatives" were selected from among the bands (parameters) based on the criterion taking into account the greatest differences in relative fields (in addition, the appearance or disappearance of significant bands was taken into account).

(**PKBN 05Eu**) Eu doping in the case of PKBN matrix leads to the following changes in their spectra: disappearance of bands localized at ~925, 830 and 764 cm^{-1} and appearance of bands at ~675, 560 and 420 cm^{-1}. The bands listed in the first group correspond to P-O-P bond vibrations associated with ring units and Bi-NBO bond vibrations. The complete disappearance of the mentioned absorptions in the case of PKBN 05Eu glass is additionally accompanied by a coincident decrease in the intensity of the band localized at ~960 cm^{-1}, which was also interpreted as the effect of P-O-P bond vibrations. Among the group of bands observed exclusively for the doped glass, they were assigned to unidentified structural changes, which, based on the findings of the previous section, occurred with the appearance of fluorine, Bi-O bond vibrations in BiO_3 units, and coupled Nb-O and O-Nb-O-P modes, respectively. The evolution of the intensities of the most important bands indicated that, as a result of the introduction of Eu dopant, the values of the relative fields of the bands associated with BiO_3 units (including the appearance of a previously absent band) and the bands described as P-O-P bond vibrations in Q_2 or Q_3 units significantly increased.

(**PF 05Eu**) The differences in the spectra of the PF 05Eu series glasses in the case of glasses containing 5 and 10 mol% include the disappearance of the ~790 cm^{-1} band, which was considered as a complementary band to the band describing the P-O-P bond vibrations, located at ~830 cm^{-1}. At the same time, the appearance of the ~690 cm^{-1} band was noted, which is the effect of modified corner-shared vibrations of NbO_6 octahedra, and in the case of PF10 05Eu, the ~427 cm^{-1} band, previously not observed for this composition, was observed, related to the deformation vibrations of the Nb-O bond. Moving on to the individual glasses, in the case of PF5 05Eu, it is necessary to mention the increase in the intensity of the bands resulting from the vibrations of P=O bonds and the weakening of the bands related to the vibrations of P-O-P, Bi-O and Nb-O bonds in NbO_6 units. The changes in the spectrum of PF10 05Eu glass, which occurred due to doping, are concentrated around the bands corresponding to the stretching vibrations of the P=O bond and the P-O-P bond in Q_2 units. Moreover, an increase in the intensity of the bending vibration bands of the P-O-P bond and the Nb-O vibrations in the edge-shared NbO_6 octahedra was observed. The case of the glass containing 15 mol% KF showed that the introduction of Eu resulted in an increase in the intensity of the bands located at ~700 cm^{-1}, which were assigned to the deformation vibrations of the NbO_6 polyhedra. An increase in the relative field was also observed for the absorptions described as the effect of the deformation vibrations of the Bi-O bond.

(**PFF 05Eu**) With the appearance of 0.5 mol% Eu dopant in the composition of PFF5 05Eu, an additional band at ~792 cm^{-1} was observed, related to the vibrations of P-O-P bonds, and in the case of PFF15 05Eu, a new feature was the band with the center at ~691 cm^{-1}, to which the

vibrations of Nb-O bonds were assigned. In terms of changes, the composition of PFF10 05Eu stood out. In its spectrum, both new bands were noted: localized at ~628 cm^{-1} corresponding to deformation vibrations in the corner-shared NbO_6 octahedra and assigned to the coupled vibration modes of Nb-O and O-Nb-O-P, the center of which is located at ~413 cm^{-1}; as well as the disappearance of the bands: located at ~614 cm^{-1} and located at about 550 cm^{-1} resulting from the vibrations of BiO_3 units. The most significant relative changes in the intensity of bands in the PFF5 05Eu spectrum were noted for the bands associated with the P-O-P bond vibrations and the edge-shared NbO_6 vibrations (intensity decrease), while in the case of the corner-shared NbO_6 vibrations and the coupled Nb-O and O-Nb-O-P vibrations, an increase in the relative field of the corresponding bands is observed. The PFF10 05Eu glass was characterized by an evolution of bands associated with NbO_6 units similar to the above case, and an additional increase in the intensity of the bands located at ~970, 530, 475 cm^{-1} was observed, which probably correspond to the P-O-P bond vibrations. The relationship between the bands describing the vibrations of differently connected NbO_6 units, described for the two above glasses, is not as clear in the case of the PFF15 05Eu sample. It is dominated by octahedra sharing edges. Additionally, an enhancement of the bands attributed to vibrations in BiO_3 units and vibrations of O-P-O bonds is observed.

(**PKA 05Eu**) In the case of the PKA series, a slightly more diverse picture of changes occurring after the introduction of the Eu dopant is observed. The spectrum of the PKA5 05Eu glass is devoid of bands located at ~780 cm^{-1} (P-O-P bond vibration component), ~751 cm^{-1} (Bi-NBO vibrations in BiO_6 units) and ~626 cm^{-1} (Nb-O bond vibrations). On the other hand, for this composition, a new band located at ~477 cm^{-1} was described, the origin of which is associated with the vibrations of BiO_3 units. The first of the above-mentioned bands also disappears in the case of PKA10 05Eu, while the ~686 cm^{-1} band associated with the appearance of fluorine in the glass compositions appears. The sample containing 15 mol% AlF_3 is characterized by a richer spectrum because three additional bands appear in it (633 cm^{-1} – Bi-O vibrations in BiO_6; 595 cm^{-1} – deformation vibrations of NbO_6 units; 415 cm^{-1} – coupled Nb-O and O-Nb-O-P modes) and one (~754 cm^{-1}) associated with the vibrations of Bi-NbO bonds occurring in BiO_6 units disappears. All 6 bands selected as representative for the spectrum of PKA5 05Eu showed an increase in intensity after the introduction of Eu dopant, in particular, the changes of the bands associated with the stretching vibrations of P-O-P and O-P-O bonds and the vibrations of Al-F bonds in AlF_6 units were distinct. Similarly to the composition described above, for PKA10 05Eu the bands associated with P-O-P vibrations were strengthened, however in this glass an additional decrease in the intensity of PO_2 and BiO_3 vibrations was noted. The composition containing the largest AlF_3 addition shows an increase in the intensity of the bands associated

with P-O-P, Al-F bond vibrations in AlF_6 polyhedra, and Nb-O bond vibrations in NbO_6 units sharing corners. At the same time, a decrease in the relative area of the band described as the effect of vibrations occurring in the edge-shared NbO_6 octahedra is observed.

The inference about the influence of the Eu dopant on the structure of the synthesized glasses turns out to be an extremely complicated issue, especially if it were necessary to clearly determine the type and scope of the induced changes. The reason for this state of affairs is mainly the fact that the structural changes induced by the addition of fluorides and those induced by the Eu dopant are strongly dependent on each other. Confirmation of this thesis can be found in the range of band parameter changes, which are much larger than would result from the amount of Eu_2O_3 used. Apparently, structural effects of different origins do not add up but create a combination. Analyzing the seemingly simpler case of the pair of glasses PKBN and PKBN 05Eu (no fluorides), the most important differences can be reduced to the conclusion that Eu_2O_3 acts on the glass network as a modifier. As a result, increased depolymerization of the phosphate network and increased presence of less complex structural units of the BiO_3 type are observed. Despite the impossibility of creating an unambiguous description of the structural evolution in the case of doped glasses containing fluoride addition, it is possible to propose general remarks. The example of the PF and PFF series shows that in addition to the type and share of fluoride, the Eu_2O_3/P_2O_5 ratio is also important. Moreover, it can be argued that the addition of Eu particularly affects the range of changes caused by fluorides and not their type.

PKBN	C_B	1368	1221	-	1087	940	925	899	866	829	799	-	764	733	-	700	-	638	628	605	-	571	-	532	-	502	478	470	439	-	409
	R_A	0.0145	0.1209	-	0.4053	0.3005	0.0063	0.0136	0.0158	0.0040	0.0089	-	0.0063	0.0135	-	0.0040	-	0.0010	0.0030	0.0090	-	0.0166	-	0.0434	-	0.0055	0.0056	0.0017	0.0010	-	0.0002
PKBN 05 Eu	C_B	1372	1225	-	1049	967	-	907	856	-	786	-	-	739	714	693	676	650	627	606	-	581	559	534	-	509	489	466	443	420	-
	R_A	0.0378	0.1574	-	0.5050	0.0229	-	0.0386	0.0867	-	0.0342	-	-	0.0189	0.0070	0.0046	0.0013	0.0003	0.0055	0.0053	-	0.0127	0.0094	0.0305	-	0.0111	0.0107	0.0044	0.0026	0.0018	-
PF5	C_B	1378	1242	1135	-	969	-	897	-	827	-	775	-	737	706	-	687	638	621	-	-	574	-	526	-	500	-	475	-	425	-
	R_A	0.0171	0.0786	0.3526	-	0.3375	-	0.0374	-	0.0471	-	0.0130	-	0.0228	0.0046	-	0.0015	0.0016	0.0065	-	-	0.0344	-	0.0414	-	0.0026	-	0.0023	-	0.0009	-
PF5 05Eu	C_B	1365	1232	1119	-	963	-	897	-	812	-	-	-	742	714	693	678	636	620	-	-	578	-	533	-	502	-	479	-	430	-
	R_A	0.0278	0.1021	0.3694	-	0.3260	-	0.0375	-	0.0502	-	-	-	0.0181	0.0045	0.0021	0.0005	0.0016	0.0059	-	-	0.0195	-	0.0325	-	0.0017	-	0.0023	-	0.0010	-
PF10	C_B	1372	1249	1146	-	972	-	907	-	861	-	790	-	737	705	-	685	637	621	-	-	585	-	529	-	499	-	474	-	-	-
	R_A	0.0265	0.0258	0.4474	-	0.2531	-	0.0122	-	0.0860	-	0.0317	-	0.0268	0.0058	-	0.0020	0.0014	0.0054	-	-	0.0149	-	0.0624	-	0.0014	-	0.0013	-	-	-
PF10 05Eu	C_B	1371	1247	1143	-	976	-	895	-	813	-	-	-	746	718	696	680	636	620	-	-	582	-	531	-	500	-	475	-	427	-
	R_A	0.0294	0.0668	0.3752	-	0.3102	-	0.0525	-	0.0608	-	-	-	0.0218	0.0073	0.0029	0.0007	0.0016	0.0055	-	-	0.0191	-	0.0427	-	0.0023	-	0.0020	-	0.0005	-
PF15	C_B	1360	1248	1161	-	999	-	901	-	814	-	-	-	746	713	693	677	637	620	-	-	580	-	532	-	503	-	478	-	426	-
	R_A	0.0346	0.0574	0.2659	-	0.4492	-	0.0469	-	0.0482	-	-	-	0.0201	0.0043	0.0017	0.0003	0.0014	0.0051	-	-	0.0189	-	0.0359	-	0.0008	-	0.0179	-	0.0026	-
PF15 05Eu	C_B	1360	1249	1169	-	1011	-	907	-	825	-	-	-	752	725	696	678	644	621	-	-	566	-	527	-	502	-	486	-	434	-
	R_A	0.0319	0.0409	0.2255	-	0.5093	-	0.0356	-	0.0539	-	-	-	0.0160	0.0072	0.0030	0.0005	0.0005	0.0053	-	-	0.0300	-	0.0229	-	0.0010	-	0.0182	-	0.0013	-
PFF5	C_B	1363	1208	-	1053	970	-	900	-	824	-	-	766	736	710	-	690	634	-	611	-	578	552	527	-	501	-	475	449	423	-
	R_A	0.0228	0.1671	-	0.4730	0.0421	-	0.1047	-	0.0636	-	-	0.0122	0.0138	0.0054	-	0.0027	0.0031	-	0.0107	-	0.0163	0.0196	0.0229	-	0.0120	-	0.0046	0.0032	0.0012	-

Table 7a. Results of modeling FT-IR spectra, for each glass the obtained band centers (C_b [cm^{-1}]) and their relative fields (R_a [%]) are included

.

PFF5	C_B	1363	1208	-	1053	970	-	900	-	824	-	-	766	736	710	-	690	634	-	611	-	578	552	527	-	501	-	475	449	423	-
	R_A	0.0228	0.1671	-	0.4730	0.0421	-	0.1047	-	0.0636	-	-	0.0122	0.0138	0.0054	-	0.0027	0.0031	-	0.0107	-	0.0163	0.0196	0.0229	-	0.0120	-	0.0046	0.0032	0.0012	-
PFF5 05Eu	C_B	1365	1209	-	1050	980	-	896	-	810	-	792	760	732	704	-	674	637	-	611	-	578	545	519	-	506	-	486	453	425	-
	R_A	0.0295	0.1807	-	0.4631	0.0230	-	0.1443	-	0.0397	-	0.0017	0.0131	0.0095	0.0113	-	0.0012	0.0023	-	0.0116	-	0.0105	0.0301	0.0108	-	0.0017	-	0.0123	0.0040	0.0027	-
PFF10	C_B	1376	1209	-	1052	974	-	896	-	809	-	-	-	729	710	692	673	632	-	614(614)	614	563	551	529	-	504	-	475	-	431	-
	R_A	0.0206	0.2073	-	0.4006	0.0447	-	0.1319	-	0.0766	-	-	-	0.0234	0.0007	0.0027	0.0005	0.0035	-	0.0078	0.0005	0.0458	0.0008	0.0178	-	0.0095	-	0.0072	-	0.0029	-
PFF10 05Eu	C_B	1364	1230	-	1084	940	-	880	-	800	-	-	-	736	710	691	676	639	628	613	-	574	-	534	-	503	-	479	-	431	413
	R_A	0.0372	0.1239	-	0.4593	0.1554	-	0.0611	-	0.0575	-	-	-	0.0165	0.0064	0.0031	0.0008	0.0010	0.0028	0.0065	-	0.0266	-	0.0317	-	0.0007	-	0.0150	-	0.0035	0.0004
PFF15	C_B	1378	1177	-	1058	973	-	893	-	810	-	-	-	730	700	-	683	632	-	614	-	573	-	541	522	503	-	483	-	427	412
	R_A	0.0168	0.3157	-	0.1801	0.1751	-	0.1263	-	0.0733	-	-	-	0.0183	0.0046	-	0.0012	0.0031	-	0.0083	-	0.0269	-	0.0233	0.0101	0.0031	-	0.0181	-	0.0026	0.0003
PFF15 05Eu	C_B	1363	1220	-	1074	944	-	881	-	803	-	-	-	736	710	691	675	634	-	617	-	577	-	536	527	504	-	479	-	432	416
	R_A	0.0287	0.1333	-	0.4663	0.1322	-	0.0717	-	0.0561	-	-	-	0.0158	0.0063	0.0035	0.0009	0.0023	-	0.0085	-	0.0254	-	0.0359	0.0003	0.0010	-	0.0120	-	0.0019	0.0002

Table 7b. Results of modeling FT-IR spectra, cont.

PKA5	C_B	1380	-	1180	1086	994	-	902	-	820	-	779	751	728	704	-	676	649	626	601	-	577	540	527	-	-	-	472	446	421	-
	R_A	0.0053	-	0.2837	0.0750	0.4370	-	0.0448	-	0.0464	-	0.0007	0.0075	0.0047	0.0072	-	0.0012	0.0014	0.0073	0.0063	-	0.0017	0.0667	0.0003	-	-	-	0.0013	0.0066	0.0007	-
PKA5 05Eu	C_B	1380	-	1191	1074	966	-	893	-	812	-	-	-	738	706	-	685	634	-	616	-	588	541	534	-	-	477	470	440	423	-
	R_A	0.0263	-	0.3150	0.1718	0.2741	-	0.0548	-	0.0706	-	-	-	0.0167	0.0056	-	0.0019	0.0019	-	0.0061	-	0.0056	0.0396	0.0011	-	-	0.0001	0.0121	0.0002	0.0014	-
PKA10	C_B	1380	-	1173	1082	990	-	900	-	821	-	782	-	742	702	-	-	639	627	607	-	580	544	531	-	-	463*	489	-	429	-
	R_A	0.0093	-	0.3015	0.0938	0.4107	-	0.0565	-	0.0359	-	0.0004	-	0.0148	0.0047	-	-	0.0009	0.0035	0.0064	-	0.0068	0.0361	0.0024	-	-	0.0023	0.0150	-	0.0024	-
PKA10 05Eu	C_B	1380	-	1170	1081	986	-	900	-	818	-	-	-	740	708	-	686	643	630	612	-	584	542	534	-	-	474	471	-	428	-
	R_A	0.0113	-	0.3443	0.0562	0.4090	-	0.0468	-	0.0451	-	-	-	0.0144	0.0048	-	0.0017	0.0006	0.0026	0.0073	-	0.0048	0.0405	0.0126	-	-	0.0005	0.0126	-	0.0016	-
PKA15	C_B	1386	-	1187	1042	974	-	904	-	816	-	-	754	721	694	-	679	-	-	617	-	579	538	-	-	502	-	471	-	427	-
	R_A	0.0247	-	0.2981	0.3480	0.0497	-	0.1386	-	0.0623	-	-	0.0073	0.0094	0.0031	-	0.0008	-	-	0.0081	-	0.0075	0.0304	-	-	0.0022	-	0.0132	-	0.0035	0.0000
PKA15 05Eu	C_B	1370	-	1200	1081	962	-	896	-	812	-	-	-	735	704	-	683	633	-	615	595	574	536	-	-	505	-	476	-	430	415
	R_A	0.0460	-	0.2694	0.2050	0.3057	-	0.0330	-	0.0621	-	-	-	0.0146	0.0065	-	0.0020	0.0024	-	0.0056	0.0001	0.0168	0.0196	-	-	0.0004	-	0.0147	-	0.0017	0.0003

Table 7c. Results of modeling FT-IR spectra, cont.

UV–Vis analysis

Absorption spectra in the range of 320 – 600 nm obtained for three series of glasses doped with 0.5 mol% Eu are presented collectively in Figure 35. Starting from the top of the figure, it contains the UV-Vis spectra of glasses from the PF 05Eu, PFF 05Eu, and PKA 05Eu series. As can be initially noticed, the spectra do not show significant changes related to the presence of fluorides in different contents, especially the occurrence of additional, unidentified absorption bands (including the measurement range of 1100 nm, which was not presented due to the desire to maintain the clarity of the figure). However, for each of the glasses, two absorption bands located in the range of 380 – 480 nm were observed (this range was additionally presented on the insets), the origin of which is related to the occurrence of 4f-4f electronic transitions of Eu^{3+} ions. The maximum located at a lower wavelength probably corresponds to the transition from the $^7F_0$ state to the $^5L_6$ excited state, and the adjacent absorption corresponds to the $^7F_0$ to $^5D_2$ transition (described in Figure 35). The presence of the above-mentioned effects confirms the effective doping of the glasses, as a result of which Eu^{3+} ions were incorporated into their structure. Another conclusion from the measurements was the determination of the approximate absorption edge - as can be seen, all of the glasses produced showed high transparency in the ultraviolet up to nearly 350 nm. Due to this characteristic, a wide range of selection of the appropriate excitation wavelength is possible in the proposed materials, which additionally supports their use for optical purposes. A specific example of the use of the presented properties is the use of wider doping with RE^{3+} ion systems, which allows for the emission of white light [141,142].

The inclusion of the spectrum obtained for the PKBN 05Eu glass in the presented comparisons allowed us to conclude on the differences resulting from the type and content of the fluoride modifiers used. However, no significant differences were noted between the spectra of glasses containing fluorides and the PKBN 05Eu matrix used as a reference. It is visible, however, that in the case of both the PF 05Eu and PKA 05Eu series, the increase in fluoride content leads to a similar shift of the absorption edge towards the ultraviolet, while the spectra of glasses from the PFF series seem not to change regardless of the composition. Additionally, taking into account the level of transmission of the glasses, they are characterized, depending on the composition, by variable values of transmittance in the visible range from ~50 to 70%. At the same time, apart from the statement that in the case of each series, the lowest transmittance value among the glasses containing fluorides was characterized by samples with 5 mol% of modifiers, there is no clear relationship between the transmission properties and the share of fluorides. These discrepancies may have their origin on the surface of the measured samples,

which were not mechanically processed due to the small thickness of the synthesized glass pellets.

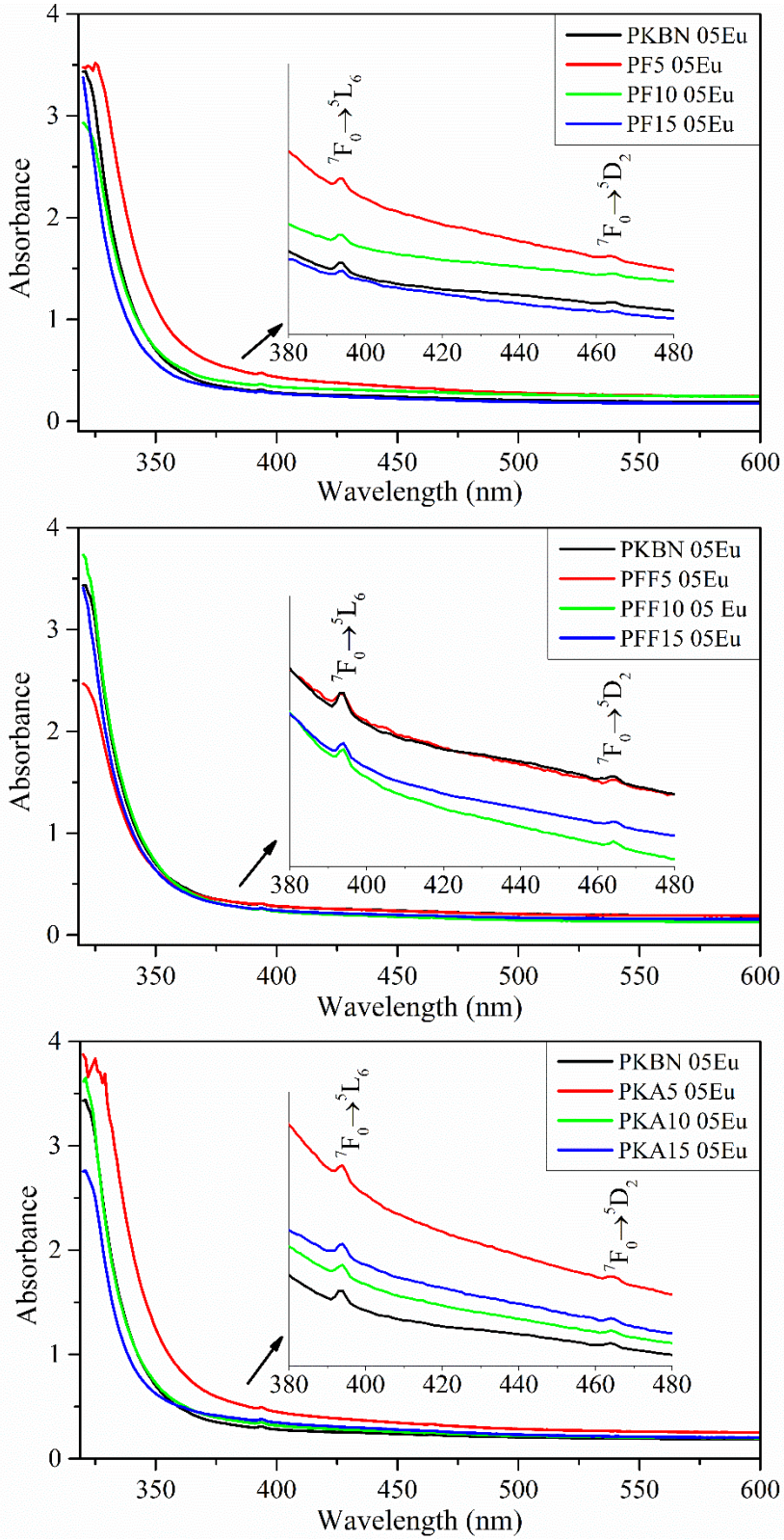

Fig. 35 Comparison of UV-Vis spectra obtained for Eu doped PF, PFF and PKA series of glasses. Enlarged spectral range include a description of Eu^{3+} absorption bands. Additionally, PKBN 05Eu spectra were added as a reference

Luminescence analysis

The luminescence measurements were conducted to determine the relationship between the emission properties of glasses doped with 0.5 mol% Eu and the introduced fluoride modifiers. The described analysis took into account both the effect of the type of fluorides and their variable content in the glass compositions, therefore, in order to obtain multi-dimensional conclusions taking into account these criteria, it was decided to present the results in two ways. Figures 36-38 contain standard sets of excitation spectra (λ_{em} = 615 nm corresponds to the $^5D_0 \rightarrow {}^7F_2$ transition in the Eu^{3+} ion) and emission spectra (λ_{ex} = 465 nm corresponds to the $^7F_0 \rightarrow {}^5D_2$ transition in the Eu^{3+} ion) taking into account samples within one glass series, in which the effect of increasing the fluoride share was distinguished, respectively PF 05Eu – Fig. 34; PFF 05Eu – Fig. 35 and PKA 05Eu – Fig. 36. Fig. 37 contains another form of data presentation, in which the spectra were grouped using the fluoride content criterion, thus emphasizing the effect of their type on the obtained luminescence. It was organized into two columns, of which the left column contains a comparison of emission spectra obtained using the excitation wavelength λ_{ex} = 465 nm, and the right column presents an analogous distribution of spectra but obtained using the excitation wavelength of λ_{ex} = 395 nm ($^7F_0 \rightarrow {}^5L_6$ transition of the Eu^{3+} ion). In order to provide an appropriate reference allowing one to follow the effects of the influence of changes in the glass compositions, the spectrum of the PKBN 05Eu matrix was included in each of the comparisons.

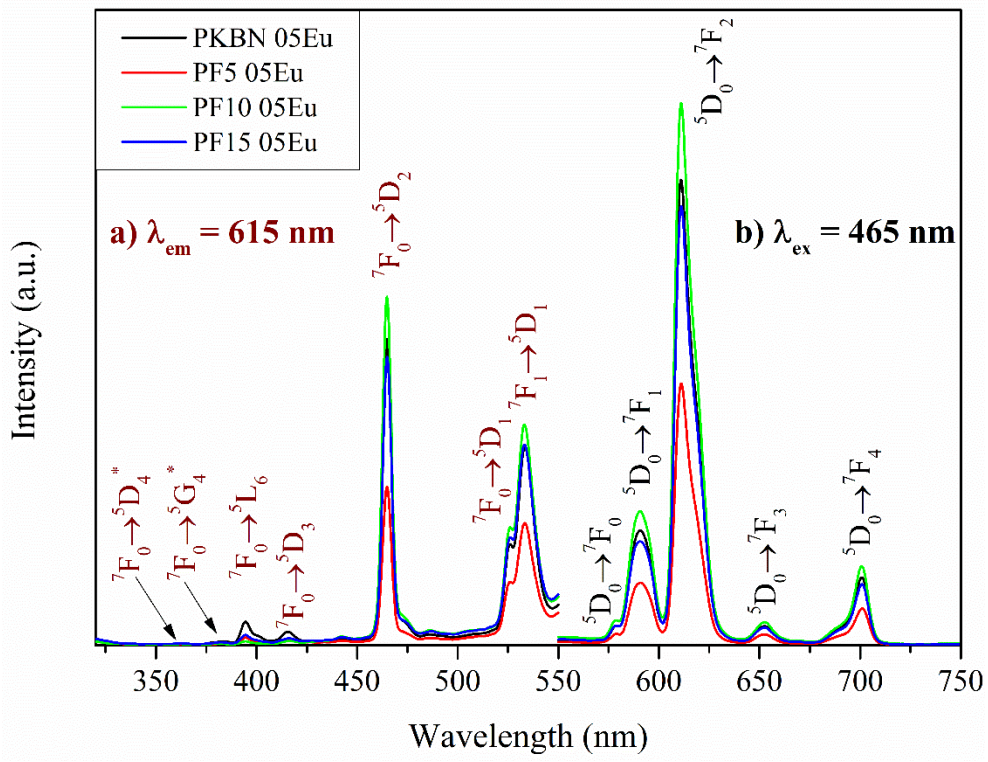

Fig. 36 Comparison of a) excitation (λ_{em} = 615 nm) and b) emission (λ_{ex} = 465 nm) spectra recorded for PF 5 – 15 glasses doped with 0.5 mol% Eu. The spectra of PKBN 05Eu are included for reference

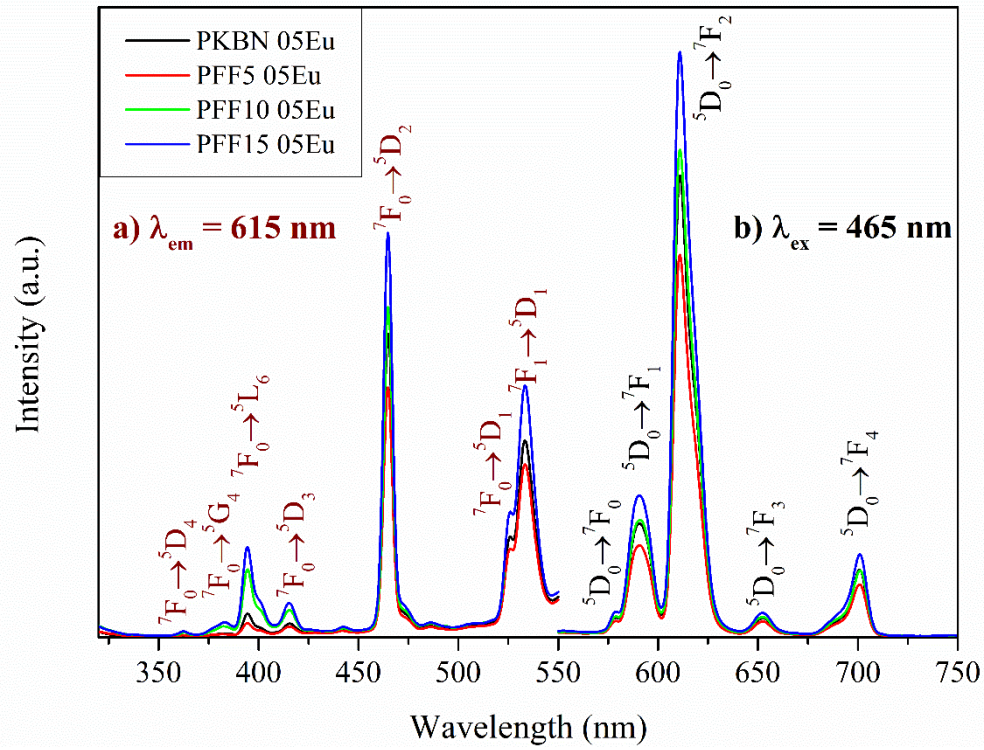

Fig. 37 Comparison of a) excitation (λ_{em} = 615 nm) and b) emission (λ_{ex} = 465 nm) spectra recorded for PFF 5 – 15 glasses doped with 0.5 mol% Eu. The spectra of PKBN 05Eu are included for reference

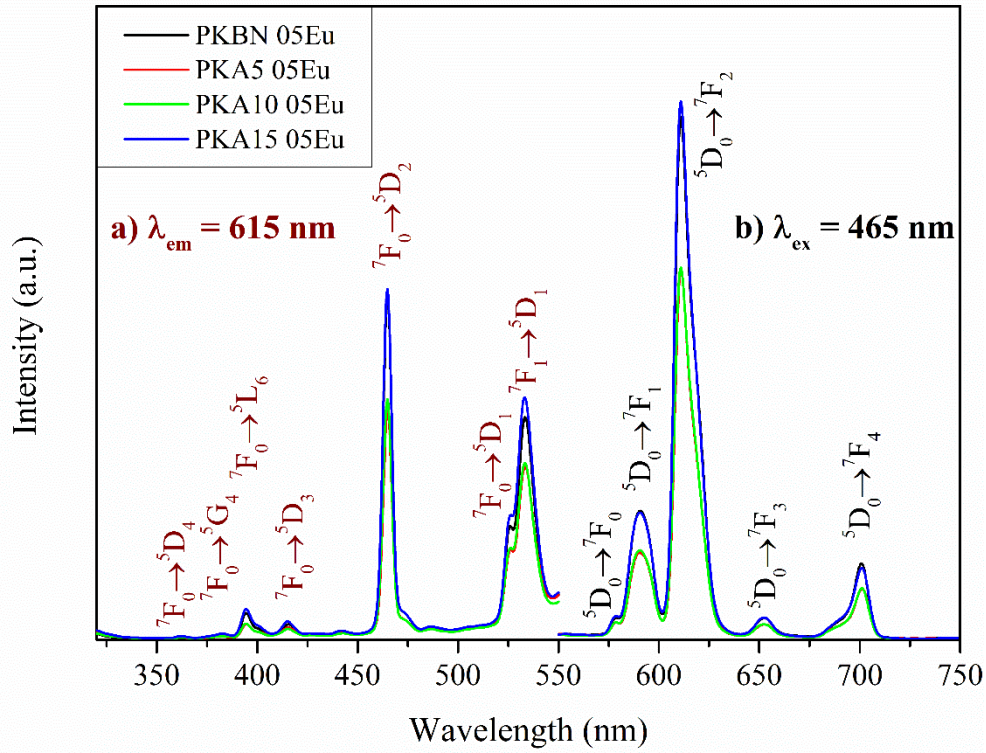

Fig. 38 Comparison of a) excitation (λ_{em} = 615 nm) and b) emission (λ_{ex} = 465 nm) spectra recorded for PKA 5 – 15 glasses doped with 0.5 mol% Eu. The spectra of PKBN 05Eu are included for reference

The recorded excitation spectra (part a of Figures 36-38) for the PFF 05Eu and PKA 05Eu series, similarly to the previously described PKBN 05Eu spectrum, were characterized by 7 well-defined maxima, to which the following electronic transitions in the Eu^{3+} ion were assigned: 362 nm ($^7F_0 \rightarrow {}^5D_4$), 383 nm ($^7F_0 \rightarrow {}^5G_4$), 394 nm ($^7F_0 \rightarrow {}^5L_6$), 415 nm ($^7F_0 \rightarrow {}^5D_3$), 465 nm ($^7F_0 \rightarrow {}^5D_2$), 525 nm ($^7F_0 \rightarrow {}^5D_1$) and 533 nm ($^7F_1 \rightarrow {}^5D_1$). Glasses that were part of the PF 05Eu series were a departure from the pattern present in the data presented so far and, in the spectra obtained for them it was possible to describe only 5 maxima unambiguously. Two of the above-mentioned transitions 362 nm ($^7F_0 \rightarrow {}^5D_4$) and 383 nm ($^7F_0 \rightarrow {}^5G_4$), except for the case of PF15 05Eu, were indistinguishable against the background of measurement noise. This does not exclude their presence, but only highlights the features of the measurement method. Except for the aforementioned anomaly, the obtained excitation and emission spectra do not show significant differences in the form of maxima shifts or the appearance of new bands, regardless of the type and content of fluorides introduced into the glasses.

It is worth emphasizing that in all presented excitation spectra there is a significant intensity disproportion between transitions located in the range of 350 – 420 nm (P1) and transitions located in the wavelength range of 450 – 550 nm (P2). As a result, the highest intensity (for all spectra) was characterized by the transition $^7F_0 \rightarrow {}^5D_2$ contained in the P2 range, while the transition considered typical for the Eu^{3+} ion, $^7F_0 \rightarrow {}^5L_6$ (located in P1), was characterized by an exceptionally low intensity. This is especially visible when confronting the above reports with the literature, in which the last of the mentioned transitions is most often recognized and observed in europium compounds as showing the highest intensity [143]. Similar conclusions were also reached in studies on glasses enriched with this dopant, in particular those based on a phosphate matrix [144–146]. However, there are also works [102,147,148] in which higher intensities were observed for the $^7F_0 \rightarrow {}^5D_2$ transition (465 nm) for materials (including glasses), and not for the $^7F_0 \rightarrow {}^5L_6$ transition (395 nm), even though the compositions and dopant contents used did not differ significantly from those proposed in the above counterexample (it is not possible to predict the spectrum variant based on the compositions alone). Considering the emission properties of the glasses studied, it is natural that in the case of potential optical applications the preferred excitation wavelength would be λ_{ex} = 465 nm.

The emission spectra obtained both at 465 nm (part b of Figures 36 - 38) and 395 nm (Figure 39) excitation wavelengths contained 5 maxima that were interpreted as electronic transitions in the Eu^{3+} ion: $^5D_0 \rightarrow {}^7F_0$ (579 nm), $^5D_0 \rightarrow {}^7F_1$ (591 nm), $^5D_0 \rightarrow {}^7F_2$ (611 nm), $^5D_0 \rightarrow {}^7F_3$ (653 nm) and $^5D_0 \rightarrow {}^7F_4$ (701 nm). Apart from the intensity differences, no deviations of other origin were observed for any of the compositions.

Moving on to the analysis of the dependence of luminescent properties on the modifier content within a single series, the first case is PF 05Eu glasses, the emission spectra of which are summarized in the right part of Figure 36. The presented summary shows the effect of the KF content, in the range from 5 to 15 mol%, on the emission intensity. As can be seen, the disproportionate addition of as little as 5 mol% fluoride caused significant changes in the PF5 05Eu glass, which resulted in a large decrease in the emission intensity (in relation to the spectra of the initial PKBN 05Eu matrix). A further increase in the modifier share resulted in obtaining luminescence enhancement for the PF10 05Eu sample, which in this case was also equivalent to achieving the highest intensity among the glasses of the tested series. Increasing the KF content to 15 mol% did not allow obtaining an intensity higher than that presented by the PKBN 05Eu matrix. This observation allows us to state that the optimal KF content (guaranteeing the highest emission) in the used range is less than 15 mol% and is probably close to 10 mol%. Accurate determination of the optimal share would require data from additional measurement points considering contents from the middle of the ranges. It is probable that the sudden change in emission intensity observed in the case of PF5 05Eu glass may be related to an unusual feature noticed in the studied PKBN matrix. In the previous chapter it was observed that the composition containing the 5 mol% fluoride (SrF_2) is characterized by a transitional character, which contains both the features typical of PKBN and those detected only in the case of a higher content of the modifier. Therefore, it is possible that in the case of PF5 05Eu glasses (due to a different type of KF additive introduction, the glass differs in stoichiometry from the equivalents from the PFF and PKA series) a similar effect occurs, but in this case the features inherited from PKBN and characteristic of PF10 and PF15 give a common effect worsening the emission properties of Eu^{3+} ions. The presented explanation can also be confirmed by the comparison of emission spectra obtained for glasses containing 5 mol% fluoride modifiers (Figure 39). As can be seen, the spectra are characterized by different intensities, but for all compositions, it is lower than in the case of PKBN glass. However, based on the conducted research it is impossible to clearly state how the above-mentioned fluorides modify the glass structure by changing the environment of Eu^{3+} ions.

Figure 37 (b) contains an analogous comparison of spectra prepared for the PFF 05Eu series. The intensity of the bands observed for the PFF5 05Eu sample, similarly to the corresponding sample from the PF series, was lower than for PKBN 05Eu, however, the disproportion in this case was not so significant. The other two samples showed luminescence enhancement, where the highest emission intensity was obtained for the PFF15 05Eu glass. Moreover, considering the differences in the band intensities between the samples containing an increasingly larger amount of KF, a trend close to proportionality becomes visible, in which

the intensity gradually increases. This emphasizes how different effects were obtained by choosing a different method of introducing KF into the composition.

As expected, the use of a different modifier in the form of AlF_3 resulted in the occurrence of other spectral dependencies, which is presented in Figure 38 b. As can be observed, the addition of 5 and 10 mol% AlF_3 led to the same effect of weakening the luminescence, in relation to the reference in the form of the PKBN 05Eu spectrum. However, a further increase in the fluoride content in PKA15 05Eu resulted in a slight increase in intensity above the mentioned reference level. A possible interpretation of the above dependencies between the compositions is the occurrence of a threshold content in the case of the used AlF_3, after exceeding which the structural configuration of the material becomes possible, promoting radiative transitions of Eu^{3+} ions and the emission enhancement is observed.

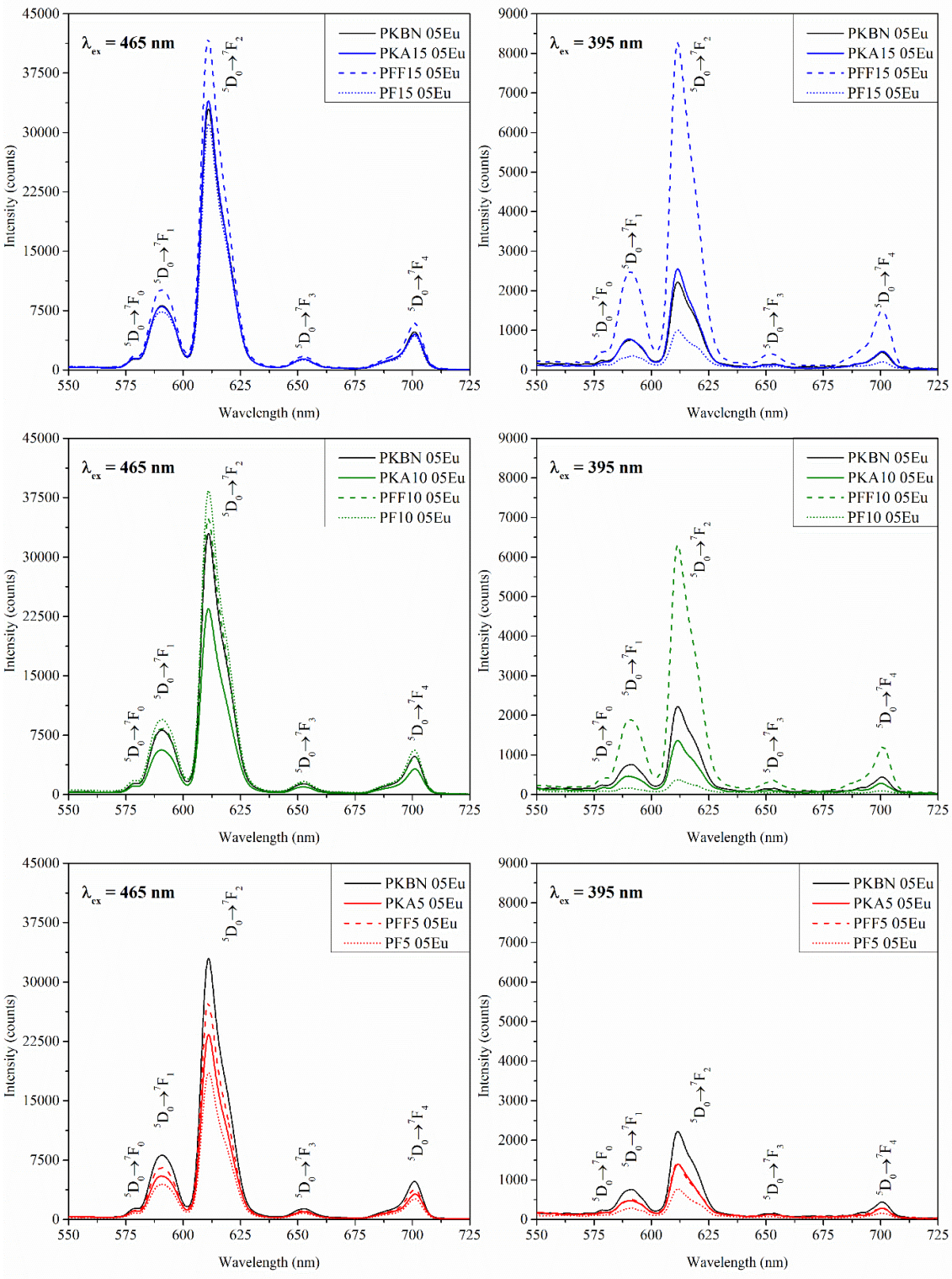

Fig. 39 Summary of emission spectra at excitation λ_{ex} = 465 nm (left column) and λ_{ex} = 395 nm (right column) of glasses illustrating the influence of fluoride content on luminescence properties. Results were grouped according to the share of modifiers

The concept of comparing spectra in the manner shown in Figure 39 allows not only to compare the samples from all 3 series corresponding to the content of modifiers but also to present how the most promising compositions of the series (PF10 05Eu, PFF15 05Eu, PKA15 05Eu) compare to other glasses. Additionally, this section has been extended to include emission spectra measured using an excitation wavelength of λ_{ex} = 395 nm, the aim of which was to provide a different perspective. Starting with the glasses with the lowest fluoride content, i.e. the lower left part of Figure 39 showing a comparison of their corresponding spectra (λ_{ex} = 465 nm), it can be stated that although the intensities were far from exceeding the level recorded for PKBN 05Eu, they are distributed with the same mutual difference. Although this distribution is random, apart from the simplified statement of which composition is the most promising (like on the podium steps), it allowed one to observe how big the difference in intensity was between the (still slightly different in composition) PF5 05Eu and PFF5 05Eu glasses. This discrepancy, although it seems to be disproportionately large, is justified, among others, by the structural evolution presented in the FTIR analysis. The graph located on the right side of the above-described comparison summarizes the emission spectra of the corresponding glasses obtained for λ_{ex} = 395 nm.

Moving on to the central part of Figure 39 containing spectra of glasses containing 10 mol% modifiers, and precisely located on the left side of the compilation of spectra obtained at excitation λ_{ex} = 465 nm, it can be noticed that the highest intensity in this range was characterized by sample PF10 05Eu. A slightly lower value was shown by the sample from the PFF 05Eu series, in which the spectra seem to change gradually with increasing KF content, in contrast to the PF series, in which the jump in intensity (between PF5 05Eu and PF10 05Eu) against the background of other spectra seems to be much more pronounced. A slightly different situation is present in the spectra with λ_{ex} = 395 nm (right central part), for PF10 05Eu the spectrum is unexpectedly characterized not only by the lowest intensity among all compositions, but also lower than that obtained for PF5 05Eu. At the same time, in the case of the twin composition PFF10 05Eu, a sudden increase in intensity (almost five-fold) was noted. Based on the collected data, it is difficult to determine the mechanism causing the sudden increase in intensity for the PFF10 05Eu sample excited with λ_{ex} = 395 nm. It is possible that as a result of the higher degree of depolymerization of the network, the glass structure became less compact, as a result of which the environment of Eu^{3+} ions changed to one that guarantees a lower probability of non-radiative transitions - the share of fluorine anions. In other words, there is a suspicion that the resulting structural changes in the environment may cause a competitive "parasitic" process, which in the case of 395 nm excitation leads to non-radiative energy dissipation. However, in the case of the PFF 05Eu series, the changes induced by the increasing addition of KF (the threshold value is

close to 10 mol%) significantly reduce the probability of this phenomenon, as a result of which much higher emission intensity is observed.

The spectra of glasses containing the highest fluoride content are presented in the upper part of the discussed figure. In the case of PFF15 05Eu, the continuing trend observed in samples with lower KF content resulted in a further increase in emission intensity, ultimately reaching the highest value among all tested compositions. The remaining two samples, as a result of the increase (PKA15 05Eu) and decrease (PF15 05Eu) of the transition intensity relative to samples containing 10 mol% fluorides, reached a level close to that presented by the spectrum of PKBN 05Eu. The spectra of these glasses obtained with UV excitation changed in a way similar to those obtained for λ_{ex} = 465 nm: for PFF15 05Eu, a further increase in intensity occurred, and for PKA15 05Eu, the bands turned out to be more intense than for PKBN 05Eu. Only in the case of PF15 05Eu the changes showed the opposite character and the lines excited with 395 nm light were slightly enhanced.

As part of an additional experiment on the subject of annealing selected samples, in addition to the structural analysis presented in the previous chapters, it was decided to conduct a luminescence analysis. Its aim was to decide whether short annealing of glasses containing the addition of "non-crystallizing" fluorides can have a beneficial effect on the emission intensity of the contained Eu^{3+} dopant ions. The implementation of the above concept, in the form of emission spectra (λ_{ex} = 465 nm) of annealed glasses, is presented in Figure 40. The layout of Figure 40 has been divided into 4 parts, each of which contains emission spectra obtained for unannealed glasses (reference), annealed at 585 °C for 8h and annealed at 585 °C for 10h, these compositions are: a) PFF5 05Eu, b) PFF15 05Eu, c) PKA5 05Eu and d) PKA15 05Eu. The abandonment of samples from the PF series was motivated by the desire to limit the variables in the analysis, and it is also probable that samples in which the proportionality of the share of components in the presence of fluorides was maintained may at least partially exhibit annealing characteristics similar to those described for glasses containing the SrF_2 additive. It should be mentioned that based on the conducted XRD measurements (Figure 27), it was established that regardless of the length of annealing time, glasses from the PFF series subjected to this process are well-defined glass-ceramics. At the same time, in the case of glasses from the PKA series, only poorly defined signs of the presence of a crystalline phase in the amorphous matrix were noted.

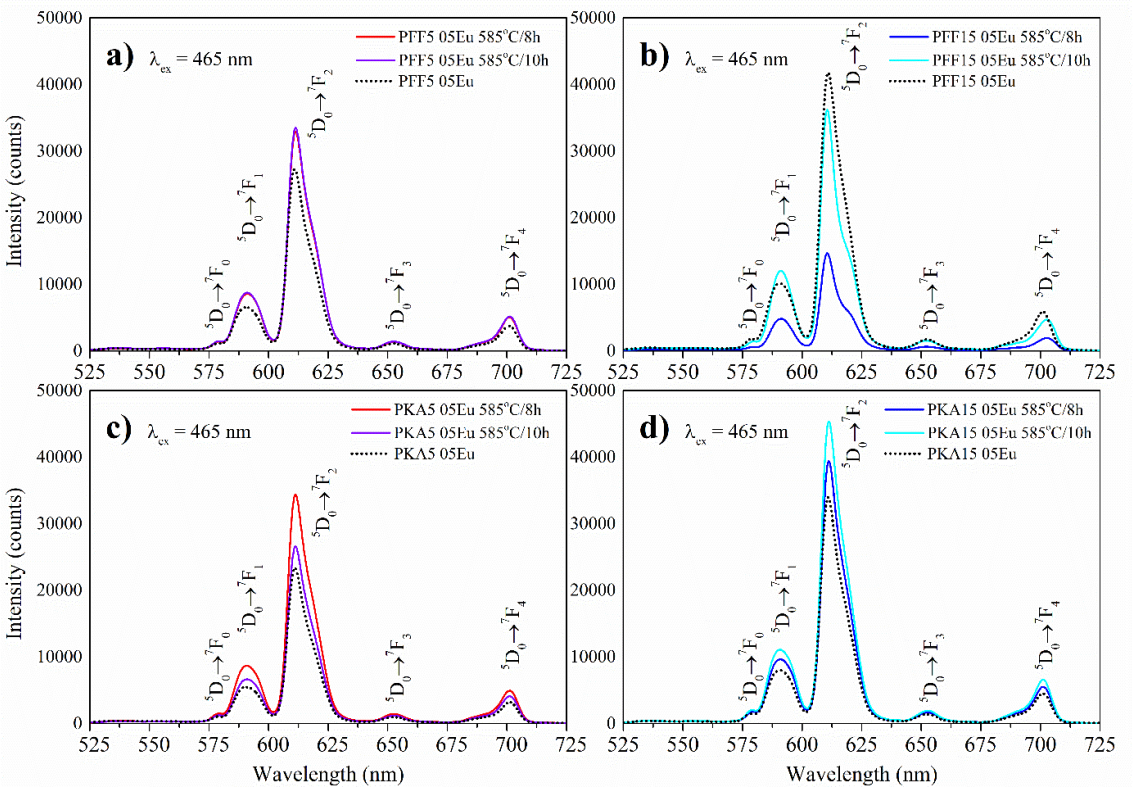

Fig. 40 Emission spectra (λ_{ex} = 465 nm) of samples a) PFF5 05Eu, b) PFF15 05Eu, c) PKA5 05Eu and d) PKA15 05Eu subjected to annealing at 585 °C for 8 or 10 h. The dashed line additionally shows the spectra of as-prepared glasses, which in this case serves as a reference

Focusing first on the compositions containing the KF additive (Figure 40 a and b), it can be observed that the spectra obtained for the PFF5 05Eu glass-ceramics, regardless of the applied heating time, are characterized by comparable intensity. It is important that, in comparison to as-prepared glass, for these samples, there was an enhancement of luminescence caused by the thermal treatment process. A different trend was noted for the glass-ceramics containing 15 mol%, depending on the heating time, the measured spectra showed an extremely different character despite the similarity of their diffraction patterns. The eight-hour heating unexpectedly resulted in a significant relative decrease in intensity, while the second process, differing only slightly in time, led to obtaining a spectrum close to the reference sample. A detailed explanation of the origin of this discrepancy would require additional studies, but due to the secondary nature of the described results, this issue was not developed. At the same time, the spectrum of the PFF1505 Eu sample annealed for 10 h contains an interesting feature in the form of a visible disproportion in the ratio of the intensity of the bands corresponding to the $^5D_0 \rightarrow {}^7F_2$ to $^5D_0 \rightarrow {}^7F_1$ transitions, known as the red/orange ratio. At first glance, it can be stated that, compared to the unannealed glass, the R/O parameter decreased significantly after annealing, which can be interpreted as a confirmation of the incorporation of Eu^{3+} ions into the crystallites formed during heat treatment.

Analogous spectra of glasses from the PKA series are included in parts c) and d) of Figure 40. In all four annealed samples, luminescence enhancement was observed, which, depending on the composition, was perversely more significant for the shorter annealing time of the PKA5 05Eu sample and for the longer annealing time in the case of PKA15 05Eu. The occurrence of a specific reversal in the response to heat treatment parameters may be related to the abrupt difference in properties observed for the glass containing 15 mol% AlF_3. Moreover, the increased thermal resistance of these materials could have determined the greater significance of features related to the amorphous structure than to the niche crystalline phase in this case. Finally, it can be stated that in the case of PKA15 05Eu glass, performing a short thermal treatment significantly improved the emission properties of the material while maintaining transparency (Figure 28 D) and a character close to amorphous (based on XRD – Figure 27).

Luminescence decay measurements

In addition to the comparative analysis of the excitation and emission spectra of the studied glasses, it was decided to carry out measurements of the luminescence decay, which provided insight into the properties of the dopant ions, especially in terms of their immediate surroundings. The measurements consisted of observing the evolution of the intensity of the emission band with a wavelength of λ_{obs} = 620 nm corresponding to the $^5D_0 \rightarrow {}^7F_2$ transition after pulsed excitation with a wavelength of 395 nm or 465 nm. Figure 41 presents exemplary sets of the obtained measurement data, where the right graph compares the results with respect to the type of fluorides used, while the left graph illustrates the evolution with increasing fluoride share. Due to the nature of the recorded curves, it was decided to model them with the expression (6), which is equivalent to their double-exponential form. The results of the fitting process are presented in Table 8, which also includes the values of the parameters calculated on their basis: the average lifetime taking into account the amplitudes $\langle\tau\rangle_{Amp}$ and the average lifetime taking into account the intensities $\langle\tau\rangle_{Int}$.

The interpretation of the obtained results is difficult due to a seemingly occurring contradiction: for homogeneous materials with experimentally confirmed amorphousness, the characterized decay curves are biexponential, which would suggest the presence of at least two different Eu^{3+} ion environments, a state usually encountered in the case of glass-ceramics. It is possible that the segregation of dopant ions, which usually occurs during controlled heating of glasses, occurred at the stage of the melting itself, taking into account at least two preferred sites with significantly different symmetries. Taking into account the number of components of the studied glasses, and thus the possible combinations of the glass network arrangement, it should be noted that these do not have to be exactly two environmental systems, but rather two sets

(with elements indistinguishable from the point of view of the described experiment), whose difference in symmetry is sufficiently large. In this approach, the structural units of the glass themselves, into which the Eu^{3+} ions are incorporated, are responsible for the biexponential decay. If we increase the scale of considerations from the atomic level created by the surroundings of individual ions to the scale of small regions (domains), the second possibility is the occurrence of micro-separation of phases in the glass matrix. From the point of view of the conducted experiment, they would be indistinguishable, so together with atomic-scale units, they constitute probable interpretations of the observed phenomena.

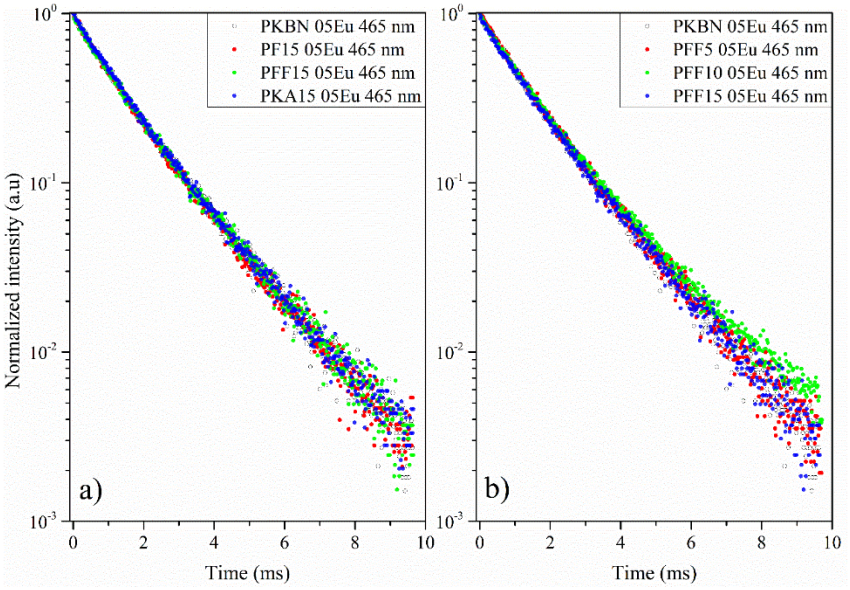

Fig. 41 Comparison of luminescence decay curves obtained for a) glasses containing 15 mol% of fluorides; b) PFF 05Eu series. Additionally decay curve of PKBN 05Eu glass was plotted

The obtained values of the parameters listed in Table 8 do not change with the sample compositions in a way that would suggest a direct relationship between them and the content or type of fluorides. No clear correlation was observed between the measured emission properties and the aforementioned parameters derived from the luminescence decay measurements. These observations suggest that the changes in lifetimes are subtle and it would be extremely difficult to draw conclusions on their basis about the properties of all three series of the presented glasses. However, it is possible to specify in an approximate way the differences that occur, and they are particularly clear in the case of the PF series. The tendency of changes in the parameters for glasses from this series stands out from the other two that were subjected to measurements, the reason for which can be sought in the different method of introducing fluorides. Thus, this example shows that the dependencies of luminescence lifetimes are not so much dependent on modifiers, but on subtle changes in the stoichiometry of the matrix, which can be confirmed by measurements carried out for glasses from the PKF series.

		PF5 05Eu	PF10 05Eu	PF15 05Eu	PFF5 05Eu	PFF10 05Eu	PFF15 05Eu	PKA5 05Eu	PKA10 05Eu	PKA15 05Eu
λ_{ex} = 395 nm	τ_1	1.117	1.046	1.108	0.870	0.561	0.484	0.663	0.414	0.744
	τ_2	2.048	1.924	2.040	1.825	1.681	1.638	1.657	1.615	1.702
	$\langle\tau\rangle_{Int}$	**1.684**	**1.661**	**1.658**	**1.636**	**1.599**	**1.590**	**1.580**	**1.577**	**1.618**
	$\langle\tau\rangle_{Amp}$	**1.535**	**1.551**	**1.499**	**1.471**	**1.415**	**1.449**	**1.457**	**1.445**	**1.540**
	A_1	0.537	0.445	0.554	0.336	0.184	0.123	0.170	0.112	0.183
	A_2	0.457	0.564	0.434	0.646	0.780	0.848	0.811	0.866	0.825
λ_{ex} = 465 nm	τ_1	0.370	0.791	0.634	0.821	0.643	0.480	0.789	0.839	0.297
	τ_2	1.489	1.678	1.562	1.693	1.631	1.527	1.647	1.676	1.451
	$\langle\tau\rangle_{Int}$	**1.452**	**1.523**	**1.467**	**1.524**	**1.539**	**1.477**	**1.495**	**1.513**	**1.430**
	$\langle\tau\rangle_{Amp}$	**1.309**	**1.350**	**1.327**	**1.410**	**1.393**	**1.332**	**1.373**	**1.398**	**1.354**
	A_1	0.117	0.299	0.214	0.333	0.202	0.133	0.309	0.325	0.084
	A_2	0.850	0.664	0.763	0.671	0.774	0.831	0.686	0.672	0.916

Table 8. Parameters obtained by fitting the luminescence decay curves of 0.5 mol% Eu doped PF, PFF and PKA glass series. Additionally, intensity and amplitude average lifetimes were calculated (lifetimes were expressed in ms)

3.3. Materials containing addition of Ag

XRD

A wide range of PB10 glass variants was structurally characterized using the XRD method, the results of which are presented in Figure 42. The first four diffraction patterns (counting from the bottom of the figure) are devoid of reflections and have only features typical of the amorphous structure of materials, thus confirming the successful synthesis process and doping of the PB10 glass matrix with both Eu and Ag. A separate case is the two upper curves from measurements of glasses heated at 500 °C for 22h, which contained 0.5 and 1 mol% Ag. As can be seen, thermal treatment did not result in the growth of any crystalline phase (in quantity/size above the detection threshold) in the matrix volumes – in particular the desired nanocrystalline Ag precipitations. They also did not occur for the glasses heated for 3 and 6 hours, which showed a purely amorphous character, but for the sake of clarity of the figure, the corresponding diffraction patterns were not included in Figure 42.

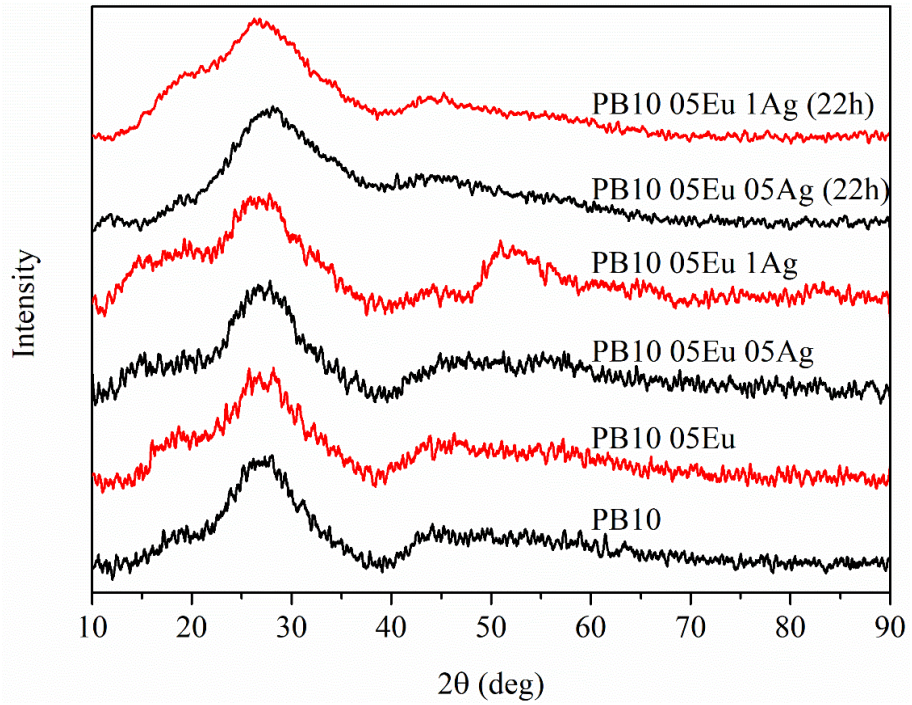

Fig. 42 The comparison of diffractograms of PB10 glasses and their Eu and Ag doped versions – the amorphous nature of these samples was confirmed. Additionally, at the top of the figure, two diffractograms of samples after the final stage of heating at 500 °C for 22h are included

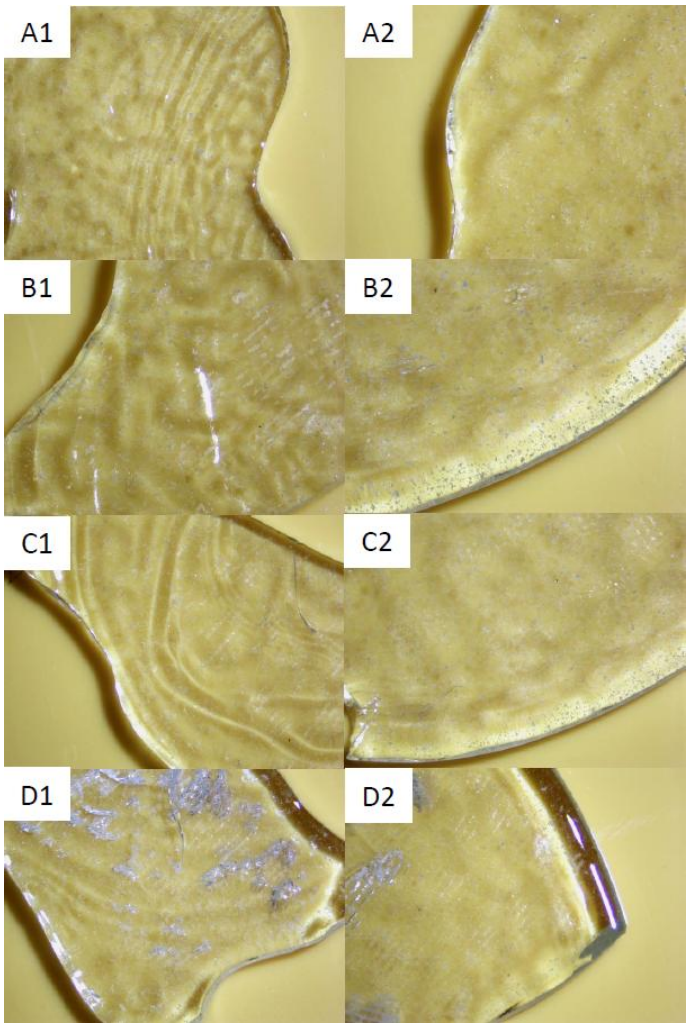

Fig. 43 Photos of the PB10 glass series. The effect of heating the PB10 05Eu 05Ag sample (left column) and the PB10 05Eu 1Ag sample (right column) at 500 °C for: A – 0h (as prepared), B – 3 h, C – 6 h, and D – 22 h is presented

At the same time, as shown in Figure 43, the described samples contained unidentified inhomogeneities in the volume regardless of the annealing process. The left column presents images obtained for different annealing times of the PF10 05Eu 05Ag glass sample, while the right side consists of corresponding pictures obtained for the PB10 05Eu 1Ag glass sample. The presence of such large inhomogeneities already in the unannealed glasses, combined with the XRD results, excludes their crystalline origin, while at the same time indicating the synthesis process, in which they must have precipitated. This directs attention to two probable causes of their presence: trapped gas bubbles or local separation of the glass phases. Analyzing the photos presented above, it was possible to show that the inhomogeneities are located in relatively large intervals throughout the glass volume, but do not occur so numerously near the sample surface itself or directly below it. Therefore, one of the probable causes is their formation during the melt quenching process itself, in which the edges of the sample being in direct contact with the mold cool down much faster, thus closing the hot interior of the sample, in which, depending on

the concept, gaseous by-products could be released in the cooling alloy or phase separation could have occurred. Additionally, the juxtaposed images show that the inhomogeneities did not change their form or size much in response to the annealing performed (ignoring changes resulting from contact with the substrate in samples subjected to 22h heating), maintaining shapes resembling glued beads, which suggests that despite their small size, they are stable up to the temperature used in the heat treatment process. The non-crystalline genesis makes it much more difficult to predict what effect the precipitates have on the properties and what factor was responsible for their appearance in the matrix.

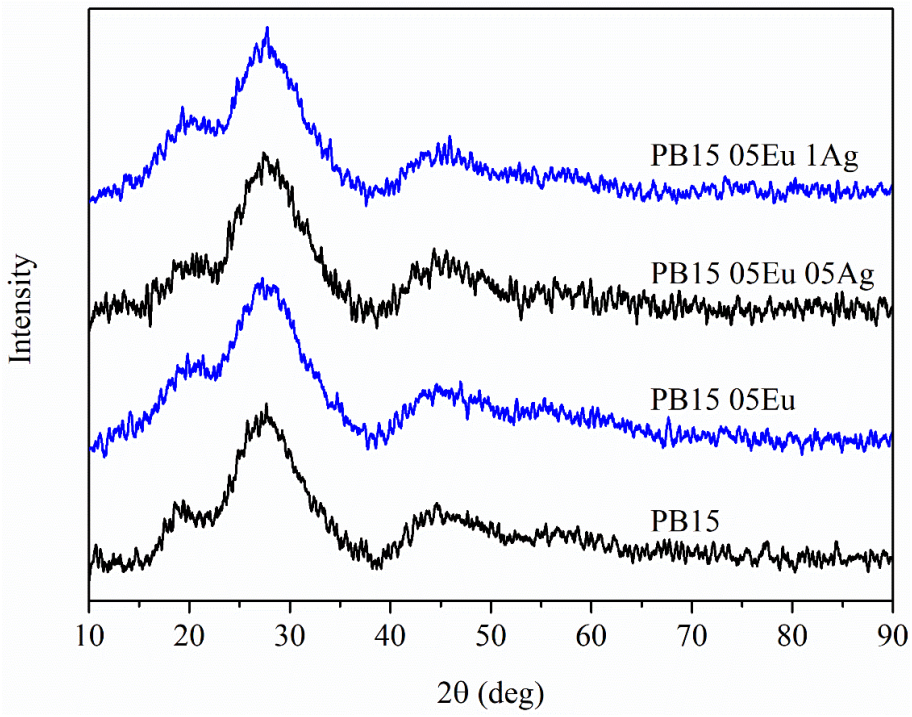

Fig. 44 Comparison of diffraction patterns of PB15 glasses and their Eu- and Ag-doped versions – the amorphous nature of these samples was confirmed

Figure 44 shows the diffraction patterns obtained for the second matrix subjected to bismuth content minimization, PB15, along with its doped versions. This confirmed the amorphous nature of the synthesized materials, especially in the presence of Eu and Ag.

DSC and DTA

The slightly different roles of the compositions based on the PB10 and PB15 matrices in the described experiment resulted in a decision to carry out a different measurement approach, which explains the differences between the thermal characteristics performed. In the case of PB10 and its doped variants, it was crucial to determine the glass transition temperature, based on which the annealing parameters were established. DSC measurements that allowed for

determining this value as T = 500 °C are presented in Figure 45. In order to compare the effect of reducing the Bi_2O_3 content on the glasses, the measurement performed for the PKBN matrix is additionally included at the bottom of mentioned figure. The T_g temperature values read for the glass transition center are collected in Table 9.

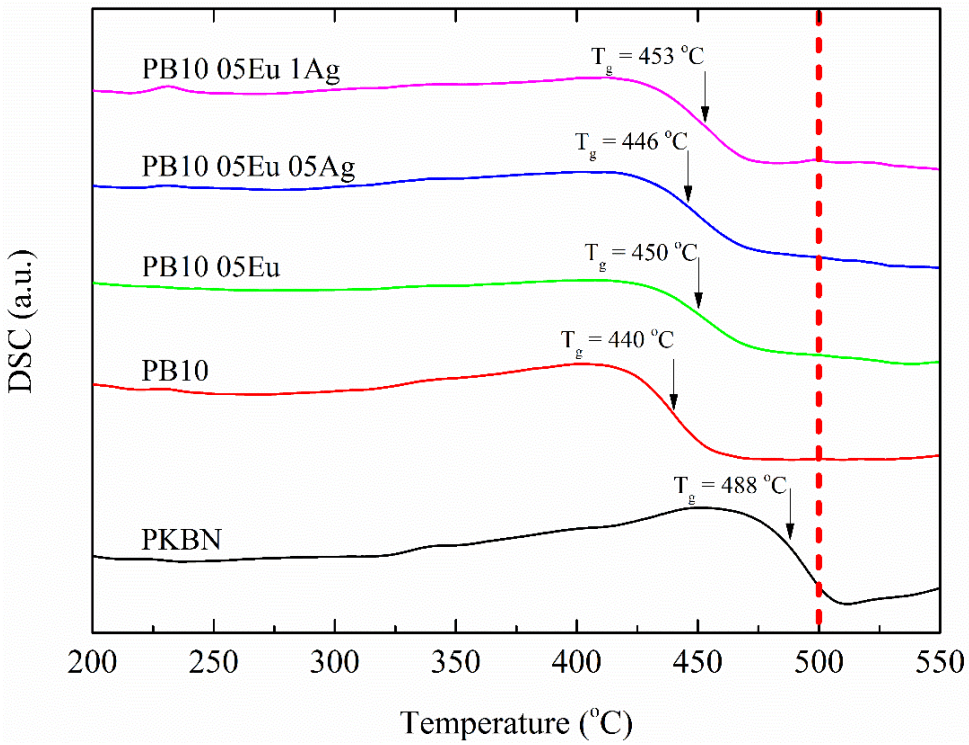

Fig. 45 Summary of DSC curves obtained for PB10 glasses and their Ag and Eu doped versions. Glass transition temperatures are indicated by arrows. The measurement result of PKBN glass is included as a reference. The vertical line indicates the temperature selected for the annealing process

As can be seen, reducing the Bi_2O_3 content in the PB10 glass composition (from 20 to 10 mol%) resulted in a large drop in the glass transition temperature, by almost ΔT = 50 °C. This revealed the extent of the structural role of Bi, the greater presence of which can be associated with greater cross-linking of the glass structure. The second factor that may affect the observed state of affairs is the distortion of the mutual proportions between the components - the "gap" created in the composition after reducing the Bi content led, among other things, to an increase in the share of K_2O controlling the degree of network depolymerization. Another observation worth emphasizing is the difference in the T_g values caused by the introduction of the Eu dopant. The structural role of small Eu_2O_3 shares, outlined earlier in this work, is in this case extremely clear because despite the above-described change caused by the reduction of Bi in the composition, and therefore a significantly different system, the introduction of Eu caused an increase in T_g by 10 °C. The addition of silver caused slight fluctuations in the glass transition position, therefore

it was decided to select 500 °C as the annealing temperature, which, being on average 50 °C higher than glass transition temperatures, could provide favorable conditions in the glass for the formation of the crystalline phase in the form of Ag nanoparticles.

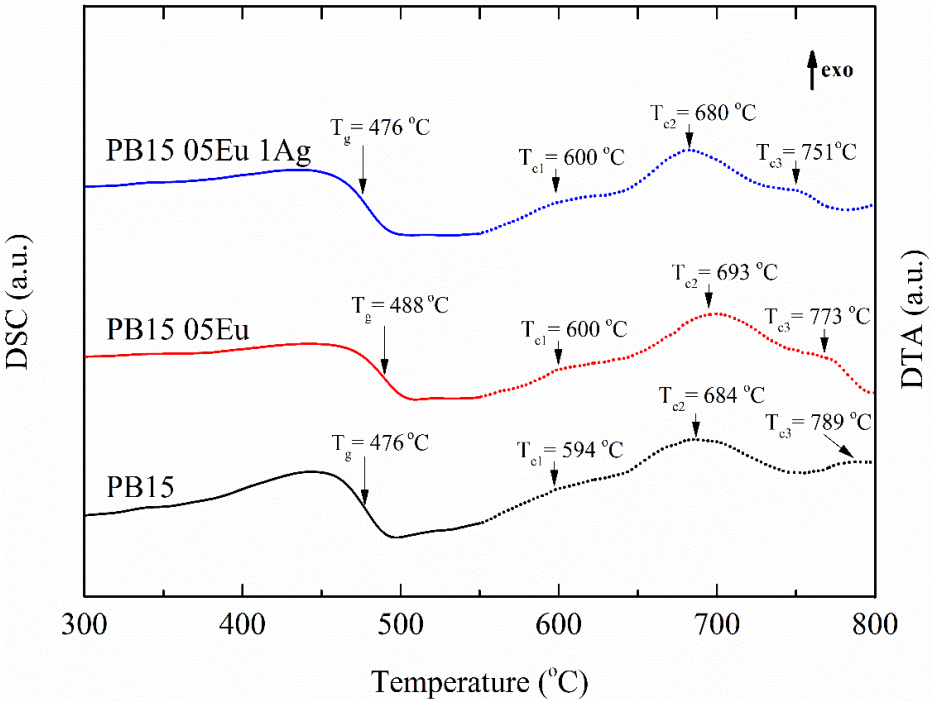

Fig. 46 Results of DSC (continuous line) and DTA (dotted line) measurements of PB15 glasses and their doped versions. The curves corresponding to the two techniques were rescaled and compared to each other to present the overall characteristics of the measured glasses. Characteristic temperatures are marked with arrows: T_g – glass transition temperature and T_c being the crystallization temperature (exothermic maximum)

Figure 46 shows the thermal analysis of glasses based on the PB15 matrix. The analysis was extended with DTA measurements, which provided additional insight into the high-temperature characteristics of the glass containing information on the exothermic phenomena occurring in them. Similarly to the case of PB10, the comparison of the glass transition temperatures enriched with the crystallization temperatures are given in Table 9.

Sample	T_g	T_{c1}	T_{c2}	T_{c3}
PKBN	488	651	698	-
PB10	440	-	-	-
PB10 05Eu	450	-	-	-
PB10 05Eu 05Ag	446	-	-	-
PB10 05Eu 1Ag	453	-	-	-
PB15	476	594	684	789
PB15 05Eu	488	600	693	773
PB15 05Eu 05Ag	482	-	-	-
PB15 05Eu 1Ag	476	600	680	751

Table 9. Characteristic temperatures (°C) determined from DTA/DSC measurements. The notations used are analogous to those introduced in Fig. 46. Gray areas indicate that the corresponding value was not measured

Referring to the previously discussed topic of the effect of Bi_2O_3 reduction on the position of the glass transition (glass transition temperature), it can be seen that a smaller "loss" in the case of PB15 glass led to a decrease in T_g of only ~10 °C. This shows that the observed change is not proportional to the size of the Bi_2O_3 content loss (ΔT = 25 °C would be expected), and therefore it can be concluded that the probable cause is a complex phenomenon and more strongly related to the mutual relations between the components than to the reduction of the Bi_2O_3 share itself. The sensitivity of the studied glasses to seemingly minor interferences in their composition is particularly interesting. It cannot be ruled out that the nonlinear relationship presented by the PB10 and PB15 compositions (being aware that two points are not the best basis) for glasses containing a Bi_2O_3 share in the range between 10 and 15 mol% could not be fulfilled in the presence of a local maximum related, for example, to an exceptionally favorable stoichiometry. The doubt expressed in this way is intended to indicate that in this system, potentially simple control of glass properties in a wide range could be capricious in its nature. However, the case of PB15 05Eu shows that the effect of the Eu dopant on the structure of the glasses, and thus the position of the glass transition, is similar to the case of PB10 glass and leads to an increase in T_g by about 12 °C. Although the presented comparison covers only two cases, it can be suggested without obligation that, taking into account the scale of the change in the T_g position caused by the reduction in the Bi_2O_3 share, the influence exerted by Eu^{3+} ions seems to be independent of this reduction and almost the same for PB10 and PB15. This would confirm the strongly modifying properties of Eu_2O_3 in the environment of the PKBN matrix and in its derivative

glasses. As a result of introducing 1 mol% silver dopant into PB15 05Eu glass, unexpectedly the T_g value (476 °C) equaled that measured for the unmodified PB15 sample. The noted change, apart from the relatively large difference ΔT = 12 °C, was a departure from the increase in T_g observed for the PB10 05Eu 1Ag sample. If the described case were treated step by step, it could be assumed that the changes introduced by the Eu dopant were to some extent leveled by the addition of Ag, as a result of which the PB15 05Eu 1Ag glass has thermal characteristics similar to the initial matrix. However, if all the changes depended solely on the (indirect) interaction between Ag^+ and Eu^{3+} ions, at least the same trend of T_g change should occur for PB10 05Eu 1Ag and the opposite is observed. This approximate description is based only on the recorded end effects, and the actual structural changes responsible for the mentioned evolution are much more complex, which does not change the fact that their large scope in the face of relatively small compositional changes constitutes an extremely interesting new research topic.

Analyzing the right part of Figure 46 containing the curves obtained in DTA measurements in the range of 550 – 800 °C for each of the tested samples, one can see three exothermic maxima (the lowest of the temperatures was marked as T_{c1}, the next ones analogously), which are identified with different crystallization processes of glass matrices. At first glance, the recorded crystallization temperatures do not show a uniform dependence, which would be consistent with the evolution of T_g. The position of the first exothermic maximum changes slightly after the introduction of 0.5 mol% Eu (T_{c1} = 600 °C), and for the PB15 05Eu 1Ag sample it remains the same. The exothermic maxima described by the T_{c2} parameters are the most intense of all three, and in this case the PB15 and PB15 05Eu 1 Ag glasses share practically the same value of T_{c2} ≈ 682 °C, while for the PB15 05Eu sample a significantly higher T_{c2} temperature of 693 °C was recorded. The last of the observed temperatures (T_{c3}) decreases gradually with the number of types of introduced dopants. The presented changes show that each of the processes associated with specific maxima interacts differently with the introduced dopants, therefore probably each of the effects should be treated independently. Using the reasoning proposed in the previous paragraph, based on the changes in the characteristic temperatures, it can be determined that the dominant influence on the form of the effect associated with T_{c1} is the Eu dopant, while in the case of T_{c2} it is the Ag dopant. The process described by T_{c3} cannot be assigned to any of the options presented and it is possible that it is based on the macroscopic crystallization processes of the matrix, which is directly influenced by the state of the glass network (the more compounds disturbing its continuity are present in the composition, the lower the T_{c3} temperature).

Based on the results presented in Figure 46, in addition to the previously determined annealing temperature T = 500 °C, it was decided to select a second, higher temperature T = 550

°C for the series of glasses based on the PB15 matrix. The PB15 series, due to the higher share of Bi_2O_3, showed higher thermal resistance, but at the same time potentially a greater chance of reducing metallic Bi instead of Ag particles. For this reason, the studies carried out on this series were of a different nature than for PB10 and focused on checking the widest possible temperature ranges and annealing times in terms of the possibility of observing plasmon resonance. In the case of the PB10 series, a subtle approach was adopted, in which the priority was to obtain Ag nanoparticles without significant deterioration of the sample properties, mainly transparency and its form.

UV-Vis analysis

Two sets of absorption spectra in the UV–Vis range obtained for the annealed PB10 05Eu 05Ag and PB10 05Eu 1Ag glasses are presented in Figures 47 and 48, respectively. They show comparison of the effect of annealing the glasses at 500 °C for 0, 3, 6 and 22 h on the transmission properties, the occurrence and changes of the absorption bands associated with the presence of Eu^{3+} ions, and in particular the presence of the absorption band associated with the surface plasmon resonance.

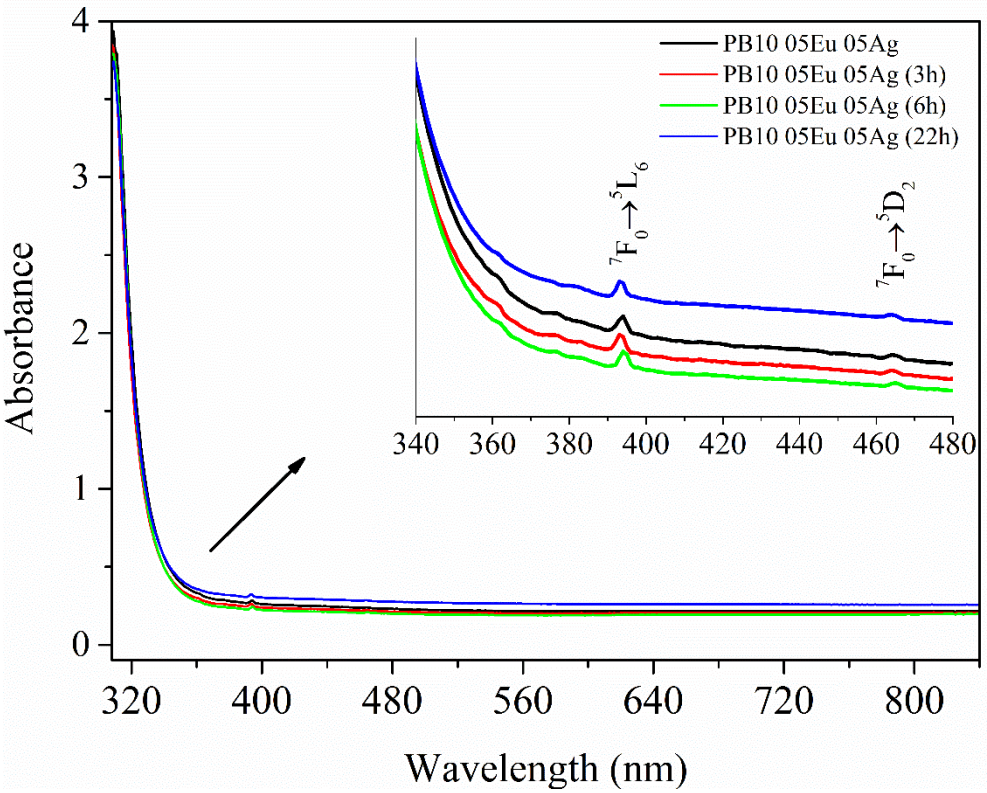

Fig. 47 Summary of UV-Vis spectra obtained for PB10 05Eu 05Ag glasses, which were annealed at 500 °C for a total of 3, 6 and 22 h. Additionally, a reference spectrum of PKBN 05Eu is included. Enlarged spectral range include a description of Eu^{3+} absorption bands

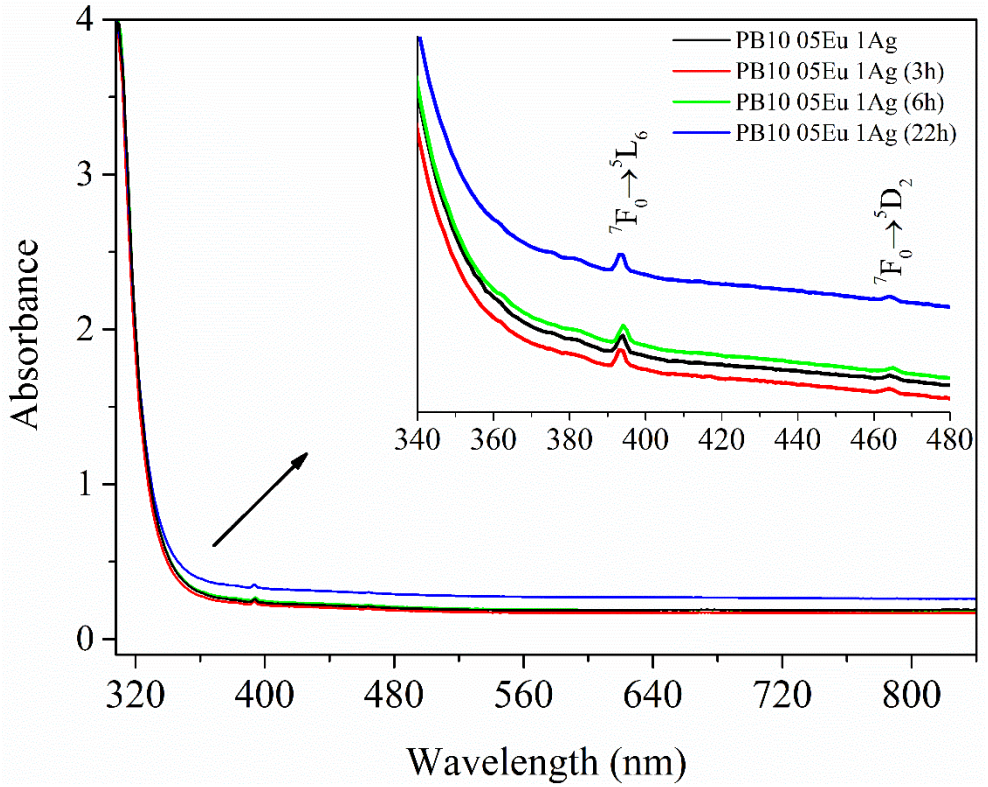

Fig. 48 Summary of UV-Vis spectra obtained for PB10 05Eu 1Ag glasses, which were annealed at 500 °C for a total of 3, 6 and 22 h. Additionally, a reference spectrum of PKBN 05Eu is included. Enlarged spectral range include a description of Eu^{3+} absorption bands

At first glance, it can be seen that for both glasses containing 0.5 mol% and 1 mol% Ag there are only minimal differences between the spectra. For all samples, two absorption bands originating from characteristic electronic transitions $^7F_0 \rightarrow {}^5L_6$ and $^7F_0 \rightarrow {}^5D_0$ of Eu^{3+} ions (inset in the graphs) were identified, however, with increasing annealing time, no evolution of their form was observed. Regardless of the applied thermal treatment parameters, no band corresponding to the surface plasmon resonance was observed for any of these samples. In accordance with the assumptions, the applied annealing temperature did not adversely affect the sample transparency (photos in Figure 43), which is evidenced by slight differences in the transmission level, which remains unchanged up to nearly 360 nm. However, it can also be stated that based on the above results, no significant differences were observed between the samples containing 0.5 and 1 mol% Ag. Attempts to apply higher annealing temperatures to PB10 glasses resulted in their clouding and crumbling, setting the modification limit for materials of this composition, and therefore they were not included in this work.

The results of absorption spectroscopy obtained for PB15 05Eu 1Ag glasses heated at 500 and 550 °C were collected in terms of the applied duration (3 – 48 h) of heat treatment in Figures 49 and 48. The spectra included in Figure 49 correspond to the samples obtained in the

heating process carried out at 500 °C, and at the outset, it can be stated that they are very similar to the measurement curves from Figures 47 and 48. Similarly to the above examples, bands related to the presence of Eu dopant appear, the form of which is unchanged with increasing annealing time. Based on the analysis of the PB10 05Eu 1Ag samples heated at 500 °C in less than 22 h, it was suspected that the process carried out for PB15 05Eu 1Ag at 500 °C in less than 22 h has a low probability of obtaining effects related to the appearance of Ag precipitations. The spectra presented below confirmed the above-mentioned assumptions and, in most cases, provided information about the absence of the surface plasmon resonance band also for the glasses subjected to annealing for 48 h. The slight change in the transmission level noted for the latter is probably related to a small deformation of the sample surface.

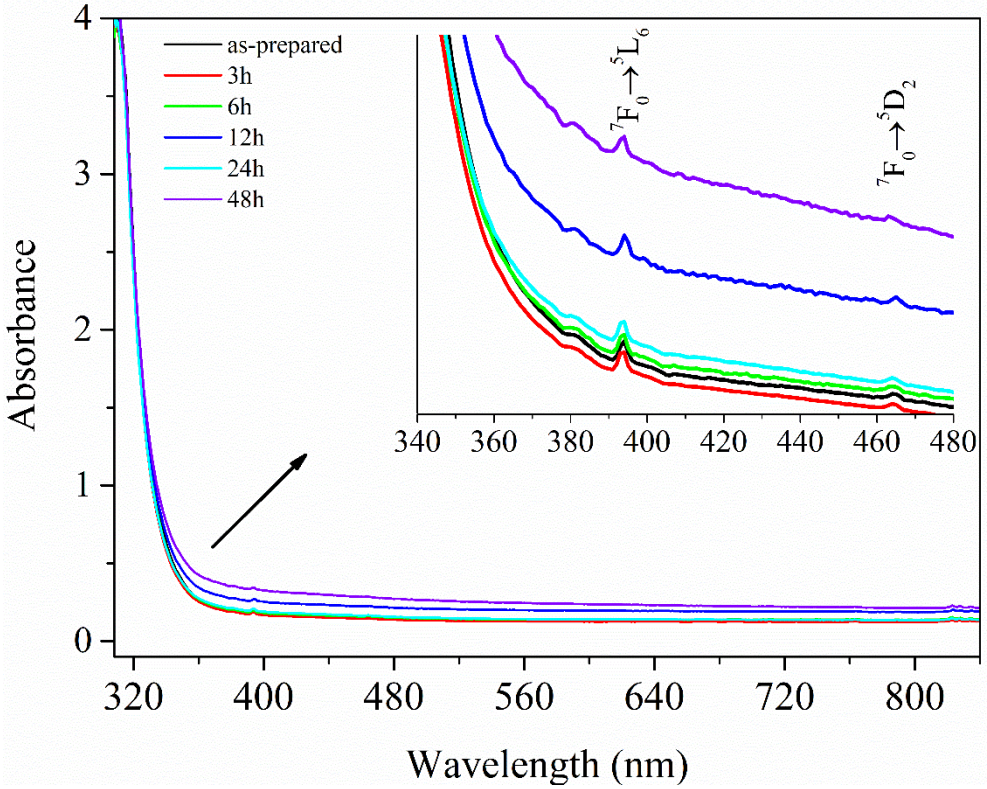

Fig. 49 Summary of UV-Vis spectra obtained for PB15 05Eu 1Ag glasses, which were subjected to a series of annealing at 500 °C in the range of total annealing time of 3–48 h. Additionally, a reference is included in the form of a spectrum of an unannealed sample of this glass. Enlarged spectral range include a description of Eu^{3+} absorption bands

The last of the presented sets of UV-Vis spectroscopy results differ significantly from the previously presented ones due to intensive changes in the shape of the curves with increasing heating time (however, absorption bands related to Eu^{3+} were observed for them). The occurring changes can be divided into two types, the first group will include spectra recorded for glasses heated for 3, 6, and 12 h, while the second group consists of spectra of samples treated for 24

and 48 h. In the first of the specified groups, with increasing heating time, an increase in absorbance is observed, followed by decreasing wavelength (in the case of 3 and 6 h more inclined in the range of 500-700 nm). For the sample heated for 12 h, the curve in the range of 500 - 700 nm is inflected, resulting in a less variable shape. The spectra classified into the second group are characterized by constant, high absorbance in the entire range beyond the absorption threshold. The uniqueness of the described results is probably related to the morphological changes of the sample surface caused by thermal treatment. It was decided to use the highest possible temperature in this case (following the DTA curve from Figure 46, the temperature just before the onset of the first exothermic maximum was selected) because it maximized the chance of agglomeration of Ag atoms while maintaining the amorphous form of the glass matrix itself. Due to the occurring temperature fluctuations and the fact that an imperfect sample was tested, and the DTA result comes from its powdered, and therefore averaged form, subsequent annealing led to the formation of inhomogeneities and progressive turbidity of the glass. As a result, despite the use of extreme conditions, it was not possible to clearly observe the surface plasmon resonance band, although the evolution of the shape of the spectra is a separate, interesting issue. There is, however, a chance that the band associated with the plasmon resonance, due to its low intensity and large width (promoted by the inhomogeneity of the environment and thus the probability of a larger dispersion of the Ag particle sizes), has blurred against the background of the spectra, changing their form only slightly, as in the case of the samples annealed for 12 h and longer presented in Figure 50. In this context, special attention should be paid to the fragment of the curves from the range from 400 to 500 nm, where an enthusiastic eye could see a faint maximum. Still, these are only loose considerations that would require further experimental confirmation.

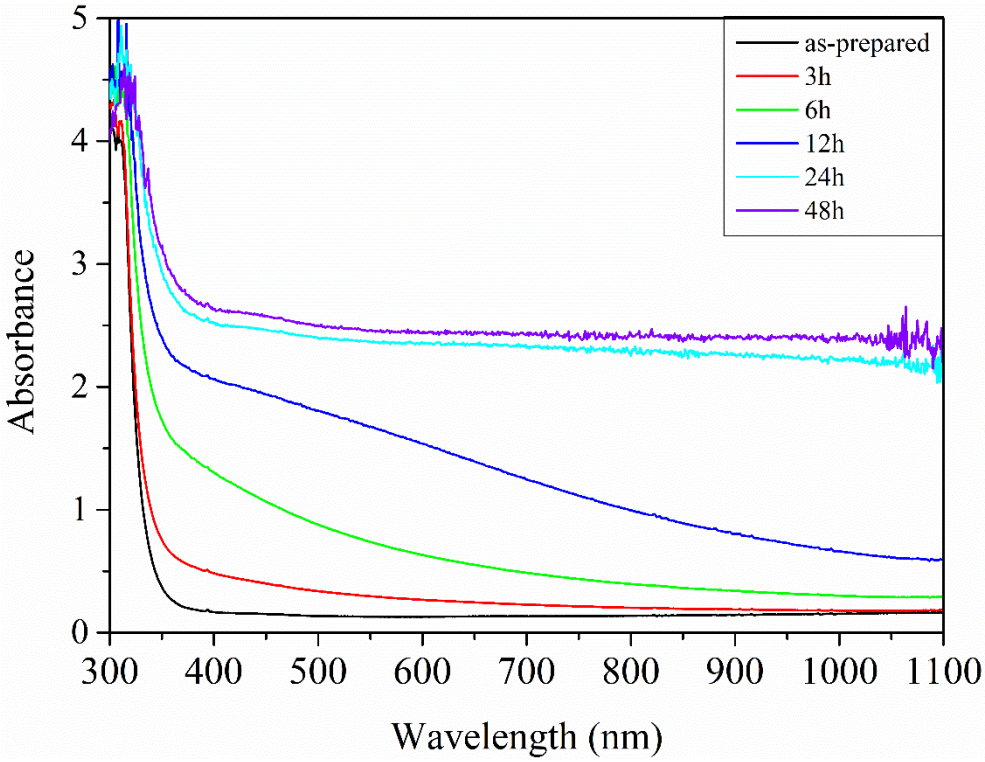

Fig. 50 Summary of UV-Vis spectra obtained for PB15 05Eu 1Ag glasses, which were subjected to a series of annealing at 550 °C for a total annealing time of 3–48 h. Additionally, a reference is included in the form of the spectrum of an unannealed sample of this glass

Luminescence analysis

The conducted heat treatment series, despite the lack of direct evidence for the presence of nanoparticles in the glasses subjected to the annealing, constituted an additional factor that could have a direct effect on the luminescent properties of Eu^{3+} ions dispersed in them. In connection with the manifested issue, the glass matrices and materials created after their controlled thermal treatment were subjected to spectrofluorimetric measurements, the effect of which is presented, among others, in Figure 51. It contains juxtaposed excitation spectra (λ_{em} = 615 nm) and emission spectra (λ_{ex} = 465 nm) measured for unannealed PB10 05Eu glasses and its two variants containing 0.5 and 1 mol% of Ag dopant.

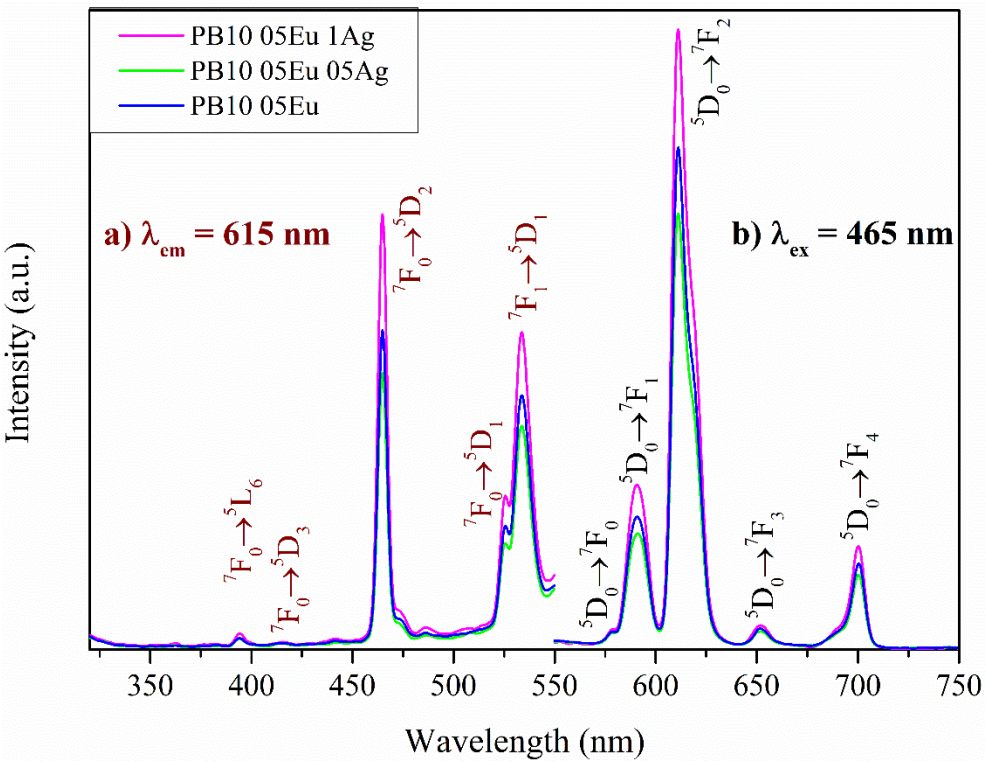

Fig. 51 Comparison of a) excitation (λ_{em} = 615 nm) and b) emission (λ_{ex} = 465 nm) spectra recorded for as-prepared PB10 glasses doped with Eu and Ag

In the excitation spectra shown on the left side of the above figure, five maxima were observed, which due to their position could be assigned to electronic transitions in the Eu^{3+} ion; their designations are shown in Figure 51. Similarly to the case described for the PF glass series, the intensity disproportion between the bands in the ultraviolet and those occurring above 450 nm was so large that it was not possible to clearly observe typical transitions $^7F_0 \rightarrow {}^5D_4$ and $^7F_0 \rightarrow {}^5G_4$. The composition that stood out in the presented comparison turned out to be PB10 05Eu 1Ag, while the slightly different composition PB10 05Eu 05Ag, in terms of intensity, turned out to be the least promising. A corresponding tendency was observed for the emission spectra presented in part b) of Figure 51. Only for the composition containing 1 mol% of Ag dopant, the luminescence enhancement was observed (compared to the glass without the addition of a noble metal). It should be mentioned that in all of the recorded emission spectra the bands occurring were assigned to the $^5D_0 \rightarrow {}^7F_J$ (J = 0 - 7) transitions characteristic of Eu^{3+} ions.

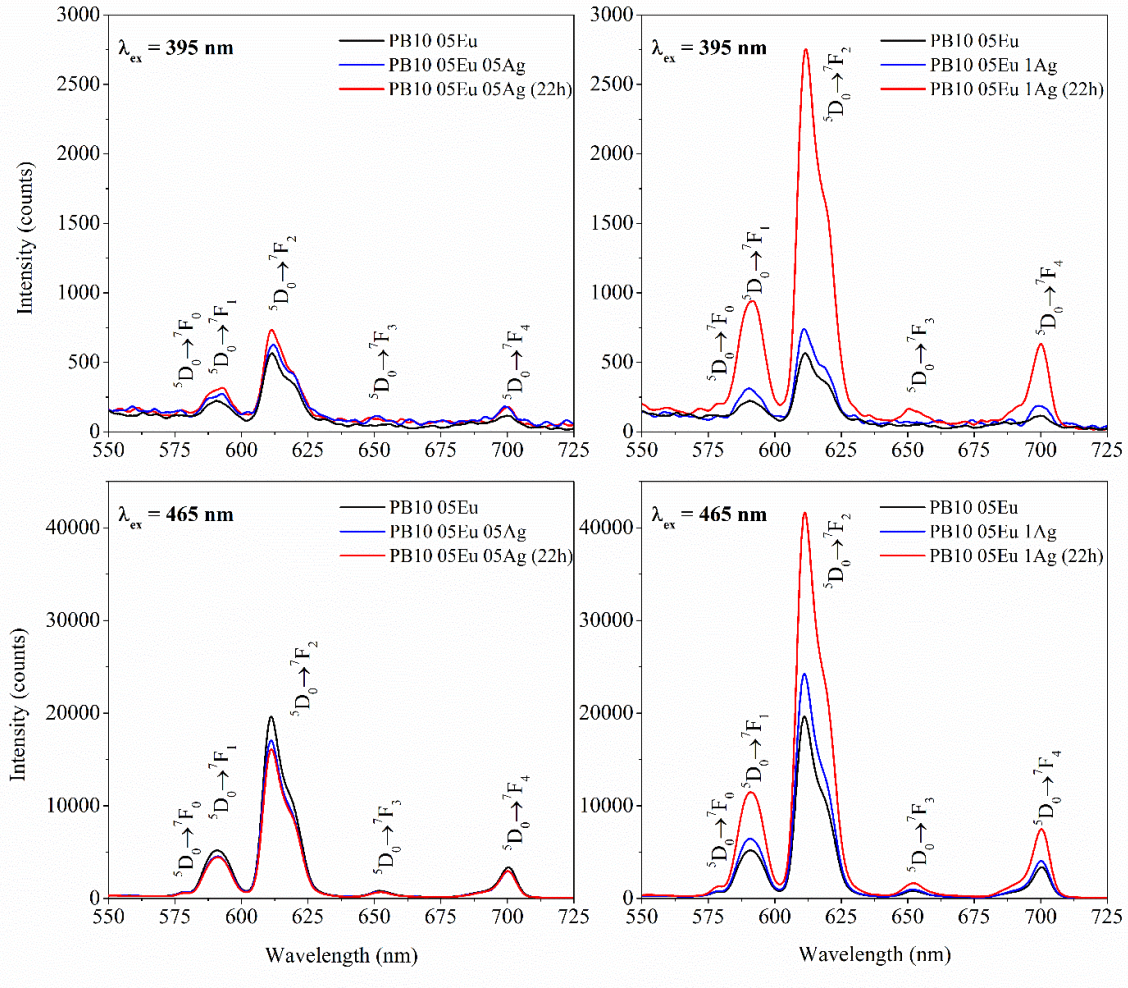

Fig. 52 Summary of emission spectra recorded for the excitation wavelength of λ_{ex} = 395 nm (top) and λ_{ex} = 465 nm (bottom) of PB10 05Eu 05Ag and PB10 05Eu 1Ag glasses, illustrating the effect of the annealing treatments (500 °C for 22 h) on the luminescent properties

Therefore, the aforementioned luminescence enhancement is a sign of a beneficial effect of the Ag dopant on the emission properties of the active centers dispersed in the glass in the form of Eu^{3+} ions. The absorption spectroscopy measurements conducted excluded the possibility of surface plasmon resonance, so the increase in the intensity of the observed emission must be related to a different mechanism, in which Ag is one of the key factors. The previously described changes in the T_g position (Figure 45) under the influence of the Ag dopant may be a clue to understanding this mechanism, in which silver modifies glass network. Treating this dopant in this way, as another element of a complex system that must take place in the amorphous structure, thereby causing local changes, it can be assumed that in a given matrix configuration, these changes had a positive effect on the probability of emission in Eu^{3+} ions. As a result, an increase in the band intensity was observed for a sufficiently high concentration of Ag ions in the composition of PB10 05Eu glasses.

Figure 52 shows four sets of emission spectra showing additionally the effect of heating the PB10 05Eu 05Ag (left side) and PB10 05Eu 1Ag (right side) glasses at 500 °C for 22 h. In addition, the upper part of the figure contains spectra obtained using an excitation wavelength of λ_{ex} = 395 nm, while the lower part contains spectra with λ_{ex} = 465 nm. Starting the analysis with two comparisons located on the left side of the figure, it can be seen that in the case of samples containing only 0.5 mol% Ag, heating did not lead to major changes in the spectra, regardless of the selected excitation wavelength. A diametrically different effect was obtained in the case of glasses containing 1 mol% Ag (right side of Figure 52). Compared to the enhancement obtained by the introduction of silver dopant alone, for the sample heated at 500 °C for 22 h, a nearly twofold increase in emission intensity was noted for the excitation with light at a wavelength of 465 nm and a fourfold increase for the excitation λ_{ex} = 395 nm (however, this is still a very low intensity compared to 465 nm). These observations additionally emphasize that there is probably a threshold Ag content above 0.5 mol%, above which it has a beneficial effect on the emission properties of the glasses. What is the reason for such a significant increase in intensity for the heated PB10 05Eu 1Ag glasses, since the presence of SPR was not directly demonstrated for them and the occurrence of crystalline phases was not observed? One of the probable options that could explain the recorded results is the summation of the beneficial effects of relaxation of the glass network (similarly to the case of heated PKA15 05Eu glasses) with local structural changes introduced by Ag ions. In addition, the presence of crystalline precipitates below the detection threshold of XRD measurement should be considered, especially in the presence of a strong amorphous halo. However, it is important to emphasize that due to the disproportion between glasses containing 0.5 mol% and 1 mol% Ag, each of the listed components would have to take into account the key presence of this dopant.

The last of the comparisons presenting the evolution of the emission spectra of PB15 05Eu 1Ag glass depending on the applied temperature (500 °C – left side, 550 °C – right side) and the times of the performed annealing is presented in Figure 53. The situation shown there is ambiguous, starting from the upper left part, the sample subjected to 6h annealing stands out in particular, thus achieving an intensity comparable to that recorded for PB10 05Eu 1Ag glass annealed for 22h at the same temperature. Longer annealing times were characterized by a similar, almost half lower intensity, but it can be seen that for different levels of the band intensity corresponding to the $^5D_0 \rightarrow {}^7F_2$ transition, the intensities of the band related to the 5D0 → 7F1 transition are almost the same. This means different values of the R/O parameter, which is the highest (among the samples heated for 12, 24, and 48 h) for the sample heated for 48 h. The emission spectra (λ_{ex} = 465 nm) obtained for the corresponding samples were compared in the lower left part of the figure 53. It was observed that they exhibit different intensity

dependence on the duration of the thermal treatment process. Invariably, for all the combinations included in Figure 53, the spectrum of the sample heated for 3 h is characterized by the lowest intensity (also in comparison to the unannealed glass), and the highest luminescence enhancement was observed for the sample heated for 48 h. The remaining spectra showed a small scatter of intensity with a peculiar result obtained for the sample heated for 6 h.

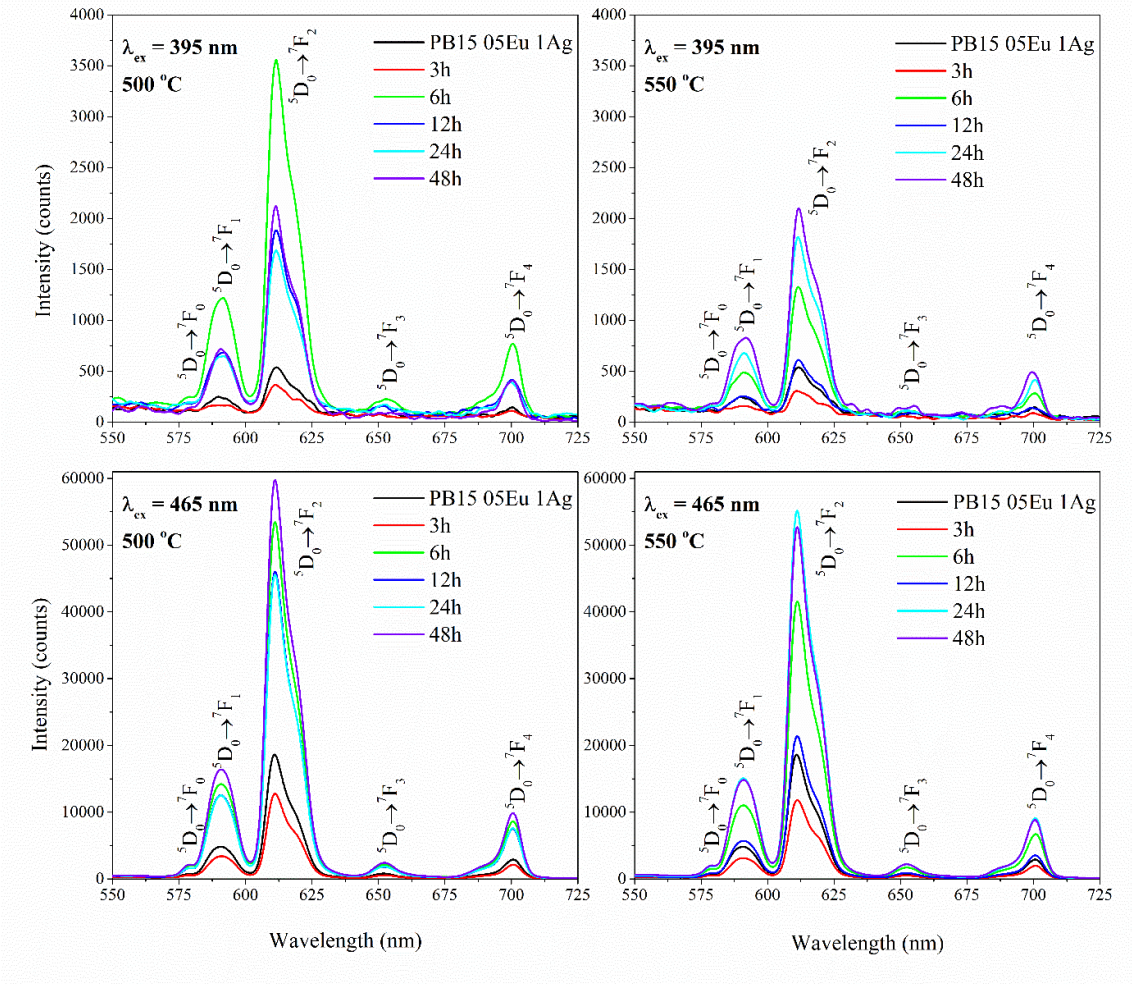

Fig. 53 Summary of emission spectra recorded for the excitation wavelength of λ_{ex} = 395 nm (top) and λ_{ex} = 465 nm (bottom) of PB15 05Eu 1Ag glasses, illustrating the effect of a series of annealing treatments at 500 and 550 °C on their luminescent properties

The right part of the above figure contains spectra of samples obtained in the process carried out only for PB15 05Eu 1Ag glasses and can be considered as an image of the effect of annealing at the limiting (conceptually the highest temperature that can meet the assumptions of the optical material) temperature on the properties of this material. Due to the smaller control of the sample form in the process, it is not possible to directly compare the results with those obtained for PB10 glasses annealed at 500 °C, but it is an interesting set of relationships that facilitates indirect conclusions about the changes taking place based on a comparison with PB15

samples annealed at 500 °C. Analyzing them for the spectra measured at excitation with a wavelength of λ_{ex} = 395 nm (top right graph), it can be seen that the intensities and mutual dependence of the bands of samples obtained in the heat treatment process lasting 24 and 48 h are similar to those noted for these samples annealed at 500 °C. However, in this case, the glass heated the longest is also the one that shows the most intense emission. Both in the described comparison and in the one presenting emission spectra at 465 nm excitation, the sample heated for 12 h showed only a slight enhancement of luminescence. In addition, this comparison revealed that the most advantageous in terms of emission intensity was the 24-hour heat treatment. The above analysis revealed that in general, the most advantageous in terms of luminescent properties of PB10 and PB15 materials is the use of a higher share of Ag in the composition and long heating times at a temperature not significantly exceeding T_g are preferred. An exception was the PB15 05Eu 1Ag sample, which after only 6 h of heating at 500 °C was characterized by an exceptionally high emission intensity, but the reason for such a sudden change in properties between 3 and 6 h is not known.

The presented results of Ag doped phosphate glasses, although they are only preliminary, revealed a potential direction of development of this material as an optical system, in which the Ag addition could be a complementary element, which together with other additions mentioned earlier in this work, could contribute to its universality of applications. Although no unambiguous confirmation of the presence of Ag nanoparticles and the occurrence of the LSPR associated with them (based on the measurements performed) was obtained, there were premises justifying further measurements. In this case, the use of the High-Resolution Transmission Electron Microscope (HR TEM) could prove particularly fruitful, the measurements of which, apart from directly demonstrating the presence of nanoparticles, could become the basis for a broader analysis, in which the structure of the materials would be correlated with the recorded absorption spectra.

4. Conclusions

Starting with the part containing the summary of the conducted research, and thus the culmination of this text, I would like to refer to one of the terms I have not used directly to describe the work so far. As we believe (based on the available literature), the produced phosphate glasses are a completely new material aspiring to be an optical matrix with great application potential. Still, in my opinion, this is not the only feature that needs to be emphasized. Based on the experience gained during both syntheses and characterization, I realized that these glasses are beautiful in their secretive universality. The combination of words proposed, which constitutes "this" term, almost draws (maybe too much) from poetry, but at the same time describes the properties of the materials I have studied so accurately that I will try to clarify this idea in the next few sentences.

So where does this secrecy come from? The simplest way to say it is that the form of these glasses does not in any way reflect their rich interior. As it turns out, an inconspicuous appearance, a slightly yellowish fragment of glass is practically indistinguishable regardless of whether it contains SrF_2, AlF_3, and KF additives or perhaps Eu or Ag dopants. The results presented in this dissertation have shown that behind this small "paradox" there is an extremely complex and delicate arrangement of the amorphous structure of phosphate glasses, in which numerous units cooperate in equilibrium to create a uniform material. In this way, a reference to the postulated universality emerged naturally, in which the matrix of PKBN glass, due to its internal structure, can be a convenient environment for various modifications without losing its typical features, including key ones such as homogeneity and transparency. Thinking about an apt comparison, at first, I thought that a container whose shape, regardless of the additives inside, does not change seemed appropriate. It is unfortunate, however, in that it suggests that the amorphous solid before modification is in some sense empty. This brief hesitation has allowed us to once again distinguish the unique properties of glasses, whose structure, although it may seem empty, is in reality not very different from that of crystalline solids, but in comparison to them still conceals within itself a creative space for further discoveries.

These observations are the result of my work, in which I conducted studies on the structure and properties of synthesized fluoride-modified luminescent phosphate glasses doped with Eu and Ag. Based on the originally produced phosphate glass matrix in the form of P_2O_5 – K_2O – $B_{i2}O_3$ – Nb_2O_5, luminescent materials were designed and produced, which are divided into 3 main variants:

- Eu-doped glasses and glass-ceramics containing SrF_2 additives;
- Eu-doped glasses and glass-ceramics containing AlF_3 and KF additives;

- Eu-doped and Ag-doped glasses with reduced Bi_2O_3 content.

The most important conclusions and observations resulting from the measurements of the above-mentioned materials and the experience gained from their synthesis process are summarized below. Based on thermal analysis measurements, a clear increase in the glass transition temperature was observed for glasses containing the SrF_2 additive, and a relationship was also revealed between its presence in the composition and the disappearance of the high-temperature exothermic maximum present for the PKBN matrix. There was also a premise about the transitional nature of the glass containing 5 mol% SrF_2, which has some common features with the PKBN matrix and with compositions containing more than 10 mol% fluoride. An observation that is particularly important was the collective increase in the characteristic temperatures of the glasses under the influence of the 0.5 mol% Eu doping, which would be evidence of its modifying function of the glass network. The crystallization characteristics carried out in the range of 485 – 605 °C allowed the selection of the temperature of 565 °C as the highest, universal temperature guaranteeing the absence of a detectable crystalline phase in 10 h of annealing and became the basis for determining the temperature of 585 °C as the optimal temperature for conducting controlled crystallization for this series of glasses. Higher annealing temperatures provided information about the emerging crystalline phases, for PKBN these were the monoclinic monazite-type $BiPO_4$ phase, its high-temperature equivalent, and $KNbO(P_2O_7)$. In the case of glasses containing 10 and 15 mol% SrF_2, the recorded reflections corresponded to the low-temperature phase of $BiPO_4$, the cubic phase of SrF_2, and the presence of an unknown phase defined as UnP was detected. The lack of reflections from high-temperature $BiPO_4$ turned out to be consistent with the disappearance of the exothermic maximum observed in the thermal analysis. We suspect that the limitation of the growth of $BiPO_4$ phases is related to the appearance of the UnP phase, hence we conclude that this phase is probably some kind of phosphate. As a result of controlled annealing of glasses doped with 0.5 mol% Eu, the appearance of faint reflections was noted, indicating their multiphase form, no glass-ceramics containing a clearly isolated crystalline phase of SrF_2 were obtained. However, the stabilization effect of glass against crystallization acquired with the addition of Eu was confirmed, and it was also observed that it becomes more significant with the increasing share of SrF_2. The changes in the structure of glasses under the influence of fluoride, apart from the evolution of the phosphate skeleton and the increase in cross-linking, turned out to be concentrated on the transition of Nb and Bi from the modifier function to the transition network former. Luminescence measurements (λ_{ex} = 465 nm) allowed us to determine the effect of SrF_2 content, and single and double annealing processes on the emission properties with the Eu dopant as the

active center. The greatest luminescence enhancement was observed for glass-ceramics obtained in the annealing process at 585 °C for 10 h, and annealing at 545 °C for 10 h was also interesting from the economic point of view, which resulted in materials showing slightly lower intensity. Considering the criterion of luminescence enhancement as a function of SrF_2 content in glass-ceramics, we observed a lack of an unambiguous relationship, but glasses containing 5 and 15 mol% SrF_2 turned out to be promising materials. At the same time, the highest emission intensity was observed for the PKBN 05Eu matrix annealed at 585 °C for 10 h, which may indicate a beneficial effect of the $BiPO_4$ crystalline phase on the emission of Eu^{3+} ions. We have also shown that the double annealing procedure achieves significantly worse results than in the case of direct application of annealing at the target temperature. The proposed explanation may be the nucleation of a foreign phase during the annealing stage at 525 °C, which adversely affects the environment of Eu ions dispersed in the matrix or indirectly reduces the probability of radiative transitions.

The 8 and 10 h of annealing of glasses containing KF and AlF_3 additives at 585 °C led to obtaining glass-ceramics, thus providing a different point of view on the role of non-crystallizing fluorides. The obtained diffractograms allowed us to state that the proportional addition of KF clearly reduces the resistance of glasses to crystallization, and this effect scales with the increasing content of fluoride, while the addition of AlF_3 has a strong stabilizing effect, therefore the recorded diffractograms contained only diffuse reflections on the amorphous envelope, making it impossible to assign crystalline phases. For glass-ceramics based on PFF5 05Eu and PFF15 05Eu, the presence of the monoclinic $BiPO_4$ phase and the UnP phase was identified, additionally, the material with 15 mol% KF contained KNb_3O_5 and Bi_2O_4 crystallites. The tests carried out on the annealed glasses from the PFF series could indicate that the observed susceptibility to crystallization will be equivalent to a lower glass transition temperature compared to PKBN, while its relative increase was noted for both PFF5 and PF5. For the aforementioned series, we observed that the different method of introducing KF leads to large differences in the T_g value only above 10 mol% share - the one read for PFF15 remains unchanged, while for PF15 it increases drastically. We observed that both the addition of 5 mol% AlF_3 and KF (in two series of glasses) manifests itself on the thermal analysis curve in the form of a small exothermic maximum, which did not occur for PKBN, but at the same time, we believe that the thermal effect, with which the maximum T_{c1} = 651 °C was associated for PKBN, is "inherited" by all compositions containing fluoride addition. It is subject to distortions and shifts, but it is a reference for other side maxima that are characteristic of a given fluoride. They are partly echoes of structural changes occurring in the glass network, the general course of which was characterized by infrared spectroscopy measurements. We have observed that for all the

glasses studied, there are indications of fluorine ion incorporation into typical structural units of glasses, but depending on the composition it is manifested in different ways. The main trend of changes in the case of the PF glass series is the formation of a more extensive phosphate network with an increasing share of disproportionate KF addition, as a direct consequence there was an increased probability of forming structural units in the form of linear chains, rings and oxygen polyhedra coordinated by Nb cations. In the case of the PFF series, the proportional addition of KF results in the intensification of the depolymerization process of the glass structure, and therefore there is an increased chance of the appearance of short phosphate chains together with Q_1 and Q_0 units. Moreover, in the case of these materials, we have noted an increased preference for the occurrence of structural units associated with Bi. The addition of AlF_3 in the PKA series glasses has been shown to have a strong effect on the increase in the cross-linking of the structure, especially through the formation of P-O-Al bonds and oxygen-fluorine units with a concentric Al atom. We suspect that the presence of Al becomes more important in the structural role compared to Nb and Bi. The analysis of the influence of Eu dopant on the structure of the glasses has led us to the conclusion that the changes induced by the presence of fluorides and Eu are strongly coupled, and the structural effects of different genesis do not create a simple sum but create a combination that makes it difficult to distinguish them. However, we believe that the Eu dopant affects in particular the extent of the structural changes induced by fluorides, not their type. Luminescence measurements (λ_{ex} = 465 nm) allowed us to notice differences between the PF 05Eu and PFF 05Eu series, in the case of the first of the mentioned only the addition of 10 mol% KF resulted in obtaining emission intensity above that measured for PKBN 05Eu, while for PFF 05Eu the luminescence enhancement was observed for 10 and 15 mol% and it was proportional to the share. In the case of the PKA series, a step change was noted in the case of increasing the share of AlF_3 from 10 to 15 mol% and only for the highest content the enhancement of Eu emission occurred.

As a result of an attempt to reduce the Bi_2O_3 content in the initial PKBN matrix, we obtained two stable, fully amorphous compositions containing 10 and 15 mol% of this substrate. Compositions in which the Bi_2O_3 content was less than 10 mol% could be obtained in an amorphous form, but were characterized by drastically lower water resistance, which determined the impossibility of their real use as optical materials. As a result of annealing samples PB10 05Eu 05Ag and PB10 05Eu 1Ag at 500 °C, materials were obtained for which the presence of any crystalline phases was not detected. At the same time, for this series, the presence of inhomogeneities was observed, independent of the annealing process parameters, the origin of which may be associated with gaseous coproducts trapped during the melting or the effects of phase separation of glasses. In the case of the PB10 series, DSC and DTA techniques

were used to determine the first annealing temperature, the value of which was T_1 = 500 °C and as a temperature on average 50 °C higher than the read T_g could potentially guarantee conditions favorable for crystallization of Ag nanoparticles. They also allowed us to observe a significant decrease in T_g after reducing the Bi_2O_3 content from 20 to 10 mol%, which suggests the importance of the structural role of this element and once again confirms the disproportionately large structural role of the Eu dopant. Also, in the case of PB15, Eu doping caused an increase in T_g - due to its nature, the structural influence of Eu seems to be independent of the change in Bi content. For PB15, 3 exothermic maxima were observed in the range of 550 - 800 °C. On their basis, we concluded that the effect behind the T_{c1} maximum is most strongly influenced by the presence of Eu, while T_{c2} is most strongly influenced by Ag. The absorption measurements performed included characterization of the effect of annealing on the optical properties of the PB10 and PB15 samples. Among the spectra of the annealed PB10 samples, no band associated with the surface plasmon resonance was observed, and there were no significant differences between the bands obtained for the samples doped with 0.5 mol% and 1 mol% Ag. We found that the use of higher annealing temperatures over 500 °C resulted in sample turbidity and cracking, setting the modification limit for this material. The spectra of the PB15 05Eu 1Ag glasses annealed at 500 °C turned out to be very similar in form and shape to analogous samples based on the doped PB10 matrix. Regardless of the glasses used and the annealing parameters, no band associated with the presence of plasmon resonance was clearly observed. We suspect that in the case of the PB15 05Eu 1Ag sample annealed at 550 °C for 12 h, a broad, diffuse maximum in the range of 400–500 nm associated with the plasmon resonance occurred, but it was distorted in the background of the spectrum and would require further confirmation. Analysis of the luminescence spectra showed that the different emission character of the as-prepared PB10 05Eu 05Ag and PB10 05Eu 1Ag glasses and their annealed versions suggests that the presence of the Ag dopant in an appropriate concentration has a beneficial effect on the emission properties of the deposited Eu^{3+} ions. In the case of PB15 05Eu 1Ag glasses heated at 500 °C, the spectra obtained at λ_{ex} = 465 nm (except for the sample heated for 3 h) showed a similar, large luminescence enhancement, of which the highest intensity was read for the sample heated for a total of 48 h.

Returning to the very beginning of this path, I can refer to the set goals and hypotheses that gave shape and meaning to this work. Although most of the goals were fulfilled, the pursuit of their fulfillment turned out to be particularly important, during which surprising issues and topics emerged, which I could not even consider when creating the original list. The discussed issue, or rather its subject itself, turned out to be a versatile material, therefore, even in terms of application as a potential luminophore, I can state that the presented work contains a set of

preliminary studies. I say this especially in relation to hypotheses because although I was not able to directly prove the presence of SrF_2 nanocrystals in the glass volume and the precipitation of Ag nanoparticles in a matrix with a reduced Bi_2O_3 content, I deeply believe that it was only a matter of limited time because this glass certainly has still much more to offer.

5. Bibliography

[1] Shelby, J.E. Introduction to Glass Science and Technology, 2nd edition. *The Royal Society of Chemistry* (2005).

[2] Turnbull, D. (1969). Under what conditions can a glass be formed*? Contemporary Physics*, 10(5), 473–488.

[3] Zallen, R. Fizyka ciał amorficznych. *PWN* (1994).

[4] Zachariasen, W. H. (1932). The atomic arrangement in glass. *Journal of the American Chemical Society*, 54(10), 3841-3851.

[5] Vogel, W. Glass Chemistry, 2nd edition. *Springer-Verlag* (1994).

[6] Uhlmann, D. R. (1972). A kinetic treatment of glass formation. *Journal of Non-Crystalline Solids*, 7(4), 337-348.

[7] Uhlmann, D. R. (1982). Kinetics of glass formation and devitrification behavior. *Le Journal de Physique Colloques*, 43(C9), C9-175.

[8] Zanotto, E. D. (2010). Bright future for glass-ceramics. *American Ceramics Society Bulletin*, *89*(8), 19-27.

[9] Deubener, J., Allix, M., Davis, M. J., Duran, A., Höche, T., Honma, T., Komatsu, T., Krüger, S., Mitra, I., Müller, R., Nakane, S., Pascual, M. J., Schmelzer, J. W. P., Zanotto, E. D., & Zhou, S. (2018). Updated definition of glass-ceramics. *Journal of Non-Crystalline Solids*, 501, 3-10.

[10] Neuville, D. R., Cormier, L., Caurant, D., & Montagne, L. From glass to crystal: Nucleation, growth and phase separation: from research to applications. *EDP Sciences* (2017).

[11] Stookey, S. D. (1959). Catalyzed crystallization of glass in theory and practice. *Industrial & Engineering Chemistry*, *51*(7), 805-808.

[12] Beall, G. H. (1992). Design and properties of glass-ceramics. *Annual Review of Materials Science*, *22*(1), 91-119.

[13] Hopper, R. W. (1985). Stochastic theory of scattering from idealized spinodal structures: II. Scattering in general and for the basic late stage model. *Journal of non-crystalline solids*, 70(1), 111-142.

[14] Beall, G. H., & Pinckney, L. R. (1999). Nanophase glass-ceramics. *Journal of the American Ceramic Society*, *82*(1), 5-16.

[15] Musgraves J.D., Hu J., Calvez L. (eds) Springer Handbook of Glass. Springer Handbooks. *Springer* (2019).

[16] Bunker, B. C., Arnold, G. W., & Wilder, J. A. (1984). Phosphate glass dissolution in aqueous solutions. *Journal of Non-Crystalline Solids*, *64*(3), 291-316.

[17] Varshneya, A. K., Maurok, J. C. Fundamentals of Inorganic Glasses, Third Edition. *Elsevier* (2019).

[18] Bunker, B. C., Arnold, G. W., Rajaram, M., & DAY, D. E. (1987). Corrosion of phosphorus oxynitride glasses in water and humid air. *Journal of the American Ceramic Society*, *70*(6), 425-430.

[19] Marchand, R., Agliz, D., Boukbir, L., & Quemerais, A. (1988). Characterization of nitrogen containing phosphate glasses by X-ray photoelectron spectroscopy. *Journal of non-crystalline solids*, *103*(1), 35-44.

[20] Reis, S. T., Karabulut, M., & Day, D. E. (2001). Chemical durability and structure of zinc–iron phosphate glasses. *Journal of Non-Crystalline Solids*, *292*(1-3), 150-157.

[21] Takebe, H., Baba, Y., & Kuwabara, M. (2006). Dissolution behavior of $ZnO–P_2O_5$ glasses in water. *Journal of Non-Crystalline Solids*, *352*(28-29), 3088-3094.

[22] Teixeira, Z., Alves, O. L., & Mazali, I. O. (2007). Structure, thermal behavior, chemical durability, and optical properties of the $Na_2O–Al_2O_3–TiO_2–Nb_2O_5–P_2O_5$ glass system. *Journal of the American Ceramic Society*, *90*(1), 256-263.

[23] Hoppe, U., Walter, G., Barz, A., Stachel, D., & Hannon, A. C. (1998). The PO bond lengths in vitreous probed by neutron diffraction with high real-space resolution. *Journal of Physics: Condensed Matter*, 10(2), 261.

[24] Hoppe, U., Walter, G., Kranold, R., & Stachel, D. (1998). An X-ray diffraction study of the structure of vitreous P_2O_5. *Zeitschrift für Naturforschung A*, 53(3-4), 93-104.

[25] Uchino, T., & Ogata, Y. (1995). Ab initio molecular orbital calculations on the electronic structure of phosphate glasses. Sodium phosphate glasses. *Journal of non-crystalline solids*, 181(1-2), 175-188.

[26] Lippmaa, E., Maegi, M., Samoson, A., Engelhardt, G., & Grimmer, A. R. (1980). Structural studies of silicates by solid-state high-resolution silicon-29 NMR. *Journal of the American Chemical Society*, *102*(15), 4889-4893.

[27] Van Wazer, J. R. (1950). Structure and properties of the condensed phosphates. II. A theory of the molecular structure of sodium phosphate glasses. *Journal of the American Chemical Society*, 72(2), 644-647.

[28] Van Wazer, J. R., & Griffith, E. J. (1955). Structure and properties of the condensed phosphates. X. General structural theory. *Journal of the American Chemical Society*, 77(23), 6140-6144.

[29] Hoppe, U. (1996). A structural model for phosphate glasses. *Journal of Non-Crystalline Solids*, 195(1-2), 138-147.

[30] Brow, R. K. (2000). The structure of simple phosphate glasses. *Journal of Non-Crystalline Solids*, 263, 1-28.

[31] Zissis, G., Bertoldi, P. and Ribeiro Serrenho, T. (2021), Update on the Status of LED-Lighting world market since 2018, EUR 30500 EN, *Publications Office of the European Union*, Luxembourg.

[32] Pattison, M., Hansen, M N. Bardsley, C. Elliott, K. Lee, L. Pattison, J. Tsao (2020), 2019 Lighting R&D Opportunities, *DOE BTO Lighting R&D Program*.

[33] Schubert, E. F. Light-Emitting Diodes (3rd Edition). *E. Fred Schubert* (2018)

[34] Shur, M. S., Žukauskas, A. (2005), Solid-State Lighting: Toward Superior Illumination, *Proc. IEEE* 93 1691-1703.

[35] Muthu, S., Schuurmans, F. J., & Pashley, M. D. (2002). Red, green, and blue LEDs for white light illumination. *IEEE Journal of selected topics in quantum electronics*, 8(2), 333-338.

[36] Muthu, S., Schuurmans, F. J., & Pashley, M. D. (2002). Red, green, and blue LED based white light generation: issues and control. In *Conference record of the 2002 IEEE industry applications conference. 37th IAS annual meeting (cat. No. 02CH37344)* (Vol. 1, pp. 327-333). IEEE.

[37] Chen, L., Lin, C. C., Yeh, C. W., & Liu, R. S. (2010). Light converting inorganic phosphors for white light-emitting diodes. *Materials*, *3*(3), 2172-2195.

[38] Trivellin, N., Meneghini, M., Buffolo, M., Meneghesso, G., & Zanoni, E. (2018). Failures of LEDs in real-world applications: A review. *IEEE Transactions on Device and Materials Reliability*, *18*(3), 391-396.

[39] Meneghesso, G., Meneghini, M., & Zanoni, E. (2010). Recent results on the degradation of white LEDs for lighting. *Journal of Physics D: Applied Physics*, *43*(35), 354007.

[40] Singh, P., & Tan, C. M. (2016). A review on the humidity reliability of high power white light LEDs. *Microelectronics Reliability*, *61*, 129-139.

[41] Geng, X., Xie, Y., Chen, S., Luo, J., Li, S., Wang, T., Zhao, S., Wang, H., Deng, B., Yu, R., & Zhou, W. (2021). Enhanced local symmetry achieved zero-thermal-quenching luminescence characteristic in the Ca_2InSbO_6: Sm^{3+} phosphors for w-LEDs. *Chemical Engineering Journal*, *410*, 128396.

[42] Qian, Y., Zhu, D., & Pu, Y. (2022). A zero-thermal-quenching phosphor $Sr_3La(AlO)_3(BO_3)_4$: Dy^{3+} for near ultraviolet excitation white-LEDs. *Journal of Luminescence*, *243*, 118610.

[43] Wang, J., Xie, Y., Guo, J., Yao, X., Geng, X., Gao, J., Feng, X., Zhou, Z., Liu, Y., Deng, B., & Yu, R. (2021). Abnormal thermal quenching behavior and optical properties of a novel apatite-type $NaCa_3Bi(PO_4)_3F$: Sm^{3+} orange-red-emitting phosphor for w-LED applications. *Ceramics International*, *47*(20), 28167-28177.

[44] Yin, Y., Yang, W., Wang, Z., Zhang, Y., Zhu, M., Dou, C., Che, Y., Sun, S., Hu, C., Teng, B., Zhao, J., Lu, J., Sun, R., & Zhong, D. (2022). Achieving zero-thermal quenching luminescence in $ZnGa_2O_4$: 0.02 Eu^{3+} red phosphor. *Journal of Alloys and Compounds*, *898*, 162786.

[45] Ofelt, G. S. (1962). Intensities of crystal spectra of rare-earth ions. *The journal of chemical physics*, 37(3), 511-520.

[46] Judd, B. R. (1962). Optical absorption intensities of rare-earth ions. *Physical review*, 127(3), 750.

[47] Wang, J., Brocklesby, W. S., Lincoln, J. R., Townsend, J. E., & Payne, D. N. (1993). Local structures of rare-earth ions in glasses: the 'crystal-chemistry'approach. *Journal of Non-Crystalline Solids*, 163(3), 261-267.

[48] Greaves, G. N. (1985). EXAFS and the structure of glass. *Journal of Non-Crystalline Solids*, 71(1-3), 203-217.

[49] Herrmann, A., Assadi, A. A., Lachheb, R., Zekri, M., Erlebach, A., Damak, K., Maalej, R., Sierka, M., & Rüssel, C. (2023). The effect of glass structure and local rare earth site symmetry on the optical properties of rare earth doped alkaline earth aluminosilicate glasses. *Acta Materialia*, 249, 118811.

[50] Zhang, J. C., Parent, C., Le Flem, G., & Hagenmuller, P. (1991). White light emitting glasses. *Journal of Solid State Chemistry*, 93(1), 17-29.

[51] Erol, E., Vahedigharehchopogh, N., Kıbrıslı, O., Ersundu, M. Ç., & Ersundu, A. E. (2021). Recent progress in lanthanide-doped luminescent glasses for solid-state lighting applications—A review. *Journal of Physics: Condensed Matter*, 33(48), 483001.

[52] Liu, Z., Chen, Q., Dai, N., Yu, Y., Yang, L., & Li, J. (2012). Tunable white light emitting glass suitable for long-wavelength ultraviolet excitation. *Journal of Non-Crystalline Solids*, 358(23), 3289-3293.

[53] Gou, J., Fan, J., Zuo, S., Luo, M., Chen, Y., Zhou, X., Yang, Y., Yu, B., & Liu, S. F. (2017). Highly thermally stable and emission color tunable borate glass for white-light-emitting diodes with zero organic resin. *Journal of the American Ceramic Society*, 100(9), 4011-4020.

[54] Bashar, K. A., Lakshminarayana, G., Baki, S. O., Mohammed, A. B., Caldiño, U., Meza-Rocha, A. N., Singh, V., Kityk, I. V., & Mahdi, M. A. (2019). Tunable white-light emission from Pr^{3+}/Dy^{3+} co-doped B_2O_3-TeO_2 PbO-ZnO Li_2O-Na_2O glasses. *Optical Materials*, 88, 558-569.

[55] Ehrt, D. (2015). Phosphate and fluoride phosphate optical glasses—properties, structure and applications. *Physics and Chemistry of Glasses-European Journal of Glass Science and Technology Part B*, 56(6), 217-234.

[56] Linganna, K., Rao, C. S., & Jayasankar, C. K. (2013). Optical properties and generation of white light in Dy^{3+}-doped lead phosphate glasses. *Journal of Quantitative Spectroscopy and Radiative Transfer*, 118, 40-48.

[57] A. Vidhi, A. Ankita, A. Anu, A.S. Rao (2022). Spectroscopic characterizations of Dy^{3+} ions doped phosphate glasses for epoxy-free white LED applications. *Optical Materials*, 132, 112863.

[58] Chen, Y., Chen, G., Liu, X., Yuan, C., & Zhou, C. (2017). Tunable luminescence mediated by energy transfer in Tm^{3+}/Dy^{3+} co-doped phosphate glasses under UV excitation. *Optical Materials*, 73, 535-540.

[59] Blasse, G., Grabmaier, B. C., Blasse, G., & Grabmaier, B. C. A general introduction to luminescent materials. *Springer Berlin Heidelberg* (1994).

[60] Jha, K., & Jayasimhadri, M. (2017). Structural and emission properties of Eu^{3+}-doped alkaline earth zinc-phosphate glasses for white LED applications. *Journal of the American Ceramic Society*, 100(4), 1402-1411.

[61] Francisco-Rodriguez, H. I., Lira, A., Soriano-Romero, O., Meza-Rocha, A. N., Bordignon, S., Speghini, A., Lozada-Morales, R., & Caldiño, U. (2018). Lithium-aluminum-zinc phosphate glasses activated with Tb^{3+} and Tb^{3+}/Eu^{3+} for green laser medium, reddish-orange and white phosphor applications. *Optical Materials*, 79, 358-365.

[62] Górny, A., Sołtys, M., Pisarska, J., & Pisarski, W. A. (2019). Effect of acceptor ions concentration in lead phosphate glasses co-doped with Tb^{3+}–Ln^{3+} (Ln= Eu, Sm) for LED applications. *Journal of Rare Earths*, 37(11), 1145-1151.

[63] Wang, Y., & Ohwaki, J. (1993). New transparent vitroceramics codoped with Er^{3+} and Yb^{3+} for efficient frequency upconversion. *Applied Physics Letters*, 63(24), 3268-3270.

[64] Auzel, F., Pecile, D., & Morin, D. (1975). Rare earth doped vitroceramics: new, efficient, blue and green emitting materials for infrared up-conversion. *Journal of the Electrochemical Society*, 122(1), 101.

[65] Méndez-Ramos, J., Lavın, V., Martın, I. R., Rodrıguez-Mendoza, U. R., Rodrıguez, V. D., Lozano-Gorrın, A. D., & Núnez, P. (2001). Role of the Eu^{3+} ions in the formation of transparent oxyfluoride glass ceramics. *Journal of Applied Physics*, 89(10), 5307-5310.

[66] Coates, J., Gay, E., & Sammes, P. G. (1997). Anion effects on the luminescence of europium complexes. *Dyes and pigments*, 34(3), 195-205

[67] Wang, X., Chen, J., Li, J., & Guo, H. (2011). Preparation and luminescent properties of Eu-doped transparent glass-ceramics containing SrF_2 nanocrystals. *Journal of Non-Crystalline Solids*, 357(11-13), 2290-2293.

[68] Qiao, X., Fan, X., & Wang, M. (2006). Luminescence behavior of Er^{3+} in glass ceramics containing BaF_2 nanocrystals. *Scripta Materialia*, 55(3), 211-214.

[69] Secu, M., Secu, C. E., Polosan, S., Aldica, G., & Ghica, C. (2009). Crystallization and spectroscopic properties of Eu-doped CaF_2 nanocrystals in transparent oxyfluoride glass-ceramics. *Journal of Non-Crystalline Solids*, 355(37-42), 1869-1872.

[70] Liu, X., Chen, G., Chen, Y., & Yang, T. (2017). Luminescent characteristics of $Tm^{3+}/Tb^{3+}/Eu^{3+}$ tri-doped phosphate transparent glass ceramics for white LEDs. *Journal of Non-Crystalline Solids*, 476, 100-107.

[71] Yu, X., Duan, L., Ni, L., & Wang, Z. (2012). Fabrication and luminescence behavior of phosphate glass ceramics co-doped with Er^{3+} and Yb^{3+}. *Optics Communications*, 285(18), 3805-3808.

[72] Kumar, M., Nagabhushana, H., & Ratnakaram, Y. C. (2021). Influence of alkali and alkaline earths on structural and luminescence properties of Sm^{3+} doped lithium fluoro phosphate glass and different (Na, Mg, K, Ca and Sr) glass ceramics. *Journal of Non-Crystalline Solids*, 573, 121146.

[73] Wyckoff, R. W. G. The Structure of Crystals, supplement for 1930-1934 to the second edition. *American Chemical Society Monograph Series*, p. 26, (1935).

[74] Ivanovskikh, K. V., Pustovarov, V. A., Kirm, M., & Shul'gin, B. V. (2005). Time-resolved vacuum ultraviolet spectroscopy of Er^{3+} ions in the SrF_2 crystal. *Journal of Applied Spectroscopy*, 72, 564-568.

[75] Shendrik, R., Radzhabov, E. (2010). Temperature dependance of Ce^{3+} and Pr^{3+} emission in CaF_2, BaF_2, SrF_2. *IEEE Transactions on Nuclear science*, 57(3), 1295-1299.

[76] Antuzevics, A., Kemere, M., & Ignatans, R. (2016). Local structure of gadolinium in oxyfluoride glass matrices containing SrF_2 and BaF_2 crystallites. *Journal of Non-Crystalline Solids*, 449, 29-33.

[77] Luo, Q., Qiao, X., Fan, X., & Zhang, X. (2010). Preparation and luminescence properties of Ce^{3+} and Tb^{3+} co-doped glasses and glass ceramics containing SrF_2 nanocrystals. *Journal of Non-Crystalline Solids*, 356(50-51), 2875-2879.

[78] Qiao, X., Fan, X., Wang, M., & Zhang, X. (2009). Spectroscopic properties of Er^{3+} and Yb^{3+} co-doped glass ceramics containing SrF_2 nanocrystals. *Journal of Physics D: Applied Physics*, 42(5), 055103.

[79] Milewska, K., Maciejewski, M., Synak, A., Łapiński, M., Mielewczyk-Gryń, A., Sadowski, W., & Kościelska, B. (2021). From structure to luminescent properties of B_2O_3-Bi_2O_3-SrF_2 glass and glass-ceramics doped with Eu^{3+} ions. *Materials*, 14(16), 4490.

[80] Walas, M., Pastwa, A., Lewandowski, T., Synak, A., Gryczyński, I., Sadowski, W., & Kościelska, B. (2016). Luminescent properties of Ln^{3+} doped tellurite glasses containing AlF_3. *Optical Materials*, 59, 70-75.

[81] Milewska, K., Maciejewski, M., Łapiński, M., Synak, A., Behrendt, M., Sadowski, W., & Kościelska, B. (2023). Structural and luminescence properties of B_2O_3-Bi_2O_3-AlF_3 glass doped with Eu^{3+}, Tb^{3+} and Tm^{3+} ions. *Journal of Non-Crystalline Solids*, 605, 122169.

[82] Liang, H., Luo, Z., Liu, X., Wang, B., Qin, C., Lei, W., & Lu, A. (2020). Effect of F/O ratio on up-conversion and down-conversion luminescence properties of Er^{3+}/Yb^{3+} co-doped SiO_2–Al_2O_3–AlF_3-Gd_2O_3–Na_2O glass. *Journal of Alloys and Compounds*, 827, 154274.

[83] Sarumaha, C. S., Rajagukguk, J., Chanthima, N., Rajaramakrishna, R., & Kaewkhao, J. (2023). Improvement of Luminescence Performance by the Addition of KF in the Eu_2O_3 Doped Li_2O-AlF_3-NaF-P_2O_5 Glass for Highly Efficient Reddish-Orange Laser Application. *Integrated Ferroelectrics*, 239(1), 167-182.

[84] Takahashi, M., Kanno, R., Kawamoto, Y., Tanabe, S., & Hirao, K. (1994). Compositional dependence of Er^{3+} upconversion luminescence in MF LiF ZrF_4 glasses (M: alkali metals). *Journal of Non-Crystalline Solids*, 168(1-2), 137-143.

[85] Malta, O. L., Santa-Cruz, P. A., De Sá, G. F., & Auzel, F. (1985). Fluorescence enhancement induced by the presence of small silver particles in Eu^{3+} doped materials. *Journal of Luminescence*, 33(3), 261-272.

[86] Amjad, R. J., Dousti, M. R., Sahar, M. R., Shaukat, S. F., Ghoshal, S. K., Sazali, E. S., & Nawaz, F. (2014). Silver nanoparticles enhanced luminescence of Eu^{3+}-doped tellurite glass. *Journal of Luminescence*, 154, 316-321.

[87] Dousti, M. R., Sahar, M. R., Rohani, M. S., Samavati, A., Mahraz, Z. A., Amjad, R. J., Awang, A., & Arifin, R. (2014). Nano-silver enhanced luminescence of Eu^{3+}-doped lead tellurite glass. *Journal of Molecular Structure*, 1065, 39-42.

[88] Saad, M., Stambouli, W., Mohamed, S. A., & Elhouichet, H. (2017). Ag nanoparticles induced luminescence enhancement of Eu^{3+} doped phosphate glasses. *Journal of Alloys and Compounds*, 705, 550-558.

[89] Assal, J., Hallstedt, B., & Gauckler, L. J. (1999). Experimental Phase Diagram Study and Thermodynamic Optimization of the Ag-Bi-O System. *Journal of the American Ceramic Society*, 82(3), 711-715.

[90] Sadecka, K., Gajc, M., Orlinski, K., Surma, H. B., Klos, A., Jozwik-Biala, I., Sobczak, K., Dluzewski, P., Toudert, J., & Pawlak, D. A. (2015). When eutectics meet plasmonics: Nanoplasmonic, volumetric, self-organized, silver-based eutectic. *Advanced Optical Materials,* 3(3), 381-389.

[91] Sanz, O., Haro-Poniatowski, E., Gonzalo, J., & Navarro, J. F. (2006). Influence of the melting conditions of heavy metal oxide glasses containing bismuth oxide on their optical absorption. *Journal of Non-Crystalline Solids*, 352(8), 761-768.

[92] - Septimio, R., Cruz, C., Silva, B., Garcia, A., Spinelli, J. E., & Cheung, N. (2021). Microstructural and segregation effects affecting the corrosion behavior of a high-temperature Bi-Ag solder alloy in dilute chloride solution. *Journal of Applied Electrochemistry*, 51, 769-780.

[93] Bojarski, Z., Łągiewka, E. Rentgenowska analiza strukturalna. *PWN* (1988).

[94] Cullity, B.D. and Stock, S.R. Elements of X-Ray Diffraction, 3rd Edition. *Pearson Education Limited*, (2014).

[95] Cox, J. N., Armstrong, J. L. Structure and Composition of Glasses and Amorphous Materials by Vibrational Spectroscopy: in: Chalmers, J. M., Griffiths, P. R. Handbook of Vibrational Spectroscopy. *Wiley* (2002).

[96] Stoch, L., & Środa, M. (1999). Infrared spectroscopy in the investigation of oxide glasses structure. *Journal of Molecular Structure*, 511, 77-84.

[97] Brown, M. E. (Ed.). Introduction to thermal analysis: techniques and applications. Dordrecht: *Springer Netherlands*, (2001).

[98] Saad, M., & Poulain, M. (1987). Glass forming ability criterion. In *Materials science forum* (Vol. 19, pp. 11-18). Trans Tech Publications Ltd.

[99] Karpukhina, N., Hill, R. G., & Law, R. V. (2014). Crystallisation in oxide glasses–a tutorial review. *Chemical Society Reviews*, *43*(7), 2174-2186.

[100] Höhne, G. W. H., Hemminger, W., & Flammersheim, H. J. Differential scanning calorimetry (Vol. 2, pp. 9-30). *Berlin: Springer*, (2003).

[101] Pelant, I., Valenta, J. Luminescence Spectroscopy of Semiconductors. *Oxford University Press,* (2012).

[102] Walas, M., Lewandowski, T., Synak, A., Łapiński, M., Sadowski, W., & Kościelska, B. (2017). Eu^{3+} doped tellurite glass ceramics containing SrF_2 nanocrystals: Preparation, structure and luminescence properties. *Journal of Alloys and Compounds*, *696*, 619-626.

[103] Kubicki, A. A., Bojarski, P., Grinberg, M., Sadownik, M., & Kukliński, B. (2006). Time-resolved streak camera system with solid state laser and optical parametric generator in different spectroscopic applications. *Optics communications*, *263*(2), 275-280.

[104] Adamski, A., Barańska, M., Bodzoń-Kułakowska, A., Chruszcz-Lipska, K., Hetmańczyk, Ł., Kaczor, A., Kraj, A., Małek, K., Migdał-Mikuli, A., Mikuli, E., Noga, M., Pietrzyk, P., Proniewicz, E., Proniewicz, L., Silberring, J., Sojka, Z., Suder, P., Szklarzewicz, J., & Wesełucha-Birczyńska, A. Wybrane metody spektroskopii i spektrometrii molekularnej w analizie strukturalnej (K. Małek & L. Proniewicz, Eds.), *Wydawnictwo Uniwersytetu Jagiellońskiego,* (2005).

[105] Pascuta, P., Rada, S., Borodi, G., Bosca, M., Pop, L., & Culea, E. (2009). Influence of europium ions on structure and crystallization properties of bismuth-alumino-borate glasses and glass ceramics. *Journal of Molecular Structure*, 924, 214-220.

[106] Mooney-Slater, R. C. (1962). Polymorphic forms of bismuth phosphate. *Zeitschrift für Kristallographie-Crystalline Materials*, *117*(1-6), 371-385.

[107] Romero, B., Bruque, S., Aranda, M. A., & Iglesias, J. E. (1994). Syntheses, crystal structures, and characterization of bismuth phosphates. *Inorganic Chemistry*, 33(9), 1869-1874.

[108] Moustafa, Y. M., & El-Egili, K. (1998). Infrared spectra of sodium phosphate glasses. *Journal of Non-Crystalline Solids*, 240(1-3), 144-153.

[109] De Araujo, E. B., De Paiva, J. A. C., De Araujo, M. A. B., & Sombra, A. S. B. (1996). Structure and optical properties of lithium niobium-phosphate glasses and glass ceramics. *Physica Status Solidi (b),* 197(1), 231-240.

[110] Wang, G., Lei, J., Yun, H., Guo, L., & Jin, B. (1991, November). XPS, IR, and Mossbauer studies of lithium phosphate glasses containing iron oxides. In *Submolecular Glass Chemistry and Physics* (Vol. 1590, pp. 229-236). SPIE.

[111] Robinson, E. A. (1963). Characteristic vibrational frequencies of oxygen compounds of phosphorus and chlorine: correlation of symmetric and asymmetric stretching frequencies of PO and ClO bonds. *Canadian Journal of Chemistry*, *41*(1), 173-179.

[112] Shaim, A., Et-Tabirou, M., Montagne, L., & Palavit, G. (2002). Role of bismuth and titanium in Na_2O–Bi_2O_3–TiO_2–P_2O_5 glasses and a model of structural units. *Materials research bulletin*, *37*(15), 2459-2466.

[113] Rani, S., Sanghi, S., Agarwal, A., & Ahlawat, N. (2009). Influence of Bi_2O_3 on optical properties and structure of bismuth lithium phosphate glasses. *Journal of Alloys and compounds*, *477*(1-2), 504-509.

[114] Sene, F. F., Martinelli, J. R., & Gomes, L. (2004). Synthesis and characterization of niobium phosphate glasses containing barium and potassium. *Journal of Non-Crystalline Solids*, *348*, 30-37.

[115] Parks, J. R., & Van Wazer, J. R. (1957). Structure and properties of the condensed phosphates. XII. Reorganization theory and some applications. *Journal of the American Chemical Society*, *79*(18), 4890-4897.

[116] Brow, R. K., Tallant, D. R., Myers, S. T., & Phifer, C. C. (1995). The short-range structure of zinc polyphosphate glass. *Journal of Non-Crystalline Solids*, *191*(1-2), 45-55.

[117] Hu, Y. I., Liu, N. H., & Lin, U. L. (1998). Glass formation and glass structure of the $BiO_{1.5}$—PbO—CuO system. *Journal of materials science*, *33*, 229-234.

[118] Tatsumisago, M., Hamada, A., Minami, T., & Tanaka, M. (1983). Structure and properties of Li_2O – RO - Nb_2O_5 glasses (R- Ba, Ca, Mg) prepared by twin-roller quenching. *Journal of Non-Crystalline Solids*, *56*(1-3), 423-428.

[119] Pascuta, P., Pop, L., Rada, S., Bosca, M., & Culea, E. (2008). The local structure of bismuth borate glasses doped with europium ions evidenced by FT-IR spectroscopy. *Journal of Materials Science: Materials in Electronics*, *19*, 424-428.

[120] Zhou, X., & Wang, X. (2013). Preparation, characterization and luminescence properties of $BiPO_4$: Eu nanophosphors. *Luminescence*, 28(5), 685-689.

[121] Naidu, B. S., Vishwanadh, B., Sudarsan, V., & Vatsa, R. K. (2012). $BiPO_4$: a better host for doping lanthanide ions. *Dalton Transactions*, 41(11), 3194-3203.

[122] Guan, M., Sun, J., Tao, F., & Xu, Z. (2008). A host crystal for the rare-earth ion dopants: synthesis of pure and Ln-doped urchinlike $BiPO_4$ structure and its photoluminescence. *Crystal Growth and Design*, 8(8), 2694-2697.

[123] Antuzevics, A., Kemere, M., Krieke, G., & Ignatans, R. (2017). Electron paramagnetic resonance and photoluminescence investigation of europium local structure in oxyfluoride glass ceramics containing SrF_2 nanocrystals. *Optical Materials*, 72, 749-755.

[124] Jin, H., Mo, Z., Zhang, X., Yuan, L., Yan, M., & Li, L. (2016). Luminescent properties of Eu^{3+}-doped glass ceramics containing $BaCl_2$ nanocrystals under NUV excitation for White LED. *Journal of Luminescence*, 175, 187-192.

[125] Sillen, A., & Engelborghs, Y. (1998). The correct use of "average" fluorescence parameters. *Photochemistry and photobiology*, 67(5), 475-486.

[126] Amjad, R. J., Santos, W., Jacinto, C., & Dousti, M. R. (2017). Luminescence dynamics in Eu^{3+} doped fluoroborate glasses. *Journal of Luminescence*, 192, 827-831.

[127] Balda, R., Fernández, J., Eilers, H., & Yen, W. M. (1994). Site-selective spectroscopy of Eu^{3+} ions in fluoride glasses. *Journal of Luminescence*, 59(1-2), 81-87.

[128] José Filho, C., Zilio, S. C., Messias, D. N., Pilla, V., Silva, A. C. A., Dantas, N. O., & Andrade, A. A. (2020). Effects of aluminum substitution by potassium in the P_2O_5–Al_2O_3–Na_2O–K_2O phosphate glasses. *Journal of Alloys and Compounds,* 815, 152359.

[129] Yue, Y., Wang, Y., Cao, Y., Chen, S., Zhou, Q., Chen, W., & Hu, L. (2018). Effect of Al_2O_3 on structure and properties of Al_2O_3-K_2O-P_2O_5 glasses. *Optical Materials Express*, 8(2), 245-258.

[130] Shapaan, M., El-Badry, S. A., Mostafa, A. G., Hassaan, M. Y., & Hazzaa, M. H. (2012). Structural and electric-dielectric properties of some bismuth-phosphate glasses. *Journal of Physics and Chemistry of Solids*, 73(3), 407-417.

[131] De Andrade, J. S., Pinheiro, A. G., Vasconcelos, I. F. D., Sasaki, J. M., De Paiva, J. A. C., Valente, M. A., & Sombra, A. S. B. (1999). Raman and infrared spectra of $KNbO_3$ in niobate glass-ceramics. *Journal of Physics: Condensed Matter,* 11(22), 4451.

[132] Garrigou-Lagrange, C., Ouchetto, M., & Elouadi, B. (1985). Infrared spectra of vitreous lithium and cadmium mixed phosphates. *Canadian Journal of Chemistry*, 63(7), 1436-1446.

[133] Karmakar, B., Kundu, P., & Dwivedi, R. N. (2001). IR spectra and their application for evaluating physical properties of fluorophosphate glasses. *Journal of Non-Crystalline Solids*, 289(1-3), 155-162.

[134] Saddeek, Y. B., Kaid, M. A., & Ebeid, M. R. (2014). FTIR and physical features of Al_2O_3–La_2O_3–P_2O_5–PbO glasses. *Journal of Non-Crystalline Solids*, 387, 30-35.

[135] Marijan, S., Klaser, T., Mirosavljević, M., Mošner, P., Koudelka, L., Skoko, Ž., Pisk, J., & Pavić, L. (2024). Exploring the Effect of V_2O_5 and Nb_2O_5 Content on the Structural, Thermal, and Electrical Characteristics of Sodium Phosphate Glasses and Glass–Ceramics. *International Journal of Molecular Sciences*, 25(5), 3005.

[136] Silva Neto, O. C., Muniz, R. F., Pedrochi, F., & Steimacher, A. (2023). Structural, Thermal, and Spectroscopic Properties of P_2O_5-KF-Al_2O_3 Glassy System. *Journal of Electronic Materials*, 52(10), 6719-6729.

[137] Pascuta, P., Pop, L., Rada, S., Bosca, M., & Culea, E. (2008). The local structure of bismuth borate glasses doped with europium ions evidenced by FT-IR spectroscopy. *Journal of Materials Science: Materials in Electronics*, 19, 424-428.

[138] Ignatieva, L. N., Zakalyukin, R. M., Fedorov, P. P., & Buznik, V. M. (2001). IR spectroscopic study of glasses based on InF_3 and AlF_3. *Journal of Structural Chemistry*, 42, 564-569.

[139] Haiyan, C., & Fuxi, G. (1989). Vibrational spectra and structure of AlF_3-YF_3 fluoride glasses. *Journal of Non-Crystalline Solids,* 112(1-3), 272-276.

[140] Liu, H., Lu, Y., Qu, Y., Lu, H., & Yue, Y. (2016). Effect of the content of Al_2O_3 on structure and properties of calcium-phosphate glasses: two experimental case studies. *Journal of Non-Crystalline Solids*, 450, 95-102.

[141] Dahiya, J., Hooda, A., Agarwal, A., & Khasa, S. (2022). Effect of Dysprosium and Samarium RE ion Co-doping on photoluminescence behavior of novel alkali fluoride bismuth borate glasses: A white LED material. *Optical Materials*, 134, 113162.

[142] Jose, A., Krishnapriya, T., George, A., Jose, T. A., Joseph, C., Unnikrishnan, N. V., & Biju, P. R. (2021). Cool/warm white light luminescent traits and energy transfer studies of Dy^{3+}/Er^{3+}/Sm^{3+} triply doped multicomponent borosilicate glasses for lighting applications. *Journal of Non-Crystalline Solids*, 562, 120775.

[143] Binnemans, K. (2015). Interpretation of europium (III) spectra. *Coordination Chemistry Reviews*, 295, 1-45.

[144] Jiang, F., Sha, S., Li, S., Xu, S., Xu, H., Mei, X., & Zhang, Y. (2021). Luminescence and structural properties of Eu^{3+}-doped calcium fluoride-bismuth oxide-phosphate glasses. *Ceramics International*, 47(10), 13776-13782.

[145] Vijaya, N., & Jayasankar, C. K. (2013). Structural and spectroscopic properties of Eu^{3+}-doped zinc fluorophosphate glasses. *Journal of Molecular Structure*, 1036, 42-50.

[146] Pisarska, J., Sołtys, M., Żur, L., Pisarski, W. A., & Jayasankar, C. K. (2014). Excitation and luminescence of rare earth-doped lead phosphate glasses. *Applied Physics B*, 116, 837-845.

[147] Dousti, M. R., Poirier, G. Y., & de Camargo, A. S. S. (2015). Structural and spectroscopic characteristics of Eu^{3+}-doped tungsten phosphate glasses. *Optical Materials*, 45, 185-190.

[148] Raju, C. N., Sailaja, S., Raju, S. H., Dhoble, S. J., Rambabu, U., Jho, Y. D., & Reddy, B. S. (2014). Emission analysis of $CdO–Bi_2O_3–B_2O_3$ glasses doped with Eu^{3+} and Tb^{3+}. *Ceramics International*, 40(6), 7701-7709.

List of figures

List of tables

Scientific achievements

Publications directly related to the doctoral dissertation

- **Maciejewski, M.**, Milewska, K., Synak, A., Sadowski, W., & Kościelska, B. (2023). Influence of controlled crystallization and SrF_2 content on the structure and properties of Eu^{3+} doped phosphate glasses. *Journal of Non-Crystalline Solids*, *616*, 122473.
- **Maciejewski, M.**, Milewska, K., Synak, A., Łapiński, M., Sadowski, W., & Kościelska, B. (2025). Effect of AlF_3 and KF addition on the structure and luminescent properties of P_2O_5–K_2O–Nb_2O_5–Bi_2O_3 glasses doped with Eu^{3+}. *Journal of Luminescence*, *277*, 120954.

Publications beyond the topics covered in the doctoral dissertation

- Milewska, K., **Maciejewski, M**., Synak, A., Łapiński, M., Mielewczyk-Gryń, A., Sadowski, W., & Kościelska, B. (2021). From structure to luminescent properties of B_2O_3-Bi_2O_3-SrF_2 glass and glass-ceramics doped with Eu^{3+} ions. *Materials*, *14*(16), 4490.
- Milewska, K., **Maciejewski, M**., Łapiński, M., Synak, A., Behrendt, M., Sadowski, W., & Kościelska, B. (2023). Structural and luminescence properties of B_2O_3-Bi_2O_3-AlF_3 glass doped with Eu^{3+}, Tb^{3+} and Tm^{3+} ions. *Journal of Non-Crystalline Solids*, *605*, 122169.
- Wysocka, I., Czaplicka, N., Pawelczyk, E., Karczewski, J., Sobczak, J., Bielan, Z., **Maciejewski, M.**, Kościelska, B., & Rogala, A. (2023). Novel sugar-based nickel-tungsten carbide catalysts for dry reforming of hydrocarbons. *Journal of Industrial and Engineering Chemistry*, 124, 431-446.
- Wysocka, I., Karczewski, J., **Maciejewski, M.**, Kościelska, B., Kubiak, A., Rogala, A., & Gębicki, J. (2023). Ni-WC/Al_2O_3 and Ni-WC/$MgWO_4$/$MgAl_2O_4$ catalysts for resource recovery via pyrolysis combined with the dry reforming of plastics (PCDR). *Journal of Environmental Chemical Engineering*, *11*, 111298.
- Wysocka, I., Karczewski, J., Gołąbiewska, A., Łapiński, M., Cieślik, B., **Maciejewski, M.**, Kościelska, B., & Rogala, A. (2023). Nickel phase deposition on V_2CT_x/V_2AlC as catalyst precursors for a dry methane reforming: The effect of the deposition method on the morphology and catalytic activity. *International Journal of Hydrogen Energy*, 48, 10922-10940.
- Milewska, K., **Maciejewski, M.** E., Žitňan, M., Velázquez, J. J., Galusek, D., Sadowski, W., & Kościelska, B. (2024). Tunable emission and energy transfer of B_2O_3–Bi_2O_3–AlF_3 glass system doped with Eu^{3+}/Dy^{3+}. *Journal of Luminescence*, *269*, 120440.
- Milewska, K., **Maciejewski, M.**, Łapiński, M., Synak, A., Narajczyk, M., Bafia, A., Sadowski, W., & Kościelska, B. (2025). Crystallization of Ag Nanoparticles in Borate–Bismuth Glass and Its Influence on Eu^{3+} Luminescence. *Applied Sciences*, *15*(8), 4495.
- Nawrot, N., Jespersen, E. A., Wojciechowska, E., Rossau, T. E., Strycharz, J., Kluska, J., Matej-Łukowicz, K., Karczewski, J., **Maciejewski, M.**, & Arias, C. A. (2025). Effect of straw and wood biochar application on growth of Miscanthus× giganteus on marginal soil: a meso-scale study with shock short-term screening. *Biomass and Bioenergy*, *200*, 107989.

- Pawelczyk, E., Frąckiewicz, I., Gil, A., Karczewski, J., **Maciejewski, M. E.**, Dymerski, T., & Gębicki, J. (2025). Ni-Mo_2C/γ-Al_2O_3 catalysts for syngas production in pyrolysis-dry reforming of plastics-the effect of amine nature on catalyst performance. *Chemical Engineering Journal*, *516*, 164181.